

**Vacuum drum drying –
a novel technology for enabling formulation
principles in the development of
oral solid dosage forms**

Dissertation
zur
Erlangung des Doktorgrades (Dr. rer. nat.)
der
Mathematisch-Naturwissenschaftlichen Fakultät
der
Rheinischen Friedrich-Wilhelms-Universität Bonn

vorgelegt von
Barbara Veronika Schönfeld
aus
Heydebreck

Bonn 2022

Angefertigt mit Genehmigung der Mathematisch-Naturwissenschaftlichen Fakultät
der Rheinischen Friedrich-Wilhelms-Universität Bonn

Gutachter*in: Prof. Dr. Karl Gerhard Wagner
Gutachter*in: Prof. Dr. Alf Lamprecht
Fachnaher Gutachter*in: Prof. Dr. Gerd Bendas
Fachfremder Gutachter*in: Prof. Dr. Andreas Schieber

Tag der Promotion: 24. Oktober 2022

Erscheinungsjahr: 2022

Danksagung

An erster Stelle möchte ich mich bei meinem Doktorvater Prof. Dr. Karl G. Wagner für die umfangreiche und hervorragende Betreuung meiner Doktorarbeit bedanken sowie für die stets hilfreichen Ratschläge, Denkanstöße und Korrekturen.

Ein besonderer Dank gilt außerdem meinem Betreuer bei AbbVie Dr. Ulrich Westedt, der mich von Beginn der Promotion an immer tatkräftig unterstützt hat – ob in fachlichen Diskussionen oder praktisch im Labor/Technikum, der immer Zeit und ein offenes Ohr hatte, der mich fachlich wie persönlich weiterentwickelt hat, und der mir immer den Rücken gestärkt und vor allem freigehalten hat. Ein großes Vorbild!

Außerdem danke ich Herrn Professor Dr. Alf Lamprecht für die Übernahme des Zweitgutachtens, sowie Professor Dr. Gerd Bendas und Professor Dr. Andreas Schieber für Ihre Bereitschaft an der Prüfungskommission teilzunehmen.

Großer Dank gilt auch Dr. Lutz Asmus, der mich gefördert und vor allem ermutigt hat, den Schritt aus der Komfortzone zu gehen und das Promotionsstudium zu beginnen, sowie Dr. Matthias Degenhardt und Dr. Gunther Berndl, die es mir ermöglicht haben die Doktorarbeit in einer Kooperation zwischen AbbVie (NCE Formulation Sciences) und der Universität Bonn anzufertigen.

Ein herzliches Dankeschön gilt dem gesamten Vakuum-Walzentrockner Projekt-Team bei AbbVie für die fachlichen Diskussionen und Ideenanstöße sowie Preamkumar Kathiresan und Mike Weinberg für die helfenden Hände am Vakuum-Walzentrockner. Danke an Raphael Eich, Harald Krull, Roger Kubitschek und Ralf Heilmann und jeweiligen Teams für die technische Unterstützung vor Ort an der Anlage. Ohne eure Expertise würde die Prototyp-Anlage heute noch nicht laufen!

Meinen AbbVie Kolleg*innen Dr. Kristin Voges, Dr. Esther Bochmann, Dr. Benjamin-Luca Keller und Dr. Cihad Anamur danke ich für die inspirierenden Gespräche in Kaffee- und Lunchpausen und ihre stets aufmunternden Worte im Arbeitsalltag. Besonderer Dank gilt außerdem meinen Bürokolleg*innen Karola Rau und Michael Preiß für den täglichen Zuspruch und die motivierenden Worte bei den ein oder anderen Tiefs. Ein weiterer, herzlicher Dank gilt einem Urgestein der Abteilung, Harald Hach – einen meiner Lieblingskollegen, der immer für einen Spaß zu haben ist, mir den Laboralltag versüßt und auch fachlich immer wieder neue Perspektiven aufzeigt.

Bedanken möchte ich mich auch bei meinem Arbeitskreis in Bonn am „Institut für pharmazeutische Technologie“ für die herzliche Begrüßung und Aufnahme im Arbeitskreis und die geselligen sowie lustigen Stunden zu Karnevals-Zeiten und bei weiteren Aktionen wie den „Christmas-Decoration Award“. Tage, die für immer in Erinnerung bleiben. Nicht zu vergessen aber auch die Unterstützung bei Laborarbeiten: Großes Dankeschön an Dr. Alexander Denninger und Tim Becker bei der Unterstützung beim BiPHa+, und Dr. Kristina Steffens, Dr. Tim Lillotte und Thilo Faber bei SEM Aufnahmen. Martina Gerlitz danke ich für die netten Gespräche bei Besuchen und für die schnelle und tatkräftige Unterstützung bei administrativen und organisatorischen Anfragen.

Abschließend möchte ich mich bei meiner Familie und bei meinen Freunden für die Ermutigungen und deren Interesse an meiner Arbeit bedanken. Stellvertretend möchte ich hier zwei besondere Menschen hervorheben: Natascha Tschukewitsch und Caroline Neuber, die mir in zahlreichen Gesprächen bei Spaziergängen wieder Energie und Kraft für die nächste Herausforderung geschenkt haben. Auf die nächsten Kilometer gemeinsam.

Mein größter und herzlichster Dank jedoch gilt meinen liebevollen Eltern, den wichtigsten Menschen in meinem Leben, die immer an mich glauben und hinter mir stehen, die mich bedingungslos in allen Lebenslagen unterstützen und immer ein offenes Ohr für mich haben. Ohne euch wäre ich nicht der Mensch geworden, der ich bin. Mein Dank ist nicht in Worte zu fassen.

Für meine Eltern

„In der Mitte von Schwierigkeiten liegen die Möglichkeiten“
(Albert Einstein)

TABLE OF CONTENTS

TABLE OF CONTENTS

ABBREVIATIONS AND SYMBOLS	VII
1. INTRODUCTION AND THEORETICAL BACKGROUND	1
1.1 Vacuum Drum Drying.....	4
1.2 Amorphous Solid Dispersion.....	8
1.2.1 Principle	8
1.2.2 Manufacturing Technologies.....	8
1.3 Solidification of Nanocrystals	11
1.3.1 Principle	11
1.3.2 Manufacturing Technologies.....	13
1.4 Tablets	15
1.4.1 Compression Mechanisms	15
1.4.2 Compression Analysis	17
1.5 References.....	18
2. AIM AND SCOPE	24
3. VACUUM DRUM DRYING - A NOVEL SOLVENT-EVAPORATION BASED TECHNOLOGY TO MANUFACTURE AMORPHOUS SOLID DISPERSIONS IN COMPARISON TO SPRAY DRYING AND HOT MELT EXTRUSION	25
3.1 Graphical Abstract	26
3.2 Abstract.....	26
3.3 Highlights	27
3.4 Keywords	27
3.5 Introduction	27
3.6 Material and methods	30
3.6.1 Materials	30
3.6.2 Methods	30
3.6.2.1 Amorphous solid dispersion (ASD) preparation	30
3.6.2.1.1 Hot-melt extrusion	31
3.6.2.1.2 Spray drying	31
3.6.2.1.3 Vacuum drum drying	31
3.6.2.2 Amorphous solid dispersions characterization	33
3.6.2.2.1 Assay & degradation products by HPLC	33
3.6.2.2.2 Residual crystallinity and glass transition temperature (T_g) by differential scanning calorimetry (DSC).....	33
3.6.2.2.3 Residual crystallinity by polarized light microscopy (PLM).....	34
3.6.2.2.4 Residual crystallinity by X-ray powder diffraction (XRPD).....	34

TABLE OF CONTENTS

3.6.2.2.5 Residual solvents by gas chromatography.....	35
3.6.2.2.6 Loss on drying	35
3.6.2.2.7 Bulk/tapped/particle (pycnometric) density.....	35
3.6.2.2.8 Flowability.....	35
3.6.2.2.9 Specific surface area.....	35
3.6.2.2.10 Particle size distribution.....	36
3.6.2.2.11 Scanning electron microscopy	36
3.6.2.3 In-vitro dissolution – BiPHa+	36
3.7 Results and discussion	37
3.7.1 Amorphous solid dispersions characterization	37
3.7.1.1 Product quality.....	37
3.7.1.1.1 Assay and degradation products.....	37
3.7.1.1.2 Residual crystallinity and glass transition temperature (T_g).....	39
3.7.1.1.3 Residual solvents and loss on drying (LOD)	40
3.7.1.2 Powder properties and downstream processability	41
3.7.1.2.1 Particle size distribution and particle morphology	41
3.7.1.2.2 Bulk/tapped/particle (pycnometric) density and flowability	44
3.7.2 In-vitro dissolution – BiPHa+	45
3.8 Conclusion	48
3.9 CRediT authorship contribution statement.....	49
3.10 Declaration of competing interest	49
3.11 Acknowledgement & Funding	49
3.12 Appendix A. Supplementary data	50
3.13 References.....	55
4. COMPRESSION OF AMORPHOUS SOLID DISPERSIONS PREPARED BY HOT-MELT EXTRUSION, SPRAY DRYING AND VACUUM DRUM DRYING	59
4.1 Graphical Abstract	60
4.2 Abstract.....	60
4.3 Highlights	61
4.4 Keywords	61
4.5 Introduction	61
4.6 Material and methods	63
4.6.1 Materials	63
4.6.2 Methods	63
4.6.2.1 Amorphous solid dispersion (ASD) preparation	63
4.6.2.1.1 Hot-melt extrusion (HME).....	64

TABLE OF CONTENTS

4.6.2.1.2	Spray drying (SD).....	65
4.6.2.1.3	Vacuum drum drying (VDD)	65
4.6.2.2	Tablet blend preparation.....	66
4.6.2.3	Glass transition temperature (T_g) by differential scanning calorimetry (DSC)	66
4.6.2.4	Bulk/tapped/particle (pycnometric) density	66
4.6.2.5	Flowability.....	67
4.6.2.6	Particle size distribution.....	67
4.6.2.7	Specific surface area (SSA)	67
4.6.2.8	Loss on drying	67
4.6.2.9	Scanning electron microscopy.....	68
4.6.2.10	Compression analysis	68
4.6.2.11	Elastic recovery	69
4.6.2.12	Tableting.....	70
4.6.2.13	X-ray micro computed tomography (X-ray μ CT).....	70
4.6.2.14	Friability	70
4.6.2.15	Disintegration.....	70
4.6.2.16	In-vitro dissolution.....	70
4.7	Results	72
4.7.1	Powder characterization of ASDs and tablet blends (TB).....	72
4.7.1.1	Particle size distribution (PSD), particle morphology and specific surface area (SSA).....	72
4.7.1.2	Densities (bulk/tapped/particle (pycnometric)) and flowability	73
4.7.1.3	Loss on drying (LOD)	74
4.7.1.4	Glass transition temperature (T_g dry).....	74
4.7.2	Compression analysis.....	76
4.7.2.1	Tabletability (out-of-die).....	76
4.7.2.2	Compactability (out-of-die)	77
4.7.2.3	Elastic recovery	79
4.7.3	Tablet characterization	80
4.7.3.1	Tablet manufacture.....	80
4.7.3.2	Tablet morphology.....	80
4.7.3.3	Friability	83
4.7.3.4	Disintegration and in-vitro dissolution.....	83
4.8	Discussion.....	85
4.8.1	Powder characterization ASDs and tablet blends (TB).....	85
4.8.2	Compression analysis.....	85

TABLE OF CONTENTS

4.8.3	Tablet characterization	87
4.9	Conclusion	89
4.10	Declaration of competing interest	90
4.11	Acknowledgments & Funding	90
4.12	Appendix A. Supplementary data	91
4.13	References.....	92
5.	COMPRESSION MODULUS AND APPARENT DENSITY OF POLYMERIC EXCIPIENTS DURING COMPRESSION – IMPACT ON TABLETABILITY.....	94
5.1	Graphical Abstract	95
5.2	Abstract.....	95
5.3	Keywords	96
5.4	Introduction	96
5.5	Materials and Methods.....	99
5.5.1	Materials	99
5.5.2	Methods	100
5.5.2.1	Hot-melt extrusion	100
5.5.2.2	Tablet blend preparation.....	100
5.5.2.3	Particle density (pycnometric density, ρ_{par}).....	101
5.5.2.4	Density under pressure (ρ_{pre}).....	101
5.5.2.5	Density ratio (ρ_{ratio}).....	101
5.5.2.6	Compression analysis	101
5.5.2.7	Compaction pressure	102
5.5.2.8	Apparent density (in-die)	102
5.5.2.9	Particle density threshold	102
5.5.2.10	Solid fraction (in-die).....	102
5.5.2.11	Elastic recovery (in-die)	102
5.5.2.12	Elastic modulus (Young's modulus)	103
5.5.2.13	Heckel analysis (in-die)	103
5.6	Results	105
5.6.1	Density ratio: particle density vs. density under pressure.....	105
5.6.2	Apparent density in-die vs. compaction pressure	106
5.6.3	Elastic recovery in-die vs. compaction pressure.....	108
5.6.4	Particle density threshold.....	111
5.6.5	Elastic modulus (Young's modulus, E_{mod}).....	112
5.6.6	Heckel analysis (in-die).....	112
5.7	Discussion.....	119

TABLE OF CONTENTS

5.7.1	Powder density in compression analysis - differences and consequences	119
5.7.2	Particle density exceeded during compression and the impact on elastic recovery	120
5.7.3	Impact of density determination on Heckel analysis	122
5.8	Conclusion	124
5.9	Author contributions	124
5.10	Conflicts of interest	125
5.11	Acknowledgments.....	125
5.12	Funding	125
5.13	Data availability statement	125
5.14	References.....	126
6.	TRANSFORMATION OF RITONAVIR NANOCRYSTAL SUSPENSIONS INTO A REDISPERSIBLE DRUG PRODUCT VIA VACUUM DRUM DRYING	130
6.1	Graphical Abstract	131
6.2	Abstract.....	131
6.3	Keywords	132
6.4	Introduction	132
6.5	Material and Methods	134
6.5.1	Materials	134
6.5.2	Methods	134
6.5.2.1	Preparation of ritonavir nanosuspensions by wet ball milling	134
6.5.2.2	Characterization of nanosuspensions	135
6.5.2.2.1	Particle size analysis by dynamic light scattering.....	135
6.5.2.2.2	Particle size analysis by laser diffraction.....	135
6.5.2.3	Solidification via vacuum drum drying	135
6.5.2.4	Redispersibility of VDD intermediates/tablets/capsules	137
6.5.2.4.1	Redispersibility by particle fractions in submicron range.....	137
6.5.2.4.2	Redispersibility index.....	137
6.5.2.5	Characterization of VDD intermediates	137
6.5.2.5.1	Bulk/tapped density	137
6.5.2.5.2	Flowability.....	138
6.5.2.5.3	Particle size distribution.....	138
6.5.2.5.4	Loss on drying	138
6.5.2.5.5	Crystallinity and glass transition temperature (T_g) by differential scanning calorimetry (DSC)	138
6.5.2.5.6	Short-term stability focussing on redispersibility	139
6.5.2.6	Downstream processability.....	139

TABLE OF CONTENTS

6.5.2.6.1	Tabletability and tabletting.....	139
6.5.2.6.2	Encapsulation.....	139
6.5.2.6.3	Disintegration	140
6.6	Results	140
6.6.1	Characterization of ritonavir nanosuspensions.....	140
6.6.2	Solidification via VDD and characterization of resulting intermediates	140
6.6.2.1	Impact of drying protectant and drum temperature on processability.....	140
6.6.2.2	Impact of drying protectant and drum temperature on powder properties of dried intermediates	141
6.6.2.3	Impact of drying protectant and drum temperature on redispersibility....	144
6.6.2.4	Impact of drying protectant and drum temperature on solid state of ritonavir	145
6.6.3	Short-term stability of selected formulation.....	146
6.6.4	Downstream processability of selected formulation.....	146
6.6.4.1	Tabletability and disintegration of selected formulations	147
6.6.4.2	Impact of tableting process on redispersibility	147
6.6.4.3	Impact of encapsulation process on redispersibility	148
6.7	Discussion.....	149
6.8	Conclusion	153
6.9	Author contributions	154
6.10	Declaration of competing interest	154
6.11	Acknowledgments.....	154
6.12	Funding statement	154
6.13	Appendix A. Supplementary data	155
6.13.1	Crystallinity and glass transition temperature (T_g) by differential scanning calorimetry (DSC).....	155
6.13.2	Crystallinity by powder X-ray diffraction (PXRD)	155
6.13.3	Encapsulation process.....	157
6.14	References.....	158
7.	SUMMARY AND OUTLOOK.....	161
8.	PUBLICATIONS	166

ABBREVIATIONS AND SYMBOLS

Abbreviations/Symbols	
A	Intercept of linear ascending part of Heckel plot
A-HP	Acid hydrolysis product
ANOVA	Analysis of variance
API	Active pharmaceutical ingredient
ASD	Amorphous solid dispersion
BET	Brunauer-Emmet-Teller
BSE	Backscattered electron
COP	Copovidone
CP	Compaction pressure
D	Tablet diameter
DLS	Dynamic light scattering
DS	Drug substance
DSC	Differential scanning calorimetry
E	Elastic modulus
E_{mod}	Elastic modulus modified (calculated via ER_{in-die} slope)
ER_{in-die}	Elastic recovery in-die
f_1	Difference factor
f_2	Similarity factor
FaSSIF-V2	Fasted state simulating fluid version 2.0
FDA	U.S. Food and Drug Administration
FFC	Flow function coefficient
FIH	First-in-human
GC	Gas chromatography
GMP	Good manufacturing practice
HDPE	High-density polyethylene
HME	Hot-melt extrusion
HPLC	High pressure liquid chromatography
HPMCSAS	Hypromellose acetate succinate
ICH	International Conference on Harmonization
k	Slope of Heckel equation
Lac	Lactose
LD	Laser diffraction
LOD	Loss on drying
Man	Mannitol
mPas	Millipascal-second
n.a.	Not applicable
n.d.	Not detected/ not determined
NMT	Not more than
NS	Nanosuspension
OP	Outer phase
P	Breaking force

ABBREVIATIONS AND SYMBOLS

Abbreviations/Symbols

P_Y	Yield pressure
PDI	Polydispersibility index
Ph. Eur.	European Pharmacopoeia
PLM	Polarized light microscopy
PQL	Practical quantification limit
PSD	Particle size distribution
PS_{min}	Minimal punch separation
PXRD	Powder X-ray diffraction
PVP	Polyvinylpyrrolidone
RDI	Redispersibility index
RTV	Ritonavir
SD	Spray drying
SDS	Sodium dodecyl sulphate
SE	Secondary electron
SEM	Scanning electron microscope
SF	Solid fraction
SSA	Specific surface area
t	Tablet thickness
TB	Tablet blend
T_{crit}	Critical drum temperature
T_g	Glass transition temperature
$T_{g, dry}$	Glass transition temperature (dry)
$T_{g, wet}$	Glass transition temperature (wet)
TB	Tablet blend
TER	Total elastic recovery
Tre	Trehalose
TriCaCi	Tricalcium citrate tetrahydrate
TS	Tensile strength
UHMWPE	Ultra-high-molecular-weight polyethylene
USP	United States Pharmacopeia
V	Volume
V_{minCP}	Volume of tablet at minimal compaction pressure after compaction
V_{minPS}	Volume of tablet at minimal punch separation
VDD	Vacuum drum drying
w	Tablet wall thickness
X-ray μ CT	X-ray microcomputed tomography
XRPD	X-ray powder diffraction
ρ_{app}	Apparent density in-die
ρ_{par}	Particle density via helium pycnometer
ρ_{pre}	Density under pressure
ρ_{pyc}	Particle density via helium pycnometer
ρ_{ratio}	Density ratio

1. INTRODUCTION AND THEORETICAL BACKGROUND

The application of computer sciences and high-throughput screenings for the identification of new chemical entities (NCE) in the pharmaceutical industry since 1990 provided immense benefits by facilitating a “target modulation candidate selection” leading to more potent and specific drugs. However, this breakthrough came along with challenges regarding the physico-chemical properties of the drug candidates [1, 2]. Most of the identified NCEs exhibit high lipophilicity and corresponding poor water solubility, which is knowingly connected with poor bioavailability [3]. Those challenges forced the pharmaceutical industry to find new approaches to overcome the solubility-issue by formulating NCEs into final solid dosage forms showing good bioavailability in the sense of therapeutic efficacy. Nowadays, several so-called “enabling formulation principles” are available to overcome the solubility challenge: chemical modifications (salts, prodrugs), physical modifications (polymorphs, amorphous systems) or carrier/delivery systems (cyclodextrins, micelles, self-emulsifying systems, liposomes) [4]. The landscape of enhancement principles is divers and innovative. However, only a few principles are scalable from small scale design or early phase development up to commercial scale. Potential reasons are lack of robustness and reproducibility, challenges to fulfil GMP (good manufacturing practices) requirements such as contact materials, sanitation and installation, operational and performance qualification of the equipment [5].

A frequently used principle in recently marketed drug products is the molecular dispersive embedment of poorly water-soluble drug substances in a polymeric matrix to form an amorphous solid dispersion (ASD) [6, 7]. Another important approach is the nanocrystal technology [8]. In this principle, the crystalline drug substance is being nanosized improving the dissolution behavior and solubility according to the Noyes–Whitney and Ostwald–Freundlich principles [9-11]. However, there is a trend towards increased numbers of ASD products approved by the Food-and-Drug-Administration (FDA) in the last two decades compared to nanocrystals as clearly observed by Jermain et. al [8].

Several manufacturing technologies exist for either ASDs [12] or solidified nanocrystals [13]. And some technologies can be even utilized for both enabling formulation principles. From pharmaceutical industry perspective a technology comprising the applicability for more than one formulation principle is highly desirable. It offers more flexibility to switch between product types within development and production. In addition, less laboratory or production space would be required increasing the economic efficiency of a pharmaceutical company. Spray

drying for example can be used for ASD manufacture and solidification of nanosuspensions. Whereas the extrusion process is applied for ASD manufacture or granulation. However, each manufacturing technology has its own advantages, disadvantages and limitations resulting in intermediates with different properties [12]. For the pharmaceutical industry not only the manufacturability including process robustness of enabling formulation principles is key, but also the downstream processability of the received intermediate powder to the final dosage forms such as tablets. Tablets are still the most accepted dosage form commonly used in marketed products [14]. To ensure proper processability to tablets especially at large scale rotary tablet presses, the intermediate powder is supposed to have good flowability and compactability properties.

Vacuum drum drying was observed to be an important continuous manufacturing technology in the food and chemical industry. Thus, equipment availability is given from laboratory to industrial scale for drying a few hundred grams per hour up to several kilograms per hour of product. However, vacuum drum drying is rarely used in the pharmaceutical field. Raghavan, Jett [15] presented drum drying as new technology for the manufacture of heparin, and Sangekar et al. [16] for a molecular dispersion composition with enhanced bioavailability. There is certainly potential for vacuum drum drying in the pharmaceutical development which hasn't been assessed in detail for different formulation principles. Thus, the present work investigated the applicability of vacuum drum drying for two enabling formulation principles in the development of solid oral dosage forms: a) manufacture of amorphous solid dispersions and b) processing crystalline drug nanosuspensions into solidified nanocrystals (see Figure 1.1).

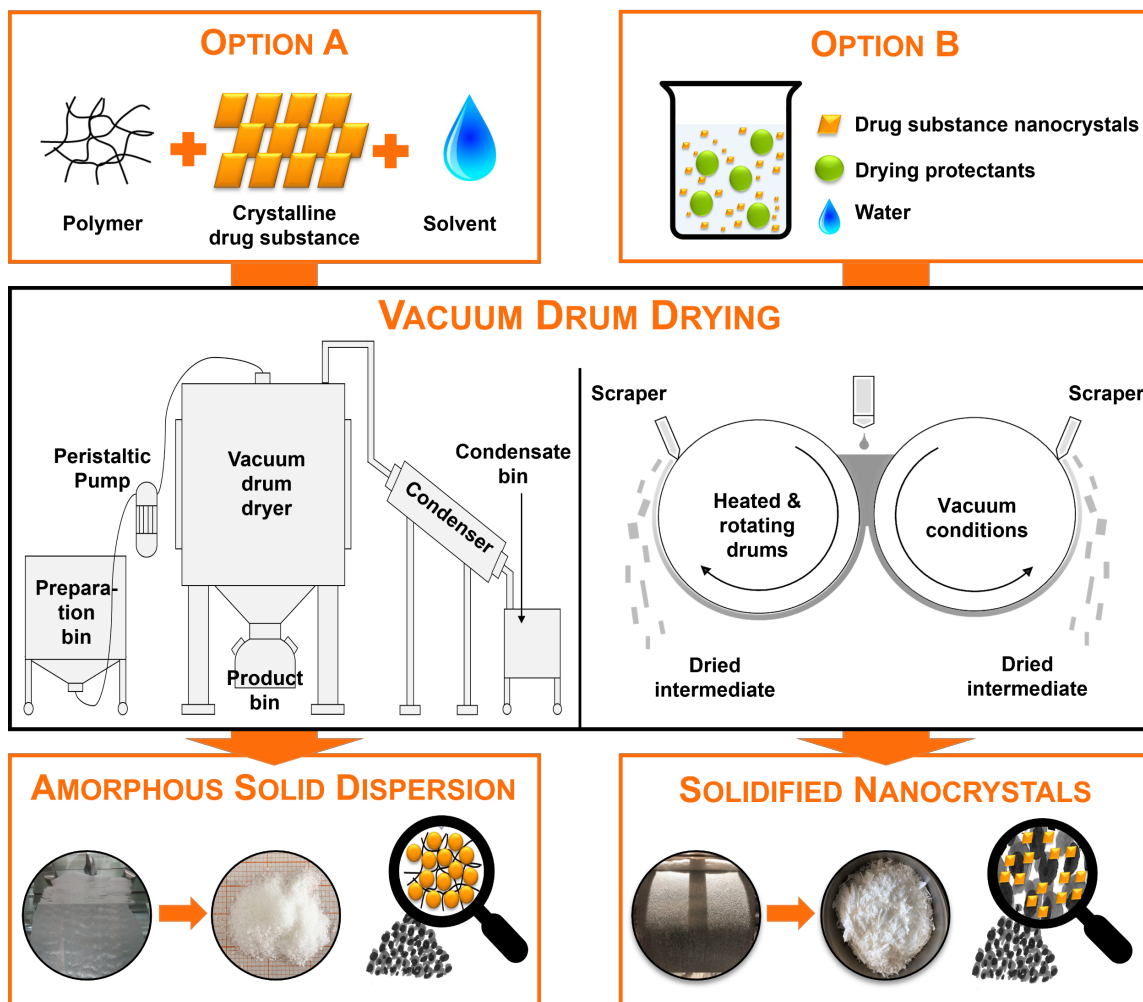


Figure 1.1: Applicability of vacuum drum drying in the development of solid oral dosage forms. Option A) manufacture of amorphous solid dispersions. Option B) processing crystalline nanosuspensions into solidified nanocrystals

1.1 Vacuum Drum Drying

Drum drying was developed in the early 1900s and is a well-known drying technology in the food and chemical industry [17]. Dried products examples out of liquids or pastes are milk powder, cereal-based baby food, yeast, pregelatinized starch for instant food or tomato puree in the food industry, and polyacrylamides, pesticides, detergents, or vitamin-containing products in the chemical industry. However, drum dryers are not of high interest within the pharmaceutical field so far [18], although drying is being an integral unit operation in the pharmaceutical development and manufacturing.

Drum dryer types on the market differ by the number of heated drums used (one or two), by the feeding mechanism (nip, single or multiple roller, spray or splash feeding), and by the pressure applied (atmospheric or vacuum) as shown in Figure 1.2 [19, 20]. Roll feeding is used in both single and double drum dryers especially if the drying solution is highly viscous. The use of multiple application rolls is beneficial if the product layer thickness on the drums should be increased to raise the throughput. Also suitable for single and double drum dryers is dip feeding where the drums are coated with liquid directly by ranging into a tray. The tray can be filled constantly with fresh liquid which might be required for thermolabile substances. Nip feeding on the other hand is much simpler and applies for liquids with broad range of viscosities (dynamic viscosity: 10 to 1040 mPas). However, it is mainly used for double drum dryers, where the gap between the drums defines the product layer thickness. For thermolabile substances the reservoir height above the drum gap should be chosen small. A more controlled application approach for the liquid onto the drum surface is spray feeding, where the liquid is atomized by a nozzle onto the drum surface. This offers the opportunity to define the product layer thickness more easily.

The most frequently used type in the food industry is the double drum dryer [21] just as the drum dryer assessed in the present work: a vacuum double drum dryer equipped with nip feeding in pilot scale fulfilling GMP requirements.

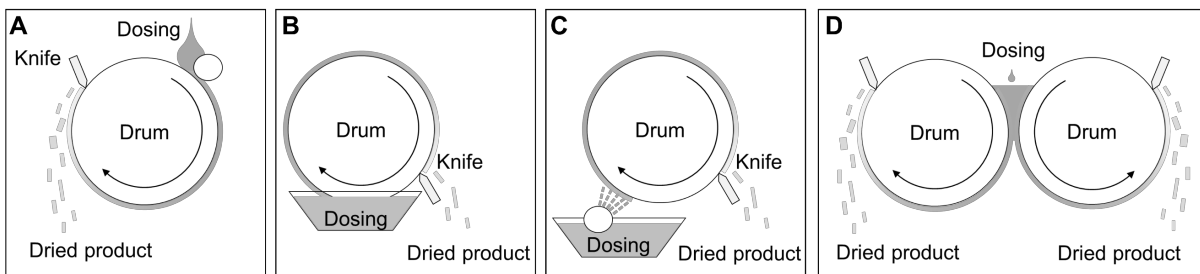


Figure 1.2: Types of drum dryers: A) Single drum dryer with single roller feed; B) Single drum dryer with dip feed; C) Single drum dryer with splash/spray feed; D) Double drum dryer with nip feed

Basically, the drum drying process can be divided into the following stages: (1) preparation of the feeding solution/suspension, (2) drying in the vacuum drum dryer and (3) sieving or milling of the produced intermediate.

During drum drying the drying solution or suspension is applied to the drum(s) spreading as thin layer onto the outer surface of the rotating, heated drum(s). A certain viscosity of the feeding solution/suspension is crucial to ensure proper product take-up onto the drum(s) as well as a wisely selected gap width for double drum dryers or feed roll application [22]. After about $\frac{3}{4}$ of a turn of the drum(s) from application of the solution/suspension, the dried product is being removed by static scraper(s)/knife(s). The efficiency of the drying process can be improved by applying vacuum, which, simultaneously offers the possibility to reduce the drum temperature for an even more gentle drying. The collected product is further processed depending on the product appearance after drum drying. Powders are sieved for deagglomeration, while sheets or flakes are milled to powder.

The thin product layer on the drum is suddenly exposed to high drum temperature for a short period of time leading to a rapid heat-up of the solution/suspension and then rapid evaporation. The rapid evaporation is even increased by applying vacuum conditions. Most of the moisture or solvent content evaporates during the initial drying phase, meaning boiling of the feed solution/suspension in the reservoir and the initial thin film formation on the drum. The subsequent drying phase is called “slow drying phase” since the moisture/solvent evaporates much slower during rotating of the drum till the knifes/scrapers remove the dried product.

The drum temperature decreases at first at the initial drying phase due to cooling by evaporation and increases during the slow drying phase. The reason for the increase is the exceeding of the energy used for evaporation by the heat of the drums. Whereas the product layer temperature stays nearly constant after heating up at the initial drying phase and increases drastically during the slow drying phase due to less evaporation. However, the

product layer temperature does not reach the drum temperature in most cases. The resulting dried product is expected to show certain porosity due to the rapid evaporation and thus, vapor bubbles formation. Those vapor bubbles form the porous structure in the thin product layer. The presumably high surface area is beneficial in terms of wettability and thus, drum drying is frequently used in the production of pregelatinized starch for instant food [17, 23].

However, the product quality such as residual solvents/moisture or degradation, and the material properties such as porosity, are a complex function of the feed solution/suspension solid load and viscosity, the feeding application mechanism, the drum speed, drum temperature and pressure conditions as visualized in Figure 1.3 [24, 25].

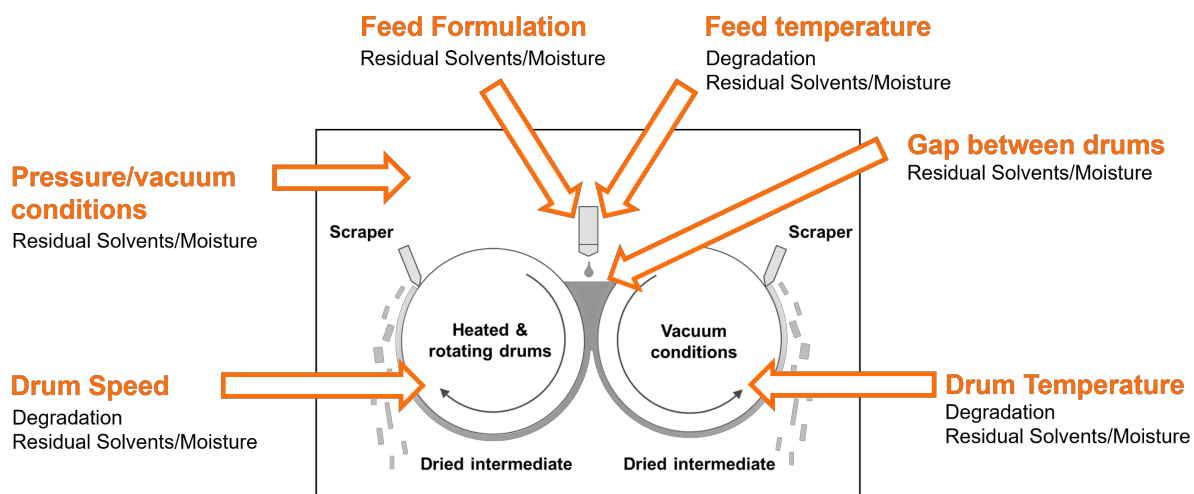


Figure 1.3: Factors impacting the product quality of products dried via vacuum drum drying

For a double drum dryer the gap width combined with the drum speed and the viscosity of the feeding solution/suspension defines the product layer thickness on the drums and thus, impacts the drying time required for the intermediate product [22, 26]. The thinner the layer, the more efficient is the drying process. Valous et al. [27] underlined the complexity of the drying process in the example of pregelatinized maize starch. Although an increase in drum speed results in reduced retention time of the product on the heated drums and a decrease in drum temperature due to more evaporation cooling, a more efficient drying was observed at higher drum speed in the specific case. This was explained by the product layer thickness being thinner at higher drum speed values. Interestingly, other research groups noted contrary findings [21]. Thus, also formulation/product specific parameters influence the drying process. Qiu et al. [28] for example observed that the bubble formation is depending on the matrix used. The bubble formation again affects the heat transfer and thus, the drying. In addition, the solid load of the solution/suspension to be dried and the related viscosity affects the drying behavior.

INTRODUCTION AND THEORETICAL BACKGROUND

as well. Other factors impacting the product quality and processability are the adhesion of the product to the drum and the homogenous spreading on the drum to ensure consistent product layer thickness all over the drum surface [22]. Both factors are mainly influenced by the formulation composition. Moreover, Valous et al. [27] investigated the impact of the reservoir level above the drums gap on moisture content, and did not find large influence related to the height of the reservoir level for low drum speeds. Besides, an increase of the drum temperature to improve the drying efficiency might result in challenges in terms of stability especially for thermolabile products as well as in terms of processability. Depending on the product composition, high drum temperatures might lead to a rubbery state of the product on the drums, which consequently complicates the removal of the dried product by the knives/scrapers due to the higher elasticity of the product. Thus, cooling mechanisms were developed to ensure proper removal of the dried product from the drums by getting the product to the glassy state [17].

1.2 Amorphous Solid Dispersion

The manufacture of amorphous solid dispersions (ASDs) is a well-known and commonly used approach in the pharmaceutical field to formulate poorly water-soluble drugs [29], which is demonstrated by the approval of several marketed products in the last two decades. Mavyret™ (AbbVie, 2017), Oriahnn® (AbbVie, 2020) and Braftovi® (Pfizer, 2020) are most recent examples of drug products manufactured by hot melt extrusion, as well as Zepatier® (Merck, 2016), Erleada® (Janssen, 2018) and Trikafta® (Vertex, 2019) by spray drying [8, 30].

1.2.1 Principle

An amorphous solid dispersion is a solid dispersion, where the drug substance is molecularly dispersed in a hydrophilic, polymeric matrix in a substantially amorphous form [6]. Since no energy is required for the amorphous form to break the crystal lattice compared to the crystalline form, the water-solubility is enhanced and thus, the bioavailability improved [31]. Despite the beneficial increased water-solubility, the higher energy level of the amorphous form leads to physical stability challenges as the drug substance may recrystallize [32]. However, kinetic stability is provided by the polymer matrix reducing the molecular mobility of the drug and thus, hindering recrystallization, especially below the ASD glass transition temperature [32, 33]. The risk for physical instability in terms of recrystallization is even reduced if the drug substance load in the ASD does not exceed the drug substance solubility in the polymer leading to thermodynamic stabilization [34]. Consequently, the polymer as well as surfactants should be chosen properly to ensure physical long-term stability. Useful tools for the prediction of physical stability are described by Baird, Taylor [35], Kyeremateng et al. [36], Lehmkemper et al. [37] and Zhang et al. [38].

1.2.2 Manufacturing Technologies

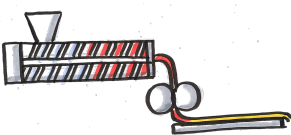
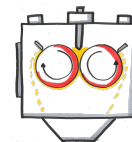
The manufacture of ASDs for pharmaceutical applications can be categorized into solvent- and fusion-based methods. The most common technologies used in commercial scale are hot-melt extrusion (HME) as example for fusion-based methods and spray drying (SD) as example for solvent-based methods [39, 40]. Vacuum drum drying is a drying technology potentially suitable for the manufacture of amorphous solid dispersions as mentioned by Sangekar et al. [16] and in addition, under investigation in the present work. The advantages as well as disadvantages of the respective technologies are listed in Table 1.1.

More manufacturing techniques are described in literature aiming to have benefits compared to conventional technologies. However, laboratory scale approaches are presented in most cases limited to the production of few to several hundred grams. Reasons might be that the processes and equipment are difficult to scale-up in terms of reproducibility and robustness, and to fulfil GMP requirements [5]. Early phase toxicology trial supplies preparations are often based on rotary evaporation, where the drug substance and excipients are dissolved in a suitable solvent system and then dried by removing the solvents at vacuum conditions while the flask rotates in a heated water bath. Despite this technique is frequently used in early stages, it was shown to be less practical for late stages. Recently Guo et al. [41] presented the acoustic fusion technique as novel method to manufacture ASDs in milligram scale, Doreth et al. [42] the amorphization directly within the tablet by microwave irradiation and Pöstges et al. [43] vacuum compressing molding for the manufacture of ternary ASDs. However, it remains to be seen if those new approaches will be optimized and transferred to larger scales.

In addition, each manufacturing technology will potentially result in ASD intermediates with different properties such as solid-state or material/powder characteristics. Studies comparing hot-melt extruded and spray dried intermediates are described in literature [44-47]. Moreover, the physical and chemical stability of the intermediate might be affected by different factors depending on the ASD manufacturing technique used. Since in hot-melt extrusion high temperatures are used to produce ASDs, degradation might occur above a certain temperature and/or energy input. Heat might also impact ASDs prepared by spray drying or vacuum drum drying, but presumably less because both techniques are known to be gentle drying processes. For those solvent-evaporation based techniques, the knowledge about the impact of the solvent on ASDs is key since residual solvents are still present after processing affecting stability. According to the ICH (international conference on harmonization) defined limitations exist for the residual solvent content tolerated within the drug product [48]. However, a complete removal of residual solvents is rarely achieved at the end of the drying process. Thus, useful predictions of the solvent impact on API solubility, sorption behavior, liquid-liquid phase separation and glass transition should be considered for formulation and solvent selection as well as for process parameter selection [49, 50].

Consequently, the technology selection should be based on the physico-chemical properties of the drug substance while focussing on the targeted drug product profile, and on the manufacturability, stability and bioavailability aspects as stated by the FDA - all crucial for obtaining a successful ASD drug product [30].

Table 1.1: Advantages and disadvantages of commonly used technologies to manufacture ASDs (hot-melt extrusion & spray drying) [20, 51] compared to assumed advantages and disadvantages of vacuum drum drying

	Hot-Melt Extrusion 	Spray Drying 	Vacuum Drum Drying 
Principle	Raw materials fed into extruder; drug substance molecularly dispersed in polymer matrix by applying heat and shear forces	Drug substance and polymer dissolved in solvent; solution atomized into droplets which are dried in heated gas stream (nitrogen)	Drug substance and polymer dissolved in solvent; solution dosed between gap of two drums spreading on rotating drums → thin film is being dried on heated drums under vacuum conditions
Advantages	<ul style="list-style-type: none"> Well-established Continuous process Easy scalability Small footprint Cost-effectiveness Deep process understanding High throughputs No solvents required Good material properties such as bulk density 	<ul style="list-style-type: none"> Well-established Gentle and fast drying → thermal exposure ↓ → suitable for thermolabile APIs Deep process understanding Good scalability 	<ul style="list-style-type: none"> Semi-continuous process Small footprint Gentle drying → thermal exposure ↓ → suitable for thermolabile APIs No viscosity limitations for feeding solution → opportunity to process new excipients and higher solid loads Most likely single drying step → no secondary drying required Certain porosity built into the dried product which is beneficial for wettability and tableting
Disadvantages	<ul style="list-style-type: none"> Thermal exposure → not suitable for thermolabile or shear-sensitive APIs (degradation ↑) Limited for APIs with high melting point Limited for some polymers/ excipients 	<ul style="list-style-type: none"> Batch process Cost-effectiveness Footprint Solvents required Residual solvents → mandatory secondary drying step + physical instability risk↑ Limited throughputs Small particles → complex downstream processing Viscosity limitations for feeding solution → low solid loads 	<ul style="list-style-type: none"> Novel technology in pharmaceutical field → no commercial scale available fulfilling GMP requirements Solvents required Limited process understanding

1.3 Solidification of Nanocrystals

Nanocrystals technique is based on the size reduction of the crystalline drug substance particles in aqueous media to nano-size ($<1\text{ }\mu\text{m}$), and is an important enabling formulation technique for the development of poorly water-soluble drug substances [52]. Several FDA-approved marketed products exist based on the nanocrystal approach, e.g., Rapamune® by Pfizer (2000) as one of the first products, or Invega Sustenna® by Janssen (2009) or Ryanodex® by Eagle Pharmaceutical (2014) as lastly approved products. In addition, crystalline drug nanosuspensions are frequently used already in early phases for toxicological studies and thus, of high importance [53].

1.3.1 Principle

Nanocrystal technology improves the solubility of poorly water-soluble drug substances via size reduction and the related increase in surface area to volume ratio, which improves drug dissolution according to Noyes–Whitney and Ostwald–Freundlich principles [9, 11]. The techniques for size reduction can be categorized in two approaches, bottom-up and top-down. Top-down approaches comprise techniques where large particles are being broken down to smaller particles via e.g., media milling or high-pressure homogenization. Bottom-up approaches consist of particle growth/ particle formation processes via e.g., precipitation. However, since controlling of particle growth in bottom-up approaches is challenging, they are not of high interest for larger scales and thus, for commercial scale production in the pharmaceutical industry [52]. In general, nanosized drug substance particles in aqueous media require stabilization compared to microparticles due to the Gibbs free energy contribution. The stabilization mechanisms are mathematically described by the Derjaguin, Landau, Verwey and Overbeek (DLVO) theory, which is applicable for the stability of colloidal systems. Common stabilizer types are ionic stabilizers functioning via thermodynamic/electrostatic stabilization, and steric stabilizers via kinetic stabilization [54, 55]. The stabilization is even more powerful when both stabilization mechanisms (ionic + steric) are combined using the so-called electro-steric stabilization [56]. In addition, amorphization can be induced by the energy applied to the drug substance particles by the size reduction technique such as wet-ball milling. Since partial amorphization increases the risk for particle growth, it should be avoided for stability reasons [57]. Thus, the selection of the formulation combined with choosing suitable parameters, e.g., for wet-ball milling, are crucial to achieve stable nanosuspensions.

However, a liquid crystalline drug nanosuspension in aqueous media is not the preferred final dosage form because of the risk for physical and chemical instability, risk for microbial growth, the known error-prone dosing combined with reduced patient compliance and the need of dosing devices. Therefore, drying technologies such as spray drying are of high interest to solidify nanosuspensions to obtain solid nanocrystals, which can be further processed to capsules or tablets for oral administration (Figure 1.4). So-called drying protectants are added to the nanosuspension prior to the drying process to avoid particle agglomeration and/or aggregation as well as crystal growth followed by sedimentation or flocculation induced by the thermal exposure during drying. Soluble sugars such as sucrose or lactose and sugar alcohols like mannitol are mostly used as drying protectants to avoid particle growth via steric hindrance. Steric hindrance means that the hydrophilic excipients bridges act as spacers avoiding drug substance crystal-to-crystal contact [58]. The nanoparticulate redispersibility and remaining crystallinity of the solidified intermediate and final drug product are key quality attributes in the solidification process to ensure the beneficial effect of nanosizing on dissolution.

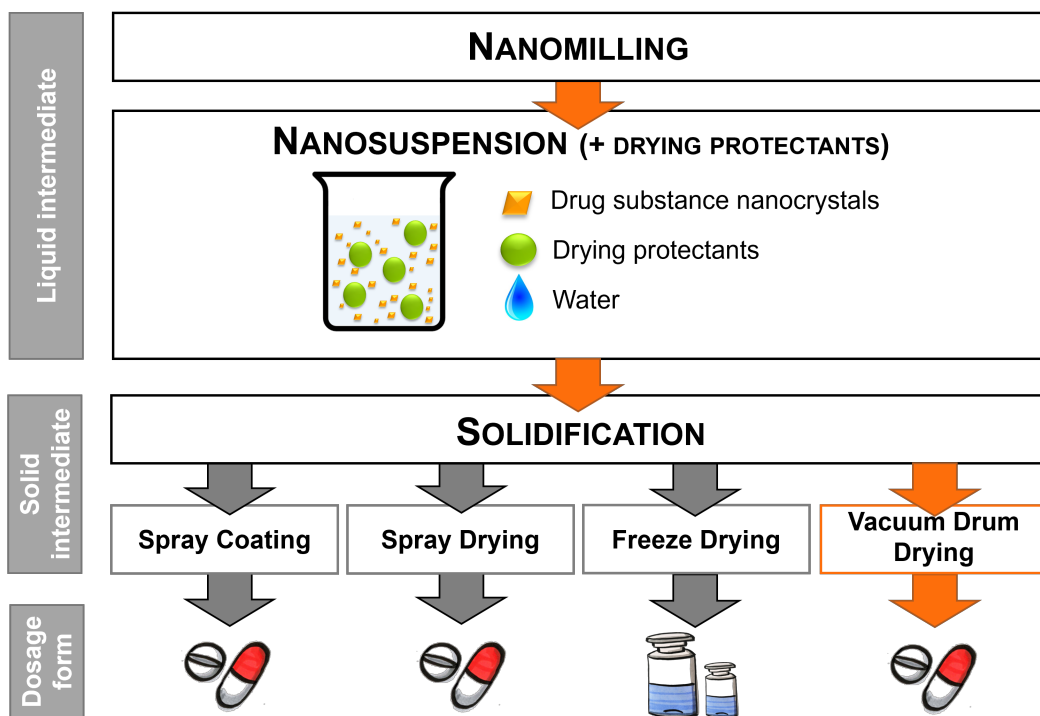
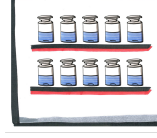


Figure 1.4: Overview of technologies for solidification of crystalline drug nanosuspensions; highlighted in orange: novel technology investigated in the present work

1.3.2 Manufacturing Technologies

Several technologies are described in literature for the solidification of crystalline drug nanosuspensions. Common techniques are spray coating (fluid-bed granulation), spray drying and freeze drying as visualized in Figure 1.4 [59, 60]. The existing solidification techniques as well as vacuum drum drying as novel technique investigated in the present work, have advantages and disadvantages which are summarized in Table 1.2. However, it should be noted that a freeze dried orally administered nanocrystal-based drug product is commercially not available presumably for the following reasons: complex scalability from laboratory scale to commercial scale and challenging powder properties for further downstream processing. Another interesting approach is the coating of inert tablet cores with crystalline drug nanosuspension as described for the commercial manufacture of Rapamune® tablets [52]. Potentially spray freeze drying might be an option as well based on work presented by Ali, Lamprecht [61, 62].

Table 1.2: Advantages and disadvantages of commonly used solidification technologies for nanocrystals (spray coating, spray drying, freeze drying) [13, 52, 60, 63] compared to assumed advantages and disadvantages of vacuum drum drying

	Spray Drying 	Spray Coating 	Freeze Drying 	Vacuum Drum Drying 
Principle	Drying of nanosuspension along with dissolved sugar or matrix polymer; atomization to fine droplets followed by drying via hot gas	Coating of suspension consisting of nanocrystals on core particles, mostly sugar cores	Freeze-drying / lyophilization: suspension is frozen along with sugars or matrix polymers, and the solvent is sublimed under vacuum	Dosing of nanosuspension along with sugar/matrix polymer between gap of drums → thin film is being dried on heated drums under vacuum conditions
Advantages	<ul style="list-style-type: none"> • Good scalability • High drug load in intermediate • Gentle drying & short thermal exposure • Good compactability • Small particles beneficial for inhalation products 	<ul style="list-style-type: none"> • Good scalability • Favorable intermediate properties such as good flowability • State-of-the-art for commercial products 	<ul style="list-style-type: none"> • Suitable screening tool to test multiple formulations • Porous intermediate readily redispersible 	<ul style="list-style-type: none"> • Semi-continuous process • Good scalability • High drug load in intermediate • Gentle drying by applying vacuum • Favorable powder properties such as bulk density • Most likely single drying step → no secondary drying required
Disadvantages	<ul style="list-style-type: none"> • Unfavorable intermediate properties such as low bulk density • Secondary drying step mandatory • Batch process • Less suitable as screening tool 	<ul style="list-style-type: none"> • Lower final drug loads achievable • Batch process • Less suitable as screening tool 	<ul style="list-style-type: none"> • Unfavorable intermediate properties such as flowability, compressibility • Batch process • Long process time • High energy consumption • Challenging scale-up 	<ul style="list-style-type: none"> • Certain thermal exposure • Novel technology in pharmaceutical field → limited process understanding + no commercial scale available so far fulfilling GMP requirements • Less suitable as screening tool

1.4 Tablets

Tablets are still the most common solid dosage form for oral administration showing vast benefits compared to others: high dose uniformity, high storage stability, easy handling and easy administration resulting in good patients' compliance, high throughputs per hour and thus, low production costs, as well as convenient packaging [64]. So, it is not surprising that about 80% of the dosage forms administered to patients are tablets [14].

Tablets are either produced by direct compression of a blend consisting of active pharmaceutical ingredient (API) and excipients, or as a subsequent step after e.g., amorphous solid dispersion manufacture or granulation (wet or dry granulation). Tablets are usually formed by powder compression in a die forcing the particles into close proximity by applying pressure. For the manufacture of tablets especially targeting throughputs of commercial scales, the powder must comprise beneficial powder properties such as easy-flowability or acceptable bulk density to ensure proper weight uniformity and to avoid tablet defects.

The mechanical strength of tablets mainly depends on the bonding points between the particles as well as on the attraction forces [65]. Although tableting is straightforward, successful manufacturing of intact tablets with sufficient mechanical strength is not always easy. Several factors impact the mechanical strength of tablets and can be classified into three categories: material and formulation factors (plasticity, elasticity, brittleness; powder morphology including particle size; crystal structure and polymorphisms), processing factors (e.g., tablet press type, tablet press speed, tooling type, resulting dwell time, compaction pressure, precompression force, etc) and environmental factors (e.g., relative humidity). But the mechanical strength might also impact the dissolution behavior of the tablets, which is crucial to ensure acceptable bioavailability.

1.4.1 Compression Mechanisms

The compression process describes the application of controlled compaction force on a defined volume of powder by punches of a certain geometry. Basically, the compression process can be generally described as follows and illustrated in Figure 1.5.

In the first phase of particle slippage and rearrangement particles are arranged in the die resulting in closer packing and thus, volume reduction [66]. Those arranging process takes place until the interparticulate friction and reduced space will prevent further interparticulate movement.

Further application of pressure is consequently linked with changes in the dimensions of the particles themselves. The changes can be temporarily and reversible by elastic deformation or permanently meaning irreversible by plastic deformation.

Particles can also break into a number of smaller particles, called particle fragmentation, which increases the surface area and thus, the number of bonding points [65]. Those particle fragments get again rearranged in the die with increasing pressure, which leads to further volume reduction of the powder bed. Then the particles can fragment further to even smaller particles at increasing pressures.

However, during the compression process all deformation mechanisms can be present either at different stages of the compaction process or even simultaneously. A high proportion of elastic deformation during compression stored as elastic energy leads to reduced mechanical strength of the tablets and most likely to tablet defects such as capping or lamination. In addition, even subsequent processing steps such as coating might be affected by defects induced by the stored elastic energy within the tablets [67, 68].

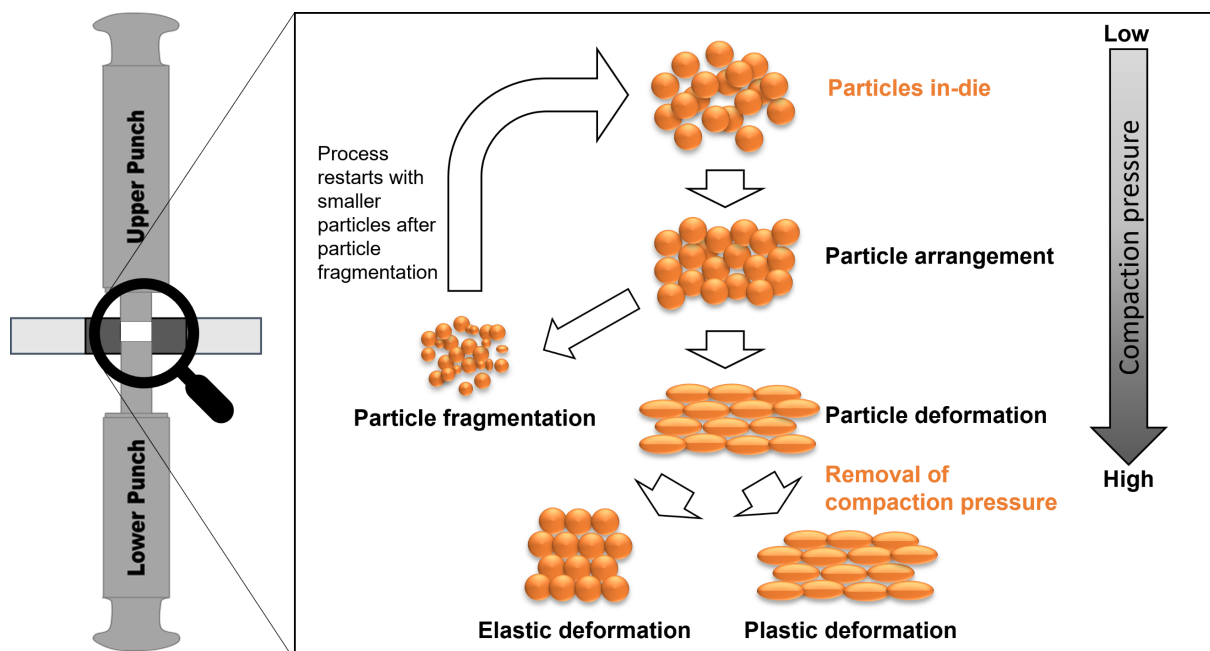


Figure 1.5: Schematic illustration of the compression mechanisms within the die during powder compression by applying increasing compaction pressure

1.4.2 Compression Analysis

Compaction simulators are often used to study the compression behavior of powders. They are instrumented to measure the forces involved in the compaction process as well as the displacement of the upper and lower punch during compression and decompression phase. The benefit of a compaction simulator is the small amount of powder necessary for the compression analysis [69]. The recorded data set is used to generate common plots to evaluate the compression behavior of materials thoroughly as described in the following [70-72].

The tabletability is defined as the ability of a powder to be transformed into a tablet with a certain mechanical strength normalized to the surface area, called tensile strength, under applied pressure. Thus, tabletability describes the relationship between the cause (compaction pressure) and the effect (strength of the compact) [73].

In contrast, the compressibility is defined as the ability of the powder to show volume reduction under applied pressure [70]. Therefore, the plot comprises the solid fraction of the tablet as function of the compaction pressure. A maximum densification results in a solid fraction of 1 meaning zero porosity. For the calculation of the solid fraction the particle density of the powder is required determined via helium pycnometer.

Lastly, the compactability describes the mechanical strength (tensile strength) of the compact as a function of solid fraction showing the dependency between compact strength and tablet porosity in a normalized way. It is a descriptor for the number of bonding points during the tableting process.

Compression analysis approaches for a deeper understanding of the compaction behavior in terms of plasticity, elasticity or brittleness were developed by Heckel, Kawakita and Lüdde, as well as Kuentz and Leuenberger [74-76]. One of the most popular approaches is the Heckel analysis considering the porosity of the tablet (either in-die or out-of-die) and the main compression force by using the force-displacement profile. It assumes that volume reduction by plastic deformation follows a first order kinetic [76]. Furthermore, it offers the opportunity to determine elastic recovery of the compact in-die also known as fast elastic recovery considering the decompression part of the Heckel plot.

1.5 References

1. Kawakami K. Current status of amorphous formulation and other special dosage forms as formulations for early clinical phases. *Journal of Pharmaceutical Sciences*. 2009;98(9):2875-85. doi: <https://doi.org/10.1002/jps.21816>.
2. Marshall GR. Computer-Aided Drug Design. *Annual Review of Pharmacology and Toxicology*. 1987;27(1):193-213. doi: <https://doi.org/10.1146/annurev.pa.27.040187.001205>.
3. Lipinski CA, Lombardo F, Dominy BW, Feeney PJ. Experimental and computational approaches to estimate solubility and permeability in drug discovery and development settings. *Advanced Drug Delivery Reviews*. 2001;46(1):3-26. doi: [https://doi.org/10.1016/S0169-409X\(00\)00129-0](https://doi.org/10.1016/S0169-409X(00)00129-0).
4. Perrie Y, Rades T. Themed issue: Improve dissolution, solubility and bioavailability of poorly soluble drugs. *Journal of Pharmacy and Pharmacology*. 2010;62(11):1517-8. doi: <https://doi.org/10.1111/j.2042-7158.2010.01199.x>.
5. Vasconcelos T, Marques S, das Neves J, Sarmento B. Amorphous solid dispersions: Rational selection of a manufacturing process. *Advanced Drug Delivery Reviews*. 2016;100:85-101. doi: <https://doi.org/10.1016/j.addr.2016.01.012>.
6. Breitenbach J. Melt extrusion: from process to drug delivery technology. *European Journal of Pharmaceutics and Biopharmaceutics*. 2002;54(2):107-17. doi: [http://doi.org/10.1016/s0939-6411\(02\)00061-9](http://doi.org/10.1016/s0939-6411(02)00061-9).
7. Szabo E, Demuth B, Galata DL, Vass P, Hirsch E, Csontos I, et al. Continuous Formulation Approaches of Amorphous Solid Dispersions: Significance of Powder Flow Properties and Feeding Performance. *Pharmaceutics*. 2019;11(12). doi: <https://doi.org/10.3390/pharmaceutics11120654>.
8. Jermain SV, Brough C, Williams RO. Amorphous solid dispersions and nanocrystal technologies for poorly water-soluble drug delivery – An update. *International Journal of Pharmaceutics*. 2018;535(1):379-92. doi: <https://doi.org/10.1016/j.ijpharm.2017.10.051>.
9. Dolenc A, Kristl J, Baumgartner S, Planinšek O. Advantages of celecoxib nanosuspension formulation and transformation into tablets. *International Journal of Pharmaceutics*. 2009;376(1):204-12. doi: <https://doi.org/10.1016/j.ijpharm.2009.04.038>.
10. Merisko-Liversidge E, Liversidge GG. Nanosizing for oral and parenteral drug delivery: A perspective on formulating poorly-water soluble compounds using wet media milling technology. *Advanced Drug Delivery Reviews*. 2011;63(6):427-40. doi: <https://doi.org/10.1016/j.addr.2010.12.007>.
11. Müller RH, Peters K. Nanosuspensions for the formulation of poorly soluble drugs: I. Preparation by a size-reduction technique. *International Journal of Pharmaceutics*. 1998;160(2):229-37. doi: [https://doi.org/10.1016/S0378-5173\(97\)00311-6](https://doi.org/10.1016/S0378-5173(97)00311-6).
12. Mendonsa N, Almutairy B, Kallakunta VR, Sarabu S, Thipsay P, Bandari S, et al. Manufacturing strategies to develop amorphous solid dispersions: An overview. *Journal of Drug Delivery Science and Technology*. 2020;55:101459. doi: <https://doi.org/10.1016/j.jddst.2019.101459>.
13. Malamatari M, Somavarapu S, Taylor KMG, Buckton G. Solidification of nanosuspensions for the production of solid oral dosage forms and inhalable dry powders. *Expert Opinion on Drug Delivery*. 2016;13(3):435-50. doi: <https://doi.org/10.1517/17425247.2016.1142524>.

INTRODUCTION AND THEORETICAL BACKGROUND

14. Jivraj M, Martini LG, Thomson CM. An overview of the different excipients useful for the direct compression of tablets. *Pharmaceutical Science & Technology Today*. 2000;3(2):58-63. doi: [https://doi.org/10.1016/S1461-5347\(99\)00237-0](https://doi.org/10.1016/S1461-5347(99)00237-0).
15. Raghavan R, Jett JL. Method to produce a solid form of heparin. International Application Published Under The Patent Cooperation Treaty: Pfizer Health AB; 2004.
16. Sangekar SA, Lee PI, Nomeir AA. Molecular dispersion composition with enhanced bioavailability. United States Patent: Schering Corporation; 2003.
17. Tang J, Feng H, Shen G-Q. Drum Drying. In: Heldman DR, editor. *Encyclopedia of Agricultural, Food, and Biological Engineering*: Marcel Dekker, Inc.; 2003.
18. Mujumdar AS. 11.6 Drum-Dried Products. *Handbook of Industrial Drying* (4th Edition). 4th ed.: Taylor & Francis; 2015.
19. Mujumdar AS. 11.3.3.1 Nip Feeding. *Handbook of Industrial Drying* (4th Edition). Taylor & Francis; 2015.
20. Karthik P, Chhanwal N, Anandharamakrishnan C. 4. Drum Drying. *Handbook of Drying for Dairy Products*. 1st Edition ed.: Wiley-Blackwell; 2017. p. 52.
21. Senevirathna SSJ, Ramli NS, Azman EM, Juhari NH, Karim R. Optimization of the Drum Drying Parameters and Citric Acid Level to Produce Purple Sweet Potato (*Ipomoea batatas* L.) Powder Using Response Surface Methodology. *Foods*. 2021;10(6):1378. doi: <https://doi.org/10.3390/foods10061378>.
22. Fritze H. Dry Gelatinized Starch Produced on Different Types of Drum Dryers. *Industrial & Engineering Chemistry Process Design and Development*. 1973;12(2):142-8. doi: <http://doi.org/10.1021/i260046a004>.
23. Daud WRW. 9. Drum Dryers. In: A.S. M, editor. *Handbook of Industrial Drying*. 3rd Edition ed.: Taylor & Francis Group, LLC.; 2006.
24. Gavrilidou MA, Valous NA, Karapantsios TD, Raphaelides SN. Heat transport to a starch slurry gelatinizing between the drums of a double drum dryer. *Journal of Food Engineering*. 2002;54(1):45-58. doi: [https://doi.org/10.1016/S0260-8774\(01\)00184-4](https://doi.org/10.1016/S0260-8774(01)00184-4).
25. Kalogianni EP, Xynogalos VA, Karapantsios TD, Kostoglou M. Effect of feed concentration on the production of pregelatinized starch in a double drum dryer. *Lebensm-Wiss Technol*. 2002;35(8):703-14. doi: [10.1006/fstl.2002.0925](https://doi.org/10.1006/fstl.2002.0925).
26. Trystram G, Vasseur J. The modeling and simulation of a drum-drying process. *International chemical engineering - New York* 1992;32:689-.
27. Valous NA, Gavrilidou MA, Karapantsios TD, Kostoglou M. Performance of a double drum dryer for producing pregelatinized maize starches. *Journal of Food Engineering*. 2002;51(3):171-83. doi: [https://doi.org/10.1016/S0260-8774\(01\)00041-3](https://doi.org/10.1016/S0260-8774(01)00041-3).
28. Qiu J, Kloosterboer K, Guo Y, Boom RM, Schutyser MAI. Conductive thin film drying kinetics relevant to drum drying. *Journal of Food Engineering*. 2019;242:68-75. doi: <https://doi.org/10.1016/j.jfoodeng.2018.08.021>.
29. Démath B, Nagy ZK, Balogh A, Vigh T, Marosi G, Verreck G, et al. Downstream processing of polymer-based amorphous solid dispersions to generate tablet formulations. *International Journal of Pharmaceutics*. 2015;486(1):268-86. doi: <https://doi.org/10.1016/j.ijpharm.2015.03.053>.
30. Bhujbal SV, Mitra B, Jain U, Gong Y, Agrawal A, Karki S, et al. Pharmaceutical amorphous solid dispersion: A review of manufacturing strategies. *Acta Pharmaceutica Sinica B*. 2021;11(8):2505-36. doi: <https://doi.org/10.1016/j.apsb.2021.05.014>.

INTRODUCTION AND THEORETICAL BACKGROUND

31. Murdande SB, Pikal MJ, Shanker RM, Bogner RH. Solubility advantage of amorphous pharmaceuticals: I. A thermodynamic analysis. *Journal of Pharmaceutical Sciences*. 2010;99(3):1254-64. doi: <https://doi.org/10.1002/jps.21903>.
32. Hancock BC, Shamblin SL, Zografi G. Molecular Mobility of Amorphous Pharmaceutical Solids Below Their Glass Transition Temperatures. *Pharmaceutical Research*. 1995;12(6):799-806. doi: <https://doi.org/10.1023/A:1016292416526>.
33. Aso Y, Yoshioka S, Kojima S. Relationship Between the Crystallization Rates of Amorphous Nifedipine, Phenobarbital, and Flopropione, and Their Molecular Mobility as Measured by Their Enthalpy Relaxation and ^1H NMR Relaxation Times. *Journal of Pharmaceutical Sciences*. 2000;89(3):408-16.
34. Prudic A, Ji Y, Sadowski G. Thermodynamic Phase Behavior of API/Polymer Solid Dispersions. *Molecular Pharmaceutics*. 2014;11(7):2294-304. doi: <https://doi.org/10.1021/mp400729x>.
35. Baird JA, Taylor LS. Evaluation of amorphous solid dispersion properties using thermal analysis techniques. *Advanced Drug Delivery Reviews*. 2012;64(5):396-421. doi: <https://doi.org/10.1016/j.addr.2011.07.009>.
36. Kyeremateng SO, Pudlas M, Woehrle GH. A fast and reliable empirical approach for estimating solubility of crystalline drugs in polymers for hot melt extrusion formulations. *Journal of Pharmaceutical Sciences*. 2014;103(9):2847-58. doi: <https://doi.org/10.1002/jps.23941>.
37. Lehmkemper K, Kyeremateng SO, Heinzerling O, Degenhardt M, Sadowski G. Long-Term Physical Stability of PVP- and PVPVA-Amorphous Solid Dispersions. *Molecular Pharmaceutics*. 2017;14(1):157-71. doi: <https://doi.org/10.1021/acs.molpharmaceut.6b00763>.
38. Zhang Z, Dong L, Guo J, Li L, Tian B, Zhao Q, et al. Prediction of the physical stability of amorphous solid dispersions: relationship of aging and phase separation with the thermodynamic and kinetic models along with characterization techniques. *Expert Opinion on Drug Delivery*. 2021;18(2):249-64. doi: <https://doi.org/10.1080/17425247.2021.1844181>.
39. Sandhu H, Shah N, Chokshi H, Malick AW. Overview of Amorphous Solid Dispersion Technologies. In: Shah N, Sandhu H, Choi DS, Chokshi H, Malick AW, editors. *Amorphous Solid Dispersions: Theory and Practice*. New York, NY: Springer New York; 2014. p. 91-122.
40. Van den Mooter G. The use of amorphous solid dispersions: A formulation strategy to overcome poor solubility and dissolution rate. *Drug Discovery Today: Technologies*. 2012;9(2):e79-e85. doi: <https://doi.org/10.1016/j.ddtec.2011.10.002>.
41. Guo Z, Boyce C, Rhodes T, Liu L, Salituro GM, Lee K-j, et al. A novel method for preparing stabilized amorphous solid dispersion drug formulations using acoustic fusion. *International Journal of Pharmaceutics*. 2021;592:120026. doi: <https://doi.org/10.1016/j.ijpharm.2020.120026>.
42. Doreth M, Hussein MA, Priemel PA, Grohganz H, Holm R, Lopez de Diego H, et al. Amorphization within the tablet: Using microwave irradiation to form a glass solution in situ. *International Journal of Pharmaceutics*. 2017;519(1):343-51. doi: <https://doi.org/10.1016/j.ijpharm.2017.01.035>.
43. Pöstges F, Kayser K, Stoyanov E, Wagner KG. Boost of solubility and supersaturation of celecoxib via synergistic interactions of methacrylic acid-ethyl acrylate copolymer (1:1) and

INTRODUCTION AND THEORETICAL BACKGROUND

- hydroxypropyl cellulose in ternary amorphous solid dispersions. International Journal of Pharmaceutics: X. 2022;4:100115. doi: <https://doi.org/10.1016/j.ijpx.2022.100115>.
44. Haser A, Cao T, Lubach J, Listro T, Acquarulo L, Zhang F. Melt extrusion vs. spray drying: The effect of processing methods on crystalline content of naproxen-povidone formulations. European Journal of Pharmaceutical Sciences. 2017;102:115-25. doi: <https://doi.org/10.1016/j.ejps.2017.02.038>.
 45. Iyer R, Hegde S, Zhang Y-E, Dinunzio J, Singhal D, Malick A, et al. The Impact of Hot Melt Extrusion and Spray Drying on Mechanical Properties and Tableting Indices of Materials Used in Pharmaceutical Development. Journal of Pharmaceutical Sciences. 2013;102(10):3604-13. doi: <https://doi.org/10.1002/jps.23661>.
 46. Patterson JE, James MB, Forster AH, Lancaster RW, Butler JM, Rades T. Preparation of glass solutions of three poorly water soluble drugs by spray drying, melt extrusion and ball milling. International Journal of Pharmaceutics. 2007;336(1):22-34. doi: <https://doi.org/10.1016/j.ijpharm.2006.11.030>.
 47. Dedroog S, Huygens C, Van den Mooter G. Chemically identical but physically different: A comparison of spray drying, hot melt extrusion and cryo-milling for the formulation of high drug loaded amorphous solid dispersions of naproxen. European Journal of Pharmaceutics and Biopharmaceutics. 2019;135:1-12. doi: <https://doi.org/10.1016/j.ejpb.2018.12.002>.
 48. EMA/CHMP/ICH/82260/2006: ICH guideline Q3C (R6) on impurities: guideline for residual solvents https://www.ema.europa.eu/en/documents/scientific-guideline/international-conference-harmonisation-technical-requirements-registration-pharmaceuticals-human-use_en-33.pdf (2019). Accessed.
 49. Dohrn S, Luebbert C, Lehmkemper K, Kyeremateng SO, Degenhardt M, Sadowski G. Solvent influence on the phase behavior and glass transition of Amorphous Solid Dispersions. European Journal of Pharmaceutics and Biopharmaceutics. 2021;158:132-42. doi: <https://doi.org/10.1016/j.ejpb.2020.11.002>.
 50. Dohrn S, Rawal P, Luebbert C, Lehmkemper K, Kyeremateng SO, Degenhardt M, et al. Predicting process design spaces for spray drying amorphous solid dispersions. International Journal of Pharmaceutics: X. 2021;3:100072. doi: <https://doi.org/10.1016/j.ijpx.2021.100072>.
 51. Haser A, Zhang F. New Strategies for Improving the Development and Performance of Amorphous Solid Dispersions. AAPS PharmSciTech. 2018;19(3):978-90. doi: <https://doi.org/10.1208/s12249-018-0953-z>.
 52. Möschwitzer JP. Drug nanocrystals in the commercial pharmaceutical development process. International Journal of Pharmaceutics. 2013;453(1):142-56. doi: <https://doi.org/10.1016/j.ijpharm.2012.09.034>.
 53. Chaubal MV. Application of formulation technologies in lead candidate selection and optimization. Drug Discovery Today. 2004;9(14):603-9. doi: [https://doi.org/10.1016/S1359-6446\(04\)03171-X](https://doi.org/10.1016/S1359-6446(04)03171-X).
 54. Li J, Wang Z, Zhang H, Gao J, Zheng A. Progress in the development of stabilization strategies for nanocrystal preparations. Drug Delivery. 2021;28(1):19-36. doi: <https://doi.org/10.1080/10717544.2020.1856224>.
 55. Liu P, Rong X, Laru J, van Veen B, Kiesvaara J, Hirvonen J, et al. Nanosuspensions of poorly soluble drugs: Preparation and development by wet milling. International Journal of Pharmaceutics. 2011;411(1):215-22. doi: <https://doi.org/10.1016/j.ijpharm.2011.03.050>.

56. Lestari ML, Müller RH, Möschwitzer JP. Systematic screening of different surface modifiers for the production of physically stable nanosuspensions. *Journal of Pharmaceutical Sciences*. 2015;104(3):1128-40. doi: <https://doi.org/10.1002/jps.24266>.
57. Kayaert P, Van den Mooter G. Is the amorphous fraction of a dried nanosuspension caused by milling or by drying? A case study with Naproxen and Cinnarizine. *European Journal of Pharmaceutics and Biopharmaceutics*. 2012;81(3):650-6. doi: <https://doi.org/10.1016/j.ejpb.2012.04.020>.
58. Zuo B, Sun Y, Li H, Liu X, Zhai Y, Sun J, et al. Preparation and in vitro/in vivo evaluation of fenofibrate nanocrystals. *International Journal of Pharmaceutics*. 2013;455(1):267-75. doi: <https://doi.org/10.1016/j.ijpharm.2013.07.021>.
59. Chaubal MV, Popescu C. Conversion of nanosuspensions into dry powders by spray drying: a case study. *Pharmaceutical Research*. 2008;25(10):2302-8. doi: <https://doi.org/10.1007/s11095-008-9625-0>.
60. Zhang X, Guan J, Ni R, Li LC, Mao S. Preparation and Solidification of Redispersible Nanosuspensions. *Journal of Pharmaceutical Sciences*. 2014;103(7):2166-76. doi: <https://doi.org/10.1002/jps.24015>.
61. Ali ME, Lamprecht A. Spray freeze drying for dry powder inhalation of nanoparticles. *European Journal of Pharmaceutics and Biopharmaceutics*. 2014;87(3):510-7. doi: <https://doi.org/10.1016/j.ejpb.2014.03.009>.
62. Ali ME, Lamprecht A. Spray freeze drying as an alternative technique for lyophilization of polymeric and lipid-based nanoparticles. *International Journal of Pharmaceutics*. 2017;516(1):170-7. doi: <https://doi.org/10.1016/j.ijpharm.2016.11.023>.
63. Lim Chin WW, Parmentier J, Widzinski M, Tan EH, Gokhale R. A Brief Literature and Patent Review of Nanosuspensions to a Final Drug Product. *Journal of Pharmaceutical Sciences*. 2014;103(10):2980-99. doi: <https://doi.org/10.1002/jps.24098>.
64. Rudnic EM, Schwartz JB. Oral solid dosage forms. Remington: the science and practice of pharmacy. Baltimore: Lippincott, Williams, & Wilkins; 2000. p. 1615-49.
65. Nyström C, Alderborn G, Duberg M, Karehill P-G. Bonding Surface area and Bonding Mechanism-Two Important Factors for the Understanding of Powder Comparability. *Drug Development and Industrial Pharmacy*. 1993;19(17-18):2143-96. doi: <https://doi.org/10.3109/03639049309047189>.
66. Jain S. Mechanical properties of powders for compaction and tabletting: an overview. *Pharmaceutical Science & Technology Today*. 1999;2(1):20-31. doi: [https://doi.org/10.1016/S1461-5347\(98\)00111-4](https://doi.org/10.1016/S1461-5347(98)00111-4).
67. Sun W-J, Kothari S, Sun CC. The relationship among tensile strength, Young's modulus, and indentation hardness of pharmaceutical compacts. *Powder Technology*. 2018;331:1-6. doi: <https://doi.org/10.1016/j.powtec.2018.02.051>.
68. Van der Voort Maarschalk K, Zuurman K, Vromans H, Bolhuis GK, Lerk CF. Stress relaxation of compacts produced from viscoelastic materials. *International Journal of Pharmaceutics*. 1997;151(1):27-34. doi: [https://doi.org/10.1016/S0378-5173\(97\)04889-8](https://doi.org/10.1016/S0378-5173(97)04889-8).
69. Michaut F, Busignies V, Fouquereau C, Huet de Barochez B, Leclerc B, Tchoreloff P. Evaluation of a Rotary Tablet Press Simulator as a Tool for the Characterization of Compaction Properties of Pharmaceutical Products. *Journal of Pharmaceutical Sciences*. 2010;99(6):2874-85. doi: <https://doi.org/10.1002/jps.22032>.

INTRODUCTION AND THEORETICAL BACKGROUND

70. Joiris E, Martino PD, Berneron C, Guyot-Hermann A-M, Guyot J-C. Compression Behavior of Orthorhombic Paracetamol. *Pharmaceutical Research.* 1998;15(7):1122-30. doi: <https://doi.org/10.1023/A:1011954800246>.
71. Leuenberger H. The compressibility and compactibility of powder systems. *International Journal of Pharmaceutics.* 1982;12(1):41-55. doi: [https://doi.org/10.1016/0378-5173\(82\)90132-6](https://doi.org/10.1016/0378-5173(82)90132-6).
72. Hagelstein V, Gerhart M, Wagner K. Tricalcium Citrate – A New Brittle Tableting Excipient for Direct Compression and Dry Granulation with Enormous Hardness Yield. *Drug Development and Industrial Pharmacy.* 2018;44:1-39. doi: <https://doi.org/10.1080/03639045.2018.1483389>.
73. Sun C, Grant DJW. Influence of Crystal Structure on the Tableting Properties of Sulfamerazine Polymorphs. *Pharmaceutical Research.* 2001;18(3):274-80. doi: <https://doi.org/10.1023/A:1011038526805>.
74. Kawakita K, Lüdde K-H. Some considerations on powder compression equations. *Powder Technology.* 1971;4(2):61-8. doi: [https://doi.org/10.1016/0032-5910\(71\)80001-3](https://doi.org/10.1016/0032-5910(71)80001-3).
75. Kuentz M, Leuenberger H. Pressure susceptibility of polymer tablets as a critical property: A modified heckel equation. *Journal of Pharmaceutical Sciences.* 1999;88(2):174-9. doi: <https://doi.org/10.1021/js980369a>.
76. Heckel RW. Density-pressure relationships in powder compaction. *Transactions of the Metallurgical Society of AIME.* 1961;221:671-5.

2. AIM AND SCOPE

Vacuum drum drying is a well-known drying technology in the food and chemical industry to produce powders out of a liquid or a paste. However, vacuum drum drying is rarely used in the development and production of pharmaceutical products so far. Therefore, the aim of the present work was to assess the applicability of vacuum drum drying as novel technology in the development of oral solid dosage forms for two enabling formulation principles.

The following topics were investigated in more detail in the present work:

- Assessment of vacuum drum drying as solvent-evaporation based technology to manufacture amorphous solid dispersions in comparison to conventional technologies, namely hot-melt extrusion and spray drying. For this, a model formulation consisting of ritonavir (15% w/w) in a copovidone/ sorbitan monolaurate matrix was studied focusing on:
 - The ASD intermediates and their solid-state characterization, powder properties and dissolution behavior using a biphasic dissolution apparatus (BiPHa+) (chapter 3)
 - The compression of ASD intermediates and their respective tablet blends including tablet characterization and disintegration/dissolution (chapter 4)
- Investigation of the compaction behavior of polymeric excipients during compression in comparison to non-polymeric excipients, and its consequences on commonly used Heckel analysis; including the assessment of an ASD manufactured via hot-melt extrusion consisting of ritonavir (15% w/w) in a copovidone/ sorbitan monolaurate matrix, and its respective tablet blend to evaluate the general impact on compaction analysis for ASDs (chapter 5)
- Evaluation of vacuum drum drying as drying technique in the solidification of aqueous, crystalline drug substance nanosuspensions prepared by wet ball milling (chapter 6)

3. VACUUM DRUM DRYING - A NOVEL SOLVENT-EVAPORATION BASED TECHNOLOGY TO MANUFACTURE AMORPHOUS SOLID DISPERSIONS IN COMPARISON TO SPRAY DRYING AND HOT MELT EXTRUSION

Barbara V. Schönfeld^{a,b}, Ulrich Westedt^b, Karl G. Wagner^{a,c}

^aDepartment of Pharmaceutical Technology, University of Bonn, Gerhard-Domagk-Straße 3, 53121 Bonn, Germany, karl.wagner@uni-bonn.de, barbara.schoenfeld@uni-bonn.de

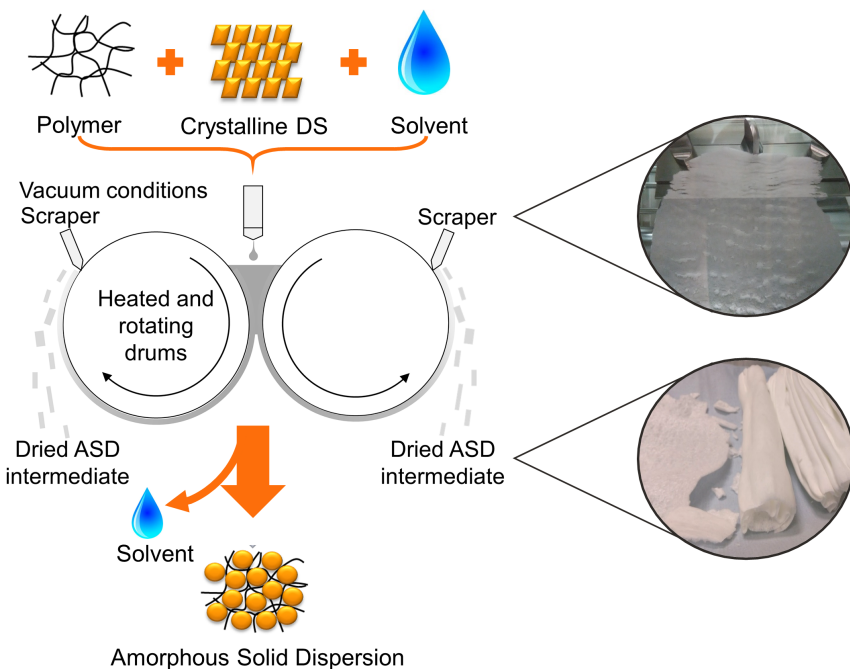
^bAbbVie Deutschland GmbH & Co. KG, Knollstraße 50, 67061 Ludwigshafen, Germany, ulrich.westedt@abbvie.com, barbara.schoenfeld@abbvie.com

^cCorresponding author

This part was published as:

B. V. Schönfeld, U. Westedt, K. G. Wagner, Vacuum drum drying – A novel solvent-evaporation based technology to manufacture amorphous solid dispersions in comparison to spray drying and hot melt extrusion, International Journal of Pharmaceutics, Volume 596, 2021, 120233, ISSN 0378-5173, <https://doi.org/10.1016/j.ijpharm.2021.120233>.

3.1 Graphical Abstract



3.2 Abstract

In this study, a novel solvent-evaporation based technology to manufacture amorphous solid dispersions (ASDs) called vacuum drum drying (VDD) was assessed in comparison to the conventional technologies hot-melt extrusion (HME) and spray drying (SD). Ritonavir (15% w/w) embedded in copovidone/sorbitan monolaurate was used to investigate the impact on the ASD quality, material properties and in-vitro dissolution. All ASDs met the critical quality criteria: absence of drug substance related crystallinity, residual solvents below ICH limit (SD, VDD) and degradation products within specification limits. Clear differences in material properties such as particle morphology and size distribution, powder densities and flowability properties were observed. Overall, the milled extrudate showed superior material properties in terms of downstream processability. The VDD intermediate performed slightly better in terms of flowability and electrostatic behavior compared to the spray dried while showing comparably unfavorable densities. However, the dissolution data suggested no significant difference between the ASDs prepared by HME, SD, and VDD and thus, no change in bioavailability is expected. In conclusion, the VDD technology might be a viable alternative to manufacture ASDs – especially for thermosensitive and shear-sensitive compounds with potential to process formulations with high solid loads and viscosities while exhibiting higher throughputs at a lower footprint.

3.3 Highlights

- Vacuum drum drying is a novel solvent-evaporation technology for ASD preparation
- Hot-melt extrusion: superior downstream processability of intermediate
- Vacuum drum drying: better flowability, less electrostatic behavior compared to SD
- No technology related difference in product quality and in-vitro dissolution

3.4 Keywords

Ritonavir; hot-melt extrusion; spray drying; vacuum drum drying; amorphous solid dispersion.

3.5 Introduction

In the last years, the number of drug candidates with poor water-solubility and related poor bioavailability increased (Jermain et al., 2018, Lipinski et al., 2001). Several strategies have been developed to tackle the solubility issue. A well-established one is the preparation of amorphous solid dispersions (ASDs), in which the active pharmaceutical ingredient (API) is embedded in a polymer matrix (Breitenbach, 2002) and stabilized in its amorphous form resulting usually in a higher water solubility compared to the crystalline form (Kennedy et al., 2008, Lehmkemper et al., 2017). The benefit of solubility enhancement is related to the higher energy level of the amorphous form, which is simultaneously a disadvantage with respect to stability of the ASD as the API may recrystallize (Hancock and Zografi, 1997). However, embedding the API into a polymer inhibits API recrystallization during storage due to the reduction of molecular mobility of the API leading to kinetic stabilization (Aso et al., 2000, Hancock et al., 1995). The risk of API recrystallization is even lower if the ASD is thermodynamically stabilized: the API drug load should not exceed the API solubility in the polymer (Prudic et al., 2014). Thus, the API drug load in the ASD is limited to ensure physical long-term stability of the ASD and should be chosen based on thermodynamic/physical tools such as the phase diagram of the API/polymer system and modelling such as Perturbed-Chain Statistical Associating Fluid Theory (PC-SAFT) predicting solubility (Kyeremateng et al., 2014, Lehmkemper et al., 2017) or Brostow Chiu Kalogeras Vassilikou-Dova (Bochmann et al., 2016). Besides, the presence of the polymer enhances the wettability of the API leading to a favourable dissolution performance (Leuner and Dressman, 2000). The FDA approved

several ASD based products in the last decade outlining the importance of this solubility enhancement strategy for the pharmaceutical industry (Szabo et al., 2019).

In general, the ASD preparation can be categorized into solvent-based and fusion-based methods. Spray drying (SD) and electro-spinning are examples for solvent-based methods, whereas hot-melt extrusion (HME) is an example for fusion-based methods as well as high-shear milling (Sandhu et al., 2014). In the pharmaceutical industry, the two most applied manufacturing technologies are SD and HME (Van den Mooter, 2012) exhibiting both advantages and limitations. HME uses thermal and mechanical energy from co-rotating screws and heated barrels (Crowley et al., 2007) followed by downstream cooling to produce solidified phase. HME technique provides several benefits such as process scalability (Dreiblatt, 2012, Repka et al., 2018, Wesholowski et al., 2019, Zecevic et al., 2018), solvent-free process, and cost-efficiency. Disadvantageously, HME is limited for APIs showing thermal and shear sensitivity resulting in chemical degradation, since processing temperatures typically above 120 °C are applied (Trasi et al., 2019). However, minimizing residence time and mechanical energy input might facilitate processing thermally labile APIs.

In comparison to HME, spray drying is known as thermally gentle technology due to the short residence time during drying and the solvent-evaporation cooling effect (Dobry et al., 2009). The SD process consists of dissolving API and polymer in organic solvent(s), the atomization of the solution into small droplets and the evaporation of the solvent used with hot drying gas. APIs, which are sensitive to shear forces or are exhibiting a high melting point, are preferably processed by solvent-evaporation techniques. To ensure the amount of residual solvents being below the ICH limit for organic solvents, postdrying is essential (EMA/CHMP/ICH/82260/2006, 2019). In addition, the residual solvents might have an impact on the stability by increasing recrystallization tendency and should be avoided in the final ASD (Sandhu et al., 2014). Moreover, SD has some limitations regarding the spraying solution viscosity and stickiness. Consequently, only solutions exhibiting a low viscosity and thus, low solid loads are feasible to be processed resulting in high costs related to the solvent amount needed and high efforts associated with solvent recycling. Another drawback arises from the properties of the spray-dried powder in terms of downstream processability to a final dosage form: the ASD intermediate may have low bulk density and might show a strong electrostatic behavior (Murtomaa et al., 2004). As a result, direct compression of the spray dried powder is often not feasible without additional measures (e.g., roller compaction step upfront).

For the pharmaceutical industry, the manufacturability including process robustness and downstream processability to the final dosage form is of high interest. In addition, economic aspects play an important role such as cost-efficiency, footprint, material consumption and process complexity. Vacuum drum drying (VDD) is a novel solvent-based technology in pharmaceutical industry to manufacture ASDs with the potential to overcome the constraints of the spray drying process. Drum drying is a well-known drying technique commonly used in the food industry to produce powders out of a liquid or a paste (Bhandari et al., 2013). Prominent drum dried products are for example milk powder, pregelatinized starch for instant food or tomato puree. Drum dryers are also used to dry chemicals such as polyacrylamides and vitamin-containing products (Mujumdar, 2015b), but rarely for pharmaceuticals (Raghavan and Jett, 2004, Sangekar et al., 2003). There are several drum dryer types on the market differing in the number of heated drums used (one or two) and in the feeding mechanism (nip feeding, roller feeding, spray and splash feeding). In this case, a vacuum double drum dryer equipped with nip feeding was investigated. The product solution is dosed between the gap of the two drums and spread out evenly on the heated, counter-rotating drums. During processing of the product solution on the heated drums under vacuum, the solution heats up immediately. Due to the temperature difference of drum surface and the wet product under vacuum, a large amount of the solvent quickly evaporates, when the boiling point is reached. The resulting thin film is dried further on the rotating drums till the scrapers remove the material from the drums (Mujumdar, 2015a). VDD is potentially suitable for thermally labile APIs due to the low residence time of the material on heated drums and due to the reduction of the temperature of the drums by application of vacuum. Moreover, oxidation of the product might be largely prevented and since it is a closed system it could be also used to handle potent substances according to safety regulations.

VDD is assumed to have several benefits compared to SD: more cost-effective, higher yields favorable for early phase development, potentially no need of a secondary drying step, no viscosity limitations for the solution to be dried since even pastes and slurries are being processed in the food industry. Consequently, high solid loads in the solution can be achieved reducing the costs for solvents and solvent recovery. Additionally, the overall production time is reduced based on the volume reduction of the solution, the higher throughput of the vacuum drum dryer and the elimination of a secondary drying step. Since viscosity is not a constraint for this technology, even uncommon polymers for spray drying could be investigated such as the high-molecular weighted PVP K90. In general, VDD is a highly effective, continuous process offering easy scalability while requiring a smaller footprint compared to SD.

The aim of this present work was to assess vacuum drum drying as novel solvent-evaporation based technology to manufacture ASDs in comparison with conventional techniques, hot-melt extrusion and spray drying. Here, a formulation composed of ritonavir (15% w/w) as model drug in a copovidone/sorbitan monolaurate matrix was selected. Ritonavir was chosen based on favorable physicochemical properties for a technology comparing study: good solubility in matrix polymer copovidone, and simultaneously, sufficient solubility in common organic solvents while showing low tendency for degradation and low risk for fast recrystallization during processing. The drug load of 15% was chosen to ensure manufacturability for all respective technologies. Furthermore, Indulkar et al. (2019) showed recently drug dissolution limitations for drug loads higher than 25%. The ASD intermediates were characterized with respect to the common critical quality attributes including assay, degradation, API related crystallinity, residual solvents. In addition, material properties were determined focussing on the downstream processability aspect ensuring manufacturability. Since material properties differences of ASDs prepared by different manufacturing processes might have an impact on bioavailability (Patterson et al., 2007), the dissolution behavior of the ASDs were assessed using the fully automated biphasic dissolution apparatus (BiPHa+) according to the Denninger model and method (Denninger et al., 2020).

3.6 Material and methods

3.6.1 Materials

Ritonavir (RTV, purity > 99.8%) was obtained from AbbVie Inc. (North Chicago, US). Copovidone (polyvinylpyrrolidone–vinyl acetate copolymer, ratio 3:2, Mw = 45,000–70,000, Kollidon® VA 64, COP) from BASF SE (Ludwigshafen, Germany), and silicon dioxide (Aerosil® 200) was purchased from Evonik Industries (Essen, Germany). Sorbitan monolaurate (Span® 20) was purchased from CRODA (Nettetal, Germany). Acetone (purity 96%) was obtained from Merck KGaA (Darmstadt, Germany).

3.6.2 Methods

3.6.2.1 Amorphous solid dispersion (ASD) preparation

The ASDs consisting of 15% (w/w) ritonavir were manufactured by hot-melt extrusion, spray drying and vacuum drum drying. The formulation composition of the ASDs including the respective functionality of each component is summarized in Table 3.1. For comparison reasons, the liquid formulation for both solvent-based manufacturing technologies (SD and VDD) was kept constant using pure acetone as solvent at a solid load of 30% (w/w).

VACUUM DRUM DRYING – A NOVEL SOLVENT EVAPORATION BASED TECHNOLOGY TO MANUFACTURE AMORPHOUS SOLID DISPERSIONS IN COMPARISON TO SPRAY DRYING AND HOT MELT EXTRUSION

Table 3.1: Formulation composition of ASDs

	Functionality	Amount [%w/w]
Ritonavir	Active Pharmaceutical Ingredient	15
Copovidone	Carrier Polymer	74
Sorbitan monolaurate	Surfactant	10
<i>Silicon Dioxide*</i>	<i>Glidant</i>	1

*= not used for spray drying and vacuum drum drying; replaced by copovidone

3.6.2.1.1 Hot-melt extrusion

The ASD material (extrudate beads) was kindly provided as benchmark material from AbbVie Deutschland GmbH & Co. KG (Ludwigshafen, Germany). Hot-melt extrusion was performed on a commercial scale co-rotating twin-screw extruder (ZSK 58, Coperion GmbH, Stuttgart, Germany). The extrudate beads were milled at a rotation speed of 6100 rpm using the impact mill Fitzmill L1A (Fitzpatrick Company, Sint-Niklaas, Belgium) equipped with an 838 µm round-hole sieve.

3.6.2.1.2 Spray drying

Ritonavir, copovidone and sorbitan monolaurate were dissolved in acetone targeting a solid load of 30% (w/w) to prepare the feed solution for the spray drying process. Spray drying was conducted using a Büchi B-290 laboratory spray dryer connected to an Inert Loop B-295 and a dehumidifier B-296 (Büchi Labortechnik GmbH, Essen, Germany). The spray dryer was equipped with a two-fluid nozzle including a 2 mm cap. The spray drying parameters were set as follows: feed rate of solution 9–10 g/min, nitrogen spray gas flow set to 60 mm corresponding to 742 l/h, aspirator rate set to 100% corresponding to a volume flow of about 35 m³/h. The inlet temperature was set to 65 °C resulting in an outlet temperature of 48 °C.

The spray dried powder was post-dried for 48 h at 40°C and vacuum conditions using a vacuum oven (Binder GmbH, Tuttlingen, Germany) to ensure complete removal of residual solvents. The yield of the process was 74%.

3.6.2.1.3 Vacuum drum drying

The vacuum drum drying (VDD) process was performed using a vacuum double drum dryer (Buflovak, New York, US) and a TAIM container (TAIM srl, Atessa, Italy) as liquid preparation vessel (Figure 3.1). Vacuum drum dryer is a semi-continuous thin-film dryer, which ensures quick and gentle contact drying on the drums under vacuum conditions. The product solution is fed between the gap of the two drums and spread out evenly on the heated, counter-rotating

VACUUM DRUM DRYING – A NOVEL SOLVENT EVAPORATION BASED TECHNOLOGY TO MANUFACTURE AMORPHOUS SOLID DISPERSIONS IN COMPARISON TO SPRAY DRYING AND HOT MELT EXTRUSION

drums. The moisture/solvent content of the thin product layer on the drums is evaporating during the contact with the heated drums under vacuum conditions. The dried product is removed from the drums by scrapers after approximately $\frac{3}{4}$ of a turn. Figure 3.2 summarizes the process workflow for a VDD process.

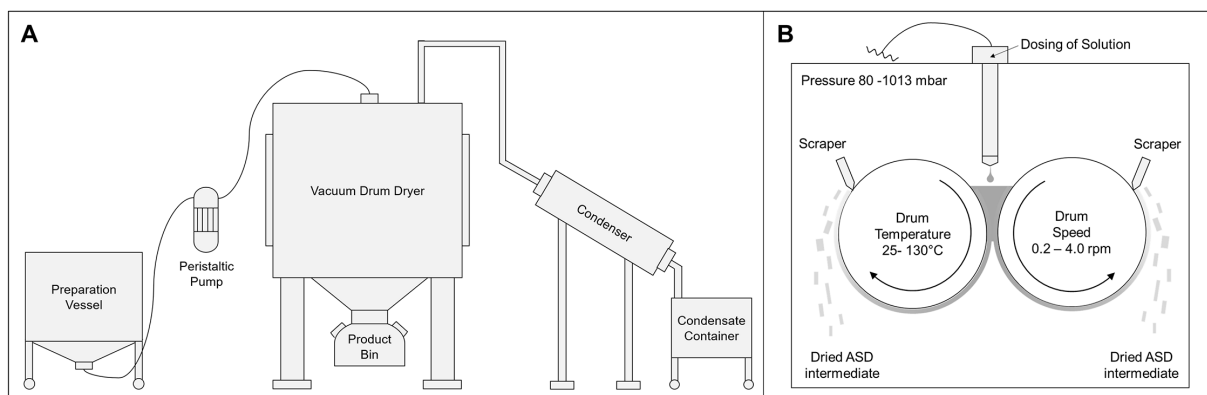


Figure 3.1: A: Schematic overview of vacuum drum drying setup including feed solution preparation vessel. B: Detailed schematic drawing of vacuum drum drying process including parameter ranges

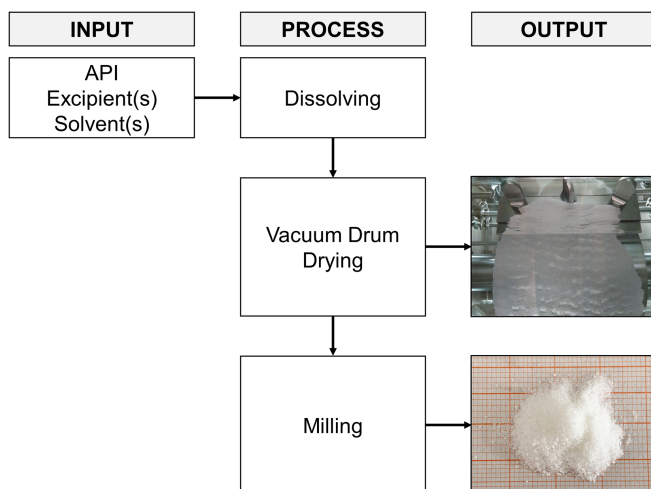


Figure 3.2: Process workflow of vacuum drum drying process

Ritonavir, copovidone and sorbitan monolaurate were dissolved in pure acetone targeting a solid load of 30% (w/w) to prepare the feed solution for the vacuum drum drying process. The feed solution was pumped into the VDD using a peristaltic pump (Watson Marlow 501RL, Rommerskirchen, Germany). The temperature of drums and casing was set to 80 °C at a pressure of 150 mbar, drum rotation speed to 0.2 rpm and gap between both drums to 0.3 mm to ensure proper drying and removal of the solvent. The dried product as flakes and thin film was collected in the product bin prior to further downstream processing. The calculated

VACUUM DRUM DRYING – A NOVEL SOLVENT EVAPORATION BASED TECHNOLOGY TO MANUFACTURE AMORPHOUS SOLID DISPERSIONS IN COMPARISON TO SPRAY DRYING AND HOT MELT EXTRUSION

throughput based on the mass of the collected ASD intermediate per processing time was approximately 600 g/hour.

The dried flakes/films were milled using a screening mill (Comil U5, Quadro Engineering, Waterloo, Canada) equipped with a 991 µm roundhole sieve.

The retention time on the drums is important for the drying process. Thus, the drum speed was selected at 0.2 rpm based on pretests performed on the vacuum drum dryer. The vacuum drum dryer used in the present study is a pilot scale prototype with a small drum diameter based on the knowhow and needs of the food industry. Consequently, to ensure a sufficient retention time the drum speed was kept quite low. The gap width between both drums was selected at 0.3 mm to prevent the solution from flowing down through the gap enabling processibility and to increase drying efficiency by creating a thin film on the drums. Notably, a gap width of 0.3 mm is within the standard range used in food industry (Karthik et al., 2017; Valous et al., 2002).

In addition to the solution at 30% (w/w) solid load, a second solution at 45% (w/w) solid load consisting of the same composition was processes by VDD (data not shown).

3.6.2.2 Amorphous solid dispersions characterization

3.6.2.2.1 Assay & degradation products by HPLC

Assay and degradation values of the ASD intermediates were determined using the high-pressure liquid chromatography system (Agilent 1100, Agilent Technologies, Waldbronn, Germany) equipped with a variable wavelength ultraviolet (UV) detector and a reversed phase column (Phenomenex Kinetex C18, 150x3 mm, 2.6 µm, maintained at 50 °C). As mobile phases 0.5% phosphoric acid in water (mobile phase A) and 0.5% phosphoric acid in acetonitrile (mobile phase B) were used in a gradient elution procedure (time [min]/mobile phase B in %: 0/15, 20/70, 22/100, 30/ 100, 30.5/15, 35/15). A mix of methanol/acetonitrile/demineralized water (40:40:20 V/V%) was used as diluent for sample preparation. The injection volume was 10 µL and the measurement was performed at 240 nm (bandwidth 4 nm). The retention time of ritonavir was 16.1 min.

3.6.2.2.2 Residual crystallinity and glass transition temperature (T_g) by differential scanning calorimetry (DSC)

Differential Scanning Calorimetry (DSC) measurements were performed to determine residual crystallinity and glass transition temperatures. The measurements were performed using a Mettler–205 Toledo DSC 1 (Mettler Toledo, Gießen, Germany) equipped with an auto-

sampler and a TC100 immersion cooler (Huber Kältemaschinenbau AG, Offenburg, Germany). All DSC samples consisting of ASD material were scanned at 10 K/min from -20 °C to 150 °C under nitrogen (gas flow 50 ml/min) as open pan method (crystallinity and dry T_g) and as closed pan method (wet T_g). Pure crystalline ritonavir was scanned at 10 K/min from -20 to 180 °C under nitrogen (gas flow 50 ml/min). The results were analyzed with STArE SW (version 16.1) (Mettler Toledo, Gießen, Germany) and are summarized in Figures 3.S1–S10 (section 3.12 Appendix A Supplementary data).

To quantify residual ritonavir crystallinity within the ASD samples, pure crystalline ritonavir was measured to determine the melting enthalpy ($n = 2$, see Figure 3.S1). The mean melting enthalpy of pure crystalline ritonavir is 88.955 J/g, and thus, for a 15% drug loaded ASD formulation as investigated in the present study 13.343 J/g.

To prove suitability of the DSC method to detect drug substance related crystallinity, milled placebo extrudate (ASD) consisting of copovidone (88.09% w/w) and sorbitan monolaurate (11.91% w/w) was spiked with 0%, 1% and 15% crystalline ritonavir and analysed using DSC (see Figures 3.S2–S4). Pure milled placebo extrudate showed no peak in the temperature region of 120–130 °C, where ritonavir has its melting point. However, the spiked samples showed a clear peak corresponding to ritonavir at approximately 125 °C. Based on the melting enthalpy of pure ritonavir, the residual crystallinity could be determined: for 1% spiked placebo the measured result for crystallinity was 0.99% and for the 15% spiked placebo 14.14%. Consequently, the method described can be used to determine residual crystallinity within the ASDs investigated in this present study.

3.6.2.2.3 Residual crystallinity by polarized light microscopy (PLM)

The absence of residual crystallinity was determined by polarized light microscopy (PLM) (10x magnification, transmission light). A DMLM optical microscope equipped with a DF320 digital camera was used (Leica Microsystems, Wetzlar, Germany).

3.6.2.2.4 Residual crystallinity by X-ray powder diffraction (XRPD)

X-ray powder diffraction (XRPD) measurements were performed to verify the absence of crystallinity in the ASD intermediates. The measurements were performed on a X'pert Pro MPD system (PANanalytical, Almelo, Netherlands) with a step size of 0.026° 2θ using Cu Ka radiation and a counting time of 8000 s. Samples were scanned on angular range of 7.5–17° 2θ, characteristic for the crystalline ritonavir. X'Pert HighScore 2.2d program from PANanalytical was used to conduct the reflex analysis (no background subtraction performed).

3.6.2.2.5 Residual solvents by gas chromatography

Residual solvent analysis was performed using capillary gas chromatography (GC) with a flame ionization detector (Agilent 6890, Agilent Technologies, Waldbronn, Germany), and equipped with a split inlet coupled to a headspace sampler (Agilent 7694, Agilent Technologies, Waldbronn, Germany).

3.6.2.2.6 Loss on drying

A halogen moisture analyzer (HB43-SSD, Mettler-Toledo GmbH, Giessen, Germany) was used to determine the moisture content/volatiles content of the ASD intermediates via loss on drying (LOD). The samples (approximately 5.5–6 g) were heated to 105 °C and held until mass was constant within ± 1 mg for 100 s.

3.6.2.2.7 Bulk/tapped/particle (pycnometric) density

Bulk and tapped density of the milled ASD intermediates was determined using a tapped density tester (Pharmatest Apparatebau AG, Hamburg, Germany) by calculating the mass and bulk volume occupied by the aerated powder filled into a 250 ml graduated cylinder according to Ph. Eur. 2.9.34. The samples were measured as triplicates.

Particle (pycnometric) density of the intermediates was measured using a helium pycnometer (AccuPyc 1340, Micromeritics GmbH, Aachen, Germany) equipped with a 10 cm³ sample chamber. The cycle fill pressure was set to 134.45 kPa and the equilibration rate to 0.0345 kPa/min. The sample chamber was purged with 10 purge cycles prior measurement. For each analysis 5 cycles were performed. The samples were measured as triplicates.

3.6.2.2.8 Flowability

The flowability properties of the milled ASD intermediates were measured using a ring shear tester (RST-XS, Dietmar Schulze, Wolfenbüttel, Germany) equipped with a 31.37 ml cell. The measurements were carried out at pre-shear normal stresses 0.250, 0.525, 0.800 and 1 kPa under ambient temperature and humidity. Samples were measured as triplicates using regression analysis for data evaluation.

3.6.2.2.9 Specific surface area

The specific surface area was determined using the TriStar II 3020 (Micromeritics Instrument Corporation, Norcross, United States). The specific surface area was calculated using single point Brunauer-Emmett-Teller (BET) equation from the adsorption data (Brunauer et al., 1938).

3.6.2.2.10 Particle size distribution

The particle size distribution of the milled ASD intermediates was determined using a laser diffraction particle size analyzer (Mastersizer 3000, Malvern Instruments GmbH, Herrenberg, Germany) equipped with a dry powder disperser module Aero S. For the measurements approximately 2–5 g of each ASD intermediate was used. The material was fed using the vibratory feeder and dispersed with 0 bar air pressure. The measurement data were analyzed according to the Fraunhofer approximation using the Mastersizer 3000 Software (version 3.71) and averaged.

3.6.2.2.11 Scanning electron microscopy

A scanning electron microscope (SEM) (SU-3500, Hitachi High Technologies, Krefeld, Germany) equipped with a secondary electron detector (SE) was used to visualize the morphology of the unmilled and milled ASD intermediates prepared by HME, SD and VDD. The samples were attached on SEM tubes and gold-sputtered under vacuum conditions to enhance electrically conduction. Images of samples at various magnifications were collected at an acceleration voltage of 10 kV.

3.6.2.3 In-vitro dissolution – BiPHa+

Dissolution was performed using the fully automated biphasic dissolution apparatus (BiPHa+) according to the Denninger model and method (Denninger et al., 2020). This method evaluates the dissolution behavior of the formulations in two phases and thus, taking the absorption process in the intestinal into account: an aqueous phase (50 ml) including three pH shifts mimicking the dissolution in the gastrointestinal tract, and an organic phase using 1-decanol (50 ml) mimicking the absorption process in the intestine.

For the dissolution measurements the ASD intermediates were filled into size 4 hard gelatine capsules resulting in a dosage strength of 10 mg ritonavir. The capsules were fixed to the sinkers to avoid floating of the dosage form during the measurement. All experiments were conducted at 37 °C for 4.5 h in total and at a magnetic stirring speed of 160 rpm avoiding an unstirred water layer in the aqueous phase. The dissolution test mimics the gastrointestinal passage by performing three pH shifts: pH 1 was set as starting pH value using 0.1 N HCl, after 30 min the pH was adjusted to pH 5.5 using buffer concentrate and after 90 min the pH was shifted to 6.8. pH 6.8 was kept constant for another 180 min. Furthermore, 333 µl of a surfactant concentrate consisting of sodium taurocholate and lecithin was added to generate Bi-FASSIF-V2 after 30 min prior to the addition of 1-decanol as organic phase on top of the aqueous phase.

3.7 Results and discussion

3.7.1 Amorphous solid dispersions characterization

3.7.1.1 Product quality

Amorphous solid dispersions consisting of ritonavir (15% w/w) were manufactured successfully using hot-melt extrusion, spray drying and vacuum drum drying (in GMP area). All ASD intermediates matched the specified quality attributes. Consequently, the investigated novel solvent-based technology vacuum drum drying seems to be a suitable technology to prepare ASDs - at least for the present formulation.

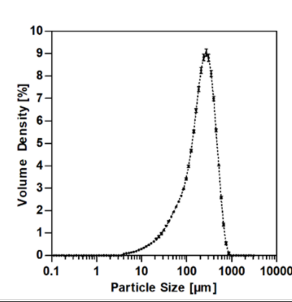
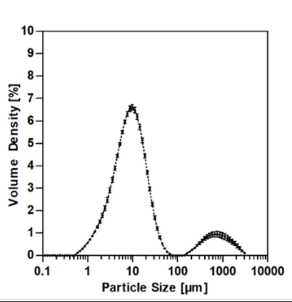
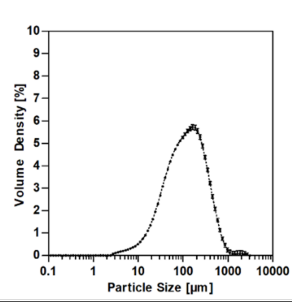
All manufacturing technologies revealed comparable results in terms of product quality except for the residual solvents criterion: at the selected process conditions, vacuum drum dried material was superior compared to SD not needing an additional drying step after the original process itself. As expected, both solvent-based approaches showed less thermal degradation compared to hot-melt extrusion.

In addition to the 30% (w/w) solid loaded solution, a 45% (w/w) solid loaded solution consisting of the same solid composition was successfully processed to a dried ASD using the VDD as well. For comparison reasons with SD, the VDD material manufactured out of the solution with the same solid load (30%, w/w) was selected for further evaluation.

3.7.1.1.1 Assay and degradation products

The assay values for ritonavir were within the specified range of 92.0–105.0% for all technologies (see Table 3.2). Ritonavir is known as thermosensitive API. The main degradation product is an acid hydrolysis product (A-HP) formed by thermal stress in the presence of water. The specification limit for A-HP is 1.6%, for sum of degradation products 2.7%. The milled extrudate showed the highest value for sum of degradation products (1.3%) including a relatively high amount of A-HP (1.2%), but still within the specifications. However, the degradation product A-HP for both solvent-based manufactured ASDs was below the practical quantification limit (PQL) of the HPLC method. Lower values for A-HP were expected for the solvent-based methods, since less thermal stress is applied to the drug substance compared to the hot-melt extrusion process with temperatures above 100 °C. Studies implied that thermal degradation of ritonavir starts above 70 °C (Gambhir et al., 2015), temperatures the product should not reach at any point due to solvent evaporation cooling and short residence times.

Table 3.2: Results of ASD intermediate characterization in terms of product quality (assay, degradation, residual crystallinity, glass transition temperature (T_g), residual solvents and loss on drying) and powder characterization (densities, flowability, particle size distribution)

		HME	ASD Intermediate	VDD
	Specification Limit		SD	
Product quality	Assay [%]	92.0-105.0	99.1	99.4
	Sum of Degradation Products [%]	NMT 2.7 (A-HP 1.6)	1.3 (A-HP 1.2)	<PQL (A-HP<PQL) (A-HP: <PQL)
	Residual Crystallinity [%]	na	n.d.	n.d.
	T_g [°C] dry (wet)	na	65.6 (46.6)	66.7 (47.0) 66.6 (46.2)
	Residual Solvents [ppm]	NMT 5000	na	6974 (441 2 nd dried) 2452
	Loss on drying	NMT 2.5	1.60	1.56 1.29
	Bulk Density [g/cm³]		0.610 ± 0.004	0.287 ± 0.007 0.197 ± 0.004
	Tapped Density [g/cm³]		0.759 ± 0.006	0.433 ± 0.004 0.310 ± 0.006
	Particle (pycnometric) Density [g/cm³]		1.2040 ± 0.0019	1.1963 ± 0.0020 1.2068 ± 0.0145
Powder characterization	Hausner Ratio		1.25 ± 0.00 (fair flow)	1.51 ± 0.10 (very poor flow) 1.57 ± 0.03 (very poor flow)
	Flowability (FFC)		8.98 ± 0.40 (easy/free flowing)	1.29 ± 0.02 (very cohesive) 2.91 ± 0.03 (cohesive flowing)
	Specific Surface Area [m²/g]		0.22	1.21 0.32
	Particle Size Distribution			
	d_{10} [μm]		52.0 ± 1.83	2.91 ± 0.06 28.8 ± 0.39
	d_{50} [μm]		226.0 ± 1.95	10.4 ± 0.18 125.0 ± 2.15
	d_{90} [μm]		477.0 ± 2.85	370.0 ± 116.0 411.0 ± 22.9
				

3.7.1.1.2 Residual crystallinity and glass transition temperature (T_g)

The absence of residual crystallinity in the ASDs was demonstrated by DSC analysis (see Table 3.2 and supplementary data Figure 3.S5 (HME), 3.S7 (SD), 3.S9 (VDD)). Moreover, the PLM images of the ASD intermediates at room temperature shown in Figure 3.3 confirmed the absence of crystals in the ASD: no birefringent spots were detected for the HME (Figure 3.3, A), SD material (Figure 3.3, B) and VDD material (Figure 3.3, C). PLM image of the VDD material (Figure 3.3, C) showed some light reflections, which can be assigned to the edges of the ASD fragments and not to residual crystals. However, milled placebo extrudate spiked with crystalline ritonavir (15% DL) was investigated as positive control to confirm absence of residual crystals in the VDD material (Figure 3.3, D): the PLM image exhibited several birefringent spots in form of long needles and thus, clear visual differences compared to the light reflections of the VDD material.

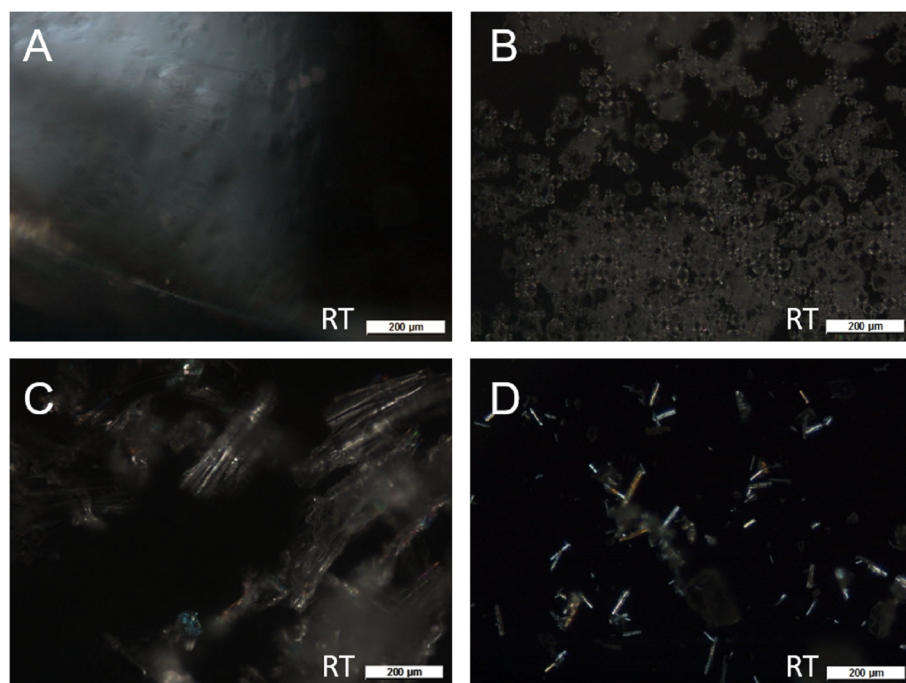


Figure 3.3: PLM images (room temperature, 10x magnification, transmission light) of ASD intermediates manufactured by (A) HME; (B) SD; (C) VDD and of the (D) physical mixture of milled placebo extrudate spiked with crystalline ritonavir (15% DL) as positive control

Next to DSC and PLM, XRPD as standard analytical method for absence of crystalline API was conducted. The results are visualized in Figure 3.4. The ASD intermediates showed no distinct reflexes in the XRPD confirming absence of crystallinity. These results were consistent with the observations made by DSC and PLM. Consequently, the HME, SD and VDD intermediates could be stated as amorphous.

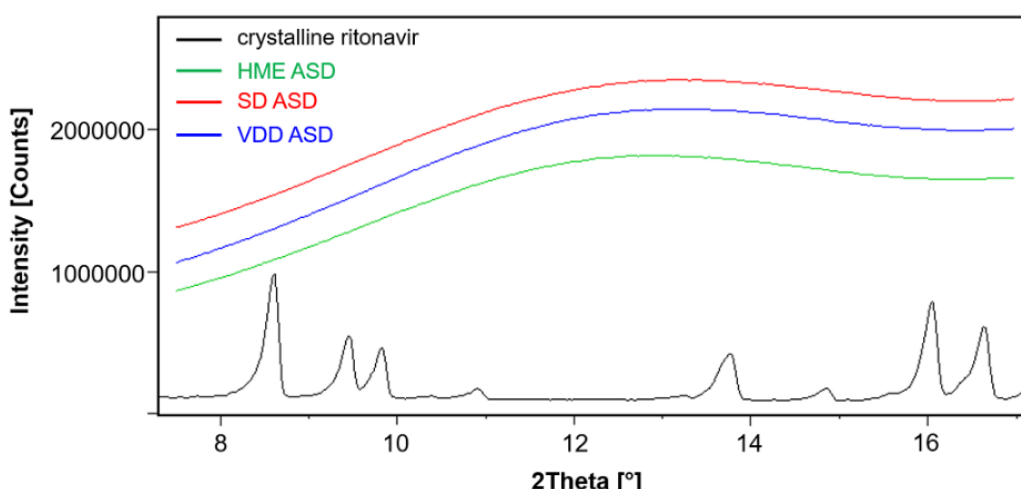


Figure 3.4: XRPD patterns of crystalline ritonavir (black) and of ASD intermediates manufactured by HME (green), SD (red), VDD (blue)

In addition, the DSC analysis (see Table 3.2 and supplementary data Figures 3.S5–S10) revealed a single T_g for each ASD indicating the API to be molecularly dispersed in the polymer phase (Lin et al., 2018). The T_g values (wet and dry T_g) are in a comparable range at about 65–67 °C (dry T_g) and 46–47 °C (wet T_g) for HME, SD, and VDD due to the same composition of the ASDs. The T_g of pure copovidone is typically at about 101 °C. Generally, the presence of sorbitan monolaurate as plasticizer reduces the T_g as a well-known fact explaining the measured data for the ritonavir/copovidone/sorbitan monolaurate formulation (Gryczke et al., 2012). However, slightly lower wet T_g values were observed for the VDD material which is related to the small amount of residual solvents still present. In general, with increasing presence of moisture (e.g., residual solvents), the T_g values decrease enhancing the molecular mobility of the polymer (Konno and Taylor, 2006). To ensure physical stability of the ASDs it is generally recommended to store the ASDs 50 °C below T_g (dry), since significant molecular mobility at this temperature range is expected (Hancock et al., 1995). This rule of thumb is not especially for ASDs but for amorphous concepts in general. Since ritonavir is embedded in a polymer and thus, kinetically stabilized and shows good miscibility in copovidone via hydrogen bonds, the risk of recrystallization at room temperature is reduced. Moreover, ritonavir seems to be an API with low recrystallization tendency (Zhou et al., 2007).

3.7.1.1.3 Residual solvents and loss on drying (LOD)

Residual solvents of acetone are summarized in Table 3.2. Both residual solvents values for the SD and VDD material were below 5000 ppm according to the ICH limit for acetone (EMA/CHMP/ICH/82260/2006, 2019). However, to fulfill this requirement the SD material had to be post-dried, because the initial value for residual solvents was at 6974 ppm (after

secondary drying 441 ppm). Consequently, the vacuum drum drying technology is beneficial compared to the spray drying in terms of residual solvents and the related number of process steps required. Furthermore, VDD technology could positively affect the physical stability of the manufactured ASD by eliminating the secondary drying step, since solvent-based methods might exhibit more relaxation leading to higher recrystallization tendency especially at elevated temperatures during the secondary drying (Bhardwaj and Suryanarayanan, 2012; Huang and Williams, 2018).

The LOD values (see Table 3.2) were between 1 and 2%, and thus, within the specified limit and acceptance range in terms of tabletability.

3.7.1.2 Powder properties and downstream processability

Amorphous solid dispersions prepared by HME, SD and VDD process resulted in material with different powder properties after milling with respect to size and morphology of the particles (see Figure 3.5, Figure 3.6 and Table 3.2). The impact of particle size and shape on powder flowability is well described and affects for example filling or feeding operations in the downstream process (Hancock et al., 2002; Sinka et al., 2004). Poor powder flowability and a high tendency of densification related to equipment vibrations can lead to tablet weight variations and nonconformity regarding hardness and assay (content uniformity) and thus, to a less robust process. Furthermore, bridging or caking of the powder while feeding could occur causing high risk for the process performance. While SD particle size and shape is being defined by the spray drying process itself, the HME and VDD particle sizes can be adjusted by the subsequent milling process.

The present study revealed that the HME intermediate showed the best downstream processability compared to the solvent-based ASD intermediates (see Table 3.2), which can be explained by the investigated powder properties of the ASD intermediates: particle size distribution and morphology, material density and flowability. Among SD and VDD, VDD is superior showing better flowability (FFC 1.29 (SD) vs 2.91 (VDD)) and less electrostatic charge. Moreover, there is potential to further improve the powder properties of the VDD material by investigating optimal processing parameters for the milling step.

3.7.1.2.1 Particle size distribution and particle morphology

Table 3.2 shows the particle size distribution (volume density vs particle size) and the d_{10} , d_{50} and d_{90} values of the ASD intermediates manufactured via HME, SD and VDD. In the case of the milled extrudate, a d_{50} value of 226 µm with a narrow particle size distribution was identified, whereas for the SD material a large content of fine particles were observed resulting

in a d_{50} value of 10.4 μm . Based on the high number of fines in the SD material, the corresponding d_{90} value might be related to agglomerates and might not reflect the actual particle sizes. Milling the VDD material resulted in a d_{50} value of 125 μm and a related slightly broader particle size distribution compared to the HME material.

Scanning electron micrographs (Figure 3.5 and Figure 3.6) were taken to provide insights into particle size and morphology of the ASD intermediates manufactured via hot-melt extrusion, spray drying and vacuum drum drying. Overall, the SEM analysis confirmed the particle sizes of the ASD intermediates measured by laser diffraction. The SEMs of the milled extrudate showed irregular shaped, comparatively large granules with sharp breaking edges including some scratches corresponding to the milling process (Figure 3.5A). Small particles of less than 10 μm adhered on the smooth surfaces of larger particles (Figure 3.5a). The shape of milled extrudate reminds of small gravel. The spray dried ASD (Figure 3.5B, b) appeared as intact hollow spheres with diameters of approximately less than 10 μm tending to build agglomerates of up to 400 μm in size. The SEMs for the spray dried material confirmed the assumption of the d_{90} value to be related to agglomerates.

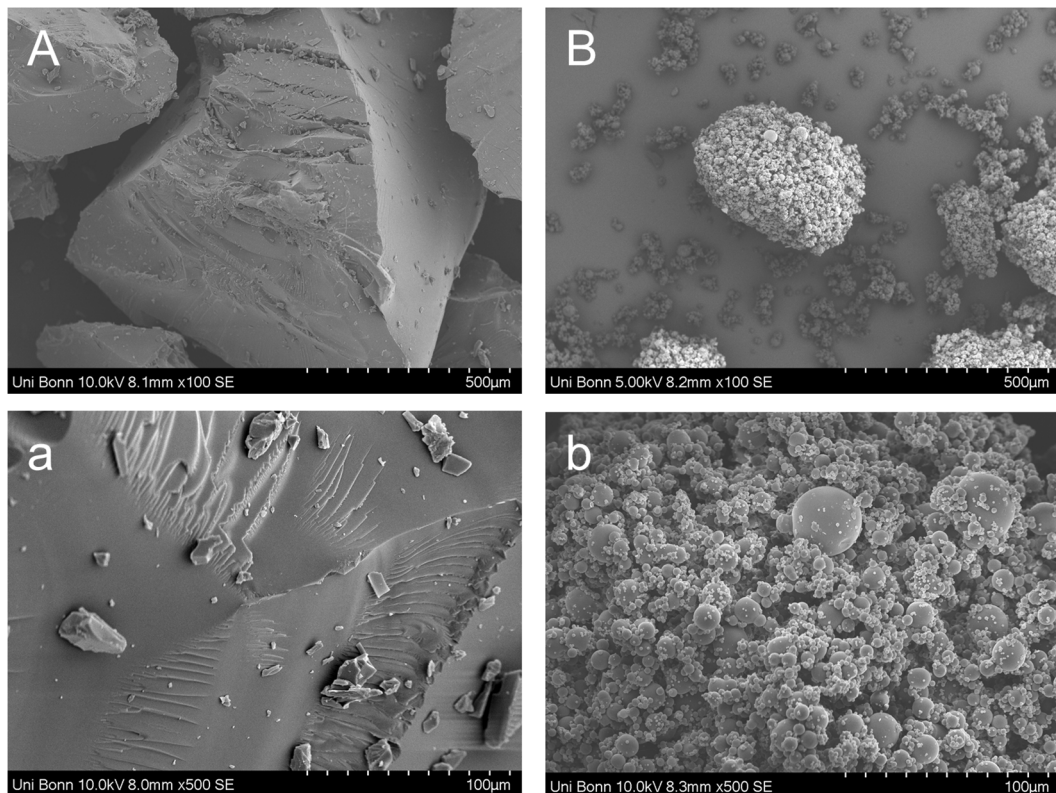


Figure 3.5: Scanning electron micrograph images of ASD intermediates manufactured by (A, a) HME (milled); (B, b) SD

The vacuum drum dried ASD showed different morphology on the top (distal) and on the bottom (proximal) side of the material. The material in direct contact with the heated drums (Figure 3.6A, a) showed a smooth surface with a wavelike appearance related to the accumulation of the material prior to the scraping off the drums. The smooth surface might be related to the heat of the drums leading to a partial softening of the material. Whereas the material without direct contact (Figure 3.6B, b) showed a plate-shaped morphology providing particles with irregular shape and sharp breaking edges. The shape of the VDD intermediate reminds of platelets.

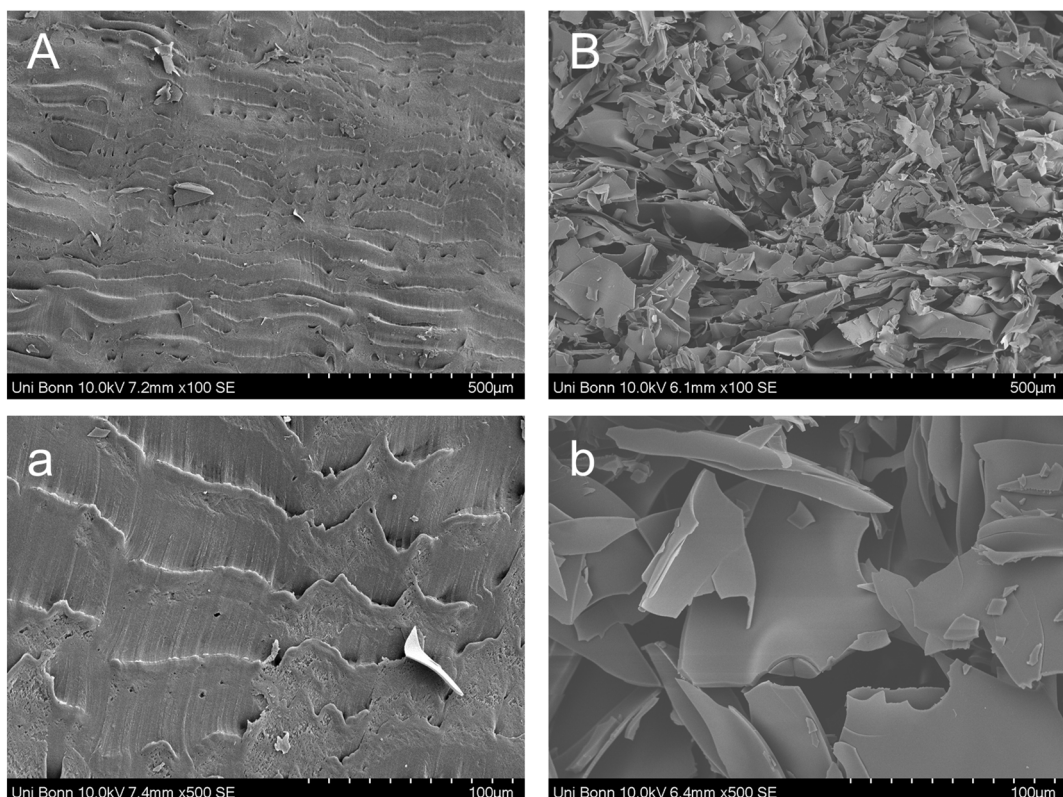


Figure 3.6: Scanning electron micrograph images of ASD intermediates manufactured by VDD (A, a) surface of material with direct contact to drums; (B, b) surface of material without direct contact to drums

Based on the SEM pictures small particles and a larger surface area of the SD and VDD material compared to HME could be detected. Besides, it is well-known from literature that the surface area of SD material compared to HME material is several times higher (Agrawal et al., 2013) which could be also confirmed by BET analysis (SD: $1.21 \text{ m}^2/\text{g}$; HME: $0.22 \text{ m}^2/\text{g}$). For the VDD material a slightly larger surface area (VDD: $0.32 \text{ m}^2/\text{g}$) was expected in comparison to HME according to the solvent-evaporation process. However, the observed difference in particle size and the related surface area could influence the moisture uptake by the ASD and thus, the physical stability. The smaller the particle size and the higher the surface area of the

ASD is, the higher the expected moisture uptake. Increasing presence of moisture decreases the T_g value of the ASD indicating enhancement of the molecular mobility of the polymer and thus, reducing physical stability of the ASD by increasing recrystallization probability (Konno and Taylor, 2006).

Since vacuum drum drying is evaluated as novel technology, the physical stability of the VDD material with respect to crystallinity was assessed. The DSC analysis showed no crystallinity and thus, physical stability at room temperature for at least 15 months.

For the sake of completeness, the extrudate as well as the vacuum drum dried material could be milled differently affecting powder properties. In this case, the ideal parameters for milling of the extrudate beads were chosen in terms of downstream processability using an impact mill (Fitzmill L1A, Fitzpatrick Company, Sint-Niklaas, Belgium) referring to the commercial process parameters. Hot-melt extrusion as fusion-based method results in a high-density material usually in the shape of extrudate lentils based on the calandering process. Particle size and particle shape of the milled extrudate are not correlated to the extrusion process itself, but dependent on the milling process and the respective formulation composition (Andrews et al., 2010). Thus, milling is the crucial step in downstream processing as particle size and morphology is affecting flowability, segregation tendency and dissolution.

3.7.1.2.2 Bulk/tapped/particle (pycnometric) density and flowability

Table 3.2 shows the results of the densities measurements (bulk, tapped and particle (pycnometric) density). Overall, all ASD intermediates consisting of the same composition showed similar particle (pycnometric) density values as expected.

The bulk density of the milled extrudate was around 0.6 g/cm³, which is typical for copovidone based extrudates. The bulk density of the SD material was substantial lower (0.29 g/cm³). The VDD material showed even lower bulk density with 0.20 g/cm³. The superior bulk density of the milled extrudate can be explained with the extrusion process itself. The melting of the components results in high-density material. In addition, the relatively regular particle shape and narrow particle size distribution of the milled extrudate containing larger particles compared to SD and VDD in the current study are favorable for a high bulk density and without electrostatic behavior. Both solvent-evaporation technologies resulted in a material with low bulk density. Higher porosity is built into the material during evaporation of the solvent leading to low-density particles like hollow spheres of the SD material. For the SD material the electrostatic and agglomeration tendency between particles increases the bulk volume and thus, lower the bulk density. Powders, as the SD material, consisting of a high number of

particles below 10 µm are usually extremely cohesive and resist flow under gravity. The presence of electrical charge might lead to a loose packing due to mutual repulsion between the particles. Plate-shaped particles as present in the VDD material mostly produce a loose packing and thus, a low bulk density, as they only contact each other by their edges and protrusions with air-filled spaces between them are prevalent.

The corresponding Hausner ratio (see Table 3.2) for the milled extrudate indicated fair flow (1.25 ± 0.00), and for the SD (1.51 ± 0.10) as well as VDD material (1.57 ± 0.03) very poor flow. The high Hausner ratio for the SD and VDD material poses potential risk for segregation caused by vibrations during processing e.g., compression, and low process robustness leading often to high weight variations of the dose units. Consequently, the risk of non-uniformity of the final dose unit might be elevated without the addition of an external phase for compression.

The flowability results described as FFC values (Freeman, 2007; Jenike, 1964) are summarized in Table 3.2. Compared to both solvent-based ASDs the milled extrudate exhibited the highest FFC value (8.98 ± 0.40) indicating an easy to free flowing powder. The FFC value for the spray dried ASD (1.29 ± 0.02) indicated very cohesive material. The FFC value for the milled VDD material (2.91 ± 0.03) was slightly higher compared to SD material indicating cohesive flow properties. The superior flowability of the milled extrudate was related to the particle shape, relatively large particles, and the narrow particle size distribution. The SD material showed high electrostatic behavior and the tendency to agglomeration related to the large content of fines resulting in bad flow properties despite the favorable spherical particle shape. The VDD intermediate in contrast, showed no electrostatic behavior and less tendency to agglomeration. The irregular particle shape of the VDD material paired with the broad particle size distribution might be the cause for the cohesive flow. Nevertheless, even a slight increase in the FFC value in the lower end of the classification can lead to a substantial improvement in downstream processability and should be assessed accordingly.

3.7.2 In-vitro dissolution – BiP_Ha+

Dissolution experiments were performed with the BiP_Ha+ biphasic dissolution test targeting fasted state conditions using 0.1 N HCl as gastric and FaSSIF-V2 as intestinal medium (Denninger et al., 2020). The drug dissolution (ritonavir concentration) was measured in two phases: the aqueous phase mimicking the gastro-intestinal lumen and the organic phase mimicking an absorption compartment. Figure 3.7 shows the dissolution profiles of ASDs manufactured by (A) hot-melt extrusion, (B) spray drying, (C) vacuum drum drying, and (D) all profiles overlapped for better comparability. The dissolution data indicated no significant

difference in dissolution behavior for the ritonavir containing ASDs with respect to the manufacturing process. The statistical significance on a difference between those dissolution data was assessed using a one-way analysis of variance (ANOVA) with an assumed significance level of $\alpha = 0.05$. A p-value of 0.13 confirmed no difference in dissolution behavior. However, a difference might occur while comparing tablets out of ASD intermediates prepared via HME, SD and VDD and should be assessed in future, since a pronounced difference in tablet porosity is expected based on the manufacturing process.

Due to the basic character of ritonavir ($pK_A = 2.4$) all ASDs showed an almost complete dissolution (approximately 94 to 100%) at pH 1 after 30 min in the aqueous phase (black lines). The presence of ASD intermediates as powder in capsule led to a fast onset in dissolution based on the large surface area of the ASD particles. Moreover, the capsules were fully disintegrated after 3 to 5 min leading only to a short delay in dissolution at the beginning of the test. After the pH adjustments (pH 5.5 at 30 min, pH 6.8 at 90 min), precipitation of ritonavir occurred: the ritonavir dissolution decreased rapidly as a fact of the low solubility of ritonavir at these pH ranges. Then, the dissolution in the aqueous phase increased initially till a plateau was reached at the end concentration of approximately 4 to 10% assuming supersaturation of the ritonavir in the dissolution medium.

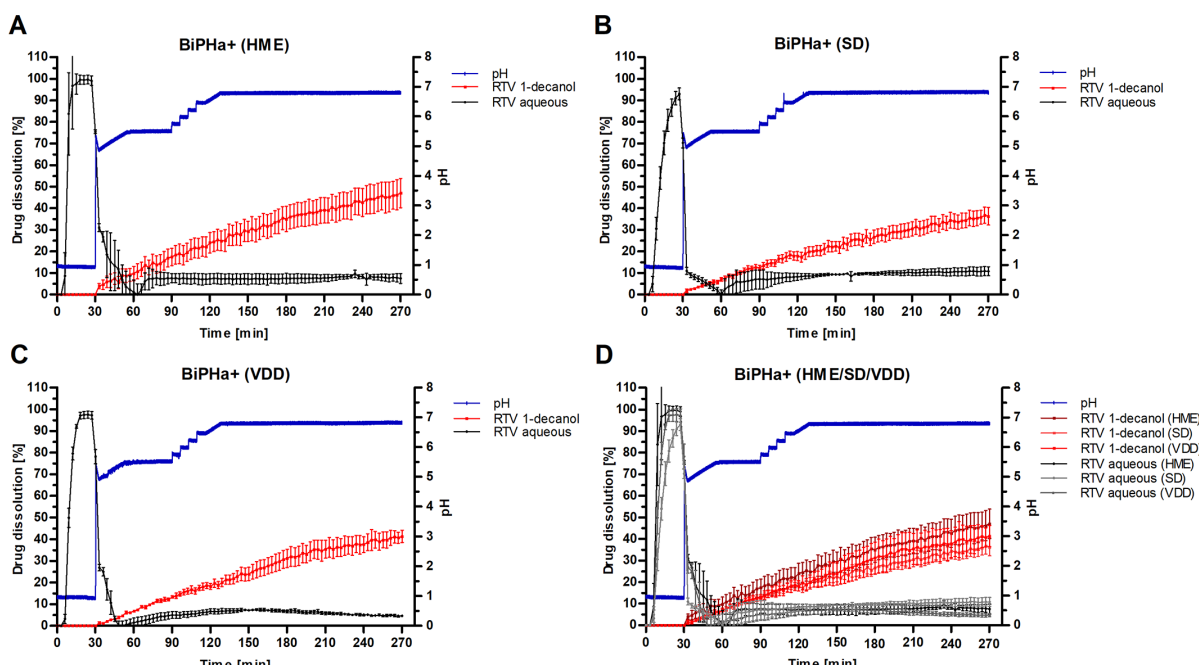


Figure 3.7. BiPha+ dissolution profiles of ritonavir containing amorphous solid dispersions (10 mg capsules) prepared by (A) HME, (B) SD, (C) VDD. (D) Dissolution profiles of ASDs prepared by HME, SD and VDD compared in one graph. Red line: API (ritonavir) concentration in the 1-decanol layer (mean value and standard deviation); black-line: dissolved ritonavir in the aqueous medium (mean value and standard deviation); blue line: pH values. All experiments were performed in triplicates ($n = 3$)

The organic phase (1-decanol) functioning as absorption compartment was added after 30 min. The dissolution profiles in the organic phase (red lines) showed an increase in ritonavir concentration over time up to a final concentration of approximately 37–45% after 270 min. All ASDs showed similar flux rates into the organic phase and a slight decrease in flux rate over time indicating a diminishing concentration of the dissolved ritonavir in the aqueous phase.

Dissolution profiles reported by Denninger et al. (2020) showed qualitatively comparable results: a fast and high onset in dissolution and a fast decrease after pH change in the aqueous phase. However, the dissolution in the aqueous phase reached a lower maximum of approximately 75% in the gastric medium and a lower ritonavir concentration with less than 5% in the intestinal medium after pH shift. Furthermore, the end concentration in the organic phase was higher at 58%. According to Indulkar et al. (2019) and Xu et al. (2017) a 15% drug loaded ritonavir ASD is supposed to show fast drug release and to form amorphous nanodroplets related to liquid-liquid-phase-separation. These nanodroplets might be responsible for the successive flux in the organic medium: nanodroplets might enable the replacement of the dissolved API, which partitioned into the absorption compartment (organic phase). Nanodroplets might function as reservoir by equilibrating rapidly in the aqueous medium during dissolution testing.

The differences in absolute values in the dissolution profiles could be related to the sample particle size (Zheng et al., 2019). In this study powder in capsules were tested whereas Denninger et al. tested cut extrudate strands. Smaller particles are expected to dissolve faster compared to coarse particles. A piece of extrudate strand could be seen as large particle steadily eroding during dissolution exhibiting a slower dissolution rate. Xu et al. (2017) reported a more rapid dissolution of ritonavir and a higher absolute dissolution value for the ASD powder compared with a ritonavir containing tablet. The ASD powder is assumed to precipitate after pH change more drastically due to the extensive amount of ritonavir dissolved in the gastric phase related to the reduced particle size. Consequently, the higher precipitation and the related slower re-dissolution of the ritonavir precipitate led to a lower flux to the organic phase mimicking the absorption and thus, eventually to a lower bioavailability.

Similar to these results, tablets containing lopinavir and ritonavir showed lower bioavailability for crushed compared to uncrushed tablets underlining the observations made in the biphasic dissolution test (Best et al., 2011).

3.8 Conclusion

The present study demonstrated the feasibility of vacuum drum drying (VDD) as novel solvent-based technology for the manufacture of ASDs (amorphous solid dispersions) – for the present formulation at defined process conditions - in comparison to hot-melt-extrusion (HME) and spray drying (SD). Although the HME intermediate showed superior powder properties and related downstream processability for the tested formulation (ritonavir 15% (w/w) in copovidone/sorbitan monolaurate matrix), the solvents-based methods (VDD and SD) are valid alternatives for the HME process - especially for APIs with challenging physicochemical properties such as high melting point, and less stability against thermal or shear stress during processing. All intermediates showed similar product quality and in-vitro dissolution profiles despite differences in particle morphology and related powder properties.

The present work indicates potential of the VDD with respect to the following aspects: the VDD enables potentially processing highly viscous solutions, e.g. due to high solid loads or polymers of high molecular weight, which cannot be processed by either HME or SD closing the gap of existing technologies. The VDD demonstrated a more efficient removal of the solvents even without an additional drying step despite the postulated slower drying kinetics – at least for the selected formulation and conditions. In fact, eliminating the second drying step could most likely affect positively the physical stability of the ASD, since the amount of residual solvents is reduced to a minimum immediately after processing, and elevated temperatures are not applied for several hours as typically common for the SD second drying step. The drying efficiency underlines the advantage of the VDD from an economical point of view: potentially higher cost efficiency due to assumed higher throughputs and a faster overall production time, while requiring less solvents. In addition, production-scale equipment for VDD has a much lower footprint compared to SD.

The improved material properties of the VDD intermediate compared to SD, such as enhanced flowability and reduced electrostatic charging, facilitate the downstream processing. However, VDD as presumed novel technology should be assessed further with respect to tabletability in comparison to ASDs from HME and SD in future studies.

3.9 CRediT authorship contribution statement

B. V. Schönenfeld: Conceptualization, Methodology, Investigation, Visualization, Writing - original draft. U. Westedt: Conceptualization, Methodology, Project administration, Supervision, Writing - review & editing. K. G. Wagner: Conceptualization, Methodology, Supervision, Writing - review & editing.

3.10 Declaration of competing interest

The authors declare the following financial interests/personal relationships which may be considered as potential competing interests: Barbara V. Schönenfeld and Ulrich Westedt are employees of AbbVie and may own AbbVie stock. Barbara V. Schönenfeld is a PhD student and Karl G. Wagner is a professor at the University of Bonn. They have no additional conflicts of interest to report.

3.11 Acknowledgement & Funding

The authors kindly thank Tim Becker (University of Bonn) for his technical assistance in BiPHa+ dissolution testing, Kristina E. Steffens (University of Bonn) and Tim Lillotte (University of Bonn) in scanning electron microscopy, Stefan Weber (AbbVie Deutschland GmbH & Co. KG) in X-ray powder diffraction and Ariane Julke in polarized light microscopy (AbbVie Deutschland GmbH & Co. KG).

This work was funded by AbbVie Deutschland GmbH & Co. KG. University of Bonn and AbbVie participated study design, research, interpretation of data, writing, data collection, analysis, reviewing, and approving the publication.

VACUUM DRUM DRYING – A NOVEL SOLVENT EVAPORATION BASED TECHNOLOGY
TO MANUFACTURE AMORPHOUS SOLID DISPERSIONS IN COMPARISON TO SPRAY
DRYING AND HOT MELT EXTRUSION

3.12 Appendix A. Supplementary data

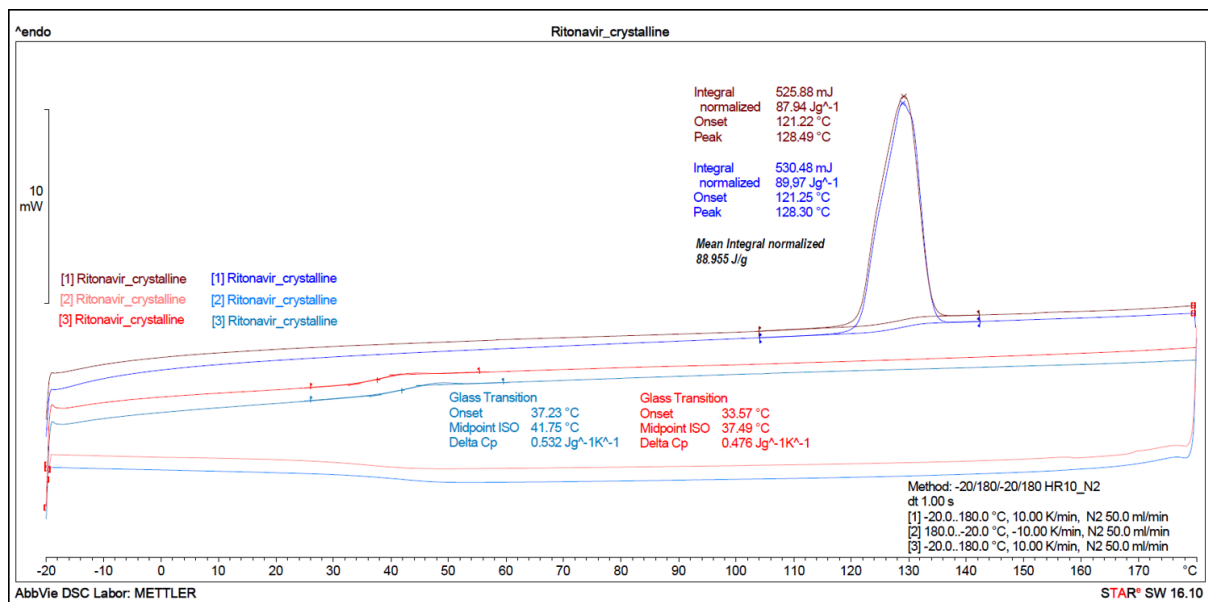


Figure 3.S1: DSC thermograms of pure crystalline ritonavir ($n=2$); red colored lines: sample 1; blue colored lines: sample 2. [1] first heating; [2] first cooling; [3] second heating. Mean melting enthalpy 88.955 J/g. Mean glass transition temperature 39.2 °C

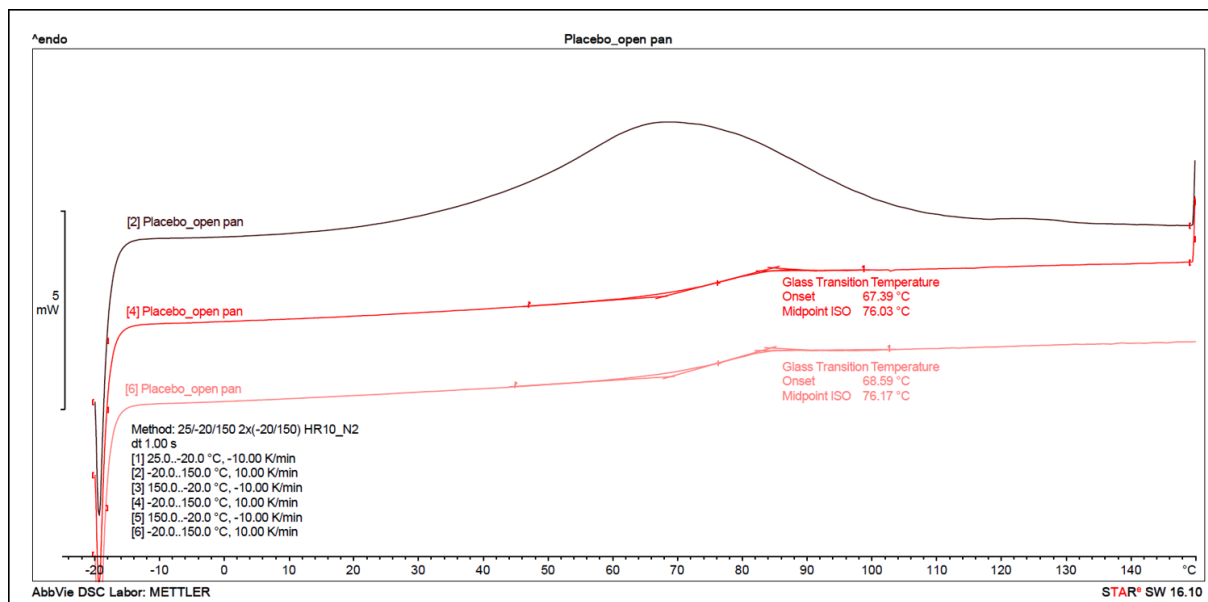


Figure 3.S2: DSC thermograms of milled placebo extrudate (open pan; [2] first heating; [4] second heating; [6] third heating). Mean glass transition temperature (dry): 76.1 °C; crystallinity: n.d.

VACUUM DRUM DRYING – A NOVEL SOLVENT EVAPORATION BASED TECHNOLOGY
TO MANUFACTURE AMORPHOUS SOLID DISPERSIONS IN COMPARISON TO SPRAY
DRYING AND HOT MELT EXTRUSION

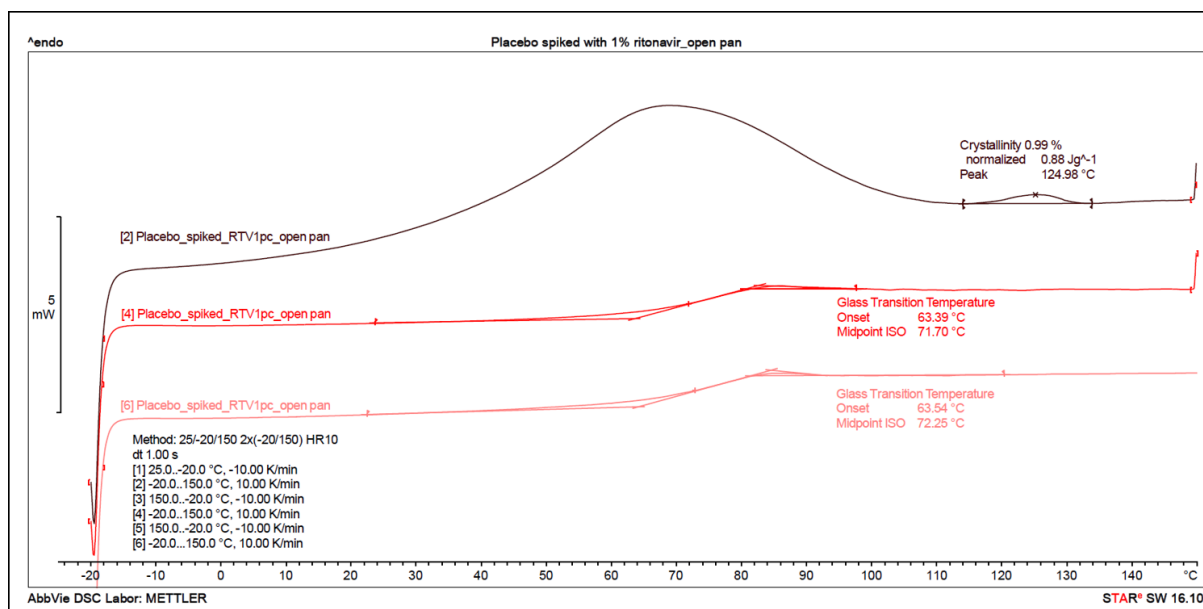


Figure 3.S3: DSC thermograms of milled placebo extrudate spiked with 1% crystalline ritonavir (open pan; [2] first heating; [4] second heating; [6] third heating). Mean glass transition temperature (dry): 72.0 °C; crystallinity: 0.99%

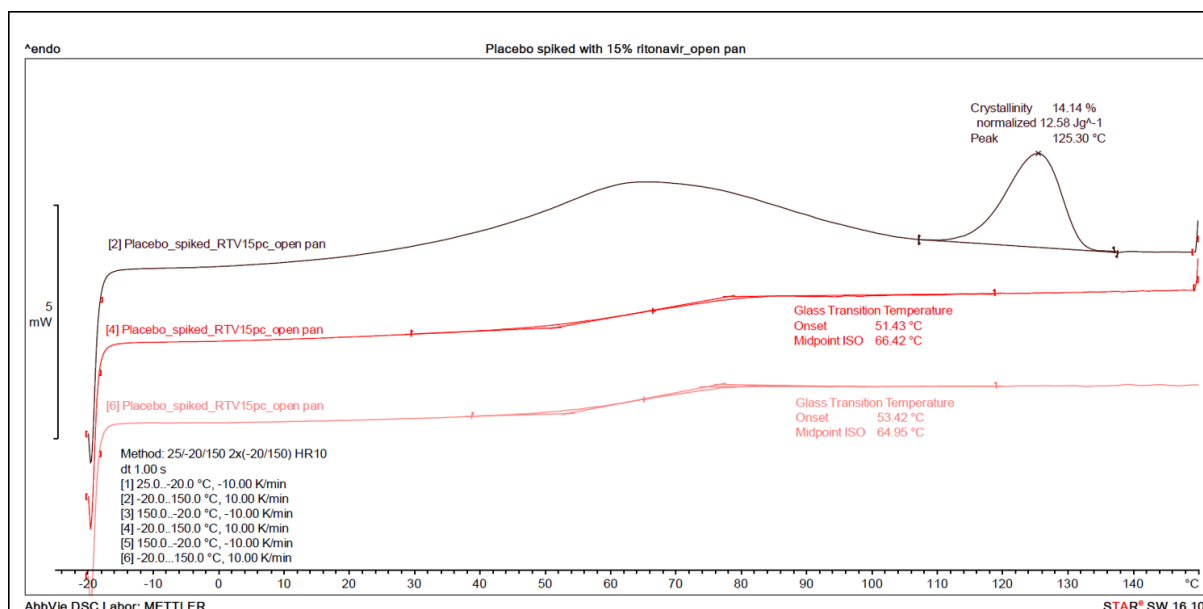


Figure 3.S4: DSC thermograms of milled placebo extrudate extrudate spiked with 15% crystalline ritonavir (open pan; [2] first heating; [4] second heating; [6] third heating). Mean glass transition temperature (dry): 65.7 °C; crystallinity: 14.14%

VACUUM DRUM DRYING – A NOVEL SOLVENT EVAPORATION BASED TECHNOLOGY
TO MANUFACTURE AMORPHOUS SOLID DISPERSIONS IN COMPARISON TO SPRAY
DRYING AND HOT MELT EXTRUSION

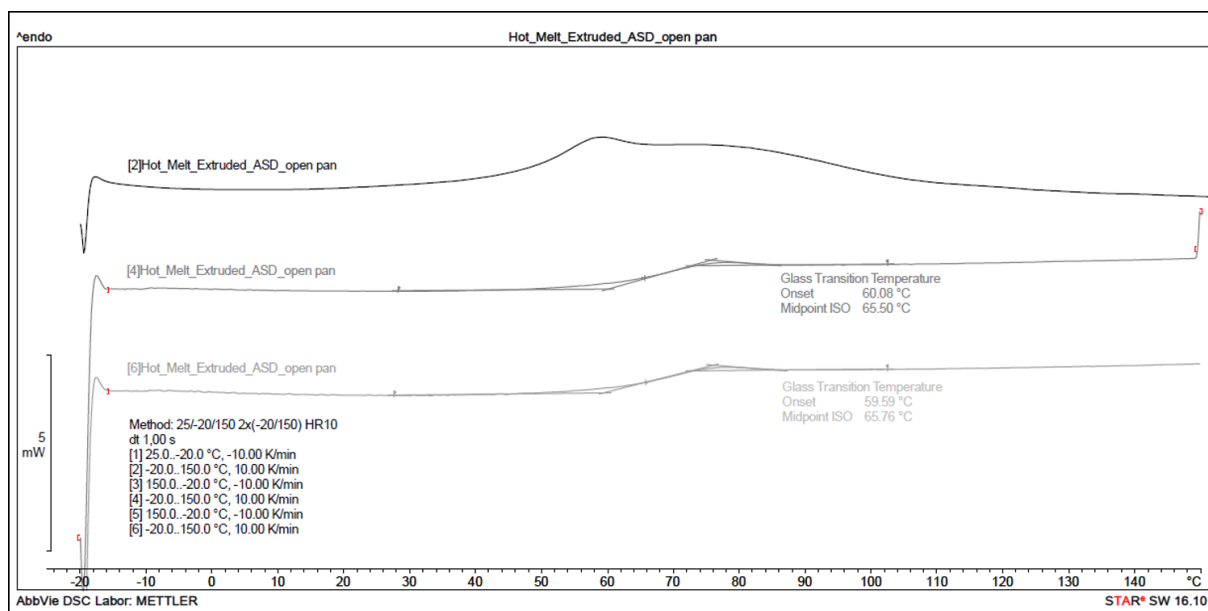


Figure 3.S5: DSC thermogram of milled HME material (open pan; [2] first heating; [4] second heating; [6] third heating). Mean glass transition temperature (dry): 65.6 °C

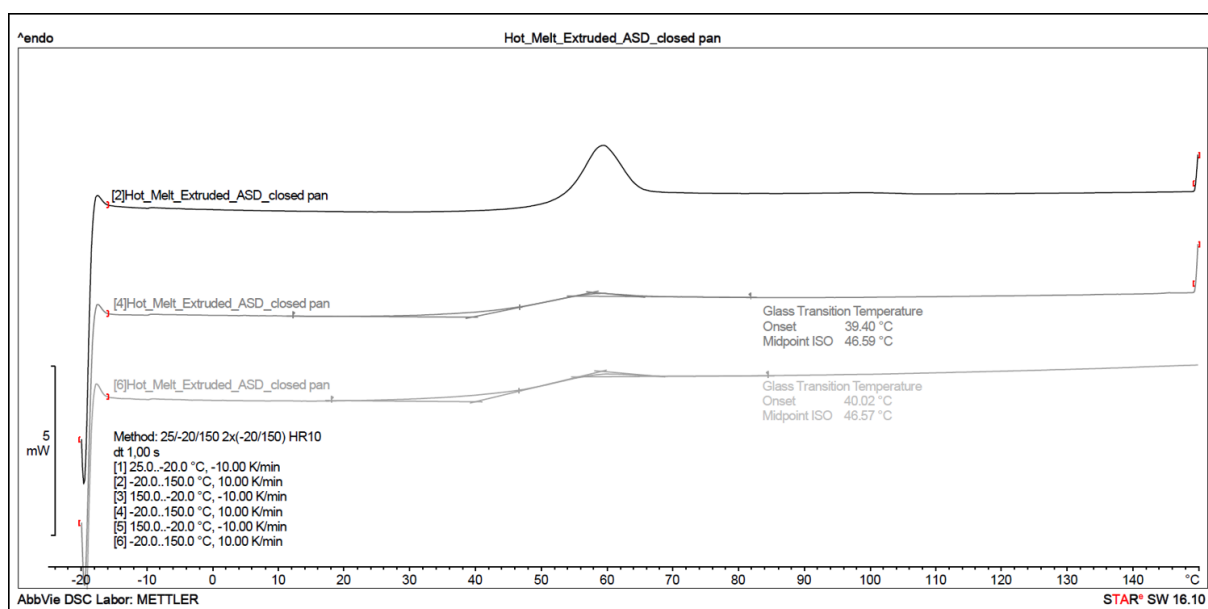


Figure 3.S6: DSC thermogram of milled HME material (closed pan; [2] first heating; [4] second heating; [6] third heating). Mean glass transition temperature (wet): 46.6 °C

VACUUM DRUM DRYING – A NOVEL SOLVENT EVAPORATION BASED TECHNOLOGY
TO MANUFACTURE AMORPHOUS SOLID DISPERSIONS IN COMPARISON TO SPRAY
DRYING AND HOT MELT EXTRUSION

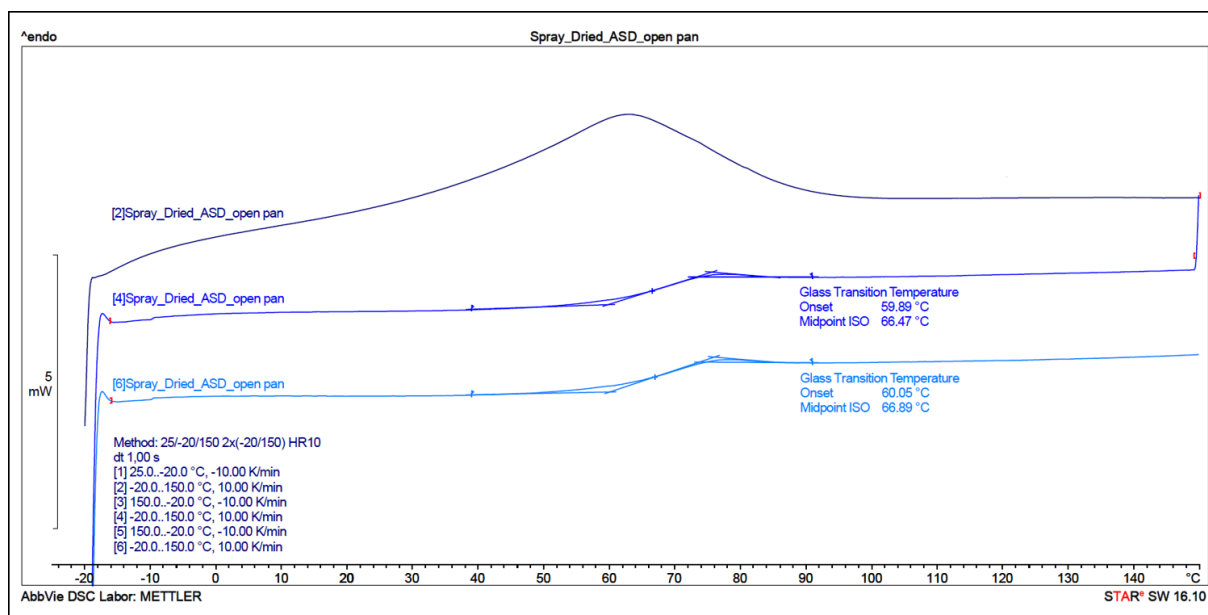


Figure 3.S7: DSC thermogram of SD material (open pan; [2] first heating; [4] second heating; [6] third heating). Mean glass transition temperature (dry): 66.7 °C

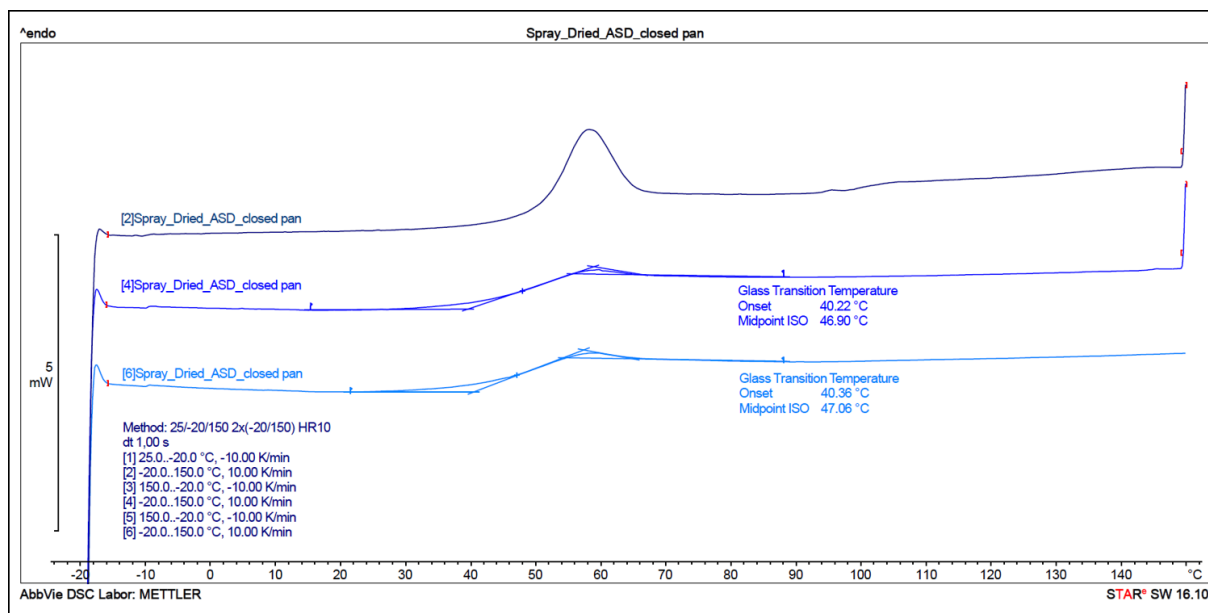


Figure 3.S8: DSC thermogram of SD material (closed pan; [2] first heating; [4] second heating; [6] third heating). Mean glass transition temperature (wet): 47.0 °C

VACUUM DRUM DRYING – A NOVEL SOLVENT EVAPORATION BASED TECHNOLOGY
TO MANUFACTURE AMORPHOUS SOLID DISPERSIONS IN COMPARISON TO SPRAY
DRYING AND HOT MELT EXTRUSION

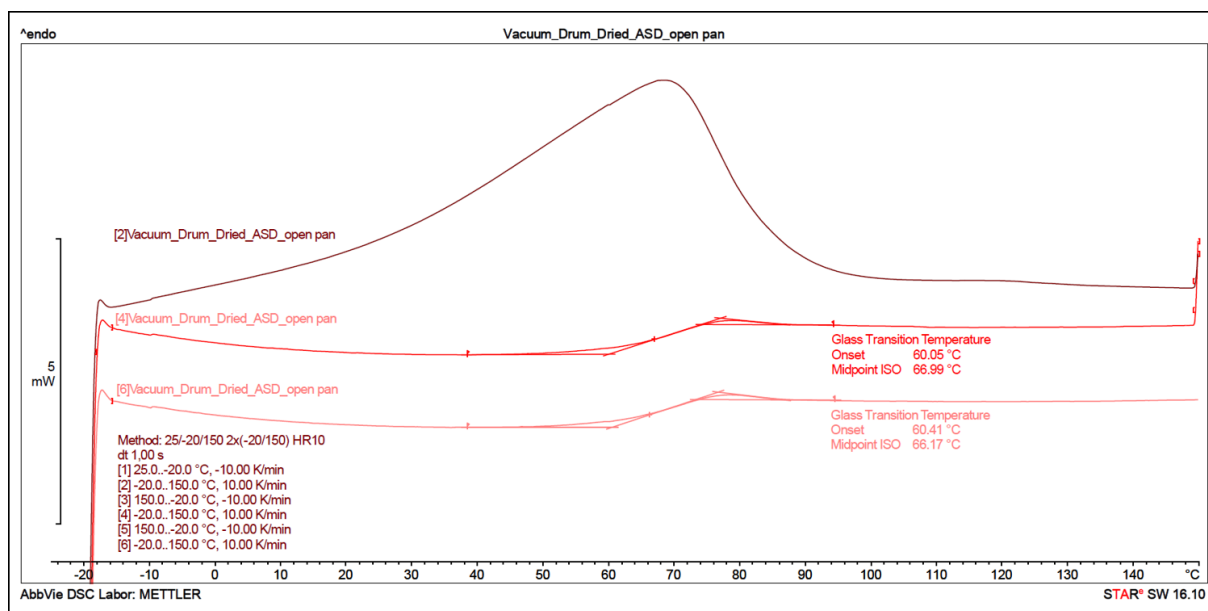


Figure 3.S9: DSC thermogram of VDD material (open pan; [2] first heating; [4] second heating; [6] third heating). Mean glass transition temperature (dry): 66.6 °C

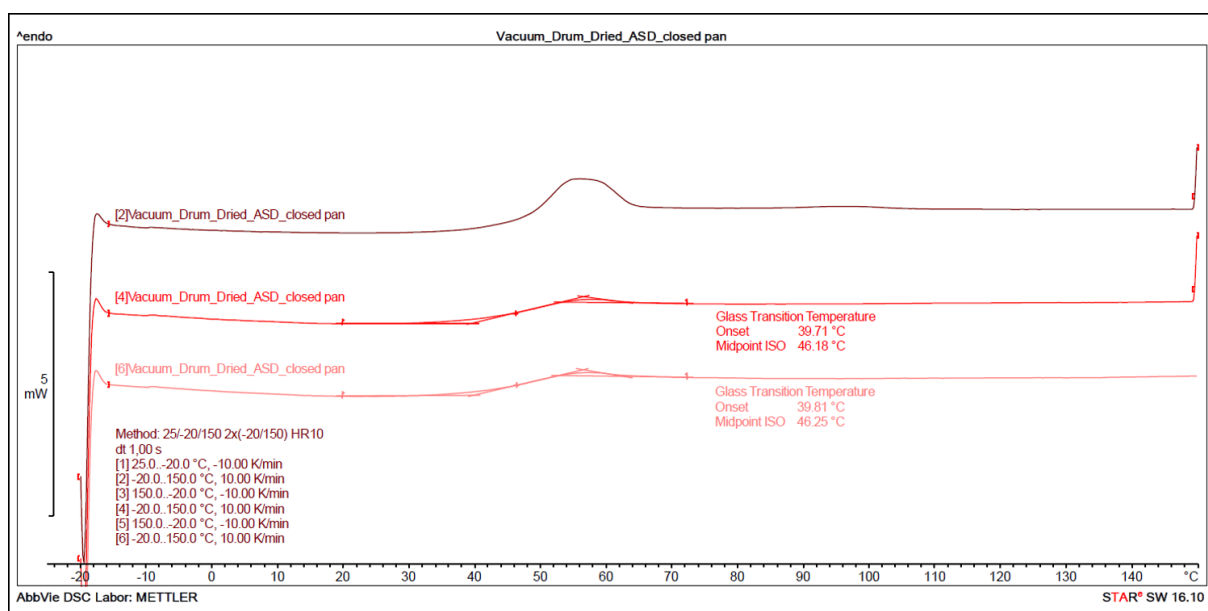


Figure 3.S10: DSC thermogram of VDD material (closed pan; [2] first heating; [4] second heating; [6] third heating). Mean glass transition temperature (wet): 46.2 °C

3.13 References

- Agrawal, A.M., Dudhedia, M.S., Patel, A.D., Raikes, M.S., 2013. Characterization and performance assessment of solid dispersions prepared by hot melt extrusion and spray drying process. International Journal of Pharmaceutics 457, 71-81 <https://doi.org/10.1016/j.ijpharm.2013.08.081>.
- Andrews, G.P., Abu-Diak, O., Kusmanto, F., Hornsby, P., Hui, Z., Jones, D.S., 2010. Physicochemical characterization and drug-release properties of celecoxib hot-melt extruded glass solutions. Journal of Pharmacy and Pharmacology 62, 1580-1590 <https://doi.org/10.1111/j.2042-7158.2010.01177.x>.
- Aso, Y., Yoshioka, S., Kojima, S., 2000. Relationship Between the Crystallization Rates of Amorphous Nifedipine, Phenobarbital, and Flopropione, and Their Molecular Mobility as Measured by Their Enthalpy Relaxation and H^1 NMR Relaxation Times. Journal of Pharmaceutical Sciences 89, 408-416 [https://doi.org/10.1002/\(SICI\)1520-6017\(200003\)89:3<408::AID-JPS11>3.0.CO;2-#](https://doi.org/10.1002/(SICI)1520-6017(200003)89:3<408::AID-JPS11>3.0.CO;2-#).
- Best, B.M., Capparelli, E.V., Diep, H., Rossi, S.S., Farrell, M.J., Williams, E., Lee, G., van den Anker, J.N., Rakhmanina, N., 2011. Pharmacokinetics of lopinavir/ritonavir crushed versus whole tablets in children. Journal of Acquired Immune Deficiency Syndromes 58, 385-391 <https://doi.org/10.1097/QAI.0b013e318232b057>.
- Bhandari, B., Bansal, N., Zhang, M., Schuck, P., 2013. 4.1 Introduction, Handbook of Food Powders - Processes and Properties. Woodhead Publishing. 2013
- Bhardwaj, S.P., Suryanarayanan, R., 2012. Molecular Mobility as an Effective Predictor of the Physical Stability of Amorphous Trehalose. Molecular Pharmaceutics 9, 3209-3217 <https://doi.org/10.1021/mp300302g>.
- Bochmann, E.S., Neumann, D., Gryczke, A., Wagner, K.G., 2016. Micro-scale prediction method for API-solubility in polymeric matrices and process model for forming amorphous solid dispersion by hot-melt extrusion. European Journal of Pharmaceutics and Biopharmaceutics 107, 40-48 <http://doi.org/10.1016/j.ejpb.2016.06.015>.
- Breitenbach, J., 2002. Melt extrusion: from process to drug delivery technology. European Journal of Pharmaceutics and Biopharmaceutics 54, 107-117 [http://doi.org/10.1016/s0939-6411\(02\)00061-9](http://doi.org/10.1016/s0939-6411(02)00061-9).
- Brunauer, S., Emmett, P.H., Teller, E., 1938. Adsorption of Gases in Multimolecular Layers. Journal of the American Chemical Society 60, 309-319 <http://doi.org/10.1021/ja01269a023>.
- Crowley, M.M., Zhang, F., Repka, M.A., Thumma, S., Upadhye, S.B., Kumar Battu, S., McGinity, J.W., Martin, C., 2007. Pharmaceutical Applications of Hot-Melt Extrusion: Part I. Drug Development and Industrial Pharmacy 33, 909-926 <https://doi.org/10.1080/03639040701498759>.
- Denninger, A., Westedt, U., Rosenberg, J., Wagner, K.G., 2020. A Rational Design of a Biphasic DissolutionSetup-Modelling of Biorelevant Kinetics for a Ritonavir Hot-Melt Extruded Amorphous Solid Dispersion. Pharmaceutics 12 <http://doi.org/10.3390/pharmaceutics12030237>.
- Dreiblatt, A., 2012. Technological Considerations Related to Scale-Up of Hot-Melt Extrusion Processes, in: Douroumis, D. (Ed.), Hot-Melt Extrusion: Pharmaceutical Applications. John Wiley & Sons, Ltd., pp. 285-300.

VACUUM DRUM DRYING – A NOVEL SOLVENT EVAPORATION BASED TECHNOLOGY
TO MANUFACTURE AMORPHOUS SOLID DISPERSIONS IN COMPARISON TO SPRAY
DRYING AND HOT MELT EXTRUSION

Dobry, D.E., Settell, D.M., Baumann, J.M., Ray, R.J., Graham, L.J., Beyerinck, R.A., 2009. A Model-Based Methodology for Spray-Drying Process Development. *Journal of Pharmaceutical Innovation* 4, 133-142 <https://doi.org/10.1007/s12247-009-9064-4>.

EMA/CHMP/ICH/82260/2006, 2019. ICH guideline Q3C (R6) on impurities: guideline for residual solvents EMA/CHMP/ICH/82260/2006

Gambhir, K., Singh, P., Jangir, D.K., Mehrotra, R., 2015. Thermal stability and hydration behavior of ritonavir sulfate: A vibrational spectroscopic approach. *Journal of Pharmaceutical Analysis* 5, 348-355 <https://doi.org/10.1016/j.jpha.2015.05.001>.

Gryczke, A., Kolter, K., Karl, M., 2012. Hot-Melt Extrusion with BASF Pharma Polymers Extrusion Compendion, 2nd Revised and Enlarged Edition ed. BASF.

Hancock, B.C., Carlson, G.T., Ladipo, D.D., Langdon, B.A., Mullarney, M.P., 2002. Comparison of the mechanical properties of the crystalline and amorphous forms of a drug substance. *International Journal of Pharmaceutics* 241, 73-85 [https://doi.org/10.1016/S0378-5173\(02\)00133-3](https://doi.org/10.1016/S0378-5173(02)00133-3).

Hancock, B.C., Shamblin, S.L., Zografi, G., 1995. Molecular Mobility of Amorphous Pharmaceutical Solids Below Their Glass Transition Temperatures. *Pharmaceutical Research* 12, 799-806 <http://doi.org/10.1023/A:1016292416526>.

Hancock, B.C., Zografi, G., 1997. Characteristics and Significance of the Amorphous State in Pharmaceutical Systems. *Journal of Pharmaceutical Sciences* 86, 1-12 <https://doi.org/10.1021/js9601896>.

Huang, S., Williams, R.O., 2018. Effects of the Preparation Process on the Properties of Amorphous Solid Dispersions. *AAPS PharmSciTech* 19, 1971-1984 <https://doi.org/10.1208/s12249-017-0861-7>.

Indulkar, A.S., Lou, X., Zhang, G.G.Z., Taylor, L.S., 2019. Insights into the Dissolution Mechanism of Ritonavir–Copovidone Amorphous Solid Dispersions: Importance of Congruent Release for Enhanced Performance. *Molecular Pharmaceutics* 16, 1327-1339 <https://doi.org/10.1021/acs.molpharmaceut.8b01261>.

Jermain, S.V., Brough, C., Williams, R.O., 2018. Amorphous solid dispersions and nanocrystal technologies for poorly water-soluble drug delivery – An update. *International Journal of Pharmaceutics* 535, 379-392 <https://doi.org/10.1016/j.ijpharm.2017.10.051>.

Karthik, P., Chhanwal, N., Anandharamakrishnan, C., 2017. Drum Drying. 4.5.1 Important operational conditions in the drum drying of milk, *Handbook of Drying for Dairy Products*, 1st Edition ed. Wiley-Blackwell, p. 52.

Kennedy, M., Hu, J., Gao, P., Li, L., Ali-Reynolds, A., Chal, B., Gupta, V., Ma, C., Mahajan, N., Akrami, A., Surapaneni, S., 2008. Enhanced bioavailability of a poorly soluble VR1 antagonist using an amorphous solid dispersion approach: a case study. *Molecular Pharmaceutics* 5, 981-993 <http://doi.org/10.1021/mp800061r>.

Konno, H., Taylor, L.S., 2006. Influence of different polymers on the crystallization tendency of molecularly dispersed amorphous felodipine. *Journal of Pharmaceutical Sciences* 95, 2692-2705 <https://doi.org/10.1002/jps.20697>.

Kyeremateng, S.O., Pudlas, M., Woehrle, G.H., 2014. A fast and reliable empirical approach for estimating solubility of crystalline drugs in polymers for hot melt extrusion formulations. *Journal of Pharmaceutical Sciences* 103, 2847-2858 <https://doi.org/10.1002/jps.23941>.

Lehmkemper, K., Kyeremateng, S.O., Heinzerling, O., Degenhardt, M., Sadowski, G., 2017. Long-Term Physical Stability of PVP- and PVPVA-Amorphous Solid Dispersions. *Molecular Pharmaceutics* 14, 157-171 <https://doi.org/10.1021/acs.molpharmaceut.6b00763>.

VACUUM DRUM DRYING – A NOVEL SOLVENT EVAPORATION BASED TECHNOLOGY
TO MANUFACTURE AMORPHOUS SOLID DISPERSIONS IN COMPARISON TO SPRAY
DRYING AND HOT MELT EXTRUSION

Leuner, C., Dressman, J., 2000. Improving drug solubility for oral delivery using solid dispersion. European journal of pharmaceutics and biopharmaceutics : official journal of Arbeitsgemeinschaft für Pharmazeutische Verfahrenstechnik e.V 50, 47-60 [https://doi.org/10.1016/S0939-6411\(00\)00076-X](https://doi.org/10.1016/S0939-6411(00)00076-X).

Lin, X., Hu, Y., Liu, L., Su, L., Li, N., Yu, J., Tang, B., Yang, Z., 2018. Physical Stability of Amorphous Solid Dispersions: a Physicochemical Perspective with Thermodynamic, Kinetic and Environmental Aspects. Pharmaceutical Research 35, 125 <https://doi.org/10.1007/s11095-018-2408-3>.

Lipinski, C.A., Lombardo, F., Dominy, B.W., Feeney, P.J., 2001. Experimental and computational approaches to estimate solubility and permeability in drug discovery and development settings¹ of original article: S0169-409X(96)00423-1. The article was originally published in Advanced Drug Delivery Reviews 23 (1997) 3–25.1. Advanced Drug Delivery Reviews 46, 3-26 [https://doi.org/10.1016/S0169-409X\(00\)00129-0](https://doi.org/10.1016/S0169-409X(00)00129-0).

Mujumdar, A.S., 2015a. 11.3.3.1 Nip Feeding, Handbook of Industrial Drying (4th Edition). Taylor & Francis.

Mujumdar, A.S., 2015b. 11.6 Drum-Dried Products, Handbook of Industrial Drying (4th Edition), 4th ed. Taylor & Francis.

Murtomaa, M., Savolainen, M., Christiansen, L., Rantanen, J., Laine, E., Yliruusi, J., 2004. Static electrification of powders during spray drying. Journal of Electrostatics 62, 63-72 <https://doi.org/10.1016/j.elstat.2004.05.001>.

Patterson, J.E., James, M.B., Forster, A.H., Lancaster, R.W., Butler, J.M., Rades, T., 2007. Preparation of glass solutions of three poorly water soluble drugs by spray drying, melt extrusion and ball milling. International Journal of Pharmaceutics 336, 22-34 <https://doi.org/10.1016/j.ijpharm.2006.11.030>.

Prudic, A., Ji, Y., Sadowski, G., 2014. Thermodynamic Phase Behavior of API/Polymer Solid Dispersions. Molecular Pharmaceutics 11, 2294-2304 <https://doi.org/10.1021/mp400729x>.

Raghavan, R., Jett, J.L., 2004. Method to produce a solid form of heparin, International Application Published Under The Patent Cooperation Treaty. Pfizer Health AB

Repka, M.A., Bandari, S., Kallakunta, V.R., Vo, A.Q., McFall, H., Pimparade, M.B., Bhagurkar, A.M., 2018. Melt extrusion with poorly soluble drugs – An integrated review. International Journal of Pharmaceutics 535, 68-85 <https://doi.org/10.1016/j.ijpharm.2017.10.056>.

Sandhu, H., Shah, N., Chokshi, H., Malick, A.W., 2014. Overview of Amorphous Solid Dispersion Technologies, Amorphous Solid Dispersions: Theory and Practice. Springer New York, New York, NY, pp. 91-122.

Sangekar, S.A., Lee, P.I., Nomeir, A.A., 2003. Molecular dispersion composition with enhanced bioavailability, United States Patent. Schering Corporation

Sinka, I.C., Schneider, L.C.R., Cocks, A.C.F., 2004. Measurement of the flow properties of powders with special reference to die fill. International Journal of Pharmaceutics 280, 27-38 <https://doi.org/10.1016/j.ijpharm.2004.04.021>.

Szabo, E., Demuth, B., Galata, D.L., Vass, P., Hirsch, E., Csontos, I., Marosi, G., Nagy, Z.K., 2019. Continuous Formulation Approaches of Amorphous Solid Dispersions: Significance of Powder Flow Properties and Feeding Performance. Pharmaceutics 11 <https://doi.org/10.3390/pharmaceutics11120654>.

Trasi, N.S., Bhujbal, S., Zhou, Q.T., Taylor, L.S., 2019. Amorphous solid dispersion formation via solvent granulation – A case study with ritonavir and lopinavir. International Journal of Pharmaceutics: X 1, 100035 <https://doi.org/10.1016/j.ijpx.2019.100035>.

VACUUM DRUM DRYING – A NOVEL SOLVENT EVAPORATION BASED TECHNOLOGY
TO MANUFACTURE AMORPHOUS SOLID DISPERSIONS IN COMPARISON TO SPRAY
DRYING AND HOT MELT EXTRUSION

Van den Mooter, G., 2012. The use of amorphous solid dispersions: A formulation strategy to overcome poor solubility and dissolution rate. *Drug Discovery Today: Technologies* 9, e79-e85 <https://doi.org/10.1016/j.ddtec.2011.10.002>.

Valous, N.A., Gavrielidou, M.A., Karapantsios, T.D., Kostoglou, M., 2002. Performance of a double drum dryer for producing pregelatinized maize starches. *Journal of Food Engineering* 51, 171-183 [https://doi.org/10.1016/S0260-8774\(01\)00041-3](https://doi.org/10.1016/S0260-8774(01)00041-3).

Wesholowski, J., Hoppe, K., Nickel, K., Muehlenfeld, C., Thommes, M., 2019. Scale-Up of pharmaceutical Hot-Melt-Extrusion: Process optimization and transfer. *European Journal of Pharmaceutics and Biopharmaceutics* 142, 396-404 <https://doi.org/10.1016/j.ejpb.2019.07.009>.

Xu, H., Vela, S., Shi, Y., Marroum, P., Gao, P., 2017. In Vitro Characterization of Ritonavir Drug Products and Correlation to Human in Vivo Performance. *Molecular Pharmaceutics* 14, 3801-3814 <https://doi.org/10.1021/acs.molpharmaceut.7b00552>.

Zecevic, D.E., Evans, R.C., Paulsen, K., Wagner, K.G., 2018. From benchtop to pilot scale—experimental study and computational assessment of a hot-melt extrusion scale-up of a solid dispersion of dipyridamole and copovidone. *International Journal of Pharmaceutics* 537, 132-139 <https://doi.org/10.1016/j.ijpharm.2017.12.033>.

Zheng, K., Lin, Z., Capece, M., Kunnath, K., Chen, L., Davé, R.N., 2019. Effect of Particle Size and Polymer Loading on Dissolution Behavior of Amorphous Griseofulvin Powder. *Journal of Pharmaceutical Sciences* 108, 234-242 <https://doi.org/10.1016/j.xphs.2018.11.025>.

Zhou, D., Grant, D.J.W., Zhang, G.G.Z., Law, D., Schmitt, E.A., 2007. A Calorimetric Investigation of Thermodynamic and Molecular Mobility Contributions to the Physical Stability of Two Pharmaceutical Glasses. *Journal of Pharmaceutical Sciences* 96, 71-83 <https://doi.org/10.1002/jps.20633>.

4. COMPRESSION OF AMORPHOUS SOLID DISPERSIONS PREPARED BY HOT-MELT EXTRUSION, SPRAY DRYING AND VACUUM DRUM DRYING

Barbara V. Schönenfeld^{a,b}, Ulrich Westedt^b, Karl G. Wagner^{a,c}

^aDepartment of Pharmaceutical Technology, University of Bonn, Gerhard-Domagk-Straße 3, 53121 Bonn, Germany, karl.wagner@uni-bonn.de, barbara.schoenfeld@uni-bonn.de

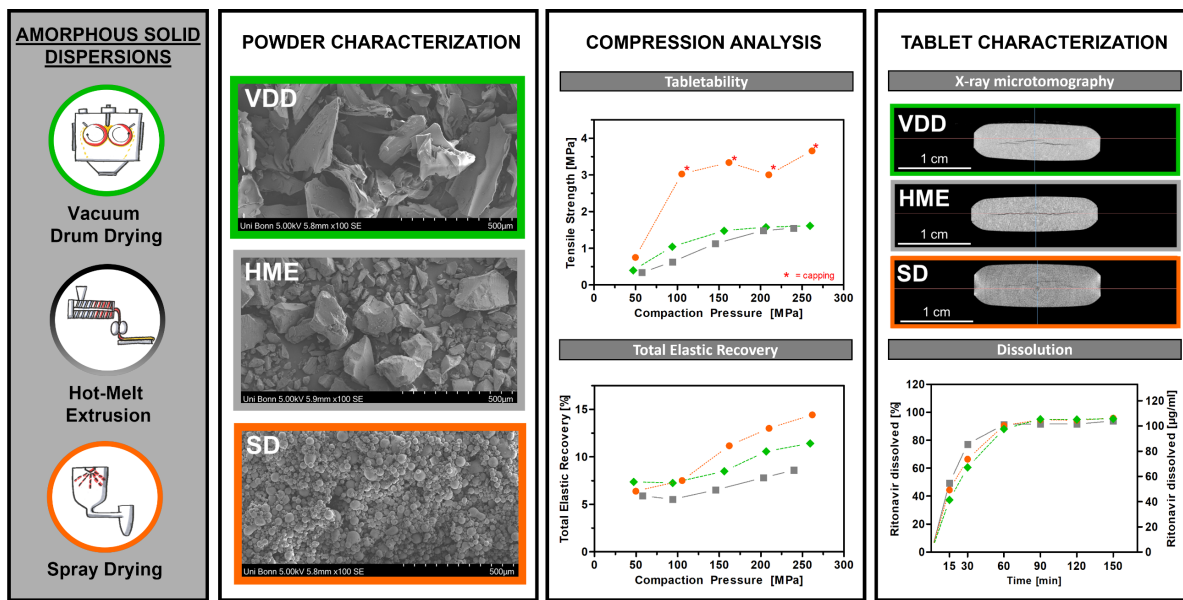
^bAbbVie Deutschland GmbH & Co. KG, Knollstraße 50, 67061 Ludwigshafen, Germany, ulrich.westedt@abbvie.com, barbara.schoenfeld@abbvie.com

^cCorresponding author

This part was published as:

B. V. Schönenfeld, U. Westedt, K. G. Wagner, Compression of amorphous solid dispersions prepared by hot-melt extrusion, spray drying and vacuum drum drying, International Journal of Pharmaceutics: X, Volume 3, 2021, 100102, ISSN 2590-1567, <https://doi.org/10.1016/j.ijpx.2021.100102>.

4.1 Graphical Abstract



4.2 Abstract

The present study explored vacuum drum drying (VDD) as an alternative technology for amorphous solid dispersions (ASDs) manufacture compared to hot-melt extrusion (HME) and spray drying (SD) focusing on downstream processability (powder properties, compression behavior and tablet performance). Ritonavir (15% w/w) in a copovidone/sorbitan monolaurate matrix was used as ASD model system. The pure ASDs and respective tablet blends (TB) (addition of filler, glidant, lubricant) were investigated. Milled extrudate showed superior powder properties (e.g., flowability, bulk density) compared to VDD and SD, which could be compensated by the addition of 12.9% outer phase. Advantageously, the VDD intermediate was directly compressible, whereas the SD material was not, resulting in tablets with defects based on a high degree of elastic recovery. Compared to HME, the VDD material showed superior tabletability when formulated as TB, resulting in stronger compacts at even lower solid fraction values. Despite the differences in tablet processing, tablets showed similar tablet performance in terms of disintegration and dissolution independent of the ASD origin. In conclusion, VDD is a valid alternative to manufacture ASDs. VDD offered advantageous downstream processability compared to SD: less solvents and process steps required (no second drying), improved powder properties and suitable for direct compression.

4.3 Highlights

- ASD technology has influence on particle morphology
- Compression behavior dominated by particle morphology
- Vacuum drum dried intermediate direct compressible into tablets
- Vacuum drum dried material shows better tabletability as milled extrudate
- ASD technology: no impact on tablet disintegration/dissolution

4.4 Keywords

Ritonavir; hot-melt extrusion; spray drying; vacuum drum drying; amorphous solid dispersion; compression analysis; downstream processing.

4.5 Introduction

One of the most promising approaches to formulate poorly water soluble drugs is the application of amorphous solid dispersions (ASDs) improving solubility and thus, bioavailability (Démuth et al., 2015). The most common ASD manufacturing technologies used in commercial scale in the pharmaceutical industry are hot-melt extrusion (HME) and spray drying (SD).

However, each manufacturing technique has its own advantages as well as disadvantages and should be chosen based on drug properties (Vasconcelos et al., 2016). Advantages of HME are continuous and solvent-free process, well-known and established technology including availability of modelling and scaling approaches, and cost-efficiency. Disadvantages are limited range of processible polymers and less suitability for APIs with thermal or shear sensitivity (Shah et al., 2013). Additionally, milling of the extrudates is usually required prior to tabletting. SD on the other hand is a thermally gentle technology reducing thermal stress related to the evaporation cooling effect (Dobry et al., 2009). Therefore, SD is suitable for thermal and shear sensitive APIs reducing degradation. Disadvantageously, SD is cost-intensive, requiring high amounts of solvents and subsequent drying energy. Furthermore, additional process steps after the drying process are required such as second drying or densification via roller compaction (Haser et al., 2017) to achieve an intermediate suitable for tablet manufacturing.

Several studies investigated the impact of HME and SD on the ASD manufacturability in terms of physico-chemical properties (Patterson et al., 2007), achievable drug load (Dedroog et al., 2019) or suitability for APIs showing high recrystallization tendency (Haser et al., 2017).

Moreover, studies observed differences in resulting ASD powder properties (Huang and Williams, 2018) and downstream processing such as tabletability (Davis et al., 2018; Démuth et al., 2015; Iyer et al., 2013).

Vacuum drum drying (VDD) was recently assessed as a promising alternative technology to prepare ASDs and compared to HME and SD on the ASD intermediate level (Schönfeld et al., 2021). VDD is a well-known drying technology in the food industry (Bhandari et al., 2013), but rarely known in the pharmaceutical field of drug product development. Raghavan and Jett (2004) presented drum drying as new technology for the manufacture of heparin. Whereas Sangekar et al. (2003) introduced drum drying for a molecular dispersion composition with enhanced bioavailability. Based on the functional principle VDD is an interesting technology for manufacturing ASDs especially in comparison to other solvent evaporation-based technologies such as SD. One benefit might be the opportunity to eliminate a second drying step by adjusting the retention time of the material on the heated rotating drums under vacuum. In addition, less solvent consumption conceivably increases cost-efficiency further since even highly viscous liquids can be processed as demonstrated in food industry applications. Consequently, higher solid loads result in higher solid throughputs and thus, lower processing times reducing overall costs. Finally, mild process temperatures combined with vacuum facilitate the processibility of even thermosensitive compounds.

Schönfeld et al. (2021) demonstrated that the solid state of the respective ASDs was similar independent of the ASD manufacturing technology. However, published information on downstream processing including product performance, is missing. Thus, the purpose of this study was to assess if the downstream processing and product performance of an ASD formulation is similar as well. For that, an ASD composition (pure ASD prepared by HME, SD and VDD, and formulated with outer phase excipients) was compared in terms of downstream processing including powder characteristics, compression behavior (tabletability, compactability), tablet morphology (scanning electron microscopy, X-ray microcomputed tomography) and product performance (friability, disintegration, dissolution).

Therefore, ritonavir in a copovidone/sorbitan monolaurate matrix (drug load: 15% w/w) was chosen as model system. Ritonavir exhibits favorable physicochemical properties for a comparative study of different ASD technologies: good solubility in matrix polymer copovidone, and simultaneously, sufficient solubility in common organic solvents while showing low tendency for degradation and low risk for fast recrystallization during processing. Furthermore, a drug load of more than 25% (w/w) limits the ritonavir dissolution as recently demonstrated by Indulkar, 2019. Consequently, ritonavir was selected to ensure manufacturability, since it

can be amorphously embedded in a copovidone-based matrix by either HME, SD or VDD resulting in an ASD intermediate with acceptable quality attributes (Schönfeld et al., 2021). And finally, a drug load of 15% (w/w) in the ASD was used to enable detection of any potential impact of ASD manufacturing technology on the quality attribute drug dissolution of the final tablet. To compensate the impact of particle size distribution (PSD) on the corresponding powder properties and compression behavior, the HME material was milled to match the PSD of the VDD intermediate. For comparison, tablet formulations based on ASD intermediates were investigated.

4.6 Material and methods

4.6.1 Materials

Ritonavir (purity >99.8%) was obtained from AbbVie Inc. (North Chicago, US). Copovidone (polyvinylpyrrolidone–vinyl acetate copolymer, Kollidon® VA 64) was purchased from BASF SE (Ludwigshafen, Germany), fumed silicon dioxide (Aerosil® 200) from Evonik Industries (Essen, Germany), sorbitan monolaurate (Span® 20) from CRODA (Nettetal, Germany), dicalcium phosphate anhydrous (DI-CAFOS® A60) from Chemische Fabrik Budenheim (Budenheim, Germany), and sodium stearyl fumarate (PRUV®) from JRS Pharma (Rosenberg, Germany). Acetone (Emprove® Essential, purity 96%) and methanol (Emprove® Essential, purity 99.5%) were obtained from Merck KGaA (Darmstadt, Germany).

4.6.2 Methods

4.6.2.1 Amorphous solid dispersion (ASD) preparation

Ritonavir (15% w/w) containing amorphous solid dispersions (ASDs) were prepared by hot-melt extrusion (HME), spray drying (SD) and vacuum drum drying (VDD). The composition of the tablets based on ASD intermediates or ASD tablet blends is summarized in Table 4.1.

COMPRESSION OF AMORPHOUS SOLID DISPERSIONS PREPARED BY HOT-MELT EXTRUSION, SPRAY DRYING AND VACUUM DRUM DRYING

Table 4.1: Formulation composition of tablets based on ASDs intermediates without outer phase excipients (Tablet (ASD)) and with outer phase excipients (Tablet (Tablet blend))

Ingredients	Functionality	Tablet (ASD)		Tablet (Tablet Blend)	
		[%w/w]	[mg/tablet]	[%w/w]	[mg/tablet]
Inner Phase (ASD)					
Ritonavir	API	15.00	100.0	13.07	100
Copovidone	Carrier Polymer	73.96	493.1	64.42	493.1
Sorbitan monolaurate	Surfactant	10.00	66.7	8.71	66.7
Silicon dioxide*	Glidant	1.04	6.9	0.91	6.9
Outer Phase (OP)					
Dicalcium phosphate anhydrous	Filler	-	-	11.70	89.6
Silicon dioxide	Glidant	-	-	0.90	6.9
Sodium stearyl fumarate	Lubricant	-	-	0.30	2.3
		100.00	666.7	100.00	765.4

*= not used for spray drying and vacuum drum drying; replaced by copovidone

4.6.2.1.1 Hot-melt extrusion (HME)

The extrudate beads were kindly provided as benchmark material from AbbVie Deutschland GmbH & Co. KG (Ludwigshafen, Germany). Hot-melt extrusion was performed on a commercial scale co-rotating twin-screw extruder (ZSK 58, Coperion GmbH, Stuttgart, Germany). The extrudate beads were milled using an impact mill (Fitzmill L1A, Fitzpatrick Company, Sint-Niklaas, Belgium) to result in a defined particle size distribution (PSD) comparable to vacuum drum drying intermediate reducing the impact of PSD on e.g., tabletability. To obtain a VDD-like PSD the extrudate beads were initially milled at different conditions, and the resulting milled extrudates were then blended within a glass bottle using a tumble blender (Turbula blender T2C, Willy A. Bachofen AG Maschinenfabrik, Muttenz, Switzerland) for 3 min at 30 rpm. The milled extrudate contained the following extrudate fractions:

- 45% (w/w) of extrudate milled at 8000 rpm through 508 µm round-hole sieve,
- 45% (w/w) of extrudate milled at 6800 rpm through 838 µm round-hole sieve,
- 10% (w/w) of sieved extrudate fraction of <63 µm.

4.6.2.1.2 Spray drying (SD)

Ritonavir, copovidone and sorbitan monolaurate were dissolved in a mix of acetone and purified water (90:10 w/w) targeting a solid load of 30% (w/w). Water was added as solvent to reduce electrostatic charging of the final powder, and thus, to ensure tabletability. A Büchi B-290 laboratory spray dryer equipped with an Inert Loop B-295 and a dehumidifier B-296 (Büchi Labortechnik GmbH, Essen, Germany) was used. The spray dryer was operated using a two-fluid nozzle including a 2 mm cap. Following spray drying conditions were applied: feed rate of solution 9 g/min, nitrogen spray gas flow 60 mm (corresponding to 742 l/h), aspirator rate 100% (corresponding to a volume flow of about 35 m³/h), inlet temperature 65 °C, and resulting outlet temperature 48 °C.

The SD intermediate was subsequently dried for 48 h under vacuum conditions (approx. 50 mbar) at 40 °C using a vacuum oven (Binder GmbH, Tuttlingen, Germany) to ensure complete removal of residual solvents. The residual solvent content for acetone after post-drying was 2339 ppm determined via gas chromatography and thus, below the ICH limit for acetone (EMA/CHMP/ICH/82260/2006, 2019). The throughput (solid) was approximately 100 g per hour.

4.6.2.1.3 Vacuum drum drying (VDD)

Ritonavir, copovidone and sorbitan monolaurate were dissolved in pure methanol (solid load 45% w/w) to obtain the feed solution for VDD. The process was performed in a vacuum double drum dryer (Buflovak, New York, US) equipped with a liquid preparation vessel (TCC-40, TAIM srl, Atessa, Italy) and a peristaltic pump (Watson Marlow 501RL, Watson Marlow, Rommerskirchen, Germany) for liquid feeding (see Figure 4.1). The process parameters of the VDD process were set as follows: drum and chasing temperature 80 °C at a pressure of 150 mbar, drum rotation speed 0.2 rpm, drum gap 0.3 mm. The dried product was collected and the throughput of the solid was approximately 600–700 g per hour. The VDD intermediate was then milled using a screening mill (Comil U5, Quadro Engineering, Waterloo, Canada) equipped with a 991 µm round-hole sieve. The residual solvent content for methanol determined via gas chromatography was below the practical detection limit (< 500 ppm) and thus, below the ICH limit for residual solvents (< 3000 ppm for methanol) immediately after processing not requiring a further drying step.

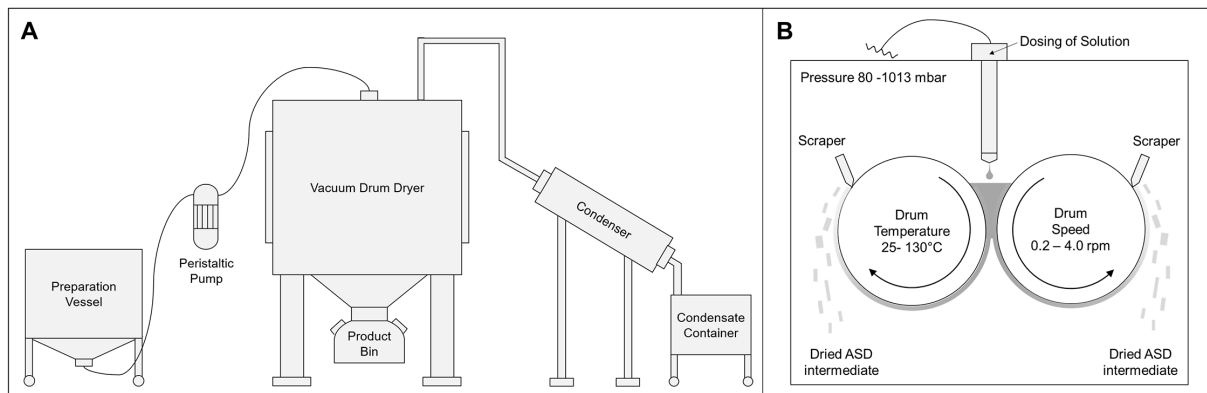


Figure 4.1: A: Schematic overview of vacuum drum drying setup; B: Detailed schematic drawing of vacuum drum drying process including parameter ranges

4.6.2.2 Tablet blend preparation

The ASD intermediates were supplemented with an outer phase consisting of dicalcium phosphate as filler/binder, fumed silicon dioxide as glidant, and sodium stearyl fumarate as lubricant (see Table 4.1) according to the Norvir® formulation. The tablet blends were prepared using a tumble blender (Turbula blender T2C, Willy A. Bachofen AG Maschinenfabrik, Muttenz, Switzerland), and a sieve with 1.0 mm mesh size (Retsch GmbH, Haan, Germany) by the following consecutive steps: (1) pre-blending for 3 min at 30 rpm, (2) sieving manually, (3) main blending for 3 min at 30 rpm. The batch size was 100 g each.

4.6.2.3 Glass transition temperature (T_g) by differential scanning calorimetry (DSC)

Differential Scanning Calorimetry (DSC) measurements were performed using a Mettler-Toledo DSC 1 (Mettler Toledo, Gießen, Germany) equipped with an auto-sampler and a TC100 immersion cooler (Huber Kältemaschinenbau AG, Offenburg, Germany). All DSC samples (ASD intermediates) were scanned at 10 K/min from (-) 20 °C to 150 °C under nitrogen (gas flow 50 ml/min) as open pan method (dry T_g). The results were analyzed with STARE SW (version 16.1) (Mettler Toledo, Gießen, Germany). All samples were measured as duplicates.

4.6.2.4 Bulk/tapped/particle (pycnometric) density

The tapped density tester (Pharmatest Apparatebau AG, Hamburg, Germany) was used to determine bulk and tapped density according to Ph. Eur. 2.9.34 (method 1). Bulk and tapped density were calculated by the mass and bulk volume occupied by the powder filled into a 250 ml graduated cylinder. The samples were measured as triplicates.

Particle (pycnometric) density was determined using a helium pycnometer (AccuPyc 1340, Micromeritics GmbH, Aachen, Germany) equipped with a 10 cm³ sample chamber under following conditions: cycle fill pressure set to 134.45 kPa and equilibration rate set to 0.0345 kPa/min. Purging of the sample chamber was conducted 10 times prior to the measurement. For each analysis 5 cycles were performed. All samples were measured as triplicates.

4.6.2.5 Flowability

ASD intermediates and tablet blends were analyzed regarding their flow properties using a ring shear tester (RST-XS, Dietmar Schulze, Schüttgutmesstechnik, Wolfenbüttel, Germany) equipped with a 31.37 ml cell. Samples were measured at pre-shear normal stresses of 0.250, 0.525, 0.800 and 1 kPa under ambient temperature (approx. 20–22 °C) and humidity (approx. 45–50% RH) in triplicates. Regression analysis was used for data evaluation.

4.6.2.6 Particle size distribution

The particle size distribution of ASD intermediates were analyzed using a laser diffraction particle size analyzer (Mastersizer 3000, Malvern Instruments GmbH, Herrenberg, Germany). For the measurements, 2–5 g of the samples were used in combination with the dry powder disperser module Aero S. The samples were dispersed with 0 bar pressure. Data were analyzed using the Mastersizer 3000 Software (version 3.71) according to the Fraunhofer approximation. Measurements were performed as triplicates and averaged.

4.6.2.7 Specific surface area (SSA)

The specific surface area was determined using the Gemini VII (Micromeritics Instrument Corporation, Norcross, United States). The specific surface area was calculated using single point Brunauer-Emmett-Teller (BET) equation from the adsorption data (Brunauer et al., 1938). The samples were analyzed as duplicates.

4.6.2.8 Loss on drying

Moisture/volatiles content was determined via the loss on drying (LOD) method using a halogen moisture analyzer (HB43-SSD, Mettler-Toledo GmbH, Giessen, Germany). The samples (approximately 5.5.-6.1 g) were heated to 105 °C and held until mass was constant within ±1 mg for 100 s.

4.6.2.9 Scanning electron microscopy

A scanning electron microscope (SEM) (SU-3500, Hitachi High Technologies, Krefeld, Germany) equipped with a secondary electron detector (SE) was used to visualize the ASD particle morphology, the tablet surface and tablet cross section. The backscattered electron detector (BSE) was used to visualize the distribution of dicalcium phosphate on the TB tablet surface. The powder samples were attached on SEM tubes using carbon conductive tabs (Plano, Wetzlar, Germany), the tablets using conductive silver liquid. All samples except for the samples for BSE analysis were platin-sputtered (at 30 mA for 40 s) under vacuum conditions using a Quorum Q150TS Coater (Quorum Technologies Ltd., Laughton, UK) to enhance electrical conductivity. Images of samples were collected at various magnifications by applying an acceleration voltage of 5 or 10 kV.

4.6.2.10 Compression analysis

Tablets ($n = 6$) targeting a mass of 200 mg were compressed on a single punch compression simulator (HB-50, Huxley Bertram Engineering Limited, Cambridge, UK) equipped with 10 mm round, flat face tooling for compression analysis. Five compaction pressures were applied ranging from 50 MPa to 250 MPa simulating a production scale tablet press Fette 3090i (61 stations) at different turret speeds to evaluate speed-dependency at 15 rpm and 80 rpm (according to a linear speed of 0.32 m/s and 1.72 m/s, and a dwell time of 19 ms and 3 ms for Euro B tooling). In addition, compression was simulated at a high turret speed (80 rpm) applying pre-compression prior to main compression to investigate the impact on the tensile strength and thus, tablettability. Pre-compression force was kept constant at 4-5 kN.

For compression analysis the compaction pressure (CP) was calculated from the applied main compression force and cross-sectional area of the punch (Eq. (4.1)).

$$CP = \frac{\text{Main Compression Force [N]}}{\text{Cross - sectional Area [mm}^2\text{]}} \quad (4.1)$$

The tensile strength (TS) is the mechanical strength of a tablet normalized by its dimensions allowing to compare tablets with different geometries. Depending on the tablet geometry different equations are required to calculate the TS of a tablet.

For round, flat tablets the TS was calculated as described in Eq. (4.2) (Fell and Newton, 1970):

$$TS = \frac{2P}{\pi Dt} \quad (4.2)$$

in which P is the breaking force, D is the tablet diameter and t is the tablet thickness.

For convex-faced elongated tablets the calculation for the tensile strength is as follows (Eq. (4.3)) (Pitt and Heasley, 2013):

$$TS = \frac{2}{3} \left(\frac{10 P}{\pi D^2 \left(2.84 \frac{t}{D} - 0.126 \frac{t}{w} + 3.15 \frac{w}{D} + 0.01 \right)} \right) \quad (4.3)$$

in which P is the breaking force, D is the tablet diameter, t is the tablet thickness, and w is the tablet wall height.

Solid fraction (SF) is the apparent density of the tablet (ρ_{app}) divided by particle (pycnometric) density (ρ_{pyc}) of the powder (Eq. (4.4)):

$$SF = \frac{\rho_{app}}{\rho_{pyc}} = \frac{m}{V \rho_{pyc}} \quad (4.4)$$

The apparent density of the tablet (ρ_{app}) was calculated from the tablet weight divided by the volume of the tablet. Depending on the tablet geometry different equations are required. For round, flat tablets the volume is calculated as described in Eq. (4.5):

$$V = \pi t \left(\frac{D}{2} \right)^2 \quad (4.5)$$

For convex-faced elongated tablets (18.0×9.5 mm) following equation (Eq. (4.6)) based on vendor's tooling drawing was used to calculate the volume:

$$V = 146.4 \text{ mm}^2 \times w \times 260 \text{ mm}^3 \quad (4.6)$$

in which w is the tablet wall height.

The calculated parameters were used to create plots to describe and compare the compression behavior. The tabletability plot (TS vs CP) shows the ability of a powder to be transformed into a tablet with a certain tensile strength under the applied compaction pressure. The compactability plot (TS vs SF) describes the ability of a powder to produce tablets of defined tensile strength under densification (Heckel, 1961).

4.6.2.11 Elastic recovery

The total elastic recovery (TER) is calculated as follows (Eq. (4.7)):

$$TER = \frac{t - PS_{min}}{PS_{min}} \times 100 \quad (4.7)$$

in which t is the tablet thickness out-of-die in mm and PS_{min} is the minimal punch separation in mm.

4.6.2.12 Tableting

Tablets ($n = 30$) consisting of either pure ASD intermediates (ASD tablets) or of tablet blends (TB tablets) were manufactured using a single punch compression simulator (HB-50, Huxley Bertram Engineering Limited, Cambridge, UK) equipped with an elongated, biconcave tooling (18.0 × 9.5 mm) (composition see Table 4.1). The TS of the tablets was kept constant for comparison reasons at 1.2–1.3 MPa.

Tablets were characterized regarding tablet weight (analytical balance, Sartorius BP 61 S-0 CE, Sartorius AG, Goettingen, Germany), thickness and diameter (caliper, Hommel Hercules Werkzeughandel GmbH & Co. KG, Viernheim, Germany) and breaking force (Erweka TBH 125, Erweka GmbH, Heusenstamm, Germany).

4.6.2.13 X-ray micro computed tomography (X-ray µCT)

The X-ray micro computed tomography scanner (Rigaku CT Lab GX130, Rigaku Americas Holding Company Inc., The Woodlands, USA) equipped with a tungsten source was used to visualize the internal structure of the tablets. Following conditions were applied for analysis: tube voltage 130 kV, tube current 60 μ A, resolution 50 μ m/pixel (voxel). The collected data were reconstructed using Rigaku software and visualized using Dragonfly software.

4.6.2.14 Friability

Friability was determined according to Ph. Eur. 2.9.7 using a friability tester (PTF 30 ERA +60 ERA, Pharma Test Apparatebau AG, Hainburg, Germany).

4.6.2.15 Disintegration

Disintegration test was performed according to Ph. Eur. 2.9.1 (test setup A) using a disintegration tester (ZT 722, Erweka GmbH, Heusenstamm, Germany).

4.6.2.16 In-vitro dissolution

Dissolution studies were performed using an USP II dissolution tester (paddle method) (Vision Elite 8, Hanson Research, Clatswoeth, US) equipped with an autosampler (AutoPlus Maximizer, Hanson Research, Clatswoeth, US). ASD and TB tablets equivalent to a dosage strength of 100 mg were analyzed (6 replicates). All experiments were performed using 900 ml of 0.06 M polyoxyethylene-10-laurylether in water, at a temperature of $37^{\circ}\text{C} \pm 0.5^{\circ}\text{C}$ for 2.5 h in total and at a paddle speed of 75 rpm. Samples (10 ml) were taken at 6 timepoints (15/30/60/90/120/150 min) filtered through a 10 μ m cannula filter (ultra-high-molecular-weight polyethylene (UHMWPE)).

For quantification, the samples were analyzed by an ultra-pressure liquid chromatography system (Agilent 1290, Agilent Technologies, Waldbronn, Germany) equipped with a variable wavelength ultraviolet (UV) detector and a reversed phase column (Phenomenex Kinetex C18, 50 × 2.1 mm, 1.7 µm, maintained at 60 °C during measurement). As mobile phases 0.1% trifluoroacetic acid (mobile phase A) and 100% acetonitrile (mobile phase B) were used in a gradient elution procedure (time [min]/mobile phase B in %: 0/5, 1.6/95, 2.2/95, 2.21/5, 2.5/5). For the sample preparation a mix of methanol/acetonitrile/0.1% trifluoroacetic acid (1:1:1 V/V%) was used as diluent (dilution factor 2). The injection volume was 5 µl for sampling timepoint 1 and 1 µl for sampling timepoint 2–6. The measurement was performed at 250 nm (bandwidth 4 nm). The retention time of ritonavir was 1.022 min.

To compare dissolution profiles of SD and VDD intermediates with the reference HME, fit factors f_1 and f_2 were calculated (Polli et al., 1997). The difference factor (f_1) calculates the difference between two curves at each time point and displays the relative error (Eq. (4.8)):

$$f_1 = \left\{ \left[\sum_{t=1}^n |R_t - T_t| \right] / \left[\sum_{t=1}^n R_t \right] \right\} \times 100 \quad (4.8)$$

where n is the number of sampling time points during dissolution testing, R_t is the reference dissolved amount of ritonavir in percentage at timepoint t , and T_t is the dissolved amount of ritonavir in percentage of the test material (SD or VDD) at timepoint t .

The similarity factor f_2 is a measurement of similarity between two curves in percentage (FDA_Guidance, 1997) (Eq.(4.9)):

$$f_2 = 50 \times \log \left\{ \left[1 + \frac{1}{n} \sum_{t=1}^n (R_t - T_t)^2 \right]^{-0.5} \times 100 \right\} \quad (4.9)$$

The difference factor (f_1) should be between 0 and 15 and the similarity factor (f_2) between 50 and 100 for curves to be considered as similar (FDA_Guidance, 1997).

4.7 Results

4.7.1 Powder characterization of ASDs and tablet blends (TB)

4.7.1.1 Particle size distribution (PSD), particle morphology and specific surface area (SSA)

Figure 4.2 visualizes the particle size distribution (PSD) and Table 4.2 shows the d_{10} , d_{50} , d_{90} values of the ASD intermediates. Laser diffraction analysis identified a relatively broad PSD for the VDD intermediate exhibiting a d_{50} of 179 μm . As targeted, the milled extrudate could mimic the VDD PSD adequately resulting in a broad PSD range with a d_{50} of 168 μm . For the SD material a large content of fine particles were detected (d_{50} : 45 μm), approximately three times smaller than the d_{50} of the VDD and HME material.

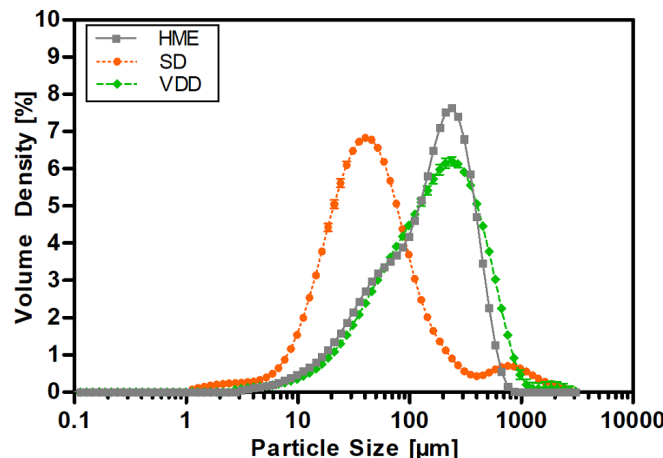


Figure 4.2: Particle size distribution of ASD intermediates determined by laser diffraction

Scanning electron micrographs (SEM) visualizing the particle morphology of the ASD intermediates confirmed the PSD data determined via laser diffraction (see Figure 4.3). The SEM of the milled extrudate showed irregularly shaped particles with a smooth surface in a broad range of particles sizes (Figure 4.3, a1–2). SEM images of the SD intermediate showed intact, whole spheres with diameters of approximately less than 10–50 μm tending to build agglomerates (Figure 4.3, b1–2). The VDD intermediate appeared as thin plate-shaped, flaky, irregular particles with sharp breaking edges (Figure 4.3, c1–2).

The specific surface area (SSA) results of the ASD intermediates are listed in Table 4.2. The SSA of the SD intermediate ($0.401 \text{ m}^2/\text{g}$) was more than three times higher compared to the SSA of the HME ($0.119 \text{ m}^2/\text{g}$) and slightly higher compared to the VDD intermediate ($0.344 \text{ m}^2/\text{g}$).

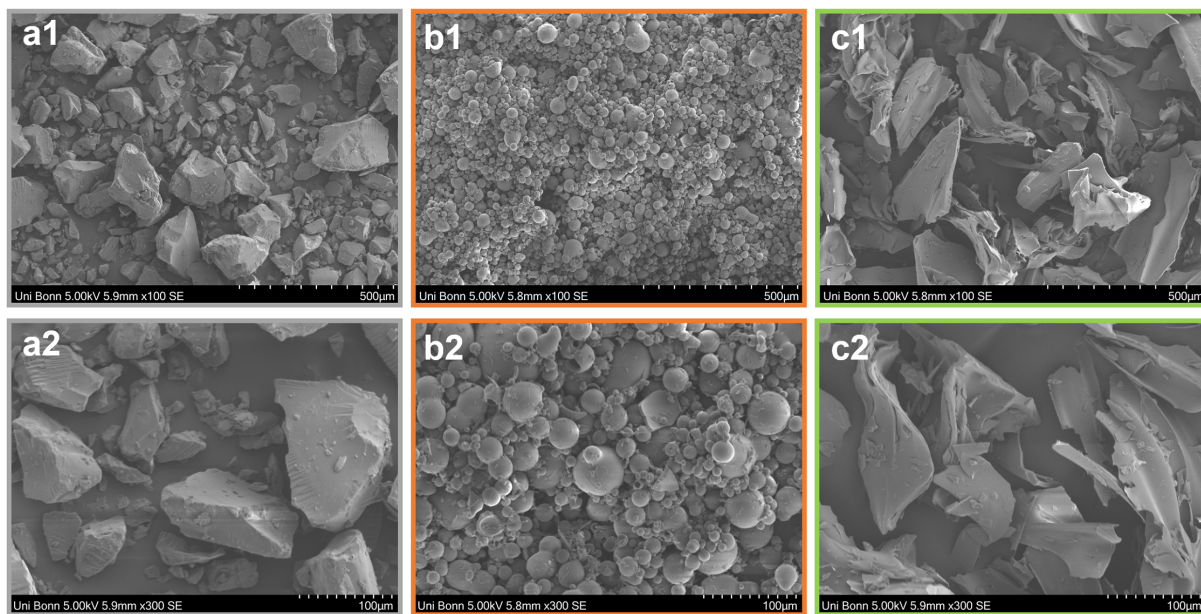


Figure 4.3: Scanning electron micrograph images of ASD intermediates at different magnifications: (a) HME; (b) SD; (c) VDD

4.7.1.2 Densities (bulk/tapped/particle (pycnometric)) and flowability

The results of the densities measurements (bulk, tapped, particle) are summarized in Table 4.2. The particle density values were very similar for all ASD intermediates at around 1.2 g/cm^3 , subsequently for the tablet blends at around 1.3 g/cm^3 .

The bulk density of the milled extrudate (0.604 g/cm^3) was three times higher than for both solvent-evaporation based materials (SD: 0.226 g/cm^3 ; VDD: 0.200 g/cm^3). Despite the similar PSD of HME and VDD, higher bulk density was observed for the HME material, which can be explained by the melting of the components during the process resulting in denser and less porous material. Interestingly, the bulk density of SD and VDD was comparable while showing substantially different PSD. This might be explained by the particle form: hollow spherical particles (SD) vs irregular shaped platelets (VDD).

The addition of outer phase excipients (dicalcium phosphate anhydrous, fumed silicon dioxide, sodium stearyl fumarate) to the ASD intermediates resulted in tablet blends with a slightly lower bulk density value for the HME material (HME TB: 0.576 g/cm^3), and slightly higher bulk density values for the solvent-evaporation technologies (SD TB: 0.317 g/cm^3 ; VDD TB: 0.246 g/cm^3).

Table 4.2 shows the flowability results assessed based on FFC values determined via ring shear testing. The HME intermediate exhibited easy flowing properties (6.84), whereas the

solvent evaporation based ASDs indicated cohesive flow (SD: 2.25; VDD: 3.85). However, the milled VDD intermediate showed a higher FFC value indicating slightly better flowability properties. Notably, a slight increase in FFC at low values between 1 and 4 improves overall processability substantially. The addition of an outer phase to ASDs resulted in tablet blends with FFC values indicating easy flow in all cases (HME: 6.99; SD: 5.64; VDD: 6.92).

4.7.1.3 Loss on drying (LOD)

The LOD values were within a range of 1–2% (see Table 4.2). An increase of LOD values after tablet blend preparation was observed for all materials related to the exposure to ambient humidity during processing.

4.7.1.4 Glass transition temperature (T_g dry)

The glass transition temperatures (T_g dry) of the respective ASD intermediates determined via DSC analysis are summarized in Table 4.2. All T_g values (dry) were in a comparable range at about 67–69 °C. In addition, all cases showed a single T_g value indicating the API to be molecularly dispersed in the polymer (Lin et al., 2018). Moreover, DSC data indicated the absence of drug substance related residual crystallinity in the ASDs.

Table 4.2: Densities, FFC, particle size distribution, specific surface area, glass transition temperature (dry) and loss on drying values of ASDs manufactured by HME, SD and VDD and their respective tablet blends (n.d.= not determined)

Material	Bulk	Tapped	Particle	Specific	FFC	Particle Size Distribution			Loss on	T_g
	Density	Density	Density	Surface Area		d_{10} [μm]	d_{50} [μm]	d_{90} [μm]	Drying	(dry) [°C]
	[g/cm ³]	[g/cm ³]	[g/cm ³]	[m ² /g]					[%]	
ASDs										
HME	0.604 ± 0.009	0.782 ± 0.005	1.201 ± 0.001	0.127 ± 0.011	6.84 ± 0.17 (easy flowing)	32.8 ± 0.41	168.0 ± 1.10	403.0 ± 3.18	1.36	68.2 ± 0.2
SD	0.226 ± 0.009	0.342 ± 0.004	1.196 ± 0.011	0.401 ± 0.010	2.25 ± 0.02 (cohesive flowing)	14.4 ± 0.16	45.3 ± 0.82	188.0 ± 9.38	1.48	67.2 ± 0.2
VDD	0.200 ± 0.001	0.300 ± 0.001	1.194 ± 0.001	0.344 ± 0.000	3.85 ± 0.20 (cohesive flowing)	37.7 ± 0.48	179.0 ± 3.91	530.0 ± 26.6	1.13	68.1 ± 1.3
TBs										
HME	0.576 ± 0.004	0.794 ± 0.008	1.299 ± 0.001	n.d.	6.99 ± 0.43 (easy flowing)		n.d.		2.01	n.d.
SD	0.317 ± 0.007	0.447 ± 0.003	1.293 ± 0.004	n.d.	5.64 ± 0.26 (easy flowing)		n.d.		1.56	n.d.
VDD	0.246 ± 0.000	0.352 ± 0.001	1.299 ± 0.003	n.d.	6.92 ± 0.71 (easy flowing)		n.d.		1.92	n.d.

Table 4.3: Results of tablet characterization (elongated, biconcave tooling, 18.0x9.5 mm) – ASD and TB tablets

Tablets	Friability	Disintegration Time	Dissolution (ritonavir dissolved) [%]								
			[%]	[min]	15 min	30min	60 min	90 min	120 min	150 min	f_1
ASDs											
HME	0.04	24.2 ± 3.1		49.35 ± 2.75	77.13 ± 2.13	91.26 ± 1.18	91.63 ± 1.21	91.57 ± 1.03	93.76 ± 0.64		Reference
SD	0.03	29.7 ± 5.2		44.48 ± 2.76	66.44 ± 4.10	90.51 ± 1.71	94.59 ± 1.66	94.28 ± 2.05	95.83 ± 0.99	4.86	65.51
VDD	0.07	28.7 ± 5.0		37.21 ± 4.21	60.60 ± 9.39	88.10 ± 5.82	94.95 ± 1.78	94.81 ± 1.57	95.36 ± 1.85	8.08	54.83
TBs											
HME	0.11	31.7 ± 5.9		27.99 ± 0.92	47.64 ± 1.54	79.15 ± 1.31	89.58 ± 1.56	91.39 ± 0.93	93.34 ± 0.31		Reference
SD	0.08	35.8 ± 2.2		40.65 ± 3.93	65.44 ± 4.95	92.83 ± 2.55	95.11 ± 0.78	95.53 ± 1.26	95.27 ± 1.91	13.04	50.34
VDD	0.00	30.2 ± 6.1		36.68 ± 1.09	57.98 ± 0.69	88.38 ± 1.80	90.78 ± 1.99	91.69 ± 1.84	92.66 ± 1.31	7.12	60.10

4.7.2 Compression analysis

4.7.2.1 Tablettability (out-of-die)

Figure 4.4 shows the tabletability plots (TS vs CP). The SD material showed unfavorable powder properties such as electrostatic charging (see section 4.7.1). Consequently, the die had to be filled manually including unavoidable slightly pre-densification of the powder. Furthermore, simulating the rotary press Fette 3090i at 80 rpm resulted in tablets showing strong capping and/or lamination, which made it impossible to measure tablet dimensions or to determine tablet hardness (see Figure 4.4 B). Thus, direct compression of SD intermediate is not feasible in terms of manufacturability.

However, focusing on the ability of the SD powder to be transformed into a tablet not taking the manufacturability into account, the SD intermediate showed the highest mechanical strength at 15 rpm (TS: 3.6 MPa, see Figure 4.4 A) and 80 rpm (TS: 3.2 MPa, see Figure 4.4 B) at an applied pre-compression force of 5 kN. Although the weight was kept constant ($200 \text{ mg} \pm 10 \text{ mg}$) for compression analysis, the variability of the results for the SD material (both ASD and TB) was high. The maximum TS of the VDD intermediate (TS: 1.6 MPa) was more than twice lower compared to SD. The HME based intermediate resulted in a maximum TS of about 1.5 MPa and thus, similar to the VDD material.

The tabletability plots of the respective tablet blends (see Figure 4.4 C + D) showed a shift to higher TSs compared to the pure ASD intermediates. The maximum tensile strength at 15 rpm turret speed for the SD TB was 6.97 MPa, for VDD TB 5.01 MPa, and for HME 3.83 MPa. Moreover, a slight speed dependency could be observed for all ASD intermediates leading to a reduced TS (see Figure 4.4 B+ D). The strongest impact was observed in case of the SD intermediate leading to strong capping and lamination. Applying pre-compression force affected the solvent-evaporation based ASDs, and respective TBs leading to increased TSs, whereas HME was less affected.

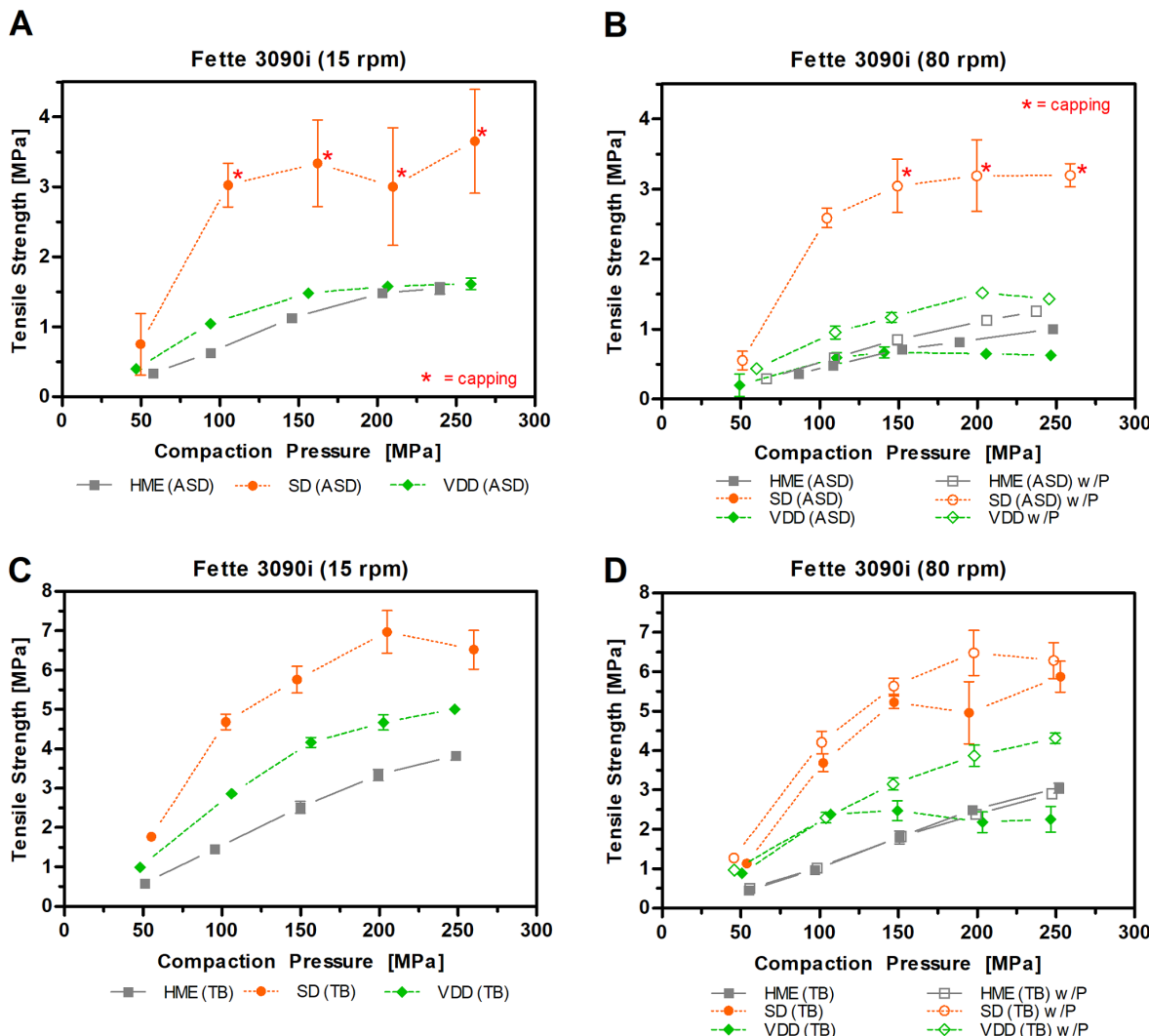


Figure 4.4: Tableability plots: (A, B) ASD tablets; (C, D) TB tablets; (A, C) simulating Fette3090i at 15 rpm; (B, D) simulating Fette3090i at 80 rpm, without and with applied pre-compression force of 4-5 kN (w/P). Note: SD ASD was manually fed into the die for compression analysis. SD ASD at 80 rpm: not feasible

4.7.2.2 Compactability (out-of-die)

Figure 4.5 summarizes the compactability plots (TS vs SF) for ASD intermediates (A, B) and tablet blends (TBs) (C, D). The SD intermediate resulted in tablets with low SF values even at high TSs corresponding to high porosity (see Figure 4.5 A). In addition, a maximum SF of about 0.89 could be identified even at increasing compaction pressures without increase in TS related to elastic deformation. Tablets based on HME intermediate exhibited the highest SF values (0.95), whereas the VDD intermediate resulted in SF values slightly lower compared to the HME intermediate. Overall, the addition of an outer phase to the ASD intermediates reduced the maximum achievable SF value. However, the data showed that high TS values could be reached at even lower SF values. Consequently, stronger compacts with higher

porosity were produced. Higher maximum SF values for the SD TB tablets were noticed compared to the SD ASD tablets.

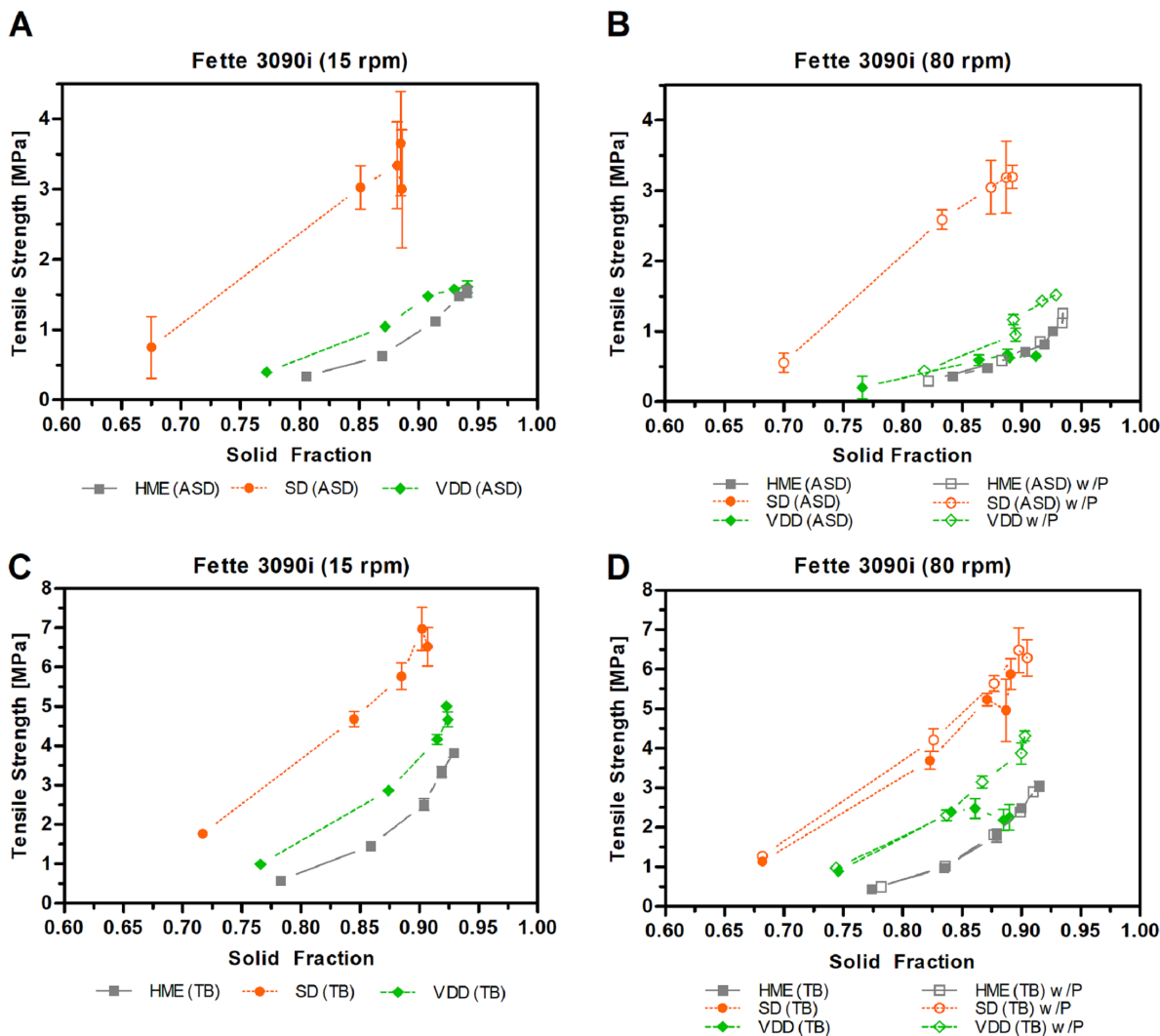


Figure 4.5: Compactability plots: (A, B) ASD tablets; (C, D) TB tablets; (A, C) simulating Fette3090i at 15 rpm; (B, D) simulating Fette3090i at 80 rpm without and with applied pre-compression force (w/P). Note: SD ASD was manually fed into the die for compression analysis. SD ASD at 80 rpm: not feasible

Increasing the turret speed caused slight decrease in maximum SF for all ASD intermediates and TBs explicable by the shortened dwell time increasing elastic deformation. However, applying pre-compression force levelled the effect (see Figure 4.5 B + D) by increasing dwell time indirectly and by allowing the powder to rearrange within the die.

Compressibility plots are visualized in Appendix A supplementary data (see section 4.12, Figure 4.S1).

4.7.2.3 Elastic recovery

Figure 4.6 shows the total elastic recovery (TER) of ASD and TB tablets. The TER values raised with increasing compaction pressures in all cases. Comparing ASD based tablets, the SD tablets showed the highest TER values at 15 rpm. The TER values for the HME tablets were lower, whereas the VDD intermediate showed slightly higher TER values compared to the HME intermediate. In addition, with increasing turret speed from 15 to 80 rpm, the TER values increased for all ASD and TB tablets. By adding dicalcium phosphate, all TER values decreased, as well as by applying pre-compression force.

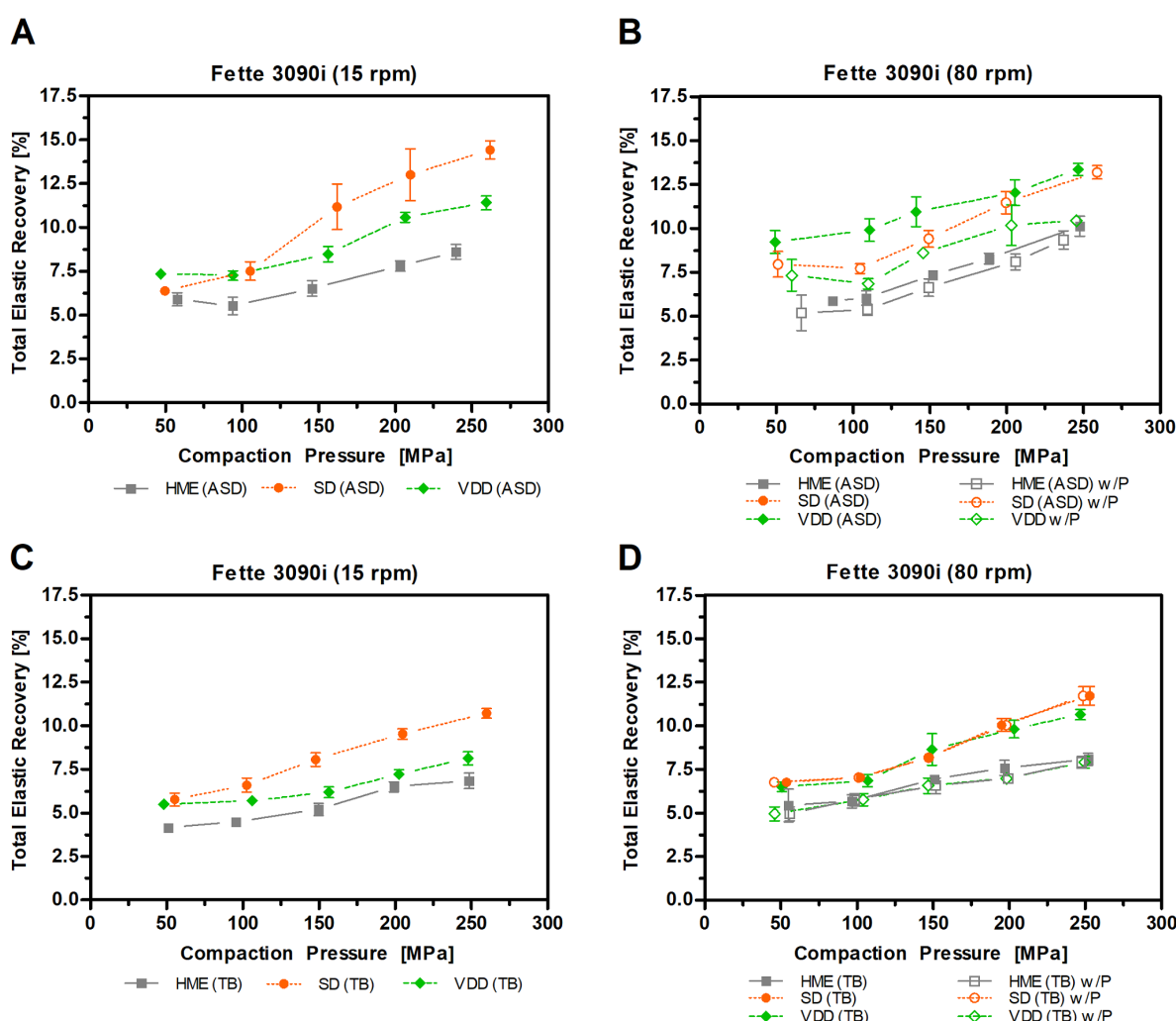


Figure 4.6: Total elastic recovery: (A, B) ASD tablets; (C, D) TB tablets; (A, C) simulating Fette3090i at 15 rpm; (B, D) simulating Fette3090i at 80 rpm without and with applied pre-compression force (w/P). Note: SD ASD was manually fed into the die for compression analysis. SD ASD at 80 rpm: not feasible

4.7.3 Tablet characterization

4.7.3.1 Tablet manufacture

Elongated, biconvex tablets out of ASD and TB were successfully manufactured targeting a dosage strength of 100 mg ritonavir, respectively (Table 4.4). The aimed common tensile strength of 1.2–1.3 MPa was achieved in all cases. However, the required compaction pressure (CP) values varied depending on the ASD origin: pure HME required the highest CP (283.40 MPa) followed by VDD (127.47 MPa) and SD (69.56 MPa). The total elastic recovery (TER) data were in accordance with the CP values: HME (67.58%) > VDD (30.03%) > SD (15.29%). Regarding tablet porosity, the HME tablets showed the highest SF values (0.97) and the SD ones the lowest (0.80). The VDD tablets were in between with a SF value of 0.93.

The same trends for CF, SF and TER were observed for the TB tablets, although showing substantial lower values generally.

Table 4.4: Results of the tablet manufacture (elongated, biconcave tooling, 18.0 x 9.5 mm) – ASD and TB tablets

Tablets	Weight [mg]	Compaction Pressure [MPa]	Tensile Strength [MPa]	Solid fraction	Total Elastic Recovery [%]
ASDs					
HME	671.2 ± 4.5	283.40 ± 9.43	1.23 ± 0.00	0.97 ± 0.00	67.58 ± 2.24
SD	664.9 ± 4.1	69.56 ± 1.44	1.33 ± 0.06	0.80 ± 0.00	15.29 ± 0.59
VDD	661.4 ± 7.9	127.47 ± 8.77	1.29 ± 0.02	0.93 ± 0.01	30.03 ± 1.41
TBs					
HME	763.3 ± 4.0	93.94 ± 2.61	1.28 ± 0.09	0.89 ± 0.00	18.78 ± 0.56
SD	761.2 ± 4.3	57.54 ± 0.97	1.29 ± 0.09	0.75 ± 0.00	12.89 ± 0.38
VDD	768.1 ± 3.0	67.64 ± 2.89	1.26 ± 0.02	0.84 ± 0.00	14.67 ± 0.72

4.7.3.2 Tablet morphology

The grey scale in the X-ray µCT images is related to the density and the average atomic number of components within the tablet: high density areas are brighter compared to low density areas (e.g., voids) (Neilly et al., 2020). Representative X-ray µCT images show radial and axial cross sections of the tablet midsection for ASD tablets (Figure 4.7) and TB tablets (Figure 4.8). ASD tablets revealed differences regarding the occurrence of voids: HME tablets (Figure 4.7 a1) showed more voids compared to SD (Figure 4.7 b1) and VDD tablets (Figure 4.7 c1). Moreover, only small voids could be observed within the SD tablet. The axial cross section images revealed cracks within all ASD tablets (Figure 4.7 a2, b2, c2). However,

tablet defects were not observed for the TB tablets (Figure 4.8). Overall, the X-ray µCT images of the TB tablets were darker compared to the ASD tablet images, since the high-dense dicalcium phosphate appeared very bright. Dicalcium phosphate seemed to be homogenously distributed within the HME and SD TB tablets. Whereas the filler within the VDD TB tablet seemed to be less homogenously distributed.

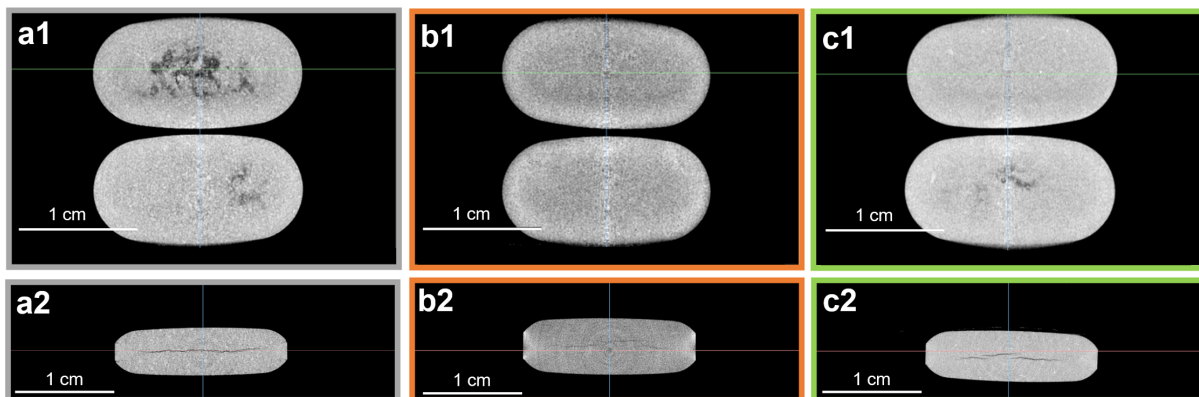


Figure 4.7: X-ray µCT images ((1) radial; (2) axial cross section) of ASD tablets: (a) HME; (b) SD; (c) VDD

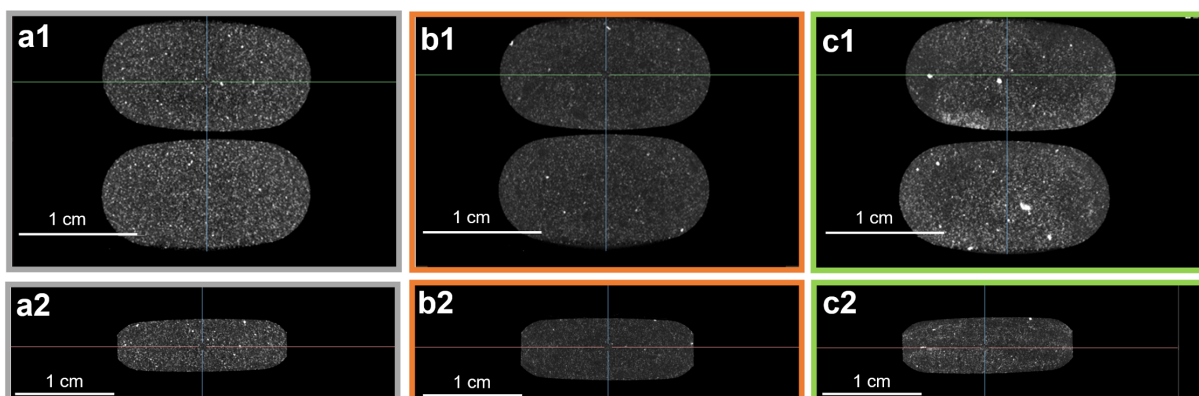


Figure 4.8: X-ray µCT images ((1) radial; (2) axial cross section) of TB tablets: (a) HME; (b) SD; (c) VDD

Figure 4.9 shows the SEM images of the tablet surface of the ASD tablets. The SD ASD tablet (Figure 4.9 b) showed the smoothest surface followed by HME ASD tablet (Figure 4.9 a). Slightly higher degree in unevenness could be observed for the VDD ASD tablet related to particle shape (Figure 4.9 c). The spherical particles of the SD intermediate were still visible on the smooth tablet surface (Figure 4.9 b). However, the SD tablets clearly showed large cracks on the surface across the intact particles. The tablet surfaces of the TB tablets visualizing the dicalcium phosphate distribution are shown in Figure 4.10. The filler distribution on the surface of the HME and VDD TBs tablets appeared homogenous. Whereas for the SD TB tablets the surface seemed to be predominantly covered with SD intermediate particles.

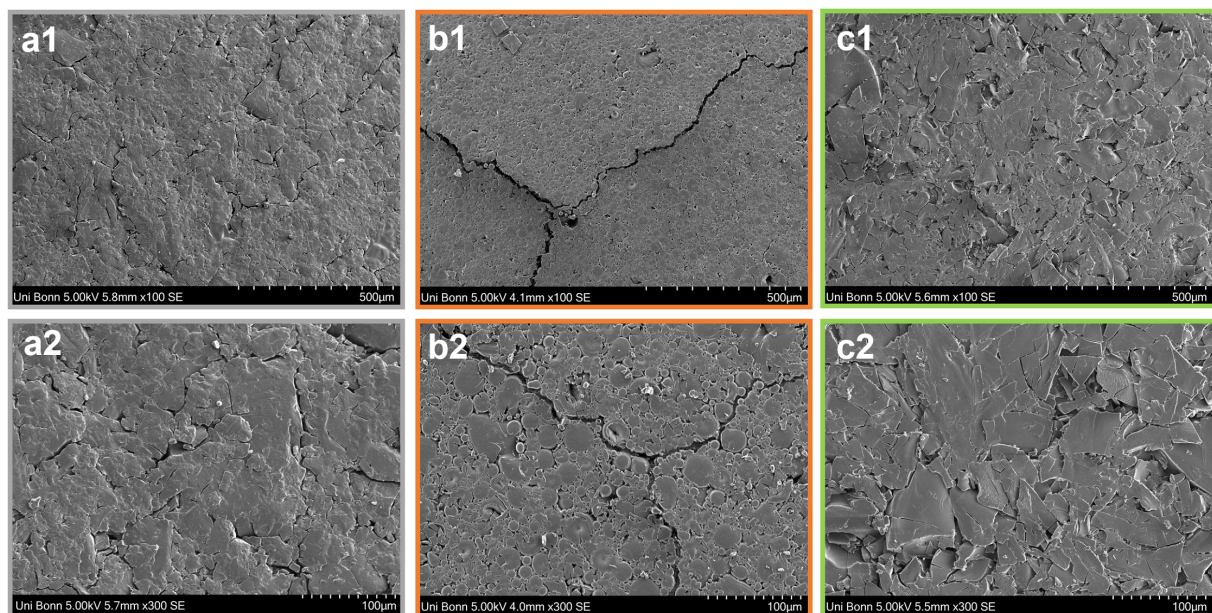


Figure 4.9: Scanning electron micrograph images of tablet surface of ASD tablets (at magnification 100x (1), 300x (2)): (a) HME, (b) SD and (c) VDD

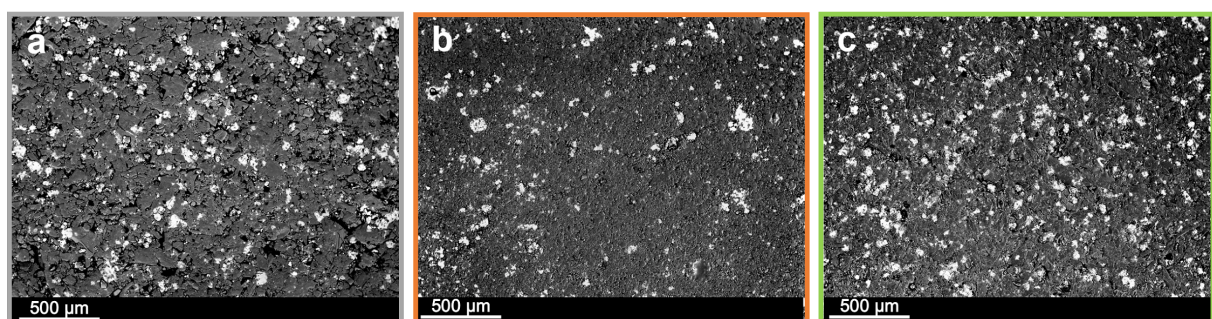


Figure 4.10: Scanning electron micrograph images of tablet surface of TB tablets: (a) HME, (b) SD and (c) VDD

Figure 4.11 (ASD tablets: a1, b1, c1 and TB tablets: A1, B1, C1) visualizes the SEM images of the respective tablet cross sections. The SEM image of the SD intermediate and SD TB cross section (Figure 4.11 b1 and B1) showed mainly intact spheres still present after compression. Interestingly, the wall of the SD spheres seemed to be relatively thick as shown in open, broken spheres. In contrast, the SEM images of the HME intermediate (Figure 4.11 a1, A1) revealed compact material without clear edges of particles. For the VDD intermediate (Figure 4.11 c1, C1) the platelet-shaped particles were still visible. However, the particles led to a coherent compact.

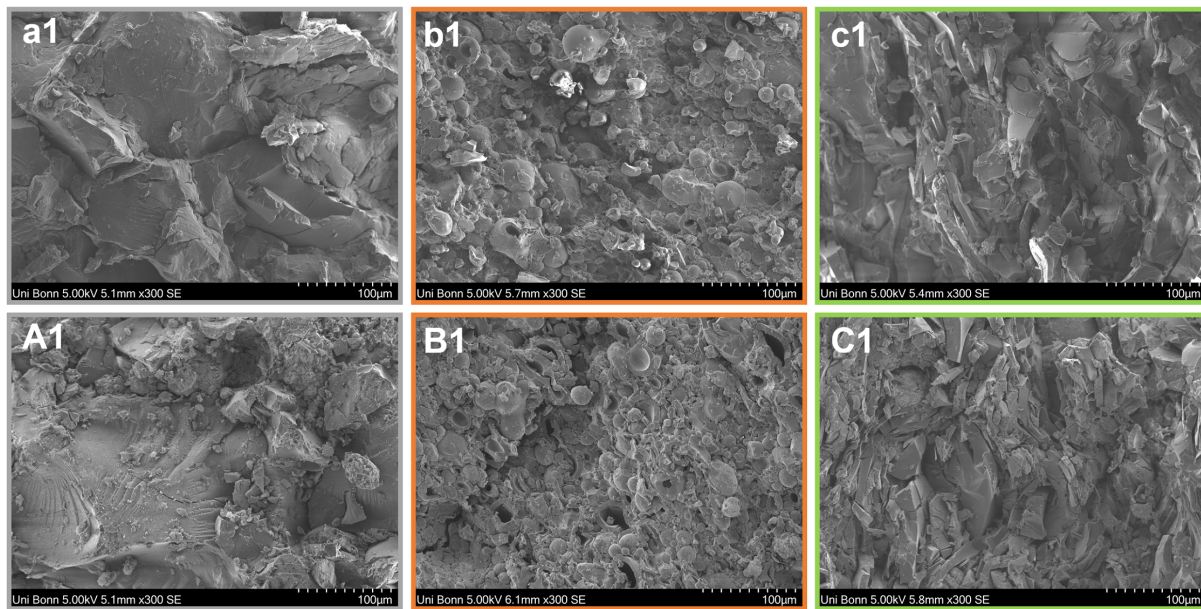


Figure 4.11: Scanning electron micrograph images of tablet cross-section of ASD tablets (a1) HME (b1) SD and (c1) VDD and of TB tablets (A1) HME (B1) SD and (C1) VDD

4.7.3.3 Friability

Table 4.3 shows the friability results of ASD and TB tablets. The friability results ranged from 0.01% to 0.11% fulfilling the criterion of the European Pharmacopoeia (Ph. Eur. (pharmacopoeia) 2.9.7), which states friability below 1% as acceptable.

4.7.3.4 Disintegration and in-vitro dissolution

Figure 4.12 shows the results of the disintegration test. The ASD tablets of similar tensile strength (1.2–1.3 MPa) disintegrated slightly faster (24–30 min) than the TB tablets of similar tensile strength (30–36 min), both showing erosion behavior. The statistical significance of the difference between the analyzed tablets was assessed using a one-way analysis of variance (ANOVA) (assumed significance level $\alpha = 0.05$). It can be assumed that the ASD manufacturing technology did not impact the tablet disintegration, because a p-value of 0.12 for ASD tablets and 0.19 for TB tablets revealed no significant difference in disintegration time.

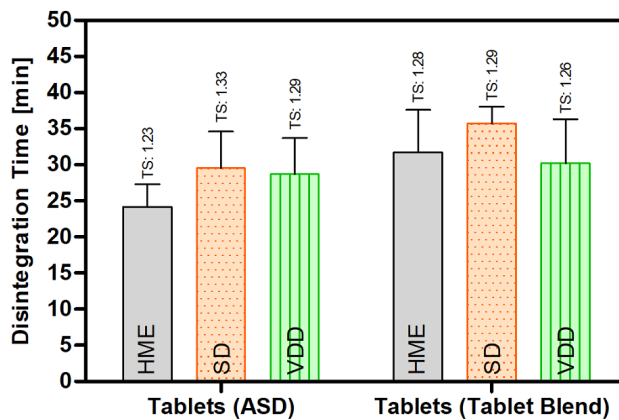


Figure 4.12: Disintegration time of tablets consisting of pure ASDs (ASD tablets) and tablets consisting of ASD containing tablet blends (TB tablets) ($n=6$, TS= tensile strength)

Figure 4.13 shows the dissolution profiles of ASD tablets (A) and TB tablets (B). In agreement with the disintegration results (see Figure 4.12), a slightly slower drug dissolution onset was observed for the TB tablets. However, all tablets showed complete drug dissolution after 120 min. Fit factors (difference factor f_1 and similarity factor f_2) were calculated to assess similarity between dissolution profiles SD and VDD in comparison to HME as reference (see Table 4.3). ASD tablets showed f_1 values between 0 and 15 (SD: 4.86; VDD: 8.08) and f_2 values between 50 and 100 (SD: 65.51; VDD: 54.83). Consequently, the dissolution profiles could be stated as similar according to the FDA guidance (FDA_Guidance, 1997). The results for the TB tablets revealed similarity for the dissolution profiles as well (f_1 values: 13.04 (SD), 7.12 (VDD); f_2 values: 50.34 (SD), 60.10 (VDD)).

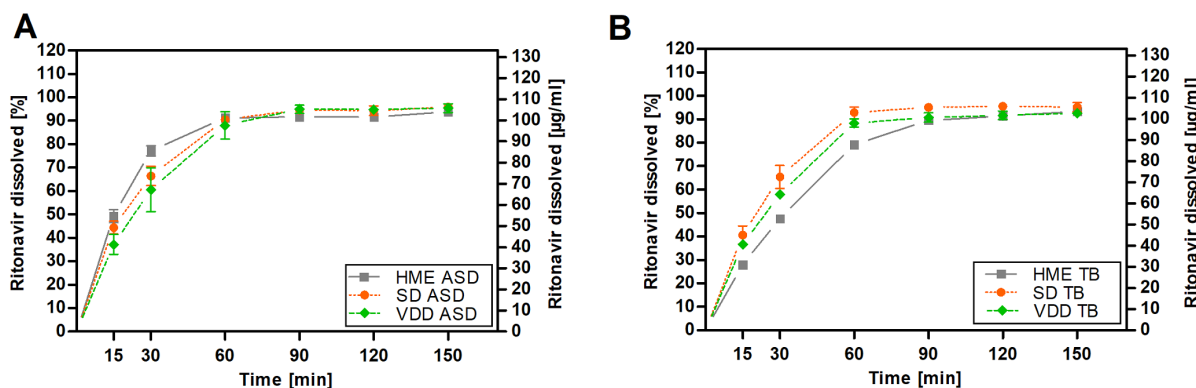


Figure 4.13: Dissolution profiles of (A) ASD tablets and (B) TB tablets using USP II paddle method at 75 rpm and non-sink conditions in 900 ml 0.06 M polyoxyethylene-10-laurylether ($37^{\circ}\text{C} \pm 0.5^{\circ}\text{C}$) ($n=6$)

4.8 Discussion

4.8.1 Powder characterization ASDs and tablet blends (TB)

The powder characterization of ASDs revealed differences in particle morphology and related powder properties based on the ASD manufacturing technology (Table 4.2). The milled extrudate is characterized by easy flowing properties, and a high bulk density value leading to an excellent downstream processability (Davis et al., 2018). Both, SD and VDD, showed cohesive flow and an essentially lower bulk density related to the porosity build into the material during solvent evaporation. The SD material tended to agglomerate and showed electrostatic charging both related to the high number of fines resulting in very poor flow despite the favorable spherical particle shape. In addition, the SSA of the SD intermediate was higher compared to HME, which is well-known from literature (Agrawal et al., 2013). Whereas the cohesive flow for the VDD material was expected based on the irregular particle shape (platelets) (Figure 4.3 c). Notably, the PSD of the VDD intermediate can be influenced by milling parameters (e.g., screen size, speed) offering the opportunity to design powder properties.

In general, observed differences could be compensated by adding outer phase excipients (filler, glidant, lubricant) and thus, no pronounced difference in terms of flowability could be observed enabling further downstream processing of tablet formulations.

The increased bulk density of the SD and VDD TBs can be explained by the addition of approx. 11.7% (w/w) dicalcium phosphate exhibiting a high bulk density itself. Furthermore, the addition of fumed silicon dioxide as glidant reduced the interparticular friction and decreased surface charge both beneficial for better flow and thus, higher bulk density (Gold et al., 1966; Tran et al., 2019; Varthalis and Pilpel, 1977). The already favorable particle shape, size, and density of the milled extrudate was not improved by the addition of an outer phase.

4.8.2 Compression analysis

The compression analysis revealed differences in compression behavior of the ASD intermediates with respect to the manufacturing technology used (see Figure 4.4, Figure 4.5 and Figure 4.6). The particle morphology (SSA, PSD, porosity, particle shape) seemed to be crucial independently from the ASD manufacturing technology category (fusion-based vs solvent-based). Moreover, no T_g related differences could be observed as T_g was similar for all ASDs (67–69 °C, Table 4.2).

The higher the SSA, the higher the bonding area increasing the mechanical strength of the compacts. Consequently, the SD intermediate showing higher SSA values and high amount of fine spherical particles produced stronger compacts compared to VDD and HME at similar compaction pressures in the present study, which was also reported for itraconazole containing ASDs in literature (Davis et al., 2018, Olsson and Nyström, 2001). Comparing HME and VDD, the SSA for VDD was higher despite the widely comparable PSDs. Hence, the VDD material showed a higher degree of inner porosity, which was underlined by the bulk density results and could be explained by the manufacturing process itself. Melting the components during hot-melt extrusion combined with applying vacuum ended up in a compact and dense material without air entrapment, whereas the VDD material got perforated during the VDD process due to solvent evaporation resulting in higher SSA and higher degree of inner porosity. Thus, the VDD material showed better tabletability resulting in stronger compacts compared to HME.

The thin irregular-shaped platelets of the VDD intermediate might behave anisotropically during compression in contrast to the rather isotropic, spherical HME particles. This assumption could be underlined by the TER values, which were higher for the VDD material in contrast to HME. In addition, the VDD material might fragment more easily compared to the compact, high-dense HME gravel-like particles due to the high inner porosity of the VDD material, increasing the bonding area under compression leading to higher TS values. In contrast to HME and VDD material, the SD particles were hollow, spherical particles exhibiting thick walls as shown in the SEM images (Figure 4.2 and Figure 4.11). These gas-filled hollow spheres were exhibiting a high fraction of elastic deformation, which was spontaneously released after ejection of the tablet resulting in tablet defects such as capping. The high degree in elastic recovery was confirmed by TER values (when compared at identical compaction pressure).

Moreover, slight speed dependency in tabletability could be observed for all ASDs independent of the ASD origin, which is likely related to viscoelastic deformation based on high amount of polymer in the formulation (74% w/w).

Applying pre-compression prior to main compression increased TSs of the VDD tablets while enabling tablet processing for the SD intermediate. The impact on HME tablets was less pronounced. In addition, pre-compression force seemed to expand the design space of the compression speed applicable for solvent-based ASD intermediates increasing the throughput.

Overall, the addition of an outer phase improved tablet processing by enhancing flowability and tabletability. Exemplarily, the SD TB could be filled automatically resulting in tablets without defects. Moreover, stronger compacts were achieved in all cases at comparable compaction pressure values showing less total elastic recovery.

4.8.3 Tablet characterization

Elongated, biconvex tablets (18.0×9.5 mm) with a dosage strength of 100 mg showed differences in required compaction pressures to reach at target TS of 1.2–1.3 MPa, as well as differences in resulting SF and TER values (Table 4.4). The trend in required compaction pressures was in accordance with the compression analysis data (e.g., tabletability plots see Figure 4.4). However, higher CP values and higher TER values for the ASD tablets were observed indicating over-compression, which is known to result in high elastic recovery and thus, in tablet defects as confirmed via μ CT (Figure 4.7) and SEM images (Figure 4.9). These observations differing from the compression analysis data might be related to the tooling (elongated tooling vs round biplane). As expected, voids could be found in the middle part of the tablets, since the relative density of the tablet is known to be lower in the tablet center for biconvex tablets (Diarra et al., 2015; Eiliazadeh et al., 2003). This effect can be explained by die wall friction enhanced in absence of lubricant in the ASD tablet. Therefore, laminar movement of particles was hindered by wall friction resulting in density distribution differences. Eiliazadeh et al. (2003) observed increasing elastic recovery with increasing density distribution differences between edge and center of the tablet. The present study confirmed this observation. In addition, the μ CT images (axial cross section, Figure 4.7) revealed cracks within all ASD tablets. These cracks might be related to elastic recovery based on density differences as described above and/or to air entrapment phenomena. Mazel et al. (2015) stated that air entrapment could lead to lamination and cracks and that the lamination tendency increases with increasing tablet thickness, compression speed and compaction pressure.

Moreover, for the ASD tablets, the interparticle bonding might not accommodate the elastic recovery at such high compaction pressures to achieve a common tensile strength of 1.2-1.3 MPa resulting in overcompression. Once the compaction pressure is removed, the elastic relaxation induced the bonds to break, diminishing the tensile strength. To reduce the probability of micro-cracking related to elastic recovery, a tapered die could be used allowing the tablet to expand radially (Garner et al., 2014). Furthermore, applying pre-compression force or changing the tooling geometry to a tooling with less curvature could be beneficial to avoid

lamination as well as increasing the dwell time by reducing tabletting speed or changing the punch head configuration (Euro-B to Euro-D).

However, cracks/lamination as well as large voids were not observed for the TB tablets (Figure 4.8 and Figure 4.10). Obviously, the addition of the filler dicalcium phosphate anhydrous increased the interparticle bonding leading to lower required compaction pressures and thus, less elastic recovery. Moreover, the selection of a brittle filler was beneficial to reduce elastic recovery since brittle fillers themselves show no to minimum elastic recovery. The addition of lubricant also reduced the die wall friction allowing particle movement during compression, which is beneficial especially for convex faced tooling. At the same time, the brittle material dicalcium phosphate anhydrous would balance potential lubricant sensitivity of the non-brittle and potentially lubricant sensitive ASD material.

Interestingly, SD ASD tablets exhibited the lowest SF values (Table 4.4) and thus, the highest porosity, despite without visible larger voids in the μ CT images (Figure 4.7b). This observation can be explained by the SEM images of the tablet cross-sections: the hollow spherical SD particles remained mostly intact after compression exhibiting elastic deformation similar to a tennis ball. This phenomenon can be explained by the relatively thick walls of the SD hollows (Figure 4.11b) in combination with entrapped air within the spherical particles. This consequently resulted in tablets of reduced density compared to HME tablets.

The distribution of the filler on the surface of the HME and VDD TBs tablets appeared homogenous (Figure 4.10). Whereas for the SD TB tablets the surface seemed to be predominantly covered with SD intermediate particles probably due to the electrostatic charging of the fine SD particles of low density (Figure 4.2). However, the X-ray μ CT images (Figure 4.8) of the cross-section within the middle of the tablet revealed a homogenous distribution of the filler within the SD tablet.

Despite the differences in powder and tablet morphology the present study indicates no pronounced differences in tablet performance with respect to friability, disintegration, and dissolution (Table 4.3) when compressed to similar TSs (1.2–1.3 MPa). In agreement with the disintegration data, the dissolution profiles showed slightly slower drug dissolution onset for the TB tablets, which might be related to the addition of the water-insoluble dicalcium phosphate as filler, and to the absence of voids/cracks within TB tablets hindering water to penetrate the tablets. In accordance with the present study, Indulkar et al. (2019) demonstrated complete drug release for ritonavir/copovidone containing ASD tablets at a drug load below 25% within 30 min. In addition, an initial lag time was observed comparable to the present

dissolution profiles. Moreover, the SD and VDD TB tablets showed a slightly faster onset compared to the HME TB tablets, which might be related to the lower relative density (low SF values) of the tablets and thus, higher porosity (Table 4.4). The tablets were slightly floating above the vessel bottom compared to the HME based tablets. Consequently, the SD and VDD tablets surfaces were all over in contact with the dissolution medium. However, at the end of dissolution testing no difference could be observed.

4.9 Conclusion

The present study revealed differences in powder properties as well as in compression behavior of ASD intermediates in dependence of the manufacturing technology (HME, SD, VDD) despite the similar solid state. Thus, the solid state of an ASD might not be exclusively determining for the downstream processability and compression behavior in the respective case. Indeed, those differences in material properties could be linked to particle morphology, as the solid state was quite similar in terms of T_g . The HME ASD consisting of large particles of high particle density showed superior powder flow and bulk density while exhibiting less favorable compression behavior such as lower overall tabletability and the need of high compaction pressures to reach sufficient TS values. In contrast, the SD material consisting of fine, hollow-spherical particles showed cohesive flow and electrostatic charging while exhibiting the best tabletability at worst manufacturability (high degree in tablet defects, e.g., capping). Interestingly, the VDD intermediate showed acceptable flow at comparable low bulk density, while exhibiting good tabletability and manufacturability. By adding the brittle filler dicalcium phosphate anhydrous in the outer phase to the ASD intermediates, the described differences were diminished.

Tablet performance such as disintegration and dissolution indicated no quality related differences between tablets consisting of either ASDs alone or tablet blends. Thus, the decision on the appropriate technology for a respective compound could be made individually based on the physico-chemical properties of the compound (e.g., chemical stability, melting point, solubility in solvents) or based on business-related aspects such as inhouse scale-up options. In the current case, HME can be stated as technology of choice for the respective formulation considering economic (e.g., high throughputs) and environmental aspects (e.g., no solvents used) next to material properties and compression behavior. Thus, it is no surprise that the ASD formulation studied here is commercially manufactured via hot-melt extrusion (Norvir® Tablet). However, comparing both solvent-evaporation based technologies the VDD showed benefits, which should be considered: residual solvents amount within limits even

without second drying step, higher solid loads feasible to be processed due to less viscosity limitations (45% w/w compared to 30% w/w) as shown in the applications of the food industry and thus, lower solvent consumption. In addition, an ASD via VDD showed direct tabletability for the present formulation offering a broader process window for tabletting speed resulting in higher throughputs. Thus, presumably eliminating process steps while requiring lower overall footprint in production scale makes the VDD cost-effective and attractive for the pharmaceutical industry.

Indeed, further experiments using the new technology vacuum drum drying should be considered in future to increase process understanding by assessing the interplay between process parameters and critical quality attributes in more detail.

4.10 Declaration of competing interest

Barbara V. Schönfeld and Ulrich Westedt are employees of AbbVie and may own AbbVie stock. Barbara V. Schönfeld is a PhD student and Karl G. Wagner is a professor at the University of Bonn. They have no additional conflicts of interest to report.

4.11 Acknowledgments & Funding

The authors kindly thank Thilo Faber (University of Bonn) for his technical assistance in scanning electron microscopy, John Roth (AbbVie Inc. North Chicago USA) for X-ray µCT analysis support and Andrew Vogt (AbbVie Inc. North Chicago USA) for specific surface area analysis support.

This work was funded by AbbVie Deutschland GmbH & Co. KG. University of Bonn and AbbVie participated study design, research, interpretation of data, writing, data collection, analysis, reviewing, and approving the publication.

4.12 Appendix A. Supplementary data

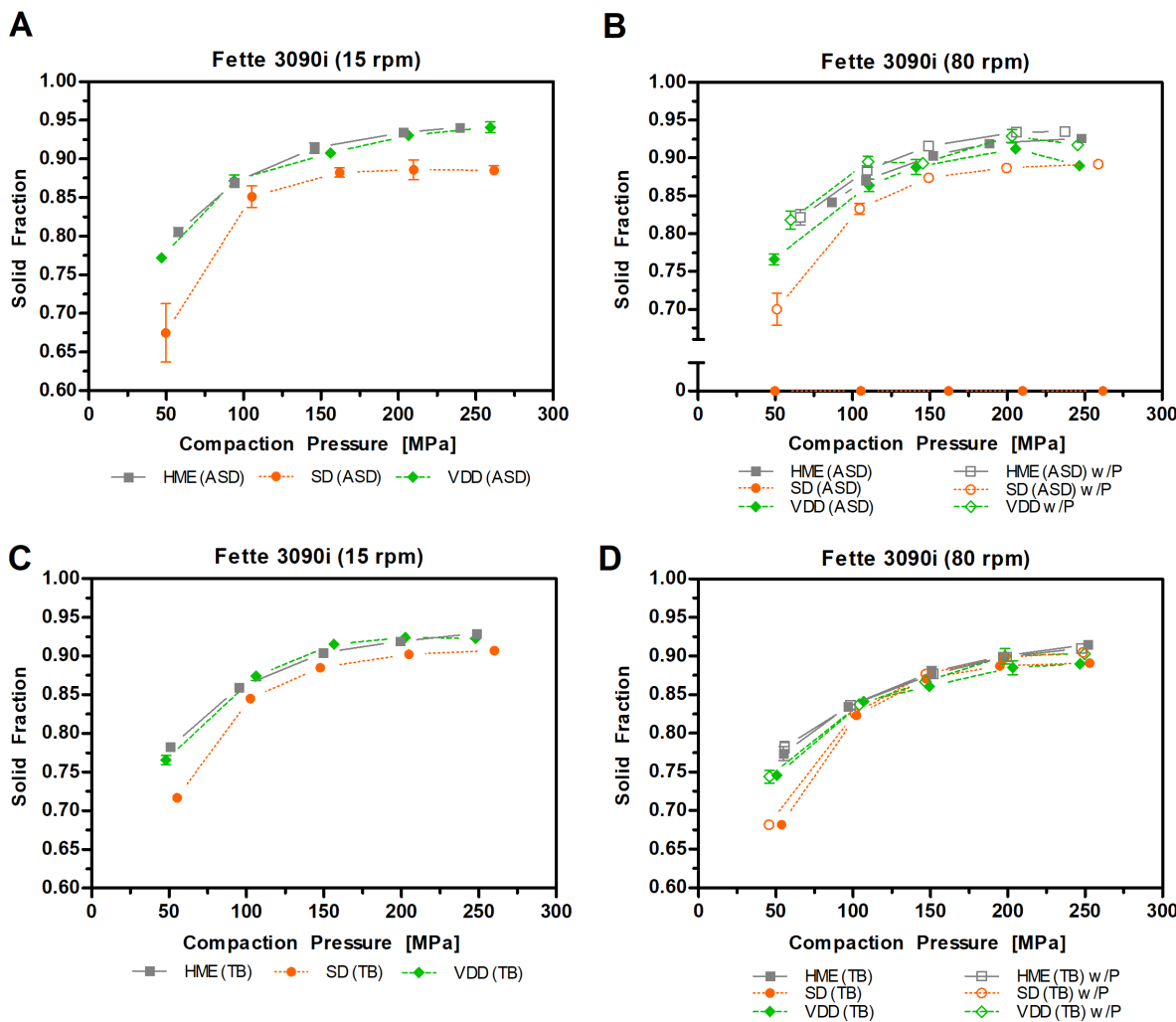


Figure 4.S1: Compressibility plots: (A, B) ASD tablets; (C, D) TB tablets; (A, C) simulating Fette3090i at 15 rpm; (B, D) simulating Fette3090i at 80 rpm without and with applied pre-compression force (w/P). Note: SD ASD was manually fed into the die for compression analysis. SD ASD at 80 rpm: not feasible

4.13 References

- Agrawal, A.M., Dudhedia, M.S., Patel, A.D., Raikes, M.S., 2013. Characterization and performance assessment of solid dispersions prepared by hot melt extrusion and spray drying process. International Journal of Pharmaceutics 457, 71-81 <https://doi.org/10.1016/j.ijpharm.2013.08.081>.
- Bhandari, B., Bansal, N., Zhang, M., Schuck, P., 2013. 4.1 Introduction, Handbook of Food Powders - Processes and Properties. Woodhead Publishing. 2013
- Brunauer, S., Emmett, P.H., Teller, E., 1938. Adsorption of Gases in Multimolecular Layers. Journal of the American Chemical Society 60, 309-319 <http://doi.org/10.1021/ja01269a023>.
- Davis, M.T., Potter, C.B., Walker, G.M., 2018. Downstream processing of a ternary amorphous solid dispersion: The impacts of spray drying and hot melt extrusion on powder flow, compression and dissolution. International Journal of Pharmaceutics 544, 242-253 <https://doi.org/10.1016/j.ijpharm.2018.04.038>.
- Dedroog, S., Huygens, C., Van den Mooter, G., 2019. Chemically identical but physically different: A comparison of spray drying, hot melt extrusion and cryo-milling for the formulation of high drug loaded amorphous solid dispersions of naproxen. European Journal of Pharmaceutics and Biopharmaceutics 135, 1-12 <https://doi.org/10.1016/j.ejpb.2018.12.002>.
- Démuth, B., Nagy, Z.K., Balogh, A., Vigh, T., Marosi, G., Verreck, G., Van Assche, I., Brewster, M.E., 2015. Downstream processing of polymer-based amorphous solid dispersions to generate tablet formulations. International Journal of Pharmaceutics 486, 268-286 <https://doi.org/10.1016/j.ijpharm.2015.03.053>.
- Dobry, D.E., Settell, D.M., Baumann, J.M., Ray, R.J., Graham, L.J., Beyerinck, R.A., 2009. A Model-Based Methodology for Spray-Drying Process Development. Journal of Pharmaceutical Innovation 4, 133-142 <https://doi.org/10.1007/s12247-009-9064-4>.
- EMA/CHMP/ICH/82260/2006: ICH guideline Q3C (R6) on impurities: guideline for residual solvents https://www.ema.europa.eu/en/documents/scientific-guideline/international-conference-harmonisation-technical-requirements-registration-pharmaceuticals-human-use_en-33.pdf (2019). Accessed.
- FDA_Guidance, 1997. Guidance for Industry Dissolution Testing of Immediate Release Solid Oral Dosage Forms, in: Research, C.f.D.E.a. (Ed.), FDA-1997-D-0187. U.S. Department of Health and Human Services Food and Drug Administration
- Fell, J.T., Newton, J.M., 1970. Determination of Tablet Strength by the Diametral-Compression Test. Journal of Pharmaceutical Sciences 59, 688-691 <https://doi.org/10.1002/jps.2600590523>.
- Gold, G., Duvall, R.N., Palermo, B.T., Slater, J.G., 1966. Powder flow studies II: effect of glidants on flow rate and angle of repose. Journal of pharmaceutical sciences 55, 1291-1295 <https://doi.org/10.1002/jps.2600551125>.
- Haser, A., Cao, T., Lubach, J., Listro, T., Acquarulo, L., Zhang, F., 2017. Melt extrusion vs. spray drying: The effect of processing methods on crystalline content of naproxen-povidone formulations. European Journal of Pharmaceutical Sciences 102, 115-125 <https://doi.org/10.1016/j.ejps.2017.02.038>.
- Heckel, R.W. Density-pressure relationships in powder compaction. Transactions of the Metallurgical Society of AIME 1961, 221, 671–675.

COMPRESSION OF AMORPHOUS SOLID DISPERSIONS PREPARED BY HOT-MELT EXTRUSION, SPRAY DRYING AND VACUUM DRUM DRYING

- Huang, S., Williams, R.O., 2018. Effects of the Preparation Process on the Properties of Amorphous Solid Dispersions. *AAPS PharmSciTech* 19, 1971-1984 <https://doi.org/10.1208/s12249-017-0861-7>.
- Iyer, R., Hegde, S., Zhang, Y.-E., Dinunzio, J., Singhal, D., Malick, A., Amidon, G., 2013. The Impact of Hot Melt Extrusion and Spray Drying on Mechanical Properties and Tableting Indices of Materials Used in Pharmaceutical Development. *Journal of Pharmaceutical Sciences* 102, 3604-3613 <https://doi.org/10.1002/jps.23661>.
- Lin, X., Hu, Y., Liu, L., Su, L., Li, N., Yu, J., Tang, B., Yang, Z., 2018. Physical Stability of Amorphous Solid Dispersions: a Physicochemical Perspective with Thermodynamic, Kinetic and Environmental Aspects. *Pharmaceutical Research* 35, 125 <https://doi.org/10.1007/s11095-018-2408-3>.
- Neilly, J.P., Yin, L., Leonard, S.-E., Kenis, P.J.A., Danzer, G.D., Pawate, A.S., 2020. Quantitative Measures of Crystalline Fenofibrate in Amorphous Solid Dispersion Formulations by X-Ray Microscopy. *Journal of Pharmaceutical Sciences* 109, 3078-3085 <https://doi.org/10.1016/j.xphs.2020.07.006>.
- Patterson, J.E., James, M.B., Forster, A.H., Lancaster, R.W., Butler, J.M., Rades, T., 2007. Preparation of glass solutions of three poorly water soluble drugs by spray drying, melt extrusion and ball milling. *International Journal of Pharmaceutics* 336, 22-34 <https://doi.org/10.1016/j.ijpharm.2006.11.030>.
- Pitt, K.G., Heasley, M.G., 2013. Determination of the tensile strength of elongated tablets. *Powder Technology* 238, 169-175 <https://doi.org/10.1016/j.powtec.2011.12.060>.
- Polli, J.E., Rekhi, G.S., Augsburger, L.L., Shah, V.P., 1997. Methods to compare dissolution profiles and a rationale for wide dissolution specifications for metoprolol tartrate tablets. *Journal of Pharmaceutical Sciences* 86, 690-700 <https://doi.org/10.1021/js960473x>.
- Raghavan, R., Jett, J.L., 2004. Method to produce a solid form of heparin, International Application Published Under The Patent Cooperation Treaty. Pfizer Health AB
- Sangekar, S.A., Lee, P.I., Nomeir, A.A., 2003. Molecular dispersion composition with enhanced bioavailability, United States Patent. Schering Corporation
- Schönenfeld, B., Westedt, U., Wagner, K.G., 2021. Vacuum drum drying – A novel solvent-evaporation based technology to manufacture amorphous solid dispersions in comparison to spray drying and hot melt extrusion. *International Journal of Pharmaceutics* 596, 120233 <https://doi.org/10.1016/j.ijpharm.2021.120233>.
- Shah, S., Maddineni, S., Lu, J., Repka, M.A., 2013. Melt extrusion with poorly soluble drugs. *International Journal of Pharmaceutics* 453, 233-252 <https://doi.org/10.1016/j.ijpharm.2012.11.001>.
- Tran, D.T., Majerová, D., Veselý, M., Kulaviak, L., Ruzicka, M.C., Zámostný, P., 2019. On the mechanism of colloidal silica action to improve flow properties of pharmaceutical excipients. *International Journal of Pharmaceutics* 556, 383-394 <https://doi.org/10.1016/j.ijpharm.2018.11.066>.
- Varthalis, S., Pilpel, N., 1977. The action of colloidal silicon dioxide as a glidant for lactose, paracetamol, oxytetracycline and their mixtures. *Journal of Pharmacy and Pharmacology* 29, 37-40 <https://doi.org/10.1111/j.2042-7158.1977.tb11234.x>.
- Vasconcelos, T., Marques, S., das Neves, J., Sarmento, B., 2016. Amorphous solid dispersions: Rational selection of a manufacturing process. *Advanced Drug Delivery Reviews* 100, 85-101 <https://doi.org/10.1016/j.addr.2016.01.012>.

5. COMPRESSION MODULUS AND APPARENT DENSITY OF POLYMERIC EXCIPIENTS DURING COMPRESSION – IMPACT ON TABLETABILITY

Barbara V. Schönenfeld^{a,b}, Ulrich Westedt^b, Karl G. Wagner^{a,c}

^aDepartment of Pharmaceutical Technology, University of Bonn, Gerhard-Domagk-Straße 3, 53121 Bonn, Germany, karl.wagner@uni-bonn.de, barbara.schoenfeld@uni-bonn.de

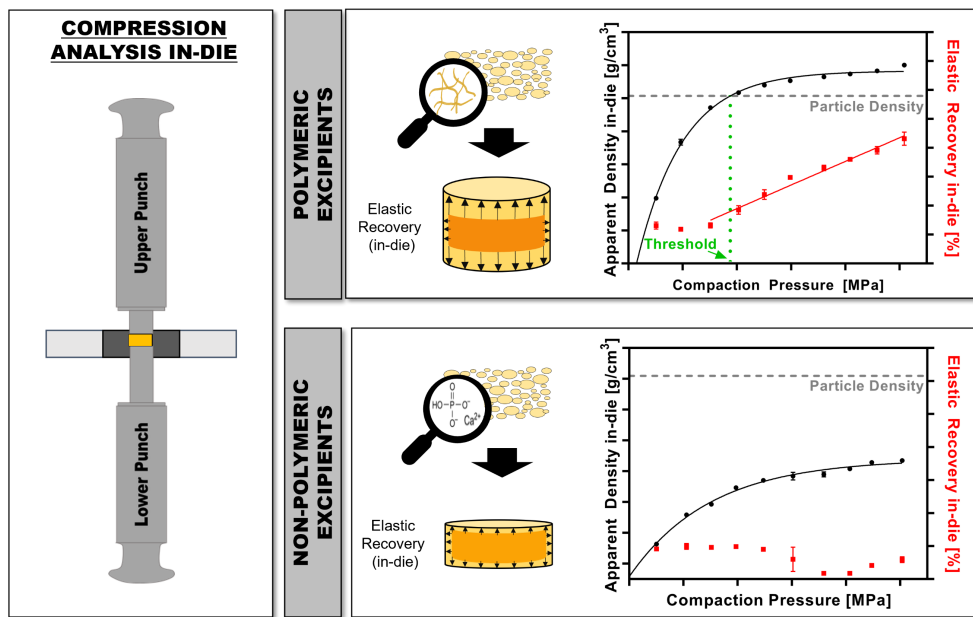
^bAbbVie Deutschland GmbH & Co. KG, Knollstraße 50, 67061 Ludwigshafen, Germany, ulrich.westedt@abbvie.com, barbara.schoenfeld@abbvie.com

^cCorresponding author

This part was published as:

B. V. Schönenfeld, U. Westedt, K. G. Wagner, Compression modulus and apparent density of polymeric excipients during compression – impact on tabletability, *Pharmaceutics*, Volume 14 (5):13, 2022, <https://doi.org/10.3390/pharmaceutics14050913>

5.1 Graphical Abstract



5.2 Abstract

The present study focuses on the compaction behavior of polymeric excipients during compression in comparison to nonpolymeric excipients and its consequences on commonly used Heckel analysis. Compression analysis at compaction pressures (CPs) from 50 to 500 MPa was performed using a compaction simulator. This study demonstrates that the particle density, measured via helium pycnometer (ρ_{par}), of polymeric excipients (Kollidon®VA64, Soluplus®, AQOAT®AS-MMP, Starch1500®, Avicel®PH101) was already exceeded at low CPs (<200 MPa), whereas the ρ_{par} was either never reached for brittle fillers such as DI-CAFOS®A60 and tricalcium citrate or exceeded at CPs above 350 MPa (FlowLac®100, Pearlitol®100SD). We hypothesized that the threshold for exceeding ρ_{par} is linked with predominantly elastic deformation. This was confirmed by the start of linear increase in elastic recovery in-die (ER_{in-die}) with exceeding particle density, and in addition, by the applicability in calculating the elastic modulus via the equation of the linear increase in ER_{in-die} . Last, the evaluation of “density under pressure” as an alternative to the ρ_{par} for Heckel analysis showed comparable conclusions for compression behavior based on the calculated yield pressures. However, the applicability of Heckel analysis for polymeric excipients was questioned in principle. In conclusion, the knowledge of the threshold provides guidance for the selection of suitable excipients in the formulation development to mitigate the risk of tablet defects related to stored elastic energy, such as capping and lamination.

5.3 Keywords

Compression analysis; compaction behavior; density under pressure; particle density; elastic recovery; Heckel analysis; yield pressure; polymers.

5.4 Introduction

Tablets are the most preferred dosage form in pharmaceutical development showing vast benefits such as high-precision dosing, manufacturing efficiency, stability, and patient compliance [1,2]. Because of their poor aqueous solubility, many drug substances in the pipeline need to be formulated via enabling technologies [3]. One enabling formulation approach commonly used in the pharmaceutical industry is the amorphous solid dispersion approach, where the active pharmaceutical ingredient (API) is molecularly dispersed in a polymeric matrix in its amorphous form to enhance solubility. Technologies used for the ASD manufacture are hot-melt extrusion, an example of a fusion-based method, or spray drying as a solvent-based method [3]. In hot-melt extrusion, thermal and mechanical energy from corotating screws and heated barrels, followed by cooling, is used to produce the solid dispersion [4], which is further downstream processed to powder (milled extrudate) via a milling step. The latter step is important as dosage forms generated from the pure melt (e.g., injection molded or calendering) often result in slow dissolution without disintegration, which can be improved by mixing the ASD powder with tabletting excipients [5]. Commonly used matrix polymers suitable for hot-melt extrusion are polyvinylpyrrolidone (PVP), polyvinylpyrrolidone/vinyl acetate (PVPVA, copovidone), polymethacrylates, hydroxypropyl methylcellulose (HPMC) or hydroxy-propyl methylcellulose acetate succinate (HPMCAS), and polyvinyl caprolactam-polyvinyl acetate-polyethylene glycol graft copolymer (Soluplus®) [6]. Nevertheless, the final dosage form of ASD-based drug products is mostly tablets, as demonstrated by recently marketed products [3,6].

Consequently, the compression of the resulting intermediates into tablets remains a key unit operation in the manufacturing process chain of a drug product. For that, tabletting excipients such as fillers or binders are added to the formulation composition. The compression process as such can be generally divided into two stages. First is slippage and particle rearrangement, resulting in a volume reduction in the powder and denser packing structure [7]. Second is the subsequent reduction in the volume via applying higher compression forces and is associated with changes in the dimensions of the particles themselves, either by irreversible plastic deformation, reversible elastic deformation, or particle

fragmentation into smaller particles [8,9]. However, during the compression of a powder, all deformation mechanisms can be present at different stages of the compaction process or can occur even simultaneously. A high proportion of elastic deformation during compression leads to the reduced mechanical strength of the tablets and probably to tablet defects such as capping or lamination [10]. In addition, even subsequent processing steps such as coating might be impacted by defects induced by the stored elastic energy within the tablets [11]. Busignies et al. [12] stated the importance of knowledge of elastic deformation to manufacture bilayer tablets.

Tableting excipients are usually categorized with respect to their main bonding mechanism and compaction behavior during compression, distinguishing between plastic or brittle deformation [9]. However, not only tableting excipients in the outer phase but also the main component of the intermediate, e.g., the matrix polymer of an amorphous solid dispersion, might profoundly affect the compaction behavior of the formulation. Thus, the selection of suitable excipients is crucial in the formulation development of solid dosage forms [13].

Compression analysis provides a deeper understanding of the compaction behavior of a powder under pressure, e.g., plasticity and elasticity. Common approaches were developed by Heckel, Kawakita and Lüdde, Kuentz and Leuenberger [14–16]. The Heckel equation considers the porosity of the tablet (either in-die or out-of-die) and the main compression force by using the force-displacement profile. It assumes that volume reduction by plastic deformation follows a first-order kinetic. In addition, it offers the opportunity to determine elastic recovery of the compact in-die, also known as fast elastic recovery, considering the decompression part of the Heckel plot.

However, limitations of the Heckel analysis were observed in several studies [17,18]. The yield pressure (P_Y), which represents the plasticity of the material, was found to be dependent on tableting parameters such as compression speed, tooling dimensions, as well as errors in porosity and pressure data used for calculation and elastic deformation [19–21]. Ilić et al. [22] observed differences in Heckel analysis comparing the “in-die” and the “out-of-die” method, stating the larger extent of error for the “out-of-die” method was due to elastic deformation. In addition, Sun, Grant [21] stated that Heckel analysis should not be considered for classification if the solid fraction of the powder during the compaction process is above 0.95. Apart from this, it was observed that the yield pressure values are lower for powders showing elastic deformation. Similar observations were made by Schlack [23], showing that starch undergoes solid-state compression and that the particle density should be corrected accordingly to ensure valid Heckel results. Heckel plots showing bending above a certain compaction pressure were

likewise observed by Wünsch et al. [24]. Accordingly, Krumme et al. [25] introduced the “true density by compression”, which should be used for Heckel calculations instead of the particle density. The difference between particle density and “true density by compression” was considered most profound for Starch1500® as elastic material and moderate for lactose as a brittle material. In conclusion, limitations for using the particle density for porosity calculations in compaction analysis were observed.

In general, several studies investigated commonly used excipients for direct compression [26–29]. However, the difference in compaction behavior between polymeric and non-polymeric materials, focusing on the apparent density in-die at different compaction pressures, has not been investigated before, especially not in correlation with the respective particle densities and the elastic recoveries (in-die). In this study, we hypothesize that the energy, which is needed to compress excipients (especially polymeric ones) beyond their particle density, correlates with predominantly elastic deformation and thus, can be measured as an increase in fast elastic recovery.

Therefore, the present study comprises the following aspects:

- Compaction analysis of nonpolymeric tabletting excipients (di-calcium phosphate (DI-CAFOS®A60)), tricalcium citrate tetrahydrate, spray-dried lactose monohydrate (FlowLac®100), mannitol (Pearlitol®100SD)) as well as common polymeric tabletting excipients (partially pregelatinized maize starch (Starch1500®), microcrystalline cellulose (Avicel®PH101)) and amorphous solid dispersion excipients (copovidone (Kollidon®VA64), polyvinyl caprolactam-polyvinyl acetate-polyethylene glycol graft copolymer (Soluplus®), and hydroxypropyl methylcellulose (AQOAT®AS-MMP)). The excipients investigated are commonly used excipients in the development of solid dosage forms [28] and were chosen as targets to include excipients with different compaction behaviors (plastic, brittle) to ensure a comprehensive evaluation. The ASD excipients are matrix polymers used in the recently marketed drug products and are thus, of high importance [3];
- Assessment of an ASD manufactured via hot-melt extrusion consisting of ritonavir, copovidone, and sorbitan monolaurate and its respective tablet blend to evaluate the general impact on compaction analysis for ASDs;
- Discussion of consequences for commonly used Heckel analysis and the use of the “density under pressure” (500 MPa, dwell time 10 s) instead of particle density.

5.5 Materials and Methods

5.5.1 Materials

Di-calcium phosphate (DI-CAFOS®A60) was obtained from Chemische Fabrik Budenheim (Budenheim, Germany), tricalcium citrate tetrahydrate (TriCaCi) from Jungbunzlauer Ladenburg GmbH (Ladenburg, Germany), microcrystalline cellulose (Avicel®PH101) from FMC (Philadelphia, PA, USA), alpha-lactose monohydrate (FlowLac®100) from Meggle Group (Wasserburg, Germany), mannitol (Pearlitol®100SD) from Roquette GmbH (Frankfurt a. M., Germany), copovidone (polyvinylpyrrolidone-vinyl acetate copolymer, Kollidon®VA 64) and polyvinyl caprolactam-polyvinyl acetate-polyethylene glycol graft copolymer (Soluplus®) from BASF SE (Ludwigshafen, Germany), hypromellose acetate succinate (HPMCAS, AQOAT®AS-MMP) from Shin-Etsu Chemical Co. Ltd. (Tokyo, Japan), and partially pregelatinized maize starch (Starch1500®) from Colorcon Limited (Kent, UK).

DI-CAFOS®A60 are aggregates of fine, almost spherical particles with an uneven surface and a d_{50} value of 60 µm [30]. TriCaCi is a powder of almost spherically shaped large agglomerates with a mean particle size of 135 µm [26]. Avicel®PH101 consists of irregularly shaped particles with a broad particle size distribution and a mean particle size of approximately 56 µm [31,32]. FlowLac®100 is manufactured via spray drying, which explains the spherical shape of the particles with a mean particle size of 110 µm [33]. In addition, Pearlitol®100SD is prepared via spray drying resulting in spherical particles with a mean particle size of 100 µm [34]. The mean particle size of Kollidon®VA 64 is 82 µm, and the particles are hollow spheres in a significant proportion [35]. Soluplus® appears as particles with a diameter of approximately 340 microns in a mostly spherical shape, according to the technical information of the vendor [36]. AQOAT®AS-MMP consists of particles with a mean particle size of approximately 300 µm. Starch1500® consists of particles with a broad particle size distribution and a mean particle size of approximately 65 µm [37].

The amorphous solid dispersion (ASD) consists of 15% (w/w) ritonavir, 74% (w/w) copovidone, 10% (w/w) sorbitan monolaurate, and 1% (w/w) silicon dioxide, and the tablet blend of 87.1% (w/w) milled extrudate (ASD), 11.7% (w/w) di-calcium phosphate, 0.9% (w/w) silicon dioxide, and 0.3% (w/w) sodium stearyl fumarate. Both ASD and tablet blend composition were in accordance with the marketed Norvir® formulation serving as model ASD formulation in the present study representative for other ASDs. The ASD was manufactured by hot-melt extrusion and was kindly provided by AbbVie Deutschland GmbH & Co. KG, Ludwigshafen, Germany.

COMPRESSION MODULUS AND APPARENT DENSITY OF POLYMERIC EXCIPIENTS DURING COMPRESSION – IMPACT ON TABLETABILITY

In detail, ritonavir (purity > 99.8%) was obtained from AbbVie Inc. (North Chicago, IL, USA) and sorbitan monolaurate (Span20[®]) from CRODA (Nettetal, Germany). Di-calcium phosphate (DI-CAFOS[®] A60) was purchased from Chemische Fabrik Budenheim (Budenheim, Germany), fumed silicon dioxide (Aerosil[®]200) from Evonik Industries (Essen, Germany), and sodium stearyl fumarate (PRUV[®]) from JRS Pharma (Rosenberg, Germany).

To ease the readability of the figures within the article, the respective excipients were displayed without their trademarks.

5.5.2 Methods

5.5.2.1 Hot-melt extrusion

Hot-melt extrusion was performed on a commercial scale co-rotating twin-screw extruder (ZSK 58, Coperion GmbH, Stuttgart, Germany) combined with a calender (COLLIN Lab & Pilot Solutions GmbH, Maitenbeth, Germany) equipped with ellipsoidal-shaped molds to obtain the ritonavir containing amorphous solid dispersion in the form of extrudate beads. The extrusion parameters were as follows: temperature profile 20/80/100/110 °C, screw speed 185 rpm, and vacuum 150 mbar. The extrudate beads were milled at 7000 rpm using an impact mill (Alpine UPZ100, Hosokawa Alpine, Augsburg, Germany) equipped with a 1.3 mm sieve.

5.5.2.2 Tablet blend preparation

Outer phase excipients were added to the milled extrudate (87.1% (w/w)) consisting of ritonavir as a drug substance according to the Norvir[®] formulation, an antiretroviral drug product (tablet) used in combination with other medications to treat the human immunodeficiency virus infection (HIV) and acquired immunodeficiency syndrome (AIDS): di-calcium phosphate as a filler (11.7% (w/w)), fumed silicon dioxide as a glidant (0.9% (w/w)), and sodium stearyl fumarate (0.3% (w/w)) as a lubricant. The tablet blend was prepared using a bin blender (Bohle PM400, L.B. Bohle Maschinen + Verfahren GmbH, Enningerloh, Germany), and a screening machine (Bohle BTS, L.B. Bohle Maschinen + Verfahren GmbH, Enningerloh, Germany) with a 1.5 mm mesh by the following consecutive steps: (1) sieving, and (2) blending for 9 min at 6 rpm.

The milled extrudate is named in the following as HME ASD and the respective tablet blend as HME TB.

5.5.2.3 Particle density (pycnometric density, ρ_{par})

Particle (pycnometric) density was determined using a helium pycnometer (AccuPyc 1340, Micromeritics GmbH, Aachen, Germany). The helium pycnometer was equipped with a 10 cm³ sample chamber and was operated at a cycle fill pressure of 134.45 kPa and an equilibration rate of 0.0345 kPa/min. Purging of the sample chamber was conducted 10 times prior to the measurement. For each analysis, 5 cycles were performed. All samples were measured as triplicates.

5.5.2.4 Density under pressure (ρ_{pre})

The density under pressure (ρ_{pre}) was determined according to Krumme et al. [25] using a single punch compression simulator (HB-50, Huxley Bertram Engineering Limited, Cambridge, UK) equipped with 10 mm round, flat face tooling. A compaction profile was designed to ensure proper air release during compaction and maximum densification, including a ramp of 20 s up to the maximum compaction pressure of 500 MPa and a dwell time of 10 s. For each respective material, 6 tablets were manufactured to determine the density under compaction pressure, which was used for further calculations.

5.5.2.5 Density ratio (ρ_{ratio})

The density ratio ρ_{ratio} between the density under pressure (ρ_{pre}) and particle density (ρ_{par}) was calculated for comparison reasons according to the following equation (Equation (5.1)):

$$\rho_{ratio}[\%] = \frac{\rho_{pre} - \rho_{par}}{\rho_{par}} \times 100 \quad (5.1)$$

5.5.2.6 Compression analysis

A single punch compression simulator (HB-50, Huxley Bertram Engineering Limited, Cambridge, UK) equipped with 10 mm round, flat face tooling was used for compression analysis. Tablets (n = 6) targeting a mass of 200 mg (400 mg for DI-CAFOS A60 due to the high bulk density) were manufactured at ten compaction pressures ranging from 50 MPa to 500 MPa. The production scale tablet press Fette 3090i (61 stations, Euro-B tooling) at a turret speed of 15 rpm (according to a linear speed of 0.32 m/s and dwell time of 19 ms) was simulated. Tablets were characterized regarding tablet weight (analytical balance, Sartorius BP 61 S 0CE, Sartorius AG, Goettingen, Germany), thickness, and diameter (caliper, Hommel Hercules Werkzeughandel GmbH & Co KG, Viernheim, Germany), and breaking force (Lab-line H4, Kraemer Elektronik GmbH, Darmstadt, Germany).

5.5.2.7 Compaction pressure

The compaction pressure (CP in N/mm² or MPa) was calculated from the applied main compression force and cross-sectional area of the punch (Eq. (5.2)) [38].

$$CP = \frac{\text{Main Compression Force [N]}}{\text{Cross - sectional Area [mm}^2\text{]}} \quad (5.2)$$

5.5.2.8 Apparent density (in-die)

The apparent density of the tablet in-die (ρ_{app}) was calculated from the tablet mass (m) divided by the volume of the tablet at minimal punch separation (V_{minSP}) (Eq. (5.3)):

$$\rho_{app} = \frac{m}{V_{minSP}} \quad (5.3)$$

5.5.2.9 Particle density threshold

The particle density threshold is defined as the value where the apparent density exceeds the particle density. For determination, the apparent density results (mean values) were plotted depending on the compaction pressure applied (mean values) and exponentially fitted (one-phase decay). The equation for the exponential fit function was used to calculate the respective particle density threshold compaction pressure (single value).

5.5.2.10 Solid fraction (in-die)

Solid fraction in-die (SF) is the apparent density of the tablet in-die (ρ_{app}) divided by the particle (pycnometric) density (ρ_{par}) of the powder (Eq. (5.4)) [38]:

$$SF = \frac{\rho_{app}}{\rho_{par}} \quad (5.4)$$

5.5.2.11 Elastic recovery (in-die)

The elastic recovery in-die (ER_{in-die}) is calculated as follows (Eq. (5.5)):

$$ER_{in-die}[\%] = \frac{V_{minCP} - V_{minPS}}{V_{minCP}} \times 100 \quad (5.5)$$

where V_{minCP} is the tablet volume at minimal compaction pressure (minCP) after the compression process, and V_{minPS} is the tablet volume at the minimal punch separation (minPS) (=minimal in-die tablet volume).

5.5.2.12 Elastic modulus (Young's modulus)

The elastic modulus displays the resistance of a material to being elastically deformed when mechanical stress is applied and can be determined via the slope of its stress–strain curve. Stiffer materials have higher elastic moduli compared to elastic materials.

The elastic modulus E is defined by the following equation (Eq. (5.6)):

$$E = \frac{F}{A} \frac{L_0}{\Delta L} \quad (5.6)$$

where F is the force applied to the surface A (“stress”), L_0 is the initial length of a solid object, and ΔL is the reduction in the length (“longitudinal strain”).

ER_{in-die} is calculated by the difference in tablet dimensions under pressure (stress) which corresponds to the reciprocal of the strain ($L_0/\Delta L$). Since a linear increase in ER_{in-die} was observed after the exceedance of the particle density, the slope of the linear equation ($a_{ER_{eq}}$) was used as a constant to determine the elastic modulus E_{mod} (Eq. (5.7)).

$$E_{mod} [MPa] = \frac{1}{a_{ER_{eq}}} \times 100 \quad (5.7)$$

5.5.2.13 Heckel analysis (in-die)

The compression behavior in terms of deformation was studied by means of the Heckel Equation (5.8) as the “in-die method” [14]. The Heckel equation assumes that volume reduction by plastic deformation follows a first-order kinetic:

$$\ln \left(\frac{1}{1 - SF} \right) = k \times CP + A \quad (5.8)$$

where CP is the compaction pressure, and SF is the solid fraction (relative density) at CP . Slope k and intercept A of the linear ascending part of the Heckel plot (phase 2, plastic deformation phase, see Figure 5.1) are material-dependent constants. The SF was calculated as the “in-die method” considering the punch gap during compression for tablet volume calculation. However, instead of just using the particle density for SF calculation, the “density under compaction pressure” (ρ_{pre}) was additionally used in accordance with Krumme et al. [25]. For comparison reasons, Heckel plots at 100 and 300 MPa were generated by using (a) the particle density (ρ_{par}) and (b) the density under pressure (ρ_{pre}) ($n = 6$). Figure 5.1 shows a typical Heckel plot with stages of powder densification during compaction: (1) particle rearrangement, (2) plastic deformation, and (3) elastic deformation. After the maximum

compaction pressure is applied, the maximum material densification is reached with a short delay before the last phase, (4) elastic recovery in-die occurs, resulting in a less dense compact at the end of the compaction process.

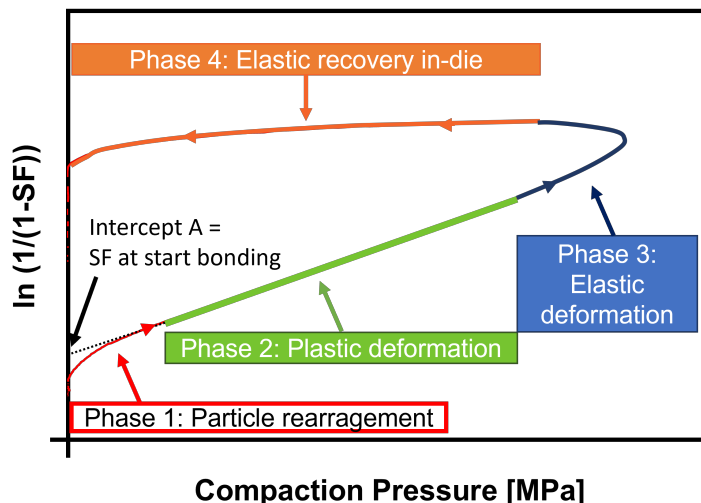


Figure 5.1: Schematic Heckel plot in-die

The linear section of the ascending part of the Heckel plot corresponds to phase 2 (see Figure 5.1) and was selected via the best correlation coefficient ($R^2 > 0.999$) for the linear regression using Igor Pro v8 (WaveMetrics Inc., Lake Oswego, OR, USA). The range for the region was set to 30 MPa for the Heckel plots at 100 MPa compaction pressure (CP) and 100 MPa for those at 300 MPa.

The yield pressure (P_Y) was calculated as reciprocal of k (slope of the linear part) and is inversely correlated to the start of plastic deformation (Eq. (5.9)) [14]:

$$P_Y = \frac{1}{k} \quad (5.9)$$

5.6 Results

5.6.1 Density ratio: particle density vs. density under pressure

The results for density (ρ_{pre} and ρ_{par}) and density ratio (ρ_{ratio}) are shown in Table 5.1 and visualized in Figure 5.2. The density under pressure values were higher compared with the particle density values determined via helium pycnometer resulting in positive density ratio values in all cases except for DI-CAFOS®A60 and TriCaCi (Figure 5.2 A). Polymeric fillers or matrix polymers for ASD manufacture showed the highest positive density ratio values, e.g., Starch1500 with 7.7% or Soluplus® with 9.8%. Brittle fillers such as TriCaCi (-3.7%) and DI-CAFOS®A60 (-14.6%) showed negative density ratio results. HME ASD and HME TB, both based on copovidone as matrix polymer, showed comparable density ratio values (6.7%) regardless of the addition of outer phase excipients in accordance with the density ratio value of pure copovidone (8.4%) (Figure 5.2 B).

Table 5.1: Results of density measurements (ρ_{pre} and ρ_{par}) and the resulting density ratio (ρ_{ratio})

Material	CP for ρ_{pre} [MPa]	ρ_{pre} [g/cm ³]	ρ_{par} [g/cm ³]	ρ_{ratio} [%]
Copovidone	503.0 ± 7.4	1.308 ± 0.026	1.207 ± 0.004	8.37
HPMC AS	505.9 ± 23.2	1.390 ± 0.004	1.281 ± 0.001	8.51
Soluplus®	500.0 ± 12.0	1.291 ± 0.004	1.176 ± 0.003	9.78
Starch1500®	507.6 ± 13.3	1.605 ± 0.005	1.490 ± 0.004	7.72
Avicel®PH101	500.8 ± 8.7	1.631 ± 0.005	1.558 ± 0.002	4.69
DI-CAFOS®A60	506.9 ± 17.7	2.407 ± 0.016	2.819 ± 0.001	-14.62
TriCaCi	501.7 ± 5.7	1.895 ± 0.011	1.967 ± 0.005	-3.66
FlowLac®100	515.1 ± 8.3	1.585 ± 0.003	1.546 ± 0.005	2.52
Pearlitol®100SD	509.8 ± 5.7	1.528 ± 0.003	1.466 ± 0.001	4.23
HME ASD	498.6 ± 5.6	1.281 ± 0.002	1.201 ± 0.001	6.66
HME TB	507.2 ± 10.9	1.386 ± 0.003	1.299 ± 0.001	6.70

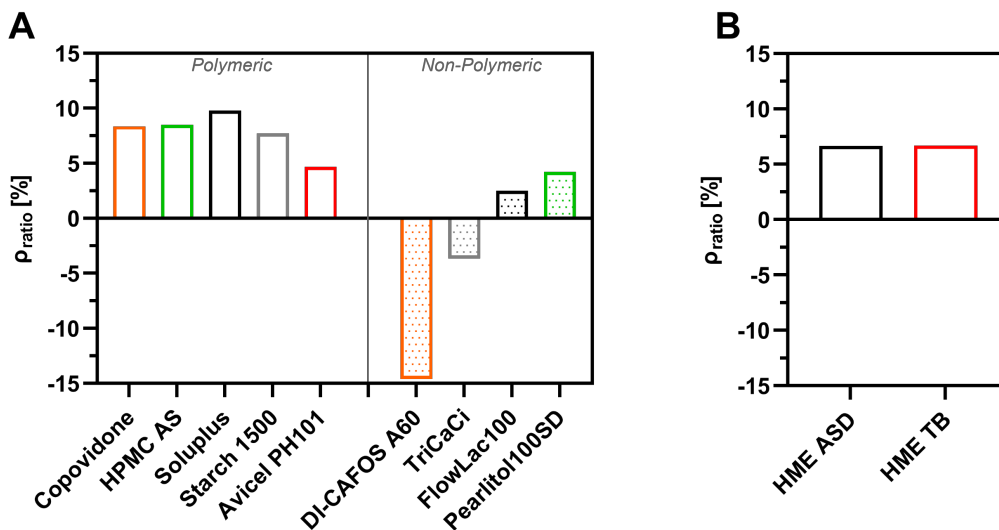


Figure 5.2: Density ratio (ρ_{ratio}) of (A) all excipients tested and (B) HME ASD and HME TB

5.6.2 Apparent density in-die vs. compaction pressure

Figure 5.3 shows the apparent density values of the tablets at minimum punch separation during compression at different compaction pressures (A1 = polymeric excipients; B1 = nonpolymeric) and the respective particle densities as dotted lines. For better interpretability, a normalized visualization via solid fraction in-die is shown in Figure 5.3 (A2) for polymeric excipients and in Figure 5.3 (B2) for nonpolymeric. The data indicated an increase in apparent density/solid fraction with increasing compaction pressure reaching a plateau at high compaction pressures. It was observed that the respective particle density values were exceeded for all polymeric excipients at the latest above a compaction pressure of 200 MPa, resulting in SF values above 1. For FlowLac®100 and Pearlitol®100SD as nonpolymeric excipients, the corresponding threshold value was at higher compaction pressures (450–500 MPa), whereas neither DI-CAFOS®A60 nor TriCaCi exceeded the particle density during compression, up to compaction pressures of 500 MPa. Considering the trend of the values, the particle density will probably not be exceeded even at higher CPs. Notably, TriCaCi showed higher SF values compared to Di-CAFOS®A60, which might be related to particle morphology. TriCaCi consists of larger agglomerates of lower micron to a submicron particle size which might shift more easily into denser structures during compression, resulting in high interaction forces and, thus, strong compacts as observed by Hagelstein et al. [27].

COMPRESSION MODULUS AND APPARENT DENSITY OF POLYMERIC EXCIPIENTS
DURING COMPRESSION – IMPACT ON TABLETABILITY

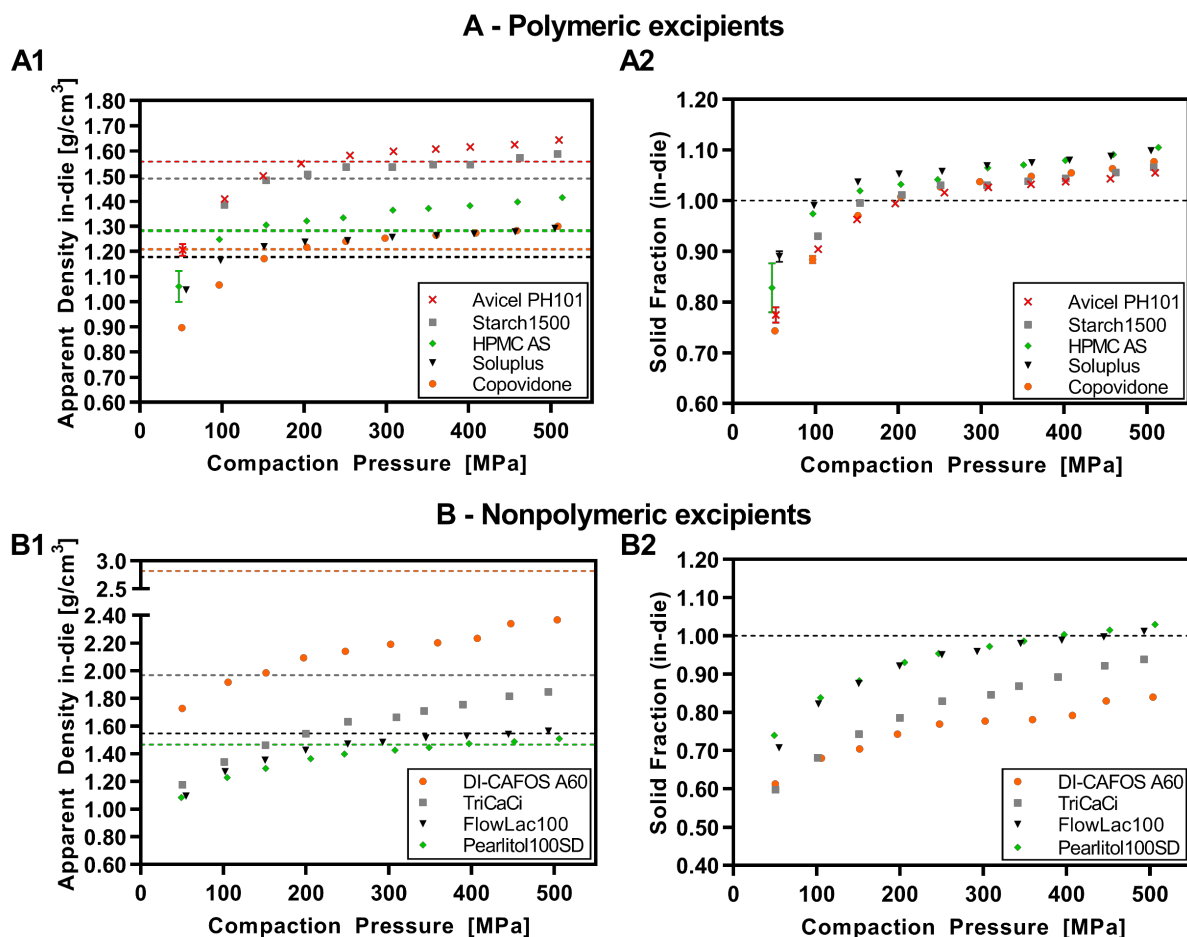


Figure 5.3: (A) Polymeric excipients: apparent density in-die vs. compaction pressure (dotted lines = respective particle densities) (A1); solid fraction in-die vs. compaction pressure (A2); (B) Nonpolymeric excipients: apparent density in-die vs. compaction pressure (dotted lines = respective particle densities) (B1); solid fraction in-die vs. compaction pressure (B2)

Figure 5.4 displays the apparent density/solid fraction in-die data for the milled extrudate (HME ASD) and the respective tablet blend (HME TB) based on copovidone as the matrix polymer. The trend was in accordance with the data for pure copovidone: the apparent density plateau was at around 1.3 g/cm³. The threshold for exceeding the particle density was in a comparable range (HME ASD: 159 MPa; HME TB: 196 MPa; copovidone: 188 MPa). However, a clear shift for the HME TB threshold to higher compaction pressure could be observed. This might be explained by the addition of 11.7% (w/w) DI-CAFOS®A60 showing no exceedance of the particle density in the investigated pressure range. Besides, the drug substance ritonavir and the surfactant sorbitan monolaurate lowered the threshold of the ASD compared to pure copovidone.

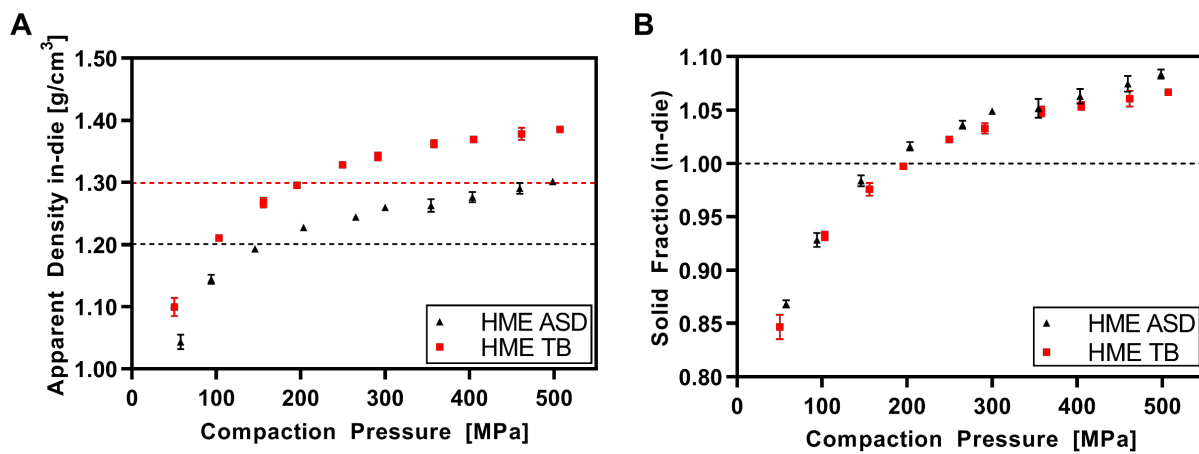


Figure 5.4: HME ASD and HME TB: (A) apparent density in-die vs. compaction pressure (dotted lines = respective particle densities); (B) solid fraction in-die vs. compaction pressure

5.6.3 Elastic recovery in-die vs. compaction pressure

The interplay of the apparent density and the elastic recovery in-die (ER_{in-die}) at different CPs for polymeric excipients is shown in Figure 5.5 and for nonpolymeric excipients in Figure 5.6. Polymeric excipients exhibited a linear increase ($R^2 > 0.90$) in ER_{in-die} with increasing CPs. Interestingly, the increase in ER_{in-die} started at about the same CP as the threshold for exceedance of the particle density during compression. The nonpolymeric excipients DI-CAFOS®A60, TriCaCi, and FlowLac®100 showed no increase in ER_{in-die} with increasing CPs up to 500 MPa, whereas Pearlitol®100SD showed an increase starting at 250-300 MPa. Overall, the ER_{in-die} values were higher for polymeric excipients even at the start (4–6%) compared with nonpolymeric excipients (<4%).

**COMPRESSION MODULUS AND APPARENT DENSITY OF POLYMERIC EXCIPIENTS
DURING COMPRESSION – IMPACT ON TABLETABILITY**

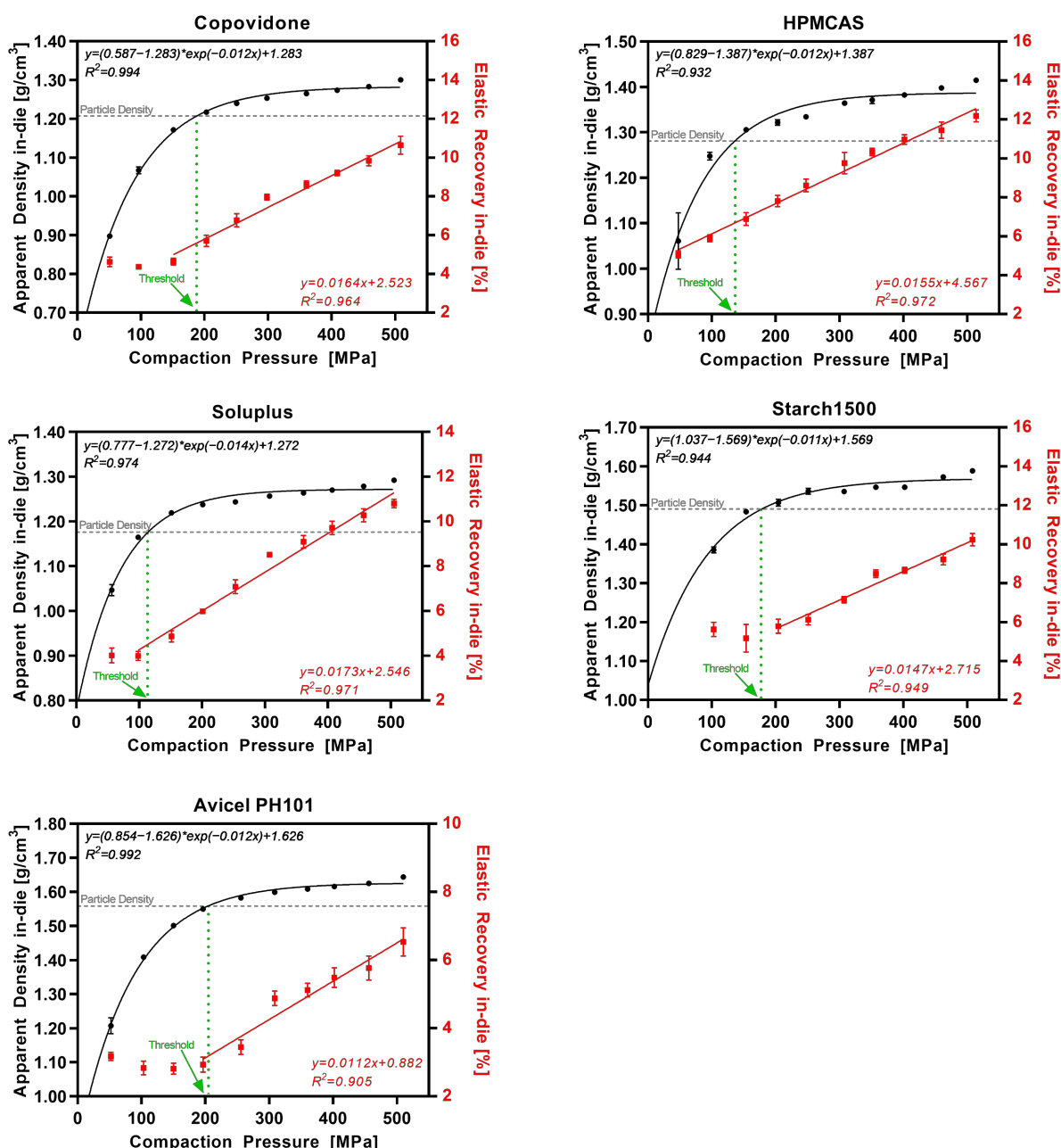


Figure 5.5: Polymeric excipients: apparent density in-die (black) and elastic recovery in-die (red) at different compaction pressures; particle density (grey dotted line); threshold in CP where $\rho_{app} = \rho_{par}$ (green dotted line)

**COMPRESSION MODULUS AND APPARENT DENSITY OF POLYMERIC EXCIPIENTS
DURING COMPRESSION – IMPACT ON TABLETABILITY**

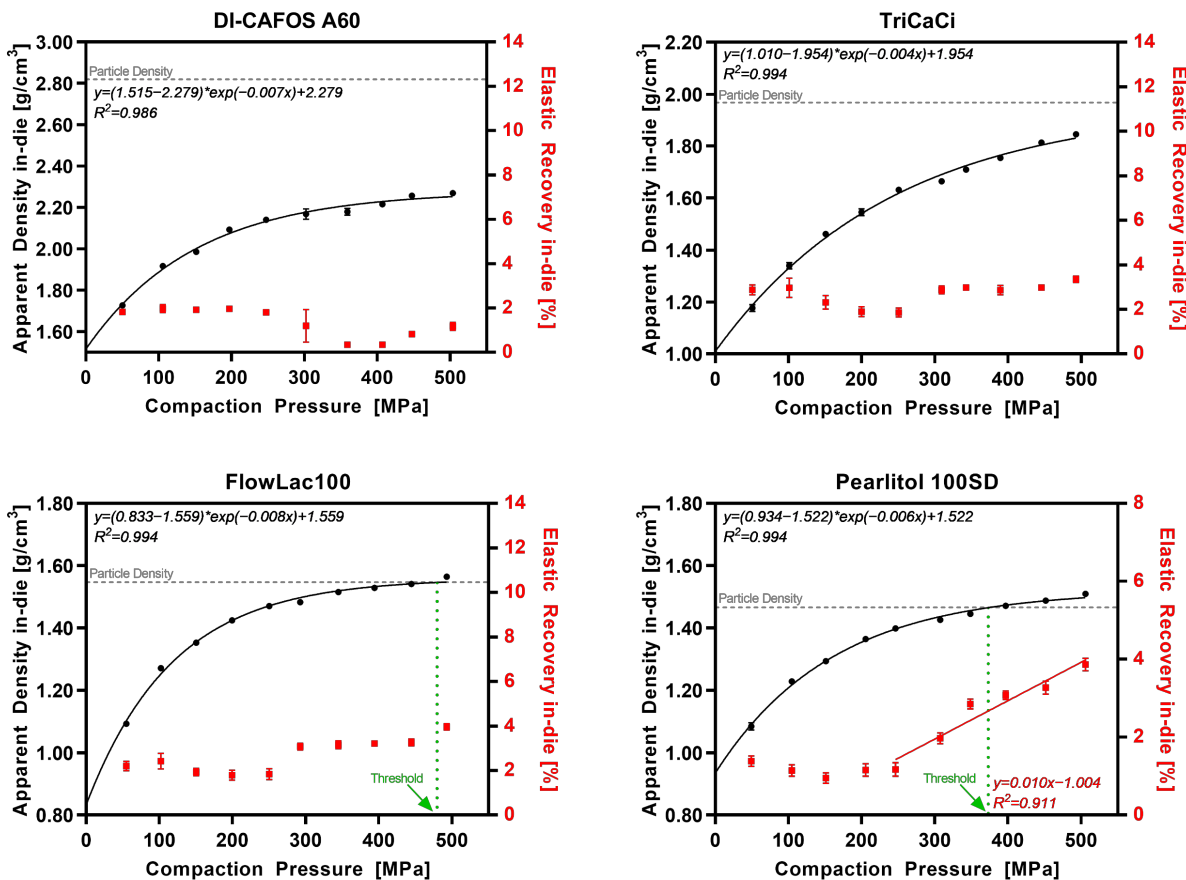


Figure 5.6: Nonpolymeric excipients: apparent density in-die (black) and elastic recovery in-die (red) at different compaction pressures; particle density (grey dotted line); threshold in CP where $\rho_{app} = \rho_{par}$ (green dotted line)

Figure 5.7 displays the results for the HME ASD and HME TB representing ASD formulations in general. Additionally, in this case, the data were in accordance with the pure copovidone data set. The ER_{in-die} increased above 150–200 MPa following linear regression with a R^2 above 0.95.

COMPRESSION MODULUS AND APPARENT DENSITY OF POLYMERIC EXCIPIENTS DURING COMPRESSION – IMPACT ON TABLETABILITY

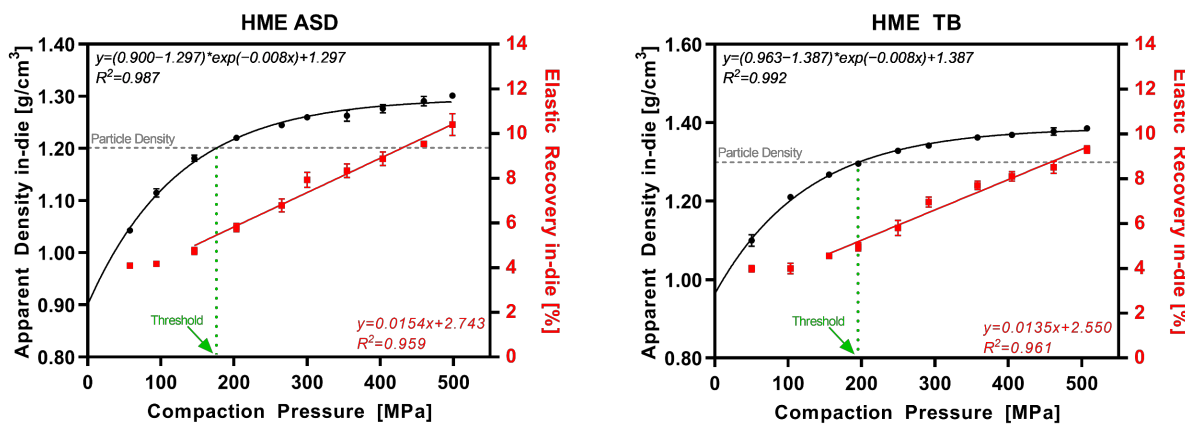


Figure 5.7: HME ASD and HME TB: apparent density in-die (black) and elastic recovery in-die (red) at different compaction pressures; particle density (grey dotted line); threshold in CP where $\rho_{app} = \rho_{par}$ (green dotted line)

5.6.4 Particle density threshold

The thresholds in CP of the investigated excipients (polymeric and nonpolymeric) for the exceedance of the particle density during compression ($\rho_{app} = \rho_{par}$) are visualized in Figure 5.8 A, whereas the thresholds for the HME ASD and HME TB in Figure 5.8 B. The threshold simultaneously indicated the start of a linear increase in elastic recovery (in-die). The threshold values for polymeric excipients were between 100–200 MPa, and thus, the particle density was already exceeded at low CPs. In contrast, the threshold values for nonpolymeric values were either above 350 MPa (FlowLac® and Pearlitol®100SD) or never reached (DI-CAFOS®A60, TriCaCi).

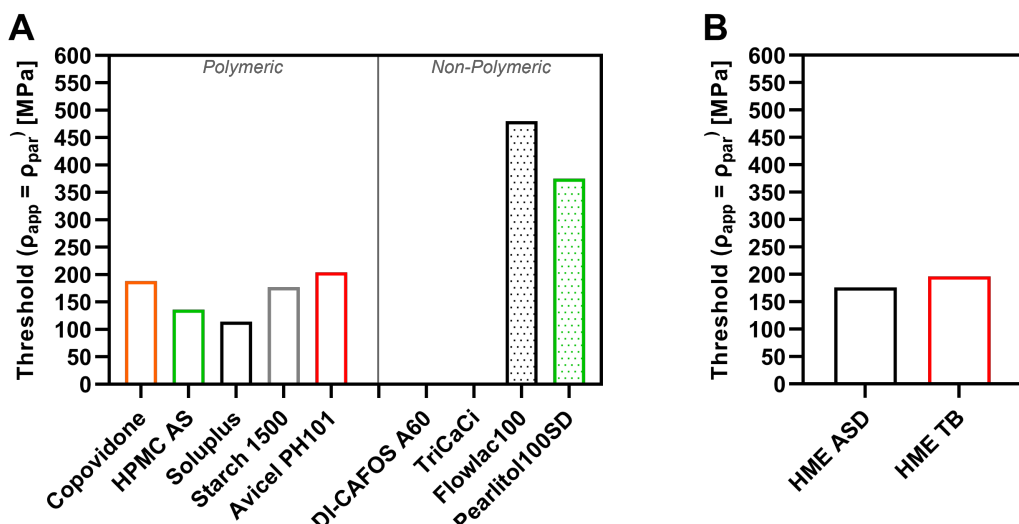


Figure 5.8: Particle density threshold in CP ($\rho_{app} = \rho_{par}$) of (A) polymeric and nonpolymeric excipients, and (B) of HME ASD and TB

5.6.5 Elastic modulus (Young's modulus, E_{mod})

Table 5.2 summarizes the elastic modulus (E_{mod}) values calculated based on the slope of the linear regression equation for ER_{in-die} . E_{mod} values for the polymeric excipients were in the range of 5.8–8.9 GPa. E_{mod} values for HME ASD (6.5 GPa) and HME TB (7.4 GPa) were similar to pure copovidone (6.1 GPa). However, the HME TB E_{mod} value was higher compared with the ASD, assuming higher stiffness of the material, which might be related to DI-CAFOS®A60, known as brittle filler.

E_{mod} values for nonpolymeric excipients could not be calculated via this approach since no linear increase in ER_{in-die} was observed for those excipients, except for Pearlitol®100SD. An E_{mod} for Pearlitol®100SD of 10.2 GPa was higher compared to nonpolymeric excipients indicating a slightly higher degree of stiffness.

Table 5.2. Results of calculated elastic modulus (E_{mod}) based on ER_{in-die} linear equation (n.a. = not applicable)

Material	$a_{ER_{eq}}$	E_{mod} (GPa)
Copovidone	0.01635	6.1
HPMC AS	0.01554	6.4
Soluplus®	0.01731	5.8
Starch1500®	0.01471	6.8
Avicel®PH101	0.01124	8.9
DI-CAFOS®A60	n.a.	n.a.
TriCaCi	n.a.	n.a.
FlowLac®100	n.a.	n.a.
Pearlitol®100SD	0.00986	10.2
HME ASD	0.01538	6.5
HME TB	0.01353	7.4

5.6.6 Heckel analysis (in-die)

The Heckel plots are visualized in Figure 5.9 (polymeric excipients), Figure 5.10 (nonpolymeric excipients), and Figure 5.11 (HME ASD and HME TB). Heckel plots could not be generated properly for CPs of 300 MPa for polymeric excipients (Figure 5.9) and the ASD model formulations (Figure 5.11) if calculated with the particle density. The particle density was exceeded at compaction pressures of 100–200 MPa, resulting in SF values above 1, i.e., an invalid Heckel model. As mentioned in section 5.5.2.13, the density under CP (ρ_{pre}) was

COMPRESSION MODULUS AND APPARENT DENSITY OF POLYMERIC EXCIPIENTS DURING COMPRESSION – IMPACT ON TABLETABILITY

additionally considered for Heckel analysis according to Krumme et al. [25], leading to valid Heckel plots even at CPs of 300 MPa.

Overall, nonpolymeric excipients showed distinct curvature at the beginning of the Heckel plot related to particle rearrangement and fragmentation, which was much less pronounced for polymeric excipients. Moreover, polymeric excipients showed a larger extent of elastic recovery in the decompression phase compared with nonpolymeric excipients.

The Heckel plots for HME ASD and TB (Figure 5.11) were widely comparable to the curve shape of pure copovidone (Figure 5.9).

**COMPRESSION MODULUS AND APPARENT DENSITY OF POLYMERIC EXCIPIENTS
DURING COMPRESSION – IMPACT ON TABLETABILITY**

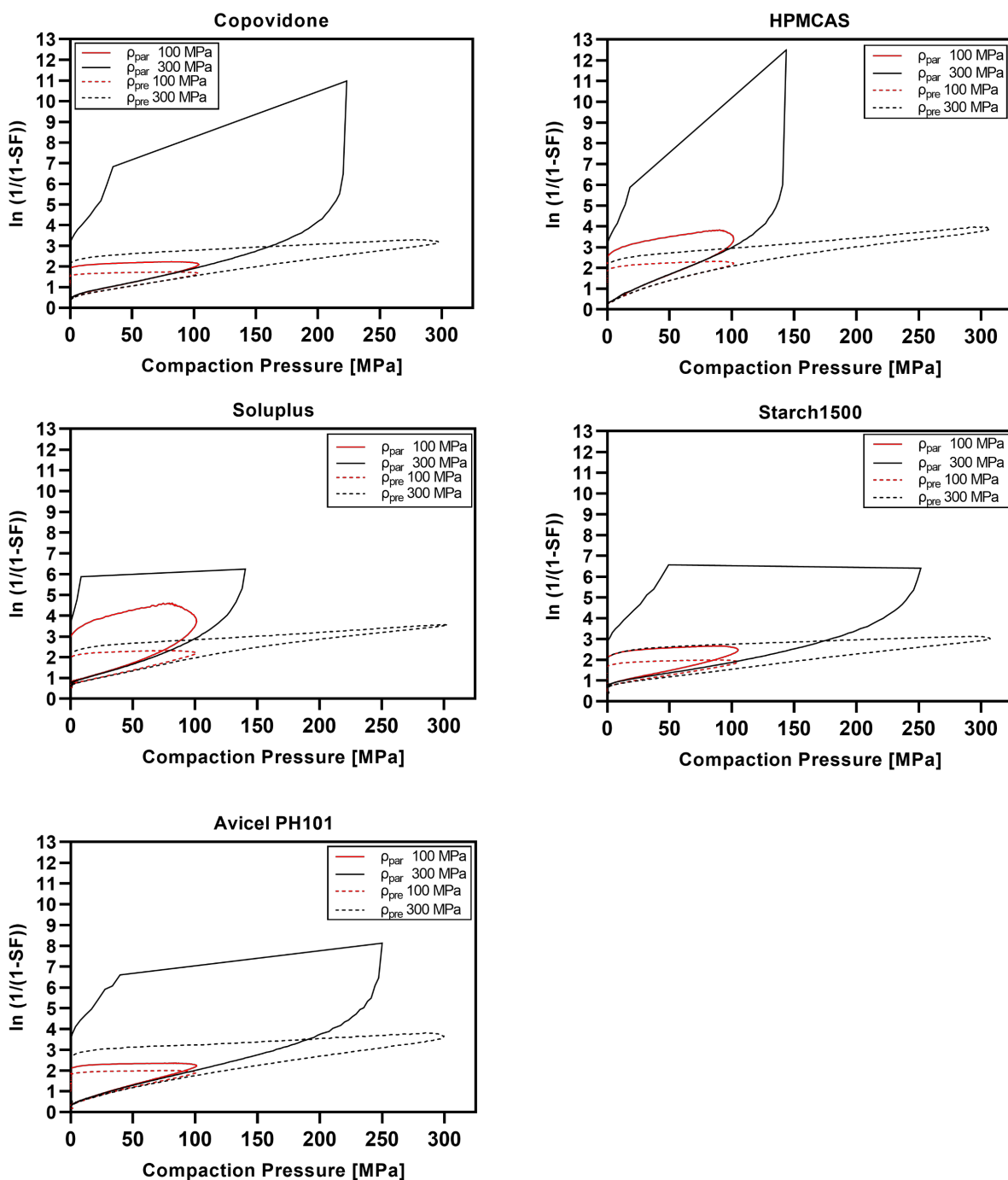


Figure 5.9. Heckel plots of polymeric excipients at 100 and 300 MPa calculated using particle density (ρ_{par}) or density under pressure (ρ_{pre})

**COMPRESSION MODULUS AND APPARENT DENSITY OF POLYMERIC EXCIPIENTS
DURING COMPRESSION – IMPACT ON TABLETABILITY**

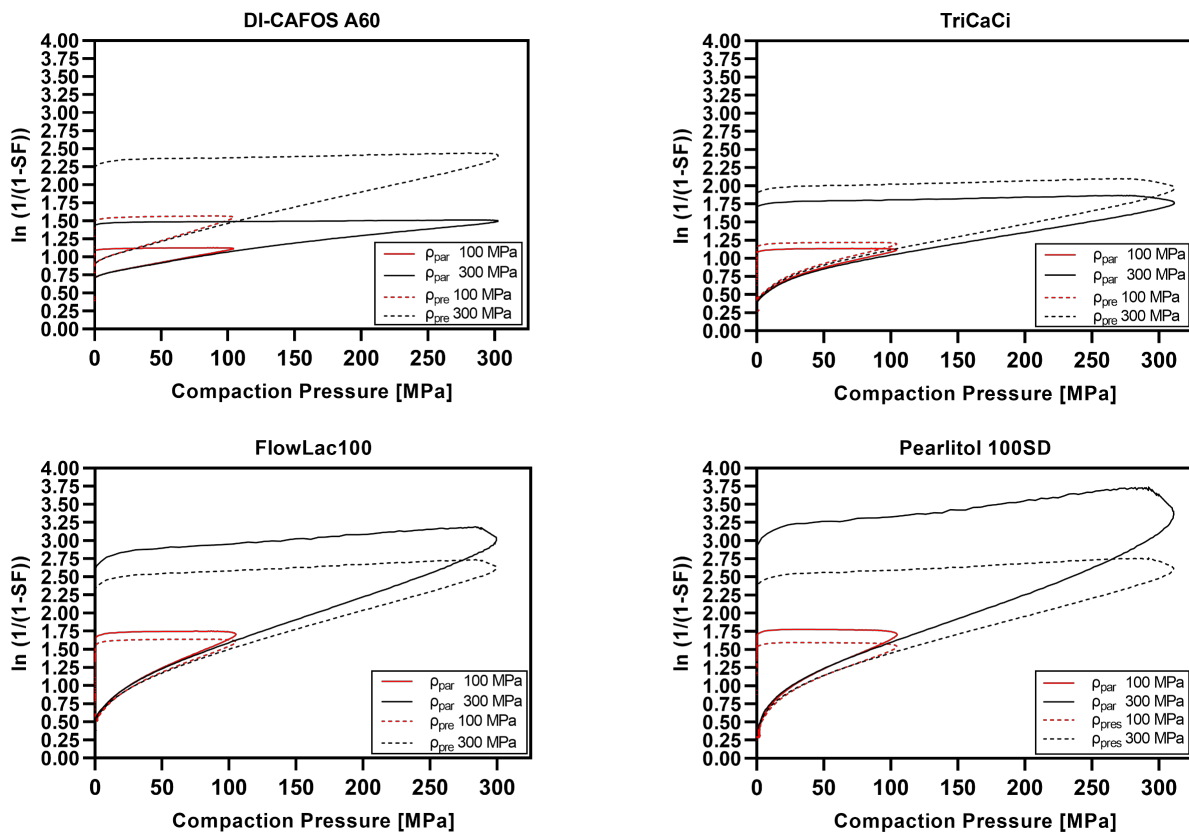


Figure 10: Heckel plots of nonpolymeric excipients at 100 and 300 MPa calculated using particle density (ρ_{par}) or density under pressure (ρ_{pre})

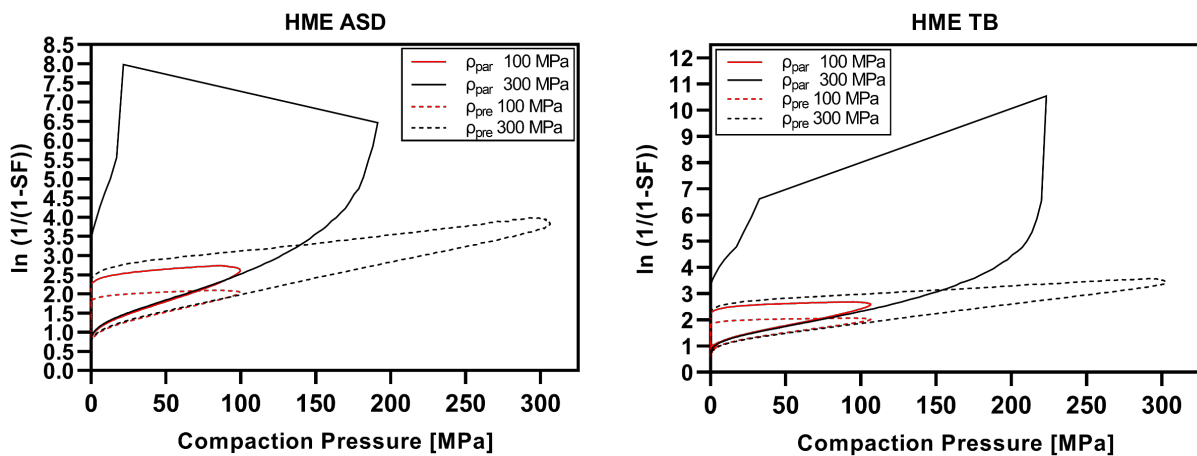


Figure 5.11: Heckel plots of HME ASD and HME TB at 100 and 300 MPa calculated using particle density (ρ_{par}) or density under pressure (ρ_{pre})

The calculated results of the Heckel analysis (in-die) are summarized in Table 5.3 for CP of 100 MPa (CP_{100}) and 300 MPa (CP_{300}) for all excipients as well as HME ASD and HME TB. The calculation of mean yield pressure (P_Y) allows an interpretation of the start of plastic flow, whereas the SF at intercept A of the linear ascending part of the Heckel plot indicates where SF bonding would occur. The highest mean yield pressures (P_Y) were observed for the nonpolymeric excipients such as DI CAFOS®A60 (ρ_{par} : 293 MPa at CP_{100} ; 585 MPa at CP_{300}) and TriCaCi (ρ_{par} : 243 MPa at CP_{100} ; 336 MPa at CP_{300}) as expected for brittle fillers. At CP_{100} (ρ_{par}), FlowLac®100 (138 MPa) and Pearlitol®100SD (130 MPa) exhibited values above 100 MPa, indicating a lower degree of brittle deformation.

In contrast, the polymeric excipients revealed P_Y values at CP_{100} (ρ_{par}) below 100 MPa, indicating viscoelastic to plastic compaction behavior (HPMCAS: 42 MPa, Soluplus®: 57 MPa, copovidone: 80 MPa, Starch1500®: 82 MPa). The respective P_Y values for HME ASD (79 MPa) and TB (88 MPa) were similar to pure copovidone, as copovidone is a major component of the formulation. Still, slightly higher values at both CPs could be observed for the HME TB, which was likely attributed to the brittle filler DI-CAFOS®A60 in the blend.

Figure 5.12 clearly visualizes the shift in yield pressures (P_Y) depending on the density used for calculation. If the density ratio was positive ($\rho_{pre} > \rho_{par}$) for the respective excipient, as seen for all polymeric excipients, the SF values were lower, resulting in a shift towards lower Y-axis values and lower slope values for the regression line in the Heckel plots. Thus, the yield pressures (P_Y) calculated with ρ_{pre} were slightly higher compared with those calculated via ρ_{par} . Exemplarily, the P_Y of HPMCAS at CP_{100} increased from 42 MPa to 69 MPa and the P_Y of Soluplus® from 57 MPa to 75 MPa. Although a clear shift could be observed, the trend between the investigated excipients stayed the same. For instance, for polymeric excipients, the ranking at CP_{100} was as follows, independently from the density used for calculation: Starch1500® > Copovidone (Kollidon®VA64) > Avicel®PH101 > Soluplus® > HPMCAS (AQOAT®AS-MMP). Since the ρ_{ratio} for DI-CAFOS®A60 and TriCaCi was negative, the P_Y values calculated with ρ_{pre} (DI-CAFOS®A60: 181 MPa, TriCaCi: 219 MPa) were lower compared with those with ρ_{par} (DI-CAFOS®A60: 293 MPa, TriCaCi: 243 MPa). For the P_Y values at CP_{300} similar shift tendencies could be observed.

COMPRESSION MODULUS AND APPARENT DENSITY OF POLYMERIC EXCIPIENTS DURING COMPRESSION – IMPACT ON TABLETABILITY

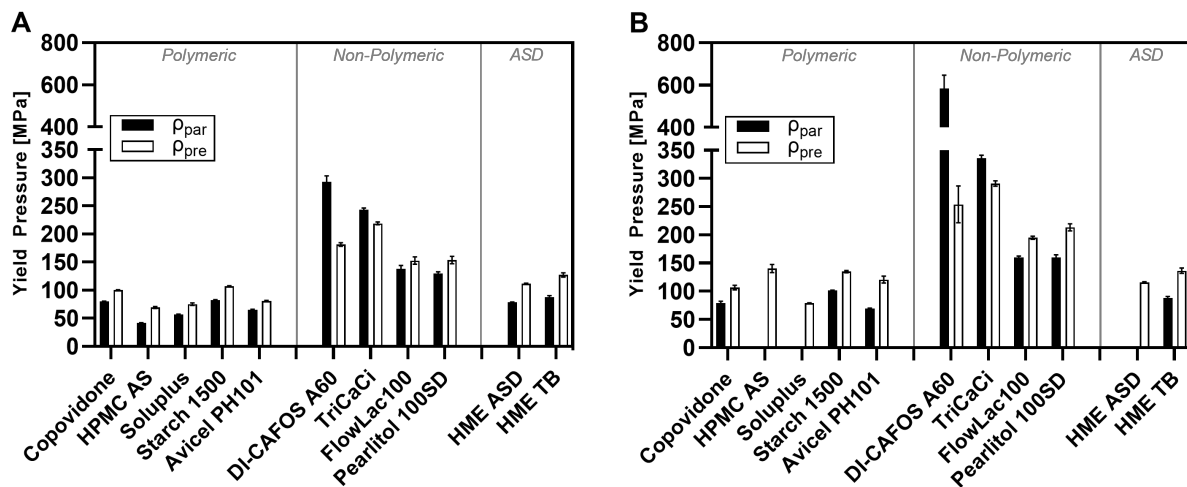


Figure 5.12: Yield pressure of excipients and HME ASD and HME TB at different compaction pressures (A) 100 MPa and (B) 300 MPa.

Table 5.3. Calculated parameters from the Heckel analysis for all excipients and HME ASD and TB compressed at 100 MPa and 300 MPa (n.a. = not applicable, no sufficient linearity)

	COMPACTON PRESSURE AT 100 MPa							
	Calculated with Particle Density (ρ_{par})				Calculated with Density under Pressure (ρ_{pre})			
	Slope k	Intercept A	Mean Yield Pressure P_Y [MPa]	SF Corresponding to A	Slope k	Intercept A	Mean Yield Pressure P_Y [MPa]	SF Corresponding to A
Copovidone	0.012 ± 0.000	0.603 ± 0.001	80.2 ± 0.2	0.453 ± 0.001	0.010 ± 0.000	0.559 ± 0.001	100.3 ± 0.3	0.428 ± 0.001
HPMC AS	0.024 ± 0.000	0.486 ± 0.006	41.8 ± 0.3	0.385 ± 0.004	0.014 ± 0.000	0.677 ± 0.026	69.1 ± 1.8	0.492 ± 0.013
Soluplus®	0.018 ± 0.000	0.816 ± 0.007	57.1 ± 0.5	0.558 ± 0.003	0.013 ± 0.000	0.713 ± 0.021	75.0 ± 2.2	0.510 ± 0.010
Starch1500®	0.012 ± 0.000	0.875 ± 0.002	82.3 ± 0.6	0.583 ± 0.001	0.009 ± 0.000	0.798 ± 0.002	107.1 ± 0.8	0.550 ± 0.001
Avicel®PH101	0.015 ± 0.000	0.544 ± 0.005	65.0 ± 0.8	0.420 ± 0.003	0.012 ± 0.000	0.587 ± 0.008	80.8 ± 1.1	0.444 ± 0.005
DI-CAFOS®A60	0.003 ± 0.000	0.776 ± 0.038	293.2 ± 10.4	0.540 ± 0.017	0.006 ± 0.000	0.956 ± 0.007	181.2 ± 3.2	0.616 ± 0.003
TriCaCi	0.004 ± 0.000	0.682 ± 0.006	243.4 ± 2.7	0.494 ± 0.003	0.005 ± 0.000	0.714 ± 0.006	218.9 ± 2.3	0.510 ± 0.003
FlowLac®100	0.007 ± 0.000	0.873 ± 0.007	137.7 ± 6.0	0.582 ± 0.003	0.007 ± 0.000	0.852 ± 0.007	152.6 ± 6.5	0.573 ± 0.003
Pearlitol®100SD	0.008 ± 0.000	0.865 ± 0.008	129.7 ± 2.9	0.579 ± 0.003	0.007 ± 0.000	0.832 ± 0.008	153.6 ± 3.5	0.565 ± 0.003
HME ASD	0.013 ± 0.000	1.158 ± 0.005	78.8 ± 0.3	0.686 ± 0.001	0.009 ± 0.000	1.072 ± 0.006	111.6 ± 0.8	0.658 ± 0.002
HME TB	0.011 ± 0.000	1.218 ± 0.007	87.5 ± 2.6	0.704 ± 0.002	0.008 ± 0.000	1.125 ± 0.006	127.1 ± 3.8	0.675 ± 0.002
COMPACTON PRESSURE AT 300 MPa								
	Calculated with Particle Density (ρ_{par})				Calculated with Density under Pressure (ρ_{pre})			
	Slope k	Intercept A	Mean Yield Pressure P_Y [MPa]	SF Corresponding to A	Slope k	Intercept A	Mean Yield Pressure P_Y [MPa]	SF Corresponding to A
	0.013 ± 0.001	0.595 ± 0.006	79.0 ± 3.2	0.448 ± 0.003	0.009 ± 0.000	0.579 ± 0.006	106.4 ± 4.1	0.440 ± 0.004
HPMC AS		n.a.			0.007 ± 0.000	1.579 ± 0.053	140.3 ± 7.3	0.794 ± 0.011
Soluplus®		n.a.			0.013 ± 0.000	0.712 ± 0.009	79.0 ± 0.4	0.509 ± 0.005
Starch1500®	0.010 ± 0.000	0.877 ± 0.001	101.4 ± 0.7	0.584 ± 0.001	0.007 ± 0.000	0.798 ± 0.007	134.8 ± 2.1	0.550 ± 0.003
Avicel®PH101	0.014 ± 0.000	0.572 ± 0.005	69.3 ± 0.7	0.436 ± 0.003	0.008 ± 0.000	1.030 ± 0.071	120.6 ± 6.1	0.642 ± 0.025
DI-CAFOS®A60	0.002 ± 0.000	0.943 ± 0.008	584.8 ± 62.0	0.610 ± 0.003	0.004 ± 0.000	1.083 ± 0.022	253.9 ± 32.7	0.661 ± 0.008
TriCaCi	0.003 ± 0.000	0.748 ± 0.002	336.0 ± 5.2	0.527 ± 0.001	0.003 ± 0.000	0.770 ± 0.002	290.9 ± 4.8	0.537 ± 0.001
FlowLac®100	0.006 ± 0.000	0.971 ± 0.002	159.5 ± 2.8	0.621 ± 0.001	0.005 ± 0.000	1.012 ± 0.006	194.9 ± 2.6	0.637 ± 0.002
Pearlitol®100SD	0.006 ± 0.000	0.945 ± 0.004	160.0 ± 4.7	0.611 ± 0.001	0.005 ± 0.000	0.978 ± 0.002	213.4 ± 6.2	0.624 ± 0.001
HME ASD		n.a.			0.009 ± 0.000	1.129 ± 0.008	115.5 ± 1.2	0.677 ± 0.002
HME TB	0.011 ± 0.000	1.163 ± 0.004	87.9 ± 2.8	0.687 ± 0.001	0.007 ± 0.000	1.117 ± 0.001	136.4 ± 4.7	0.673 ± 0.000

5.7 Discussion

5.7.1 Powder density in compression analysis - differences and consequences

The importance of the correct particle density determination for compression analysis, which significantly influences the resulting compaction parameters such as yield pressure (P_Y) within the Heckel model, has already been reported in the literature [18,21,23,25,39–42]. Gabaude et al. [42] clearly demonstrated that errors in measuring particle density have a greater effect on P_Y than the errors incurred from not correcting the displacement measurements due to punch elasticity. Thus, several publications focus on a suitable determination of the particle density considering the true conditions during compression analysis. For example, Sun [43] introduced a new method to determine the true density by calculating it via compaction data. This method involves the nonlinear regression of compaction pressure–tablet density data based on a modified Heckel equation. The intention is to avoid the impact of releasing water during the determination of the true density via helium pycnometer. Krumme et al. [25] introduced the “true density by compression” determined by compression experiments at a very high load level (0.73 GPa) under vacuum conditions. In most cases, the alternative approaches to determine the density used for compression analysis were observed to lead to higher absolute P_Y values. Krumme et al. [25] observed the strongest deviation from the pycnometric (true/particle) density for Starch1500® assumed to be related to a high number of internal pores, whereas the deviation for lactose was much smaller. The present study corroborated these findings exceeding them to other polymeric excipients showing pronounced positive ρ_{ratio} values, whereas nonpolymeric excipients had “density under pressure” values below the particle density (negative ρ_{ratio}) or less pronounced deviations from the ρ_{par} . The density values (e.g., ρ_{par} vs. ρ_{pre}) differ depending on the method used. This suggests that deriving compaction behavior parameters should be assessed relatively and not absolutely. Meaning, comparability between calculated values might only be given if the same method for density determination is used. Therefore, no clear boundaries for categories can be set considering all kinds of methods. Taking into account that even more variables such as simulated tablet press, tooling, compression speed, and applied force have an influence on compaction behavior parameters, the suggested approach seems reasonable.

5.7.2 Particle density exceeded during compression and the impact on elastic recovery

The present study observed exceeding particle densities for polymeric excipients and the amorphous solid dispersion (ASD) model formulation already at low CPs (e.g., Starch1500® at 177 MPa and Avicel®PH101 at 204 MPa). Similar results have been reported by Van der Voort Maarschalk et al. [11] for pregelatinized potato starch, by Schlack [23] for Starch1500®, as well as for microcrystalline cellulose (Avicel®PH102) assuming solid-state compression. However, the absolute exceedance threshold was slightly higher, with values around 240 MPa for Starch1500® and 280 MPa for Avicel®PH102. This might be related to differences in tablet press type (eccentric vs. rotary press) and dwell time differences. Accordingly, Wünsch et al. [24] showed in their recently published work that solid-state compression for microcrystalline cellulose (Vivapur®102) and paracetamol at CPs around 250–300 MPa and for lactose (anhydrous) at 400 MPa. Consequently, the bulk modulus measured by mercury porosimetry was used to characterize the deformation behavior of powders instead of ρ_{par} .

The current study showed a clear difference in threshold values between polymeric and nonpolymeric excipients. In addition, processing polymeric excipients used for ASD manufacture via hot-melt extrusion led to a threshold value in a similar CP range which was exemplarily shown for copovidone. Consequently, it seems worthy to consider the threshold value in CP as a potential alternative approach to categorize materials based on their compaction behavior; excipients with threshold values below 300 MPa showed predominantly viscoelastic/plastic deformation, whereas excipients with values above 350 MPa or without any determinable threshold value exhibit brittle compaction behavior. However, Yost et al. [44] clearly demonstrated that for tablet formulation development, the API plays an important role in showing lesser suitability being classified by the common approaches. In addition, the results offer the opportunity to rate the risk for tablet defects based on stored elastic energy depending on the required compaction pressure for a certain mechanical strength of the tablet. However, considering tabletability, there are more factors involved in influencing the mechanical strength of the tablets, such as particle morphology, as demonstrated in previous work [45]. It was shown that tabletability as such is mostly influenced by the particle morphology comparing ASDs with similar solid-state by hot-melt extrusion, spray-drying, or vacuum drum drying. Besides, the threshold of increasing total elastic recovery was comparable for all investigated ASDs independent of the technology.

Moreover, the present study indicated that exceeding the particle density might be linked with the start of a linear increase in fast (initial) elastic recovery (ER_{in-die}), especially for

polymeric excipients. Consequently, the energy applied to the compact over the threshold value was converted into elastic deformation of the material itself and not just of the particles. This energy was then released immediately during the in-die decompression phase. Thus, a solid-state compression can be suggested according to this data set. The demonstrated applicability of calculating the elastic modulus of a powder based on the linear increase in the ER_{in-die} above the particle density threshold confirmed this conclusion. In general, the absolute values for the elastic modulus depend on the determination method. However, similar trends could be observed using the method presented here compared to common literature. Iyer et al. [46] indicated that polymeric excipients such as copovidone (6.3 GPa), HPMCAS (3.0 GPa), or Avicel[®]PH101 (8.1 GPa) exhibit lower elastic modulus values corresponding to higher elasticity compared to nonpolymeric excipients such as dibasic calcium phosphate anhydrous (41 GPa) or lactose monohydrate (11.3 GPa) assuming higher degree in stiffness. E_{mod} values determined in the current study were in the range of 5–9 GPa (copovidone 6.1 GPa, Starch1500[®] 6.8 GPa, Avicel[®]PH101 8.9 GPa) for polymeric excipients. Consequently, our results led to similar conclusions about elasticity/stiffness and thus, demonstrated proof of predominantly elastic deformation via solid-state compression at compaction pressures above the particle density threshold.

Similar conclusions were drawn by Christian [47] for Eudragit[®] RS PO polymer used in sustained-release tablets. By comparing the in-die with the out-of-die porosity in dependency of the CP, it was observed by Christian [47] that the porosity of the tablets out-of-die was not changing, although the porosity in-die was being further reduced. The plateau was reached with exceeding particle density which was at CPs of about 150 MPa and in line with the values for polymeric excipients of the present study.

For nonpolymeric excipients, an increase in ER_{in-die} was not observed in the investigated CP range except for Pearlitol[®]100SD. However, Pearlitol[®]100SD exhibited a threshold in this CP range, explaining the observed increase in ER_{in-die} .

Overall, the extent of the ER_{in-die} for polymeric and nonpolymeric excipients was in accordance with the literature. Tanner [48] noted ER_{in-die} values for calcium phosphate grades of 1–5%, lactose grades of 1–6%, microcrystalline cellulose grades of 7–12%, HPMC of 14–17%, and starch grades of 14–18%. The present study determined values in similar ranges for nonpolymeric excipients, e.g., <4% for FlowLac[®]100 and <3% for DI-CAFOS[®]A60. For polymeric excipients, the values were slightly lower, as reported by Tanner [48] (HPMCAS: 5–13%, Starch1500[®]: 5–11%). Zhang et al. [49] observed higher ER_{in-die} values from

15–340 MPa for Avicel®PH101 (3–3.5%) as a polymeric excipient, whereas lactose monohydrate, mannitol, or dibasic calcium phosphate showed values around 1.5–2%.

The elastic recovery caused by stored elastic energy is assumed to be one of the main causes of capping or lamination defects, according to van der Voort Maarschalk et al. [50]. Moreover, it is known to diminish the tensile strength of tablets by rupturing bonds between particles. Consequently, determining and considering the threshold for formulation and process development purposes might be useful to mitigate the risk of tablet defects related to stored elastic energy. It is certainly conceivable to include the threshold for exceedance of the particle density in a risk assessment for drug product development.

5.7.3 Impact of density determination on Heckel analysis

The Heckel plots of polymeric excipients indicated pronounced viscoelastic/plastic deformation based on the strong elastic recovery and the less distinct particle rearrangement/fragmentation phase. Nonpolymeric excipients instead showed a long particle rearrangement/fragmentation phase and much less elastic recovery. The shapes of the Heckel plots presented in the current study were in accordance with the literature [23,25,26].

However, the present work demonstrated that Heckel plots were not valid for CPs exceeding the threshold of particle density if the particle density is used for porosity calculation. Similar observations were made by Schlack [23] for Starch1500® and Avicel®PH102. It was stated that Heckel plots could not be plotted properly above a CP of 250 MPa. Wünsch et al. [24] observed bending of the Heckel curve for microcrystalline cellulose and paracetamol above 250–300 MPa to high y-axis values assuming less suitability for Heckel analysis if using noncorrected density data. Additionally, Mahmoodi et al. [51] presented Heckel plots showing strong bending towards higher y-axis values in the ascending part already at CPs below 250 MPa for PEG 6000, maize starch, Starch1500®, PVP, and aspirin. Moreover, recently, Yost et al. [44] stated that Heckel results should be taken with caution for elastic materials.

The yield pressure (P_Y) values calculated based on the linear regression within the ascending part of the Heckel plot were consistent with current literature [13,26]. In general, we observed a shift to higher P_Y values for polymeric excipients by using the “density under pressure” approach for calculation. Similar observations were made for Starch1500® by Schlack [23], and for Avicel by Krumme et al. [25] and Krumme [52]. An explanation was provided by Sonnergaard [53], demonstrating that the derived Heckel parameters such as yield pressure are predominantly influenced by the particle density; the higher the density value

COMPRESSION MODULUS AND APPARENT DENSITY OF POLYMERIC EXCIPIENTS DURING COMPRESSION – IMPACT ON TABLETABILITY

used for calculation, the higher the respective yield pressures. It was stated that there might be an influence on P_Y based on the particle density value per se.

Based on the observations made in the current study, the question arises if the Heckel equation is applicable for polymeric excipients or, in general, for excipients showing densification under pressure above particle density. It should be considered in defining a common compaction pressure limit for the applicability of the Heckel analysis for excipients showing exceeding particle density might be reasonable. In addition, it should be discussed whether the porosity calculation for compression analysis should be adapted by means of the “density under pressure” in such cases. Moreover, if comparing different kinds of excipients, e.g., polymeric with nonpolymeric ones, whether it makes sense to use the same porosity calculation approach or if it should be tailored for each excipient based on the excipient’s properties; “density under pressure” for excipients exceeding the particle density and particle density for excipients showing no exceeding.

All this leads to the ultimate question: what benefit remains for the Heckel analysis in the development of solid oral dosage forms if it requires a complex assessment of its applicability considering its limitations combined with a high error susceptibility in determining related measurands such as density? For us, it is certainly conceivable to use the particle density threshold instead. The threshold value can be assessed easily using any instrumented tablet press, providing knowledge of the compaction pressure above which elastic deformation occurs predominantly during compression. Knowing the threshold compaction pressure offers the opportunity to rate the risk of tablet defects caused by the stored elastic energy during formulation and process development.

5.8 Conclusion

The present study revealed that during compression of polymeric excipients, the particle density was already exceeded at low compaction pressures (CPs). In comparison, the particle density of compressed nonpolymeric excipients was reached either at higher CPs or never. We found that the threshold for this exceedance correlated with the start of a linear increase in elastic recovery (in-die). This means that the energy needed to achieve higher densification than the particle density was directly linked to the elastic deformation of the material itself (solid-state compression). Consequently, the threshold exceedance during tabletting might increase the risk for tablet defects due to stored elastic energy and thus, should be avoided. Similar trends were seen for a model amorphous solid dispersion (ASD) containing ritonavir as a drug substance and copovidone as a matrix polymer. However, it was observed that the addition of a brittle filler (DI-CAFOS®A60) led to a threshold shift towards higher CPs, reducing the risk for tablet defects and increasing the design space for the compression process during development.

In addition, the common Heckel compression analysis was shown not to be valid at high CPs, considering the particle density for calculation. In general, it might be questioned if the Heckel analysis is useful for polymeric excipients.

To conclude, the knowledge about the pressure threshold, where the density under compression exceeds the particle density during compression, could reduce the risk in tablet development as suitable fillers might be selected to either compensate for pronounced elasticity or assign safe pressure windows for production.

5.9 Author contributions

B. V. Schönenfeld: Conceptualization, Methodology, Investigation, Visualization, Writing - original draft. U. Westedt: Conceptualization, Methodology, Project administration, Supervision, Writing - review & editing. K. G. Wagner: Conceptualization, Methodology, Supervision, Writing - review & editing.

5.10 Conflicts of interest

Barbara V. Schönfeld and Ulrich Westedt are employees of AbbVie and may own AbbVie stock. Barbara V. Schönfeld is a Ph.D. student, and Karl G. Wagner is a professor at the University of Bonn. They have no additional conflict of interest to report.

5.11 Acknowledgments

The authors kindly thank Wolfgang Erker (AbbVie Deutschland GmbH & Co. KG) for his support in Igor Pro v8 (WaveMetrics Inc., Lake Oswego, OR, USA).

5.12 Funding

This work was funded by AbbVie Deutschland GmbH & Co. KG. The University of Bonn and AbbVie participated in study design, research, interpretation of data, writing, data collection, analysis, reviewing, and approving the publication.

5.13 Data availability statement

The data presented in this study are available in the research article.

5.14 References

1. Patel, S.; Kaushal, A.M.; Bansal, A.K. Compression Physics in the Formulation Development of Tablets. *Critical Reviews in Therapeutic Drug Carrier Systems* 2006, 23, 1–66. <https://doi.org/10.1615/CritRevTherDrugCarrierSyst.v23.i1.10>.
2. Sohail Arshad, M.; Zafar, S.; Yousef, B.; Alyassin, Y.; Ali, R.; AlAsiri, A.; Chang, M.-W.; Ahmad, Z.; Elkordy, A.A.; Faheem, A.; et al. A review of emerging technologies enabling improved solid oral dosage form manufacturing and processing. *Advanced Drug Delivery Reviews* 2021, 178, 113840. <https://doi.org/10.1016/j.addr.2021.113840>.
3. Jermain, S.V.; Brough, C.; Williams, R.O., 3rd. Amorphous solid dispersions and nanocrystal technologies for poorly water-soluble drug delivery—An update. *International Journal of Pharmaceutics* 2018, 535, 379–392. <https://doi.org/10.1016/j.ijpharm.2017.10.051>.
4. Crowley, M.M.; Zhang, F.; Repka, M.A.; Thumma, S.; Upadhye, S.B.; Battu, S.K.; McGinity, J.W.; Martin, C. Pharmaceutical Applications of Hot-Melt Extrusion: Part I. Drug Development and Industrial Pharmacy 2007, 33, 909–926. <https://doi.org/10.1080/03639040701498759>.
5. Agrawal, A.; Dudhedia, M.; Deng, W.; Shepard, K.; Zhong, L.; Povilaitis, E.; Zimny, E. Development of Tablet Formulation of Amorphous Solid Dispersions Prepared by Hot Melt Extrusion Using Quality by Design Approach. *AAPS PharmSciTech* 2016, 17, 214–232. <https://doi.org/10.1208/s12249-015-0472-0>.
6. Bhujbal, S.V.; Mitra, B.; Jain, U.; Gong, Y.; Agrawal, A.; Karki, S.; Taylor, L.S.; Kumar, S.; Zhou, Q. Pharmaceutical amorphous solid dispersion: A review of manufacturing strategies. *Acta Pharmacologica Sinica B* 2021, 11, 2505–2536. <https://doi.org/10.1016/j.apsb.2021.05.014>.
7. Joiris, E.; Martino, P.D.; Berneron, C.; Guyot-Hermann, A.-M.; Guyot, J.-C. Compression Behavior of Orthorhombic Paracetamol. *Pharmaceutical Research* 1998, 15, 1122–1130. <https://doi.org/10.1023/A:1011954800246>.
8. Jain, S. Mechanical properties of powders for compaction and tableting: An overview. *Pharmaceutical Sciences & Technology Today* 1999, 2, 20–31. [https://doi.org/10.1016/S1461-5347\(98\)00111-4](https://doi.org/10.1016/S1461-5347(98)00111-4).
9. Nyström, C.; Alderborn, G.; Duberg, M.; Karehill, P.-G. Bonding Surface area and Bonding Mechanism-Two Important Factors for the Understanding of Powder Comparability. *Drug Development and Industrial Pharmacy* 1993, 19, 2143–2196. <https://doi.org/10.3109/03639049309047189>.
10. Sun, W.-J.; Kothari, S.; Sun, C.C. The relationship among tensile strength, Young's modulus, and indentation hardness of pharmaceutical compacts. *Powder Technology* 2018, 331, 1–6. <https://doi.org/10.1016/j.powtec.2018.02.051>.
11. Maarschalk, K.V.D.V.; Zuurman, K.; Vromans, H.; Bolhuis, G.K.; Lerk, C.F. Stress relaxation of compacts produced from viscoelastic materials. *International Journal of Pharmaceutics* 1997, 151, 27–34. [https://doi.org/10.1016/S0378-5173\(97\)04889-8](https://doi.org/10.1016/S0378-5173(97)04889-8).
12. Busignies, V.; Mazel, V.; Diarra, H.; Tchoreloff, P. Role of the elasticity of pharmaceutical materials on the interfacial mechanical strength of bilayer tablets. *International Journal of Pharmaceutics* 2013, 457, 260–267. <https://doi.org/10.1016/j.ijpharm.2013.09.009>.

COMPRESSION MODULUS AND APPARENT DENSITY OF POLYMERIC EXCIPIENTS
DURING COMPRESSION – IMPACT ON TABLETABILITY

13. Li, X.H.; Zhao, L.J.; Ruan, K.P.; Feng, Y.; Xu, D.S.; Ruan, K.F. The application of factor analysis to evaluate deforming behaviors of directly compressed powders. *Powder Technology* 2013, 247, 47–54. <https://doi.org/10.1016/j.powtec.2013.06.040>.
14. Heckel, R.W. Density-pressure relationships in powder compaction. *Transactions of the Metallurgical Society of AIME* 1961, 221, 671–675.
15. Kawakita, K.; Lüdde, K.-H. Some considerations on powder compression equations. *Powder Technology* 1971, 4, 61–68. [https://doi.org/10.1016/0032-5910\(71\)80001-3](https://doi.org/10.1016/0032-5910(71)80001-3).
16. Kuentz, M.; Leuenberger, H. Pressure susceptibility of polymer tablets as a critical property: A modified heckel equation. *Journal of Pharmaceutical Sciences*. 1999, 88, 174–179. <https://doi.org/10.1021/js980369a>.
17. Rue, P.J.; Rees, J.E. Limitations of the Heckel relation for predicting powder compaction mechanisms. *Journal of Pharmacy and Pharmacology* 1978, 30, 642–643.
18. Sonnergaard, J.M. A critical evaluation of the Heckel equation. *International Journal of Pharmaceutics* 1999, 193, 63–71. [https://doi.org/10.1016/S0378-5173\(99\)00319-1](https://doi.org/10.1016/S0378-5173(99)00319-1).
19. Denny, P.J. Compaction equations: A comparison of the Heckel and Kawakita equations. *Powder Technology* 2002, 127, 162–172. [https://doi.org/10.1016/S0032-5910\(02\)00111-0](https://doi.org/10.1016/S0032-5910(02)00111-0).
20. Patel, S.; Kaushal, A.M.; Bansal, A.K. Mechanistic investigation on pressure dependency of Heckel parameter. *International Journal of Pharmaceutics* 2010, 389, 66–73. <https://doi.org/10.1016/j.ijpharm.2010.01.020>.
21. Sun, C.; Grant, D.J.W. Influence of Elastic Deformation of Particles on Heckel Analysis. *Pharmaceutical Development and Technology* 2001, 6, 193–200. <https://doi.org/10.1081/PDT-100000738>.
22. Ilić, I.; Govedarica, B.; Šibanc, R.; Dreu, R.; Srčić, S. Deformation properties of pharmaceutical excipients determined using an in-die and out-die method. *International Journal of Pharmaceutics* 2013, 446, 6–15. <https://doi.org/10.1016/j.ijpharm.2013.02.001>.
23. Schlack, H. Kompressibilität Und Kompaktibilität Von Hilfsstoffen Bei Der Tablettierung; Albert-Ludwigs-University Freiburg: Freiburg, Germany, 2001; p. 149. urn:nbn:de:bsz:25-opus-1741
24. Wünsch, I.; Finke, J.H.; John, E.; Juhnke, M.; Kwade, A. A Mathematical Approach to Consider Solid Compressibility in the Compression of Pharmaceutical Powders. *Pharmaceutics* 2019, 11, 121. <https://doi.org/10.3390/pharmaceutics11030121>.
25. Krumme, M.; Schwabe, L.; Frömming, K.-H. Development of computerised procedures for the characterisation of the tableting properties with eccentric machines: Extended Heckel analysis. *European Journal of Pharmaceutics and Biopharmaceutics* 2000, 49, 275–286. [https://doi.org/10.1016/S0939-6411\(00\)00067-9](https://doi.org/10.1016/S0939-6411(00)00067-9).
26. Hagelstein, V.; Gerhart, M.; Wagner, K. Tricalcium Citrate—A New Brittle Tableting Excipient for Direct Compression and Dry Granulation with Enormous Hardness Yield. *Drug Development and Industrial Pharmacy* 2018, 44, 1631–1641. <https://doi.org/10.1080/03639045.2018.1483389>.
27. Lawal, M.V. Modified starches as direct compression excipients—effect of physical and chemical modifications on tablet properties: A review. *Starch-Stärke* 2019, 71, 1800040.
28. Jivraj, M.; Martini, L.G.; Thomson, C.M. An overview of the different excipients useful for the direct compression of tablets. *Pharmaceutical Science & Technology Today* 2000, 3, 58–63. [https://doi.org/10.1016/S1461-5347\(99\)00237-0](https://doi.org/10.1016/S1461-5347(99)00237-0).

29. Hentzschel, C.M.; Sakmann, A.; Leopold, C.S. Comparison of traditional and novel tabletting excipients: Physical and compaction properties. *Pharmaceutical Development and Technology* 2012, 17, 649–653. <https://doi.org/10.3109/10837450.2011.572897>.
30. Steffens, K.E.; Wagner, K.G. Improvement of tabletability via twin-screw melt granulation: Focus on binder distribution. *International Journal of Pharmaceutics* 2019, 570, 118649. <https://doi.org/10.1016/j.ijpharm.2019.118649>.
31. Zhang, Y.; Law, Y.; Chakrabarti, S. Physical properties and compact analysis of commonly used direct compression binders. *AAPS PharmSciTech* 2003, 4, 489–499. <https://doi.org/10.1208/pt040462>.
32. Kolakovic, R.; Peltonen, L.; Laaksonen, T.; Putkisto, K.; Laukkonen, A.; Hirvonen, J. Spray-Dried Cellulose Nanofibers as Novel Tablet Excipient. *AAPS PharmSciTech* 2011, 12, 1366–1373. <https://doi.org/10.1208/s12249-011-9705-z>.
33. Hauschild, K.; Picker, K.M. Evaluation of a new coprocessed compound based on lactose and maize starch for tablet formulation. *AAPS PharmSci* 2004, 6, 27–38. <https://doi.org/10.1208/ps060216>.
34. Paul, S.; Tajarobi, P.; Boissier, C.; Sun, C.C. Tableting performance of various mannitol and lactose grades assessed by compaction simulation and chemometrical analysis. *International Journal of Pharmaceutics* 2019, 566, 24–31. <https://doi.org/10.1016/j.ijpharm.2019.05.030>.
35. Chaudhary, R.S.; Patel, C.; Sevak, V.; Chan, M. Effect of Kollidon VA®64 particle size and morphology as directly compressible excipient on tablet compression properties. *Drug Development and Industrial Pharmacy* 2018, 44, 19–29. <https://doi.org/10.1080/03639045.2017.1371735>.
36. Technical Information Soluplus; BASF: Ludwigshafen am Rhein, Germany, 2019. Available online: <https://pharma.bASF.com/technicalinformation/30446233/soluplus> (accessed on 11 April 2022).
37. Starch 1500 Partially Pregelatinized Maize Starch Technical Bulletin; Colorcon: 2020. Available online: <https://www.colorcon.com/es/products-formulation/all-products/excipients/tablets/starch-1500/download/2920/4729/34> (accessed on 11 April 2022).
38. United States Pharmacopeia. General Chapter, (1062) Tablet Compression Characterization; United States Pharmacopeia: Rockville, MD, USA, 2022. Available online: https://doi.org/10.31003/USPNF_M99395_02_01 (accessed on 11 April 2022).
39. Paul, S.; Chang, S.-Y.; Sun, C.C. The phenomenon of tablet flashing—Its impact on tabletting data analysis and a method to eliminate it. *Powder Technology* 2017, 305, 117–124. <https://doi.org/10.1016/j.powtec.2016.09.054>.
40. Sun, C.C. Quantifying Errors in Tableting Data Analysis Using the Ryshkewitch Equation Due to Inaccurate True Density. *Journal of Pharmaceutical Sciences* 2005, 94, 2061–2068. <https://doi.org/10.1002/jps.20421>.
41. Paul, S.; Sun, C.C. The suitability of common compressibility equations for characterizing plasticity of diverse powders. *International Journal of Pharmaceutics* 2017, 532, 124–130. <https://doi.org/10.1016/j.ijpharm.2017.08.096>.
42. Gabaude, C.M.D.; Guillot, M.; Gautier, J.C.; Saudemon, P.; Chulia, D. Effects of true density, compacted mass, compression speed, and punch deformation on the mean yield pressure. *Journal of Pharmaceutical Sciences* 1999, 88, 725–730. <https://doi.org/10.1021/jf9803050>.

43. Sun, C. A Novel Method for Deriving True Density of Pharmaceutical Solids Including Hydrates and Water-Containing Powders. *Journal of Pharmaceutical Sciences* 2004, 93, 646–653. <https://doi.org/10.1002/jps.10595>.
44. Yost, E.; Mazel, V.; Sluga, K.K.; Nagapudi, K.; Muliadi, A.R. Beyond Brittle/Ductile Classification: Applying Proper Constitutive Mechanical Metrics to Understand the Compression Characteristics of Pharmaceutical Materials. *Journal of Pharmaceutical Sciences* 2022, article in press. <https://doi.org/10.1016/j.xphs.2022.01.004>.
45. Schönenfeld, B.V.; Westedt, U.; Wagner, K.G. Compression of amorphous solid dispersions prepared by hot-melt extrusion, spray drying and vacuum drum drying. *International Journal of Pharmaceutics X* 2021, 3, 100102. <https://doi.org/10.1016/j.ijpx.2021.100102>.
46. Iyer, R.; Hegde, S.; Zhang, Y.-E.; Dinunzio, J.; Singhal, D.; Malick, A.; Amidon, G. The Impact of Hot Melt Extrusion and Spray Drying on Mechanical Properties and Tableting Indices of Materials Used in Pharmaceutical Development. *Journal of Pharmaceutical Sciences* 2013, 102, 3604–3613. <https://doi.org/10.1002/jps.23661>.
47. Christian, S. Sustained Release Matrix Granules for Multiple Unit Dosage Forms Prepared by Dry Granulation; Eberhard Karls University Tübingen: Tübingen, Germany, 2005. Available online: <http://nbn-resolving.de/urn:nbn:de:bsz:21-opus-21602> (accessed on 11 April 2022).
48. Tanner, T. Evaluating Mechanical Properties and Tableting of Pharmaceutical Powders with a Novel Gravitation-Based High-Velocity Compaction Method; University of Helsinki: Helsinki, Finland, 2021. Available online: <http://urn.fi/URN:ISBN:978-951-51-7148-1> (accessed on 11 April 2022).
49. Zhang, J.; Wu, C.-Y.; Pan, X.; Wu, C. On Identification of Critical Material Attributes for Compression Behaviour of Pharmaceutical Diluent Powders. *Materials* 2017, 10, 845.
50. Maarschalk, K.V.D.V.; Zuurman, K.; Vromans, H.; Bolhuis, G.K.; Lerk, C.F. Porosity expansion of tablets as a result of bonding and deformation of particulate solids. *International Journal of Pharmaceutics* 1996, 140, 185–193. [https://doi.org/10.1016/0378-5173\(96\)04584-X](https://doi.org/10.1016/0378-5173(96)04584-X).
51. Mahmoodi, F.; Klevan, I.; Nordström, J.; Alderborn, G.; Frenning, G. A comparison between two powder compaction parameters of plasticity: The effective medium A parameter and the Heckel 1/K parameter. *International Journal of Pharmaceutics* 2013, 453, 295–299. <https://doi.org/10.1016/j.ijpharm.2013.06.040>.
52. Krumme, M. Entwicklung rechnergestützter Verfahren zur Kompressions- und Festigkeitsanalyse von Tabletten; Freie Universität Berlin: Berlin, Germany, 1992.
53. Sonnergaard, J.M. Impact of particle density and initial volume on mathematical compression models. *European Journal of Pharmaceutical Sciences* 2000, 11, 307–315. [https://doi.org/10.1016/S0928-0987\(00\)00119-6](https://doi.org/10.1016/S0928-0987(00)00119-6).

6. TRANSFORMATION OF RITONAVIR NANOCRYSTAL SUSPENSIONS INTO A REDISPERSIBLE DRUG PRODUCT VIA VACUUM DRUM DRYING

Barbara V. Schönfeld^{a,b}, Ulrich Westedt^b, Benjamin-Luca Keller^b, Karl G. Wagner^{a,c}

^aDepartment of Pharmaceutical Technology, University of Bonn, Gerhard-Domagk-Straße 3, 53121 Bonn, Germany, karl.wagner@uni-bonn.de, barbara.schoenfeld@uni-bonn.de

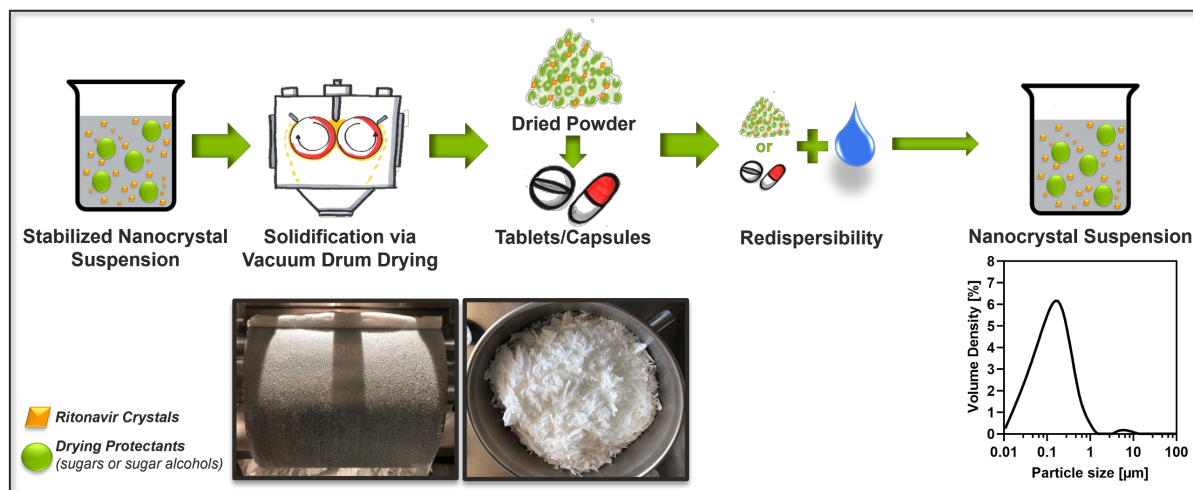
^bAbbVie Deutschland GmbH & Co. KG, Knollstraße 50, 67061 Ludwigshafen, Germany, ulrich.westedt@abbvie.com, benjamin-luca.keller@abbvie.com, barbara.schoenfeld@abbvie.com

^cCorresponding author

This part was published as:

B. V. Schönfeld, U. Westedt, B.-L. Keller, K. G. Wagner, Transformation of ritonavir nanocrystal suspensions into a redispersible drug product via vacuum drum drying, AAPS PharmSciTech, Volume 23, 137 (2022), <https://doi.org/10.1208/s12249-022-02283-z>

6.1 Graphical Abstract



6.2 Abstract

The present study explored vacuum drum drying (VDD) as potential drying technique for the solidification of crystalline ritonavir nanosuspensions prepared by wet-ball milling. In detail, the impact of drying protectants (mannitol, lactose, trehalose) added to the ritonavir nanosuspension was assessed in dependence of the drum temperature with respect to processability via VDD, resulting intermediate powder properties, remaining nanoparticulate redispersibility and crystallinity. A clear impact of the glass transition temperature (T_g) of the drying protectant on the redispersibility/crystallinity of the VDD intermediate was observed. Increased T_g of the drying protectant was associated with improved redispersibility/crystallinity at a defined drum temperature. Consequently, the high T_g -substances trehalose and lactose showed a better performance than mannitol at higher drum temperatures. However, the processability and related powder properties were not in accordance with this observation. Mannitol containing formulations showed superior processability to those containing trehalose/lactose. Moreover, the impact of the tableting and encapsulation process on the redispersibility of the VDD intermediate was studied for a selected formulation. Neither process demonstrated a negative impact on redispersibility. In conclusion, vacuum drum drying is a promising drying technique for the solidification of nanosuspensions to result in dried powder still containing ritonavir nanoparticles while demonstrating acceptable to good downstream processability to tablets/capsules.

6.3 Keywords

Ritonavir; vacuum drum drying; solidification; nanocrystals; drying protectants.

6.4 Introduction

The importance of addressing the poor water-solubility of drug candidates in pharmaceutical development has become more pronounced in the last years, since nearly 90% of the drug candidates are poorly soluble, resulting in limited bioavailability [1-3]. One strategy to tackle the solubility issue is the nanocrystal approach, whereby the crystalline drug substance is nanosized to improve dissolution behavior and saturation solubility according to the Noyes-Whitney and Ostwald-Freundlich principles [4-6]. The nanocrystal formulations are generally based on a liquid, aqueous nanocrystal suspension (nanosuspension) in the nanometer size range (100-1000 nm). However, nanoparticles in aqueous media require stabilization since nanoparticles are much less stable than microparticles due to the Gibbs free energy contribution. Two types of stabilizers with different functional principles are described in literature: ionic stabilizers via thermodynamic/electrostatic stabilization, and steric stabilizers via kinetic stabilization [7,8]. The combination of both is most commonly utilized, demonstrating the highest stabilization effectiveness due to a synergistic effect which is also referred to as electrosteric stabilization [9-11].

Nanosuspensions can be prepared by either top-down (e.g., wet ball milling) or bottom-up (e.g., precipitation) approaches [12-13]. However, in the pharmaceutical industry top-down approaches are far more relevant due to their simplicity, reproducibility and scalability [9,13]. The most prominent methods are NanoCrystal® (wet ball milling) and IDD-P™ (insoluble drug delivery microparticle technology, high pressure homogenisation) [13] which are used in the manufacture of drug products such as Invega® Sustenna™ (Paliperidone palmitate via NanoCrystal®, Janssen 2009) or Triglide® (Fenofibrate via IDD-P™, Sciele Pharma, Skye Pharma 2005) [9].

Nanocrystals in aqueous suspensions are still associated with a certain risk of instabilities, either physical (e.g., Ostwald ripening and agglomeration), chemical (e.g., hydrolysis), as well as a risk for microbial growth leading to limited product shelf life [14-16]. Another disadvantage of the administration of nanosuspensions as a liquid dosage form is the error-prone dosing step for patients, which may affect patient compliance and trigger the need for dosing devices. These disadvantages can be overcome by transforming the liquid nanocrystal suspension into

a solid dosage form such as tablets or powder filled capsules. State-of-the-art solidification (drying) techniques include spray-drying, spray-coating (also termed spray granulation) and freeze drying [11-13].

In general, drying is a critical and essentially destabilizing procedure for the nanocrystal system which may lead to particle agglomeration and/or aggregation as well as crystal growth followed by sedimentation or flocculation. Consequently, redispersibility of nanoparticles upon reconstitution of the dried powder could be affected, which in turn reduces the beneficial effect of nanosizing on dissolution. For this reason, drying protectants are usually added to the final nanosuspension prior to the drying process to avoid particle growth. Common drying protectants include soluble sugars, such as lactose, sucrose or trehalose, or sugar alcohols like mannitol [14, 17]. However, no nanocrystal-based drug product was approved by the FDA from 2009 to 2018 although drying protectants enable processability [9][1]. This demonstrates how challenging and less economically efficient the common drying processes for solidification of nanocrystal suspensions are compared to other enabling technologies such as solid dispersion technology for solubility enhancement. This is particularly relevant in light of the observation that nanosizing technology is frequently used for early toxicology studies supply, which would be a straightforward approach for FIH development. Recently, vacuum drum drying (VDD) has been introduced as alternative approach to manufacture amorphous solid dispersions showing benefits especially compared to spray drying [18, 19]. This technology is well-established in the food industry, but rarely known in the development of pharmaceuticals [20]. The manufacture of ASDs as one enabling formulation principle consists of the embedment of the drug substance molecularly dispersed (i.e., amorphous) in a matrix polymer. Using vacuum drum drying as technology requires the dissolution of the drug substance and respective excipients in a common organic solvent.

In contrast, the nanocrystal approach essentially bases on the size reduction of a crystalline drug substance into nanosized particles (nanocrystals) in aqueous media followed by a solidification (drying) step. Consequently, the focus of the present case study was to investigate the suitability of vacuum drum drying as solidification (drying) technique for nanosuspensions with the potential to overcome obstacles and disadvantages of currently available drying technologies by e.g., not needing a secondary drying step and by showing no viscosity related limitations for the solution to be dried and potentially higher yields. Thus, the suitability of vacuum drum drying for another enabling formulation principle, entirely different to the ASD approach, was examined to broaden the applicability in the pharmaceutical development.

The nanosuspension analyzed in this study consisted of ritonavir as model drug substance, sodium dodecyl sulfate as ionic stabilizer and copovidone as steric stabilizer. More detailed, the impact of the drying protectant (mannitol, lactose, trehalose) on the processibility via VDD, on the dried powder properties, the remaining nanoparticulate redispersibility and crystallinity was assessed in dependence of the drum temperature. Subsequently, the most promising formulation was selected for further downstream processibility evaluation, with a particular focus on redispersibility. Therefore, the impact of compaction pressures during tableting was investigated as well as the impact of the encapsulation process on a pilot scale machine.

6.5 Material and Methods

6.5.1 Materials

Ritonavir (RTV, purity > 99.8%) was obtained from AbbVie Inc. (North Chicago, US). Copovidone (polyvinylpyrrolidone–vinyl acetate copolymer, Kollidon® VA 64, COP) was purchased from BASF SE (Ludwigshafen, Germany), sodium dodecyl sulfate (SDS), mannitol (Parteck M 200 Emprove® Essential) and trehalose dihydrate (Emprove® Expert) from Merck KGaA (Darmstadt, Germany), and lactose (InhaLac®140) from MEGGLE Pharma (Wasserburg am Inn, Germany). Zirconium oxide beads were obtained from NETZSCH (Selb, Germany). Capsules (Quali-V HPMC capsules, size 0, color opaque grey) were purchased from Qualicaps (Madrid, Spain).

6.5.2 Methods

6.5.2.1 Preparation of ritonavir nanosuspensions by wet ball milling

The ritonavir nanosuspension was prepared by wet ball milling (top-down approach, batch sizes 1.50-1.85 kg). Ritonavir (15% w/w) and 0.5 mm zirconium oxide beads as grinding media (bead to ritonavir ratio: 1:18) were added to a stabilizer-containing solution (SDS (1% w/w) and copovidone (3% w/w)) into a 5L- HDPE (high density polyethylene) bottle. The nanosizing was performed using a tumble blender (Turbula blender T10B, Willy A. Bachofen AG Maschinenfabrik, Muttenz, Switzerland) at 45 rpm for 69 hours. Then, the zirconium beads were separated via filtration using a sieve with 200 µm mesh size. Prior to vacuum drum drying, drying protectants (mannitol, lactose, or trehalose; amount: 7.5%, 10%, 15% or 25% w/w (see Table 6.1)) as well as copovidone (7% w/w) were added to the ritonavir nanosuspension while stirring on a magnetic stirrer (IKA GmbH & Co KG, Staufen, Germany). Copovidone was added to increase the viscosity of the liquid formulation (drying dispersion) and thus, to increase the adhesion of the suspension to the drums.

TRANSFORMATION OF RITONAVIR NANOCRYSTAL SUSPENSIONS INTO A REDISPERSIBLE DRUG PRODUCT VIA VACUUM DRUM DRYING

The nanosuspension formulation and the liquid formulations (drying dispersions) including drying protectant and copovidone, were selected based on prior knowledge and formulation screening data (data not shown). The drying protectants investigated in the present study are commonly used excipients in the solidification of crystalline nanosuspensions (see section 6.4).

6.5.2.2 Characterization of nanosuspensions

6.5.2.2.1 Particle size analysis by dynamic light scattering

Dynamic light scattering (DLS) method was applied using a Zetasizer Ultra (Malvern Instruments GmbH, Herrenberg, Germany) to determine the z-average and the polydispersity index (PDI) of the nanosuspensions after wet-ball milling. Z-average represents the hydrodynamic diameter and PDI expresses the width of the particle size distribution. The samples were diluted in water (1:20) and polystyrene single-use cuvettes (DTS0012) were used. The measurements were performed in back scatter mode (173°) as triplicates at 25 °C prior to an equilibration time of 120 s. The results were analyzed using ZS Xplorer software (version 1.3.2.27).

6.5.2.2.2 Particle size analysis by laser diffraction

Laser diffraction particle size analyzer (Mastersizer 3000, Malvern Instruments GmbH, Herrenberg, Germany) equipped with the automated dispersion unit "HydroMV" module was used to determine the particle size distribution of the nanosuspensions. For the measurements, nanosuspension was added to water until a laser obscuration of approximately 2-2.5% was reached. Data were analyzed according to the MIE theory using the Mastersizer 3000 Software (version 3.71). Measurements were performed as triplicates and averaged.

6.5.2.3 Solidification via vacuum drum drying

The liquid formulations (drying dispersion: ritonavir nanosuspension + drying protectant + copovidone) were dosed into the gap of the two drums of the vacuum double drum dryer (Buflovak, New York, US) for solidification. A thin film spread out evenly on the heated, counter-rotating drums covering full drum width. The water fraction of the liquid formulation (drying dispersion) evaporated during contact with the heated drums under vacuum conditions. The dried product was scraped off the drums by knifes showing flake-like to powder-like appearance. The following process parameters were kept constant during drying for all formulations tested: casing temperature 80 °C, pressure of 100 mbar, drum rotation speed 0.3 rpm, drum gap 0.2 mm. The listed parameters were selected based on prior knowledge in the field of vacuum drum drying to result most likely in a dried product with reasonable quality

TRANSFORMATION OF RITONAVIR NANOCRYSTAL SUSPENSIONS INTO A REDISPERSIBLE DRUG PRODUCT VIA VACUUM DRUM DRYING

properties. Since the suspension to be dried was aqueous, the pressure was selected as low as applicable to ensure proper drying. The drum speed was set to a low value to increase the retention time of the product on the drums. In addition, a small drum gap was chosen, which effected the product thickness and thus, indirectly the required drying time. Just the drum temperature was varied in the range of 55 to 105 °C for the formulations depending on the drying protectant used. The formulation-based adaption of the drum temperature ranges studied was chosen to consider the known differences in glass transition temperatures of the respective pure drying protectants (approx. 87-115 °C) properly. The batch sizes were 350-500 g liquid formulation (drying dispersion) for small-scale runs and 1900 g for the large-scale run. Table 6.1 summarizes the formulations tested and the corresponding drum temperature during solidification.

The VDD intermediates of the small-scale runs were further processed into powder via manual sieving (mesh size 0.8 mm). For the large-scale evaluation, the VDD intermediate was milled at 2000 rpm using a screening mill (Comil U5, Quadro Engineering, Waterloo, Canada) equipped with an 813 µm round-hole sieve. The resulting powders of the small-scale runs were used for powder characterization and tableting, whereas the large-scale run was used for the encapsulation process.

Table 6.1: Overview of formulations processed via VDD incl. drum temperatures and associated short names

Formulation Composition of drying dispersion (liquid formulation)	Drum	Ritonavir	Short Name
	Temperature [°C]	content in dried product [w/w%]	
83% (w/w) RTV NS +10% (w/w) Man +7% (w/w) COP	75	38	Man10_75
78% (w/w) RTV NS +15% (w/w) Man +7% (w/w) COP	55	32	Man15_55*
78% (w/w) RTV NS +15% (w/w) Man +7% (w/w) COP	65	32	Man15_65
78% (w/w) RTV NS +15% (w/w) Man +7% (w/w) COP	75	32	Man15_75
68% (w/w) RTV NS +25% (w/w) Man +7% (w/w) COP	75	23	Man25_75
78% (w/w) RTV NS +15% (w/w) Lac +7% (w/w) COP	75	32	Lac15_75*
78% (w/w) RTV NS +15% (w/w) Lac +7% (w/w) COP	85	32	Lac15_85
78% (w/w) RTV NS +15% (w/w) Lac +7% (w/w) COP	95	32	Lac15_95
78% (w/w) RTV NS +15% (w/w) Tre +7% (w/w) COP	75	32	Tre15_75*
78% (w/w) RTV NS +15% (w/w) Tre +7% (w/w) COP	90	32	Tre15_90
78% (w/w) RTV NS +15% (w/w) Tre +7% (w/w) COP	105	32	Tre15_105
78% (w/w) RTV NS +7.5% (w/w) Man +7.5% (w/w) Lac +7% (w/w) COP	75	32	Man7.5/Lac7.5_75*
73% (w/w) RTV NS +10% (w/w) Man +10% (w/w) Lac +7% (w/w) COP	75	21	Man10/Lac10_75
78% (w/w) RTV NS +7.5% (w/w) Man +7.5% (w/w) Tre +7% (w/w) COP	75	32	Man7.5/Tre7.5_75*
73% (w/w) RTV NS +10% (w/w) Man +10% (w/w) Tre +7% (w/w) COP	75	21	Man10/Tre10_75

RTV NS= ritonavir nanosuspension, Man= mannitol, Lac= lactose, Tre= trehalose, COP= copovidone, *= used for compression analysis

TRANSFORMATION OF RITONAVIR NANOCRYSTAL SUSPENSIONS INTO A REDISPERSIBLE DRUG PRODUCT VIA VACUUM DRUM DRYING

6.5.2.4 Redispersibility of VDD intermediates/tablets/capsules

For redispersibility evaluation, the VDD intermediates, tablets or capsule-fillings were dispersed in an appropriate amount of water targeting the ritonavir concentration of the original nanosuspension (ritonavir: 15% w/w). The resulting suspension was mixed using a vortexer (IKA Vortexer VG3, Staufen, Germany) and subsequently characterized by laser diffraction and/or dynamic light scattering (see section 6.5.2.2).

6.5.2.4.1 Redispersibility by particle fractions in submicron range

The redispersibility was evaluated by means of laser diffraction to increase the understanding of the agglomeration state of the ritonavir particles, since larger particles could sediment during DLS analysis not being detected then. The percentage of particles below 1 µm in a cumulative volume-based particle size distribution was selected as criterion to determine the redispersibility.

6.5.2.4.2 Redispersibility index

For better comparability of the redispersed suspension with the initial nanosuspension, the redispersibility index (RDI) was calculated by normalizing the particle size describing variable (z-average or d_{50}) to the respective variable of the initial nanosuspension (see Eq. 6.1).

$$RDI = \frac{d_{50} \text{ (or } z\text{-average)}_{\text{redispersed}}}{d_{50} \text{ (or } z\text{-average)}_{\text{initial}}} \quad (6.1)$$

Consequently, an RDI value close to 1 indicates a sufficient preservation of the nanoparticulate drug substance particles after solidification. For processability evaluation, the particle size describing variable of the tablets/capsule powder fill was compared with the respective one of the VDD intermediate (powder).

6.5.2.5 Characterization of VDD intermediates

6.5.2.5.1 Bulk/tapped density

Determination of bulk and tapped density was performed using tapped density tester (Pharmatest Apparatebau AG, Hamburg, Germany) according to Ph. Eur. 2.9.34 (method 1). VDD intermediate was filled into a 250 ml graduated cylinder and the mass and bulk/tapped volume occupied by the material was determined. All measurements were conducted as triplicates.

6.5.2.5.2 Flowability

Determination of flow properties was performed using ring shear tester (RST-XS, Dietmar Schulze, Schüttgutmesstechnik, Wolfenbüttel, Germany) equipped with a 31.37 ml cell. VDD intermediates were measured as triplicates at following conditions: pre-shear normal stresses of 0.250, 0.525, 0.800 and 1 kPa, and ambient temperature (approx. 20-22 °C). Data were evaluated using regression analysis.

6.5.2.5.3 Particle size distribution

Determination of particle size distribution of VDD intermediates (powder) was performed using a laser diffraction particle size analyzer (Mastersizer 3000, Malvern Instruments GmbH, Herrenberg, Germany) equipped with a dry powder disperser module Aero S. The samples (approx. 2-5°g) were dispersed with 0 bar pressure and measured as triplicates. Data were analyzed using the Mastersizer 3000 Software (version 3.71) according to the Fraunhofer approximation.

6.5.2.5.4 Loss on drying

Determination of moisture content via loss on drying (LOD) method was performed using a halogen moisture analyzer (HB43-SSD, Mettler-Toledo GmbH, Giessen, Germany). The samples (approximately 5.5.-6.1 g) were heated to 105 °C and held until mass was constant within ± 1 mg for 100 s. The VDD intermediates were measured as triplicates.

6.5.2.5.5 Crystallinity and glass transition temperature (T_g) by differential scanning calorimetry (DSC)

Quantification of ritonavir related crystallinity as well as determination of the glass transition temperature ($T_{g,wet}$) was performed via differential scanning calorimetry (DSC) using a Mettler-Toledo DSC 3+ (Mettler Toledo, Gießen, Germany) equipped with an auto-sampler. All DSC samples (VDD intermediates) were scanned at 1.5 K/min from 25 °C to 140 °C under nitrogen (gas flow 50 ml/min) as open pan method (crystallinity) and at 10 K/min from 25°C to 150 °C as closed pan method ($T_{g,wet}$). Pure crystalline ritonavir was measured (open pan method) to determine the melting enthalpy (n=2, mean: 80.24 J/g) for quantification purposes of the VDD intermediates. The results were analyzed with STARe SW (version 16.1) (Mettler Toledo, Gießen, Germany). All VDD intermediate samples were measured as triplicates. The DSC thermograms are not shown in the present study except for Man7.5/Tre7.5_75_large representatively for all formulations in Figure 6.S1.

TRANSFORMATION OF RITONAVIR NANOCRYSTAL SUSPENSIONS INTO A REDISPERSIBLE DRUG PRODUCT VIA VACUUM DRUM DRYING

To verify the DSC results on quantification of the crystalline ritonavir content, powder X-ray diffraction (PXRD) was performed for one selected VDD intermediate (Man7.5/Tre7.5_75, see section 6.13 Appendix A. Supplementary data).

6.5.2.5.6 Short-term stability focussing on redispersibility

The physical stability of the selected VDD intermediate for downstream evaluation was determined by DLS and LD after storage for 2 and 6 months at uncontrolled conditions at room temperature and relative humidity (approximately 45-50%) and compared with initial nanosuspension data and initial powder characterization after solidification (drying).

6.5.2.6 Downstream processability

6.5.2.6.1 Tabletability and tabletting

For tabletability evaluation, round, biplane tablets (10 mm, mass: 200 mg, n=6) of selected formulations (small-scale runs, see Table 6.1) were manufactured using a single punch compression simulator (HB-50, Huxley Bertram Engineering Limited, Cambridge, UK) simulating a KorschXL100 (turret speed: 20 rpm, linear speed: 124 mm/s, dwell time: 78 ms). Different compaction pressures were applied targeting defined tensile strengths (0.4, 0.8, 1.2, 1.6, 2.0 MPa). The tensile strength range was selected around the commonly targeted tensile strength of 1.2 MPa for tablets [21]. Tablets were subsequently analyzed regarding tablet weight (analytical balance, Sartorius BP 61 S-0CE, Sartorius AG, Goettingen, Germany), thickness and diameter (caliper, Hommel Hercules Werkzeughandel GmbH & Co. KG, Viernheim, Germany), and breaking force (ErwekaTBH 125, Erweka GmbH, Heusenstamm, Germany).

6.5.2.6.2 Encapsulation

The selected VDD intermediate (Man7.5/Tre7.5_75; large-scale run) was encapsulated into size 0 Quali-V capsules in opaque grey targeting a fill weight of 157.2 mg (corresponding to 50 mg ritonavir). Encapsulation process was performed using an automated capsule filling machine (Modu-C LS, Harro Höfliger, Allmersbach im Tal, Germany) equipped with an inline in-process (weight) control unit. Process parameters were set as follows: 20 cycles/min, 100% check weighing (net weight). In-process control samples were taken at start, middle, and end of the encapsulation process and evaluated according to Ph. Eur. 2.9.5 (uniformity of mass of single-dose preparation). In addition, a process sample (n=100) was taken and analyzed (gross weight). The machine protocol was used for process assessment (net weight).

6.5.2.6.3 Disintegration

Disintegration test was performed according to Ph. Eur. 2.9.1 (test setup A) using a disintegration tester (ZT 722, Erweka GmbH, Heusenstamm, Germany).

6.6 Results

6.6.1 Characterization of ritonavir nanosuspensions

Wet ball milling of ritonavir was successfully conducted in 5 sub-batches (runs) at different batch sizes (1.5-2.0 kg). The particle size analysis results are shown in Figure 6.1. The z-average values determined via dynamic light scattering (DLS) were below 400 nm (in a range of 300-370 nm) and the PDIs were below 0.15 indicating monodispersed ritonavir nanosuspensions (see Figure 6.1 a). Laser diffraction (LD) analysis confirmed the DLS results showing absence of large particles (e.g., agglomerates), which could be potentially missed via DLS due to sedimentation. The d_{50} values obtained by LD were in a range between 113-315 nm and more than 98.5% of the particles were in the submicron range (<1 µm) (see Figure 6.1 b).

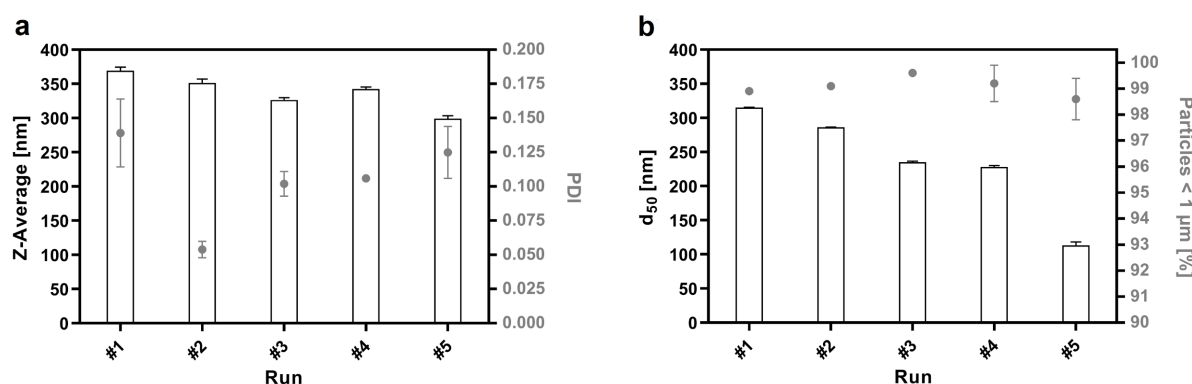


Figure 6.1: Mean particle size results of ritonavir nanosuspensions (wet-ball milling run 1-5);
a: dynamic light scattering – z-average and polydispersity index (PDI);
b: laser diffraction – d_{50} and number of particles below 1 µm in %

6.6.2 Solidification via VDD and characterization of resulting intermediates

6.6.2.1 Impact of drying protectant and drum temperature on processability

A clear dependency of the drying protectant used on processability could be observed as shown in Table 6.2. Yield values were consistently low for lactose-containing formulations ranging from 53 to 62%. Mannitol-containing formulations showed yield values of 65-86% indicating a better process performance compared to lactose-containing formulations. Whereas trehalose-containing formulations showed a pronounced drum temperature

dependence: the higher the drum temperature, the better the yield (75 °C: 63.3%, 105 °C: 92.8%). Combining mannitol with either lactose or trehalose as drying protectants resulted in formulations with acceptable yield values of 65-87% for small scale runs on a pilot scale VDD. The LOD values were between 1-3% for all other formulations except for the trehalose formulation (processed at 75 °C with LOD of 4.90%) and the mannitol formulation (processed at 55 °C with LOD of 4.87%).

6.6.2.2 Impact of drying protectant and drum temperature on powder properties of dried intermediates

Dried VDD intermediates have been characterized with respect to flowability (ring shear analysis), powder density (bulk/tapped) and solid particle size distribution (PSD). The results are summarized in Table 6.2. The results indicated an impact of drying protectant type on flowability. All mannitol containing formulations exhibited easy flowing properties, whereas the lactose or trehalose containing powders showed cohesive flow independent of the drum temperature. Flow function coefficient values (FFC) for trehalose containing formulations indicated cohesive flow at lower temperatures and borderline easy flow at the highest drum temperature.

The bulk density values (Table 6.2) were most favorable for further downstream processing for mannitol containing formulations with values at around 0.30-0.46 g/cm³. The lactose and trehalose containing formulations showed lower bulk density ranging from 0.11-0.17 g/cm³ indicating a fluffy powder. The formulations with two drying protectants, either mannitol/lactose (Man7.5/Lac7.5_75: 0.35 g/cm³) or mannitol/trehalose (Man7.5/Tre7.5_75: 0.35 g/cm³), resulted in powders with bulk density values in the same ranges of the pure mannitol containing formulation (Man15_75: 0.34 g/cm³). Consequently, mannitol might be the dominant component within the formulation with respect to bulk density. This could be confirmed by the results of mannitol containing formulations at different mannitol levels: the higher the mannitol content within the dried product, the higher the bulk density: The bulk density for Man10_75 was 0.30 g/cm³, that for Man15_75 was 0.34 g/cm³, and the one for Man25_75 was 0.46 g/cm³. For mannitol and lactose containing formulations, a minor dependence between drum temperature and bulk density values could be observed: the lower the drum temperature, the higher the bulk density. For trehalose no trend could be observed.

The particle size distribution of the intermediates indicated relatively large particles of d_{90} values even above 1000 µm due to the selected sieve. However, trehalose and lactose containing intermediates tended to lower d_{90} values at around 600-650 µm for trehalose and 535-844 µm for lactose compared to mannitol (981-1120 µm). In addition, the mannitol level

TRANSFORMATION OF RITONAVIR NANOCRYSTAL SUSPENSIONS INTO A
REDISPERISIBLE DRUG PRODUCT VIA VACUUM DRUM DRYING

within the formulation impacted the d_{90} value: the higher the mannitol content, the higher the d_{90} value (Man10_75: 796 μm ; Man15_75: 981 μm , Man25_75: 1330 μm). Furthermore, mannitol seemed to substantially impact the particle size distribution when combined with other drying protectants. The d_{50} and d_{90} values for Man7.5/Lac7.5_75 (d_{50} : 425 μm , d_{90} : 1170 μm) and Man7.5/Tre7.5_75 (d_{50} : 371 μm , d_{90} : 1030 μm) were widely comparable to those of Man15_75 (d_{50} : 388 μm , d_{90} : 981 μm).

Table 6.2: Results of drying of ritonavir nanosuspension formulations and respective vacuum drum dried intermediates (Man= mannitol, Lac= lactose, Tre= trehalose, DL= drug load, FFC = flow function coefficient, RDI= redispersibility index, T_g = glass transition temperature, n.d. = not determined)

Formulation Code	Yield [%]	Loss on Drying [%]	Crystallinity in comp. to DL [%]	$T_{g,wet}$ [°C]	FFC	Bulk Density [g/cm ³]	Tapped Density [g/cm ³]	Particle size distribution (dried powder)			Particles< 1 µm [%] (liquid)	RDI (d_{50} , liquid)	
								d_{10} [µm]	d_{50} [µm]	d_{90} [µm]			
143	Man10_75	67.1	1.38 ± 0.07	79.7 ± 1.5	n.d.	6.96 ± 0.68 (easy flow)	0.302 ± 0.001	0.413 ± 0.001	122.0 ± 13.1	357.0 ± 34.5	796.0 ± 62.5	29.06 ± 0.69	16.8
	Man15_55	65.2	4.87 ± 0.04	85.4 ± 3.7	24.4 ± 0.4	4.97 ± 0.25 (easy flow)	0.435 ± 0.003	0.558 ± 0.005	242.0 ± 28.3	564.0 ± 36.3	1120.0 ± 59.9	95.03 ± 0.02	1.1
	Man15_65	83.5	2.95 ± 0.05	59.7 ± 0.5	n.d.	7.86 ± 4.86 (easy flow)	0.417 ± 0.004	0.535 ± 0.011	117.0 ± 8.2	442.0 ± 27.2	1120.0 ± 33.8	59.44 ± 4.40	2.0
	Man15_75	78.8	1.45 ± 0.06	57.1 ± 8.6	n.d.	9.00 ± 3.72 (easy flow)	0.336 ± 0.011	0.458 ± 0.019	102.0 ± 2.0	388.0 ± 3.8	981.0 ± 24.0	20.55 ± 0.36	19.1
	Man25_65	86.2	0.96 ± 0.09	74.0 ± 6.1	n.d.	4.09 ± 0.26 (easy flow)	0.348 ± 0.002	0.460 ± 0.003	122.0 ± 6.9	383.0 ± 27.6	850.0 ± 34.5	56.95 ± 0.73	2.2
	Man25_75	78.7	1.47 ± 0.20	75.3 ± 4.1	n.d.	6.66 ± 2.45 (easy flow)	0.458 ± 0.012	0.571 ± 0.004	168.0 ± 30.5	621.0 ± 35.4	1330.0 ± 35.0	40.86 ± 2.67	13.4
	Lac15_75	62.4	1.48 ± 0.07	77.5 ± 5.0	n.d.	3.77 ± 0.19 (cohesive)	0.140 ± 0.001	0.212 ± 0.002	90.5 ± 2.1	261.0 ± 13.4	535.0 ± 53.2	93.84 ± 0.23	1.1
	Lac15_85	59.1	2.29 ± 0.06	75.6 ± 0.1	49.3 ± 0.3	3.16 ± 0.12 (cohesive)	0.124 ± 0.001	0.183 ± 0.004	118.0 ± 3.5	362.0 ± 18.0	743.0 ± 26.9	92.59 ± 0.39	1.2
	Lac15_95	53.9	1.42 ± 0.03	58.2 ± 1.1	n.d.	3.14 ± 0.19 (cohesive)	0.105 ± 0.003	0.159 ± 0.003	119.0 ± 2.7	374.0 ± 5.9	844.0 ± 4.5	23.85 ± 5.30	175.7
	Tre15_75	63.3	4.90 ± 0.08	76.0 ± 5.6	n.d.	3.31 ± 0.32 (cohesive)	0.140 ± 0.003	0.211 ± 0.001	98.7 ± 1.8	301.0 ± 10.1	608.0 ± 38.7	94.47 ± 1.07	1.1
	Tre15_90	68.7	1.06 ± 0.17	67.6 ± 3.2	55.7 ± 0.4	3.60 ± 0.03 (cohesive)	0.116 ± 0.001	0.175 ± 0.007	84.6 ± 3.3	296.0 ± 14.7	650.0 ± 21.7	97.02 ± 0.41	1.2
	Tre15_105	92.8	1.30 ± 0.05	36.6 ± 1.3	n.d.	4.04 ± 0.36 (easy flow)	0.169 ± 0.002	0.258 ± 0.002	49.5 ± 1.8	230.0 ± 12.7	600.0 ± 76.2	10.26 ± 0.19	396.6
	Man7.5/Lac7.5_75	86.7	1.00 ± 0.04	69.2 ± 0.9	n.d.	2.75 ± 0.72 (cohesive)	0.352 ± 0.002	0.499 ± 0.002	87.1 ± 6.6	425.0 ± 37.0	1170 ± 79.4	99.78 ± 0.05	1.0
	Man10/Lac10_75	64.6	1.86 ± 0.10	86.0 ± 4.9	n.d.	2.32 ± 0.17 (cohesive)	0.393 ± 0.001	0.541 ± 0.003	139.0 ± 10.8	509.0 ± 39.3	1210 ± 48.7	93.92 ± 0.27	1.0
	Man7.5/Tre7.5_75_small	84.8	1.02 ± 0.10	75.1 ± 3.0	n.d.	2.98 ± 0.30 (cohesive)	0.347 ± 0.009	0.474 ± 0.002	95.1 ± 7.7	371 ± 20.5	1030 ± 7.8	98.12 ± 0.15	1.0
	Man7.5/Tre7.5_75_large	n.d.	0.89 ± 0.10	73.1 ± 0.8	n.d.	4.72 ± 0.82 (easy flow)	0.347 ± 0.004	0.483 ± 0.002	57.3 ± 2.3	193.0 ± 5.0	429.0 ± 5.6	99.81 ± 0.33	1.2
	Man10/Tre10_75	84.3	1.74 ± 0.04	90.1 ± 2.6	n.d.	2.73 ± 0.29 (cohesive)	0.333 ± 0.004	0.462 ± 0.001	121.0 ± 4.9	379.0 ± 4.7	864.0 ± 20.2	97.43 ± 0.17	1.1

6.6.2.3 Impact of drying protectant and drum temperature on redispersibility

The impact of the drying protectant (mannitol, lactose, trehalose) at a defined amount (15% w/w within the liquid formulation (drying dispersion)) was assessed with respect to particle size and PDI after redispersing the VDD intermediate (redispersibility) dried at various drum temperatures via LD. Process conditions and the results are summarized in Table 6.2. A clear trend could be observed for all three drying protectants investigated: with increasing drum temperature the number of particles in the submicron range decreased and the RDI increased indicating particle agglomeration/ crystal growth and thus, rated non-redispersible VDD intermediate. Consequently, a critical drum temperature (T_{crit}) could be identified at which the desired redispersibility of the dry VDD intermediate was still given (particles in submicron range >90% and RDI < 1.3). Figure 6.2 illustrates the T_{crit} and $T_{g,wet}$ for the respective formulations and the $T_{g,dry}$ of the pure drying protectants according to literature [2]. A clear dependency between the $T_{g,dry}$ values of the respective drying protectants, the resulting formulation $T_{g,wet}$ values, and the T_{crit} values could be observed. Formulation Man15 with the lowest $T_{g,wet}$ showed the lowest T_{crit} (55 °C) meaning that a redispersible intermediate is feasible at the lowest drum temperature tested. Consequently, applying drum temperatures above the T_{crit} during solidification would lead to a dried, less to non-redispersible product. In contrast, dried material with trehalose displayed the highest $T_{g,wet}$ value, and also the highest T_{crit} value with 90 °C. However, the identified T_{crit} values were approximately 30-35 °C above the wet $T_{g,wet}$ for all formulations.

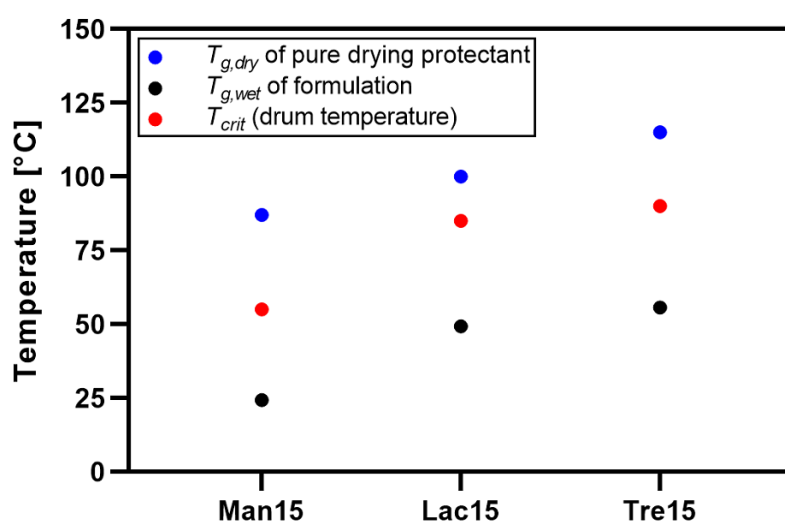


Figure 6.2: Critical process (drum) temperature (T_{crit}) and glass transition temperature ($T_{g,wet}$) of formulations containing different drying protectants (mannitol, lactose, trehalose) and $T_{g,dry}$ of the pure drying protectants according to literature [2]

6.6.2.4 Impact of drying protectant and drum temperature on solid state of ritonavir

Figure 6.S1 (Appendix A Supplementary Data) displays the DSC thermograms of the pure microcrystalline ritonavir as reference for quantification of the remaining ritonavir-related crystallinity fraction ($n=2$), and of the vacuum drum dried intermediate (Man7.5/Tre7.5_75_large) representative for all DSC measurements (data not shown). The crystalline fraction within the Man7.5/Tre7.5_75_large VDD intermediate was 23.2% corresponding to 73.0% remaining crystallinity. This is in accordance with the small-scale batch data (75.1%) of the same formulation. Additionally, an estimation of ritonavir-related crystallinity was determined via powder X-ray diffraction (PXRD) for the formulation Man7.5/Tre7.5_75_large. The remaining ritonavir-related crystallinity value was 89.93 % (see Figure 6.S2 (Appendix A Supplementary data)).

Figure 6.3 shows the impact of the drum temperature during vacuum drum drying on ritonavir-related crystallinity determined via DSC for formulations containing mannitol, lactose, or trehalose as drying protectant. Data indicated a dependency between drum temperature and ritonavir-related crystallinity: the higher the drum temperature for the respective formulation, the lower the crystalline ritonavir content within the VDD intermediate. A strong decrease in crystallinity could be observed for VDD intermediates processed at drum temperatures above T_{crit} . The crystallinity values at T_{crit} were in a range of 75-85%.

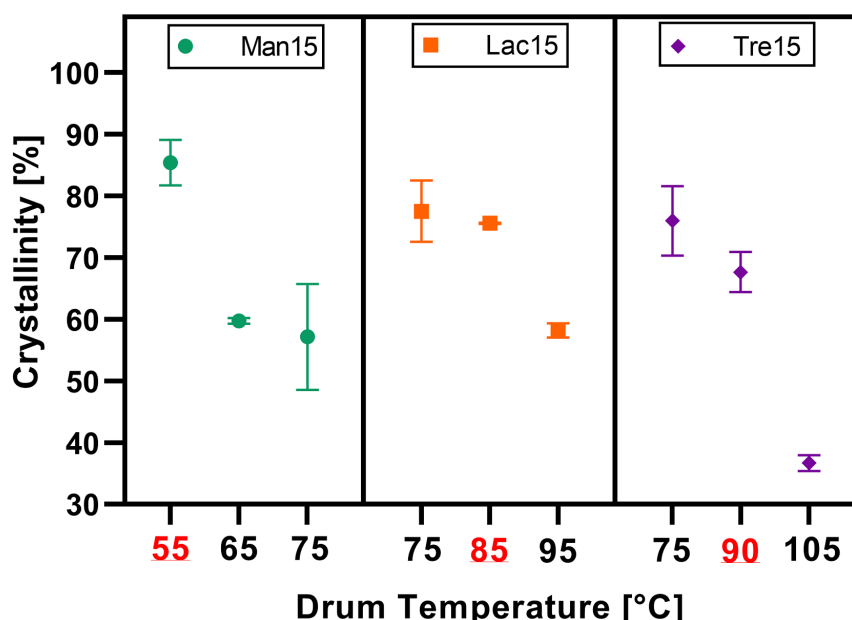


Figure 6.3: Ritonavir-related crystallinity dependent on drum temperature of formulations containing mannitol (Man15), lactose (Lac15) and trehalose (Tre15) as drying protectant; Critical drying temperature (T_{crit}) for each formulation displayed in red

6.6.3 Short-term stability of selected formulation

The short-term stability study was carried out on the selected formulation Man7.5/Tre7.5_75. The VDD intermediate was analyzed after 2- and 6-months storage at uncontrolled conditions (room temperature; relative humidity of approx. 45-50%) using LD and/or DLS. Results were compared with VDD intermediate at study start (T0) and the corresponding nanosuspension. Results are given in Table 6.3 comprising the d_{50} values, the cumulative number of particles in the submicron range as well as the z-average and PDI values. The d_{50} values ranged from 111 to 139 nm indicating no distinctive change over time regarding particle size. The number of particles in the submicron range were consistently above 97% and comparable to the corresponding nanosuspension with an initial value of 98.2%. However, z-average values indicated a slight shift to larger particles during storage: 299 nm (nanosuspension), 330 nm (after 2 months) and 353 nm (after 6 months). Consequently, it is recommended to store the dried product at lower temperatures and low humidity to avoid further particle agglomeration and/or crystal growth.

Table 6.3: Short-term stability results by laser diffraction and dynamic light scattering analysis at study start (T0), after 2 (T2) and 6 months (T6)

	Timepoint [months]			
	T0 (Nanosuspension)	T0 (Dried powder)	T2	T6
d_{50} [nm]	113.0 ± 5.2	130.0 ± 1.8	139.0 ± 0.8	111.0 ± 0.8
Particles <1µm [%]	98.6 ± 0.8	98.4 ± 0.3	97.2 ± 0.0	98.4 ± 0.3
z-Average [nm]	299.1 ± 4.30	not determined	330.1 ± 6.98	352.5 ± 4.63
PDI ^a	0.125 ± 0.019	not determined	0.119 ± 0.022	0.139 ± 0.003

^a polydispersibility index

6.6.4 Downstream processability of selected formulation

Formulation Man7.5/Tre7.5_75 was selected as prototype formulation to evaluate downstream processability comprising several benefits compared to other formulations tested. It showed good remaining nanoparticulate redispersibility, remaining crystallinity, and favorable powder properties such as bulk density (see Table 6.2). The small-scale batch intermediate was used for tabletability evaluation to ensure proper comparability to the other formulations processed into powder intermediates using similar equipment (manually milled VDD intermediate). The large-scale batch intermediate was used for encapsulation experiments.

6.6.4.1 Tableting and disintegration of selected formulations

Figure 6.4a shows the tabletability plot (tensile strength vs compaction pressure) of selected formulations simulating the rotary press Korsch XL100 at 20 rpm turret speed (linear speed: 124 mm/s). All formulations were easily compressible leading to tablets with sufficient hardness even at low compaction pressures. Still, differences were observed depending on the drying protectant used in the formulation composition. Trehalose showed the best tabletability followed by lactose. Mannitol exhibited the least favoured tabletability profile, but still showed sufficient tensile strength. Mannitol-containing formulations with lactose or trehalose in combination revealed comparable tabletability to the mannitol-only formulation. Consequently, mannitol affected tabletability most. Moreover, no tablet defects were observed for all formulations tested.

Figure 6.4b shows the impact of tensile strength on tablet disintegration for different formulations. All tablets showed fast disintegration time (< 12.5 min), which decreased with decreasing tensile strength.

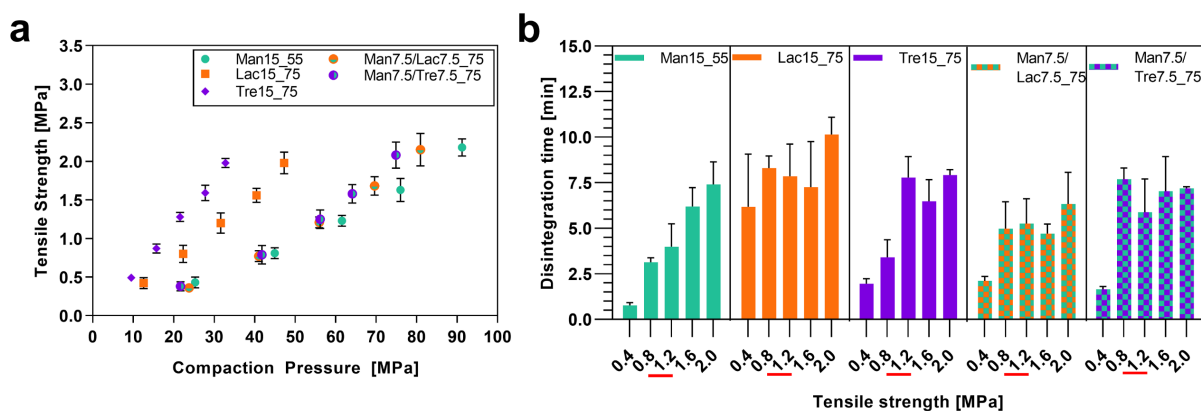


Figure 6.4: a: Tabletability plots of selected formulations simulating a Korsch XL100 at 20 rpm ($n=6$); b: Disintegration time of selected formulations compressed to tablets of defined tensile strengths ($n=6$); Man= mannitol, Lac= lactose, Tre= trehalose

6.6.4.2 Impact of tableting process on redispersibility

Tablets of different formulations with a tensile strength of 1.2 MPa were investigated regarding redispersibility after tableting by laser diffraction. The results are summarized in Table 6.4. The d_{50} values of the redispersed tablets were similar to the initial VDD powder intermediates. RDI values of 1.0-1.1 indicated no substantial change in PSD of redispersed particles with a large number of particles (> 93%) smaller than 1 μm . Consequently, no impact on tableting on redispersibility could be observed.

TRANSFORMATION OF RITONAVIR NANOCRYSTAL SUSPENSIONS INTO A
REDISPERSEABLE DRUG PRODUCT VIA VACUUM DRUM DRYING

Table 6.4: Tablets (TS: 1.2 MPa) redispersibility of different formulations by laser diffraction (Man= mannitol, Lac= lactose, Tre= trehalose, RDI = redispersibility index)

Formulation	Particles < 1 µm [%]	RDI	Disintegration time [min]
Man15_55	92.67 ± 0.05	1.0	3.99 ± 1.25
Lac15_75	95.46 ± 0.23	1.0	7.86 ± 1.76
Tre15_75	93.26 ± 0.14	1.0	7.79 ± 1.14
Man7.5/Lac7.5_75	99.68 ± 0.72	1.0	5.25 ± 1.37
Man7.5/Tre7.5_75	96.47 ± 0.72	1.0	5.88 ± 1.83

In addition, the impact of tableting on redispersibility was studied with tablets of different tensile strengths via DLS and LD for a selected formulation (Man7.5/Tre7.5_75). As shown in Figure 6.5, the z-average values by DLS were in a comparable range (342 - 367 nm) for all tensile strengths. Measured PDIs (0.100-0.175) indicated monodispersed nanosuspensions. RDI values of 1.0 to 1.1 demonstrated good redispersibility. LD results were in accordance with those from DLS measurements: the d_{50} values varied from 196 - 239 nm with 95.1 – 99.8% of the particles in the submicron range. The RDI values of LD measurement did not indicate any particle size change induced by the tableting process.

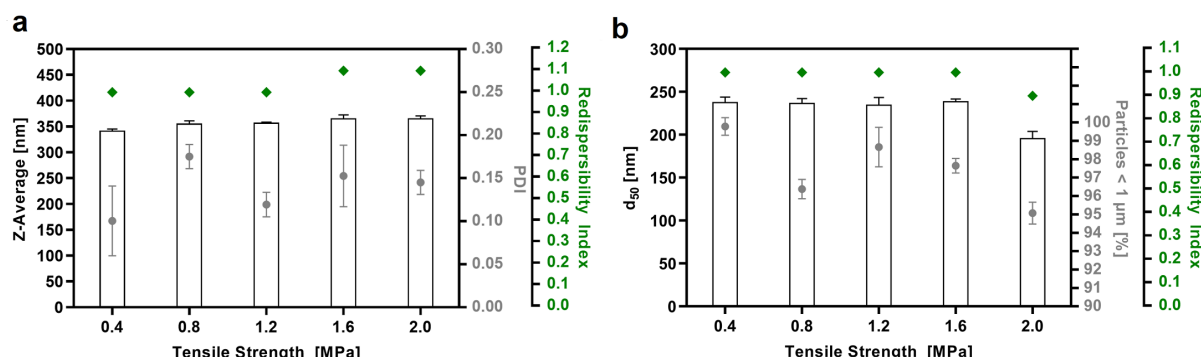


Figure 6.5: Mean particle size results of tablets with different tensile strength values; a: dynamic light scattering – z-average and polydispersity index (PDI); b: laser diffraction – d_{50} and number of particles below 1 µm in %; RDI= redispersibility index compared to powder

6.6.4.3 Impact of encapsulation process on redispersibility

The selected VDD intermediate (Man7.5/Tre7.5_75) was successfully encapsulated into size 0 HPMC capsules targeting a fill weight of 157 mg (RTV dose of 50 mg). Approximately 1000 capsules were manufactured. The results of the analyzed in-process control and process samples combined with machine protocol data are summarized in Table 6.S2 (Appendix A. Supplementary Data) reflecting an acceptable encapsulation process.

Redispersibility of the capsule powder fill (powder) was assessed via DLS and LD for the in-process control samples (see Figure 6.6). The z-average values ranged from 320 to 333 nm and the PDI from 0.114 to 0.126 assuming monodispersed nanosuspensions. The RDI values were constantly at 1.0. The particle size analysis data via LD were in accordance with the DLS data: the d_{50} values were between 135 – 140 nm with 99% of the particles in the submicron range without variation with respect to processing time. And the RDI values were at 1.0 indicating no change in particle size compared to the VDD powder. Thus, the encapsulation process did not impact the remaining nanoparticulate redispersibility of the capsule powder fill.

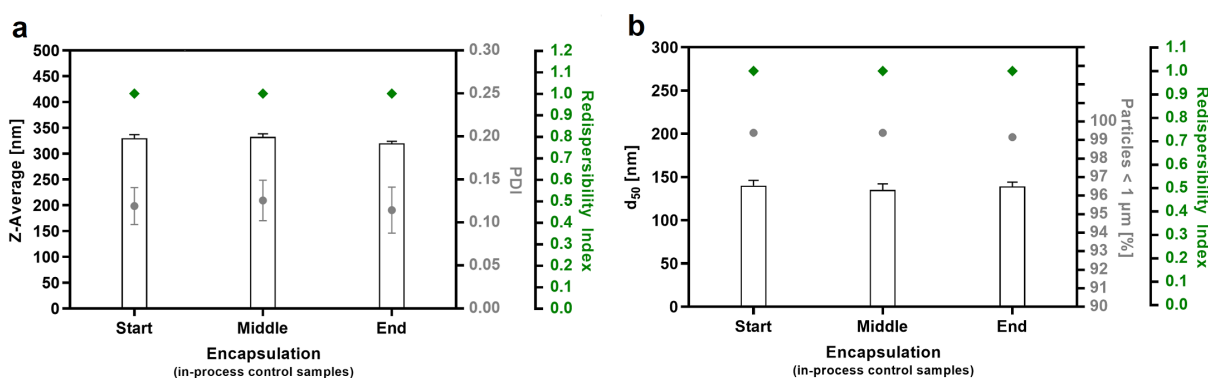


Figure 6.6: Mean particle size results of in-process control samples of the encapsulation process; a: dynamic light scattering – z-average and polydispersity index (PDI); b: laser diffraction – d_{50} and number of particles below 1 μm in %; RDI= redispersibility index compared to powder

6.7 Discussion

Ritonavir nanocrystal suspensions could be successfully manufactured with good reproducibility via wet-ball milling using zirconium oxide beads using a classic tumble blender.

The data revealed that processability of the tested nanocrystals containing liquid formulations (drying dispersions) during vacuum drum drying were impacted by the drying protectant. Mannitol was identified as best drying protectant for product solidification in terms of visual behavior on the drums, LOD and yield. Similar observations were made by Chaubal, Popescu [12] comparing lactose, mannitol, sucrose and dextrose containing spray dried powders of itraconazole nanosuspensions: mannitol was rated as most favorable carrier for spray drying of nanoparticles providing most desirable particle morphology, flowability, and LOD values.

The redispersibility was mostly affected by the interplay between drying protectant and drum temperature. An individual critical process temperature (T_{crit}) correlating with the $T_{g,wet}$ of the formulation could be identified for all formulations tested. Similar observations were recently published for the spray drying process by Czyz et al. [14]. Researchers reported that the outlet temperature during spray drying seemed to be critical and correlated with the $T_{g,wet}$ of the formulation, which was shown to be drug load related. The temperature difference between $T_{g,wet}$ of the formulation and T_{crit} (outlet) was similar for all formulations tested (approx. 20–25 °C). In the present study the difference between $T_{g,wet}$ of the formulation and T_{crit} (drum) was 30–35 °C and thus, approx. 10 degrees higher compared to the spray drying data. This might be explained by the fact that the drum temperature did not reflect the product temperature, which is probably lower due to the cooling effect during water evaporation. In contrast, the outlet temperature during spray drying is much better linked to the real product temperature. Consequently, it can be assumed that a T_{crit} related to the $T_{g,wet}$ of the formulation might be process independent. An explanation for the temperature impact on redispersibility could be as follows: process temperatures above the $T_{g,wet}$ of the material knowingly increase the fluidity of the material and potentially facilitate nanocrystals aggregation and growing. Interestingly, Malamatari et al. [22] identified the ratio of drying protectant to drug as another important, formulation related factor for redispersibility. The present study confirmed their findings, as the amount of submicron particles was increased at higher mannitol to ritonavir ratio (20% for Man15_75, 40% for Man25_75) at constant drum temperature. This stabilizing effect was likely caused by steric hindrance by the drying protectant. Zuo et al. [23] explains this steric hindrance as follows: the presence of water-soluble additives such as Mannitol could form hydrophilic excipient bridges interconnecting the nanoparticles and thus, avoiding crystal-to-crystal contact and in the end crystal growth. The same stabilizing effect is seen in lyophilization processes where mannitol is used as so called lyo-protectant [24]. Surprisingly, Man10_75 showed better redispersibility compared to Man15_75, despite containing a lower amount of drying protectant. In this case, the T_g impact would be more pronounced as stabilizing principle than the steric hindrance. Reducing the mannitol content resulted in a higher relative content of copovidone in the formulation, which has a higher $T_{g,dry}$ (101 °C) compared to mannitol. Consequently, the $T_{g,wet}$ of the formulation might be higher and thus, leading to a higher stabilizing effect against temperature. In addition, copovidone acts as matrix polymer still providing sufficient stabilization. Hence, the stabilizing effect of drying protectants on the nanocrystals might be dominated by two principles: steric hindrance (acting as spacers by building excipient bridges) and T_g influence. However, other components of the formulation might influence the T_g significantly as well (e.g., drug substance, ionic or polymeric stabilizers or adhesion enhancers).

The remaining ritonavir-related crystallinity data determined via DSC showed a clear ritonavir melting peak visible in the thermograms of all analyzed samples. However, a temperature shift to a lower melting temperature was observed for the VDD intermediates containing ritonavir nanoparticles compared to the pure microcrystalline ritonavir measurements. Based on literature, melting point depression is expected with reduction of crystal particle size as described by the Gibbs-Thomson equation [25]. In fact, this has been already reported for several nanosuspensions dried via spray drying in previously published studies [26, 27]. Consequently, measuring the remaining crystallinity at nanometer size via DSC might potentially not reflect the true crystallinity. Few percent of crystallinity might get lost due to fast melting of nanocrystals at even lower temperatures which is also implied by the left skewed melting peak in the VDD intermediate thermograms. In fact, even PXRD data represent only an estimation, because a reference standard had to be used for quantification. Consequently, the true crystallinity might be a bit higher compared to the estimated values by DSC in this study.

However, DSC data clearly indicated that a portion of the ritonavir was converted into a non-crystalline (most likely amorphous) form even at the lowest process (drum) temperatures. This observation was in accordance with the results of a recently published study, where a risperidone nanosuspension was processed by spray drying [28]. Kayaert, Van den Mooter [29] stated that the cause of amorphization is most likely the interplay between drug and stabilizer during drying, rather than the nanosizing via wet-ball milling. Indeed, if the drug substance is soluble in the stabilizer, especially if the stabilizer is a polymer, it enhances the probability of an amorphous layer formed at the interface. In the present formulations copovidone was used to increase the adhesion to the drums of the vacuum drum dryer, next to its function as polymeric stabilizer of the liquid nanosuspension. Consequently, the level of copovidone within the final dried intermediate was quite high (25% w/w) enabling the solubilization process of ritonavir. This solubilization was even more enhanced by the presence of nanocrystals instead of microcrystals. In addition, this study clearly showed a drum temperature dependency for the remaining crystallinity: the higher the drum temperature, the higher the amorphous fraction. Interestingly, the critical drum temperature for remaining crystallinity corresponded with the T_{crit} value for redispersibility.

Since non-crystalline API, e.g., amorphous API, can recrystallize during storage [29], this partial change in solid state might have an impact on stability. Consequently, different solid states after manufacturing and after drying of the nanosuspension should be avoided to ensure stability as key design requirement. This might be even more critical for substances showing

pronounced polymorphisms. Thus, future research should investigate the impact of non-crystalline API within a solidified nanocrystal drug product on storage stability.

The short-term stability evaluation of the present study indicated a slight increase in particle size determined via DLS (see Table 6.3). However, an increase in particle size could not be detected via LD. Kumar et al. [30] found out that all indomethacin nano-formulations were stable after spray drying and during storage stability which contained small molecular weight sugars such as mannitol, lactose and trehalose. However, the ratio between the drying protectant and API was much higher (1 to 5 w/w) compared to the formulation tested in this present study (1 to 1.3 w/w). A higher drying protectant to API ratio is known to be beneficial ensuring better steric stabilization, and thus, redispersibility as stated by Malamatari et al. [22]. Yet, the API load would be significantly lower.

As mitigation concept for crystal growth/aggregation, stability and amorphization, the T_g of the formulation should be determined prior to the drying step to choose the processing temperature, accordingly, meaning below the T_{crit} of the respective formulation. This applies presumably for both, spray drying and vacuum drum drying. However, the composition of the nanosuspension prior drying needs to be selected carefully considering the type of drying protectant, its T_g , and the ratio of drying protectant to API. Drying protectants with higher T_g might be preferred enabling lower drying protectant to API ratio, and thus, higher API loads of the final dosage form. Moreover, the solubility of the API within the polymeric stabilizer needs to be assessed to avoid unintended amorphization of the API.

The compression into tablets revealed a dependence on the drying protectant in the formulation. This might be related to the compression behavior of the neat drying protectant and the particle size and shape of the VDD intermediates. Nevertheless, all formulations showed acceptable tabletability, since resulting tablets exhibited sufficient tensile strength even at low compaction pressures.

Results from the redispersibility assessment indicated that tabletting did not impact redispersibility for all formulations at a tensile strength of 1.2 MPa. This was surprising, since nanosized ritonavir particles were assumed to proximate to each other during the tabletting process. But even at higher compaction pressures and higher tablet tensile strength respectively, only disintegration was affected, however, not redispersibility. Moreover, it could be demonstrated that encapsulation of VDD intermediate to capsules did not affect redispersibility of the final drug product.

To sum up, the drying process of a stabilized nanosuspension seems to be the most critical step during the manufacture of a nanocrystal drug product. The selection of the formulation components is important for several reasons. Selected excipients should enable the following:

- Stabilizing the liquid nanosuspension by preventing particle growth, agglomeration, precipitation
- Enabling the spreading of the nanosuspension, and in turn ensure uniform drying on the heated drums
- Achieving acceptable flow and density of the dried and subsequently screened intermediate to ensure downstream processability for encapsulation or compression.

6.8 Conclusion

The present study demonstrated the feasibility of using vacuum drum drying (VDD) for the solidification of ritonavir nanosuspensions resulting in redispersible solids. VDD offers advantages for downstream processing. First, no second drying step is required. Second, the powder properties of the dried intermediate, such as particle size distribution, can be adjusted during milling and by this, potentially optimized for subsequent encapsulation or compression into tablets, which was demonstrated for a selected model formulation.

Moreover, first insights were gathered on the interplay between formulation composition and VDD process conditions (drum temperature), on the resulting impact on powder redispersibility, and on the remaining ritonavir related crystallinity as follows:

- For all studied formulations redispersibility and DS-crystallinity substantially decreased exceeding a formulation specific drum temperature (T_{crit}).
- As T_{crit} is formulation dependent, it should be identified for each formulation as part of the process development.
- T_{crit} might be correlated with the glass transition temperature ($T_{g,wet}$) of the formulation, which is mostly dominated by the T_g of the pure drying protectant. However, this needs further mechanistic clarification.
- Particle growth during drying can be prevented by taking advantage of the principles of steric hindrance in combination with possibly high T_g of the formulation leading to less fluidity.
- As the stabilizers for the nanosuspension will affect the overall T_g , the type and amount should be carefully selected for formulation composition.

6.9 Author contributions

B. V. Schönenfeld: Conceptualization, Methodology, Investigation, Visualization, Writing - original draft. B.-L. Keller: Conceptualization, Methodology, Writing - review & editing. U. Westedt: Conceptualization, Methodology, Project administration, Supervision, Writing - review & editing. K. G. Wagner: Conceptualization, Methodology, Supervision, Writing - review & editing.

6.10 Declaration of competing interest

Barbara V. Schönenfeld, Benjamin-Luca Keller and Ulrich Westedt are employees of AbbVie and may own AbbVie stock. Barbara V. Schönenfeld is a PhD student and Karl G. Wagner is a professor at the University of Bonn. They have no additional conflicts of interest to report.

6.11 Acknowledgments

The authors kindly thank Stefan Weber (AbbVie Deutschland GmbH & Co. KG) for his support in powder X-ray diffraction and Harald Hach (AbbVie Deutschland GmbH & Co. KG) for his support during preparation of the formulations.

6.12 Funding statement

This work was funded by AbbVie Deutschland GmbH & Co. KG. The university of Bonn and AbbVie participated in study design, research, interpretation of data, writing, data collection, analysis, reviewing, and approving the publication.

6.13 Appendix A. Supplementary data

6.13.1 Crystallinity and glass transition temperature (T_g) by differential scanning calorimetry (DSC)

For method details see manuscript section 6.5.2.5.5.

Figure 6.S1 displays the DSC thermograms of the pure microcrystalline ritonavir as reference for quantification of the remaining ritonavir-related crystallinity fraction ($n=2$), and of the vacuum drum dried intermediate (Man7.5/Tre7.5_75_large) representative for all DSC measurements (data not shown).

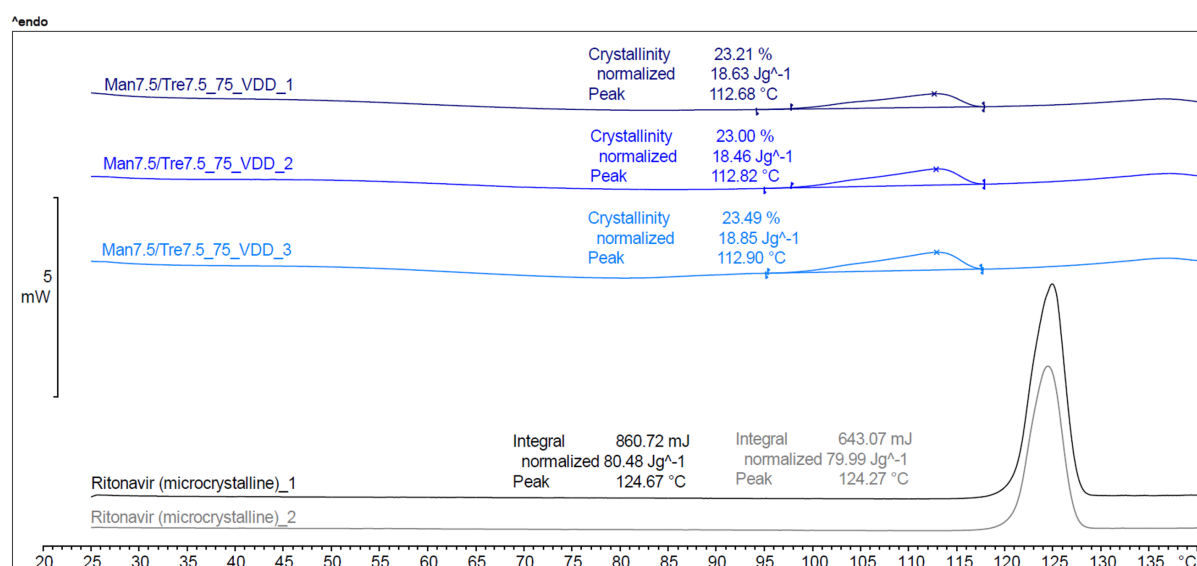


Figure 6.S1: DSC thermograms (open pan) of pure ritonavir (microcrystalline, grey/black colored lines mean melting enthalpy: 80.2 J/g, $n=2$) and vacuum drum dried intermediate (Man7.5/Tre7.5_75_large), blue colored lines, mean crystallinity: 23.2%, $n=3$)

6.13.2 Crystallinity by powder X-ray diffraction (PXRD)

Powder X-ray diffraction (PXRD) was performed for a selected VDD intermediate (Man7.5/Tre7.5_75) to verify the DSC results on quantification of the crystalline ritonavir content within the VDD intermediates. The measurement ($n=2$) was conducted using a X'pert Pro MPD system (PANalytical, Almelo, Netherlands) in reflection mode with a step size of 0.026° 2θ using Cu Kα radiation, a counting time of 1000 s on an angular range of 5-39° 2θ as characteristic for ritonavir. Since a ritonavir reference in nanosize is not available without amorph parts, lithium carbonate (Li₂CO₃) was used as internal standard for quantification as estimation by applying the Rietveld method. The suitability of using an internal standard for quantification was assessed upfront in mixtures of Li₂CO₃ with micro-crystalline ritonavir and the copovidone. The VDD intermediate was spiked with the internal standard (Li₂CO₃)

TRANSFORMATION OF RITONAVIR NANOCRYSTAL SUSPENSIONS INTO A
REDISPERSEABLE DRUG PRODUCT VIA VACUUM DRUM DRYING

corresponding to the targeted drug load of ritonavir within the sample, and then cryo-milled for 10 seconds prior to the PXRD measurement. A diffractogram of copovidone was scaled and fitted to the background diffractogram. The reflex analysis was conducted using the HighScore Pro 4.9 program from PANalytical.

The diffractograms of the pure components (copovidone, mannitol, ritonavir, lithium carbonate (Li_2CO_3)) and the VDD sample (formulation Man7.5/Tre7.5_75_large) spiked with lithium carbonate are shown Figure 6.S2. The remaining ritonavir-related crystallinity value was estimated to 89.93 %, which is in accordance with available DSC data.

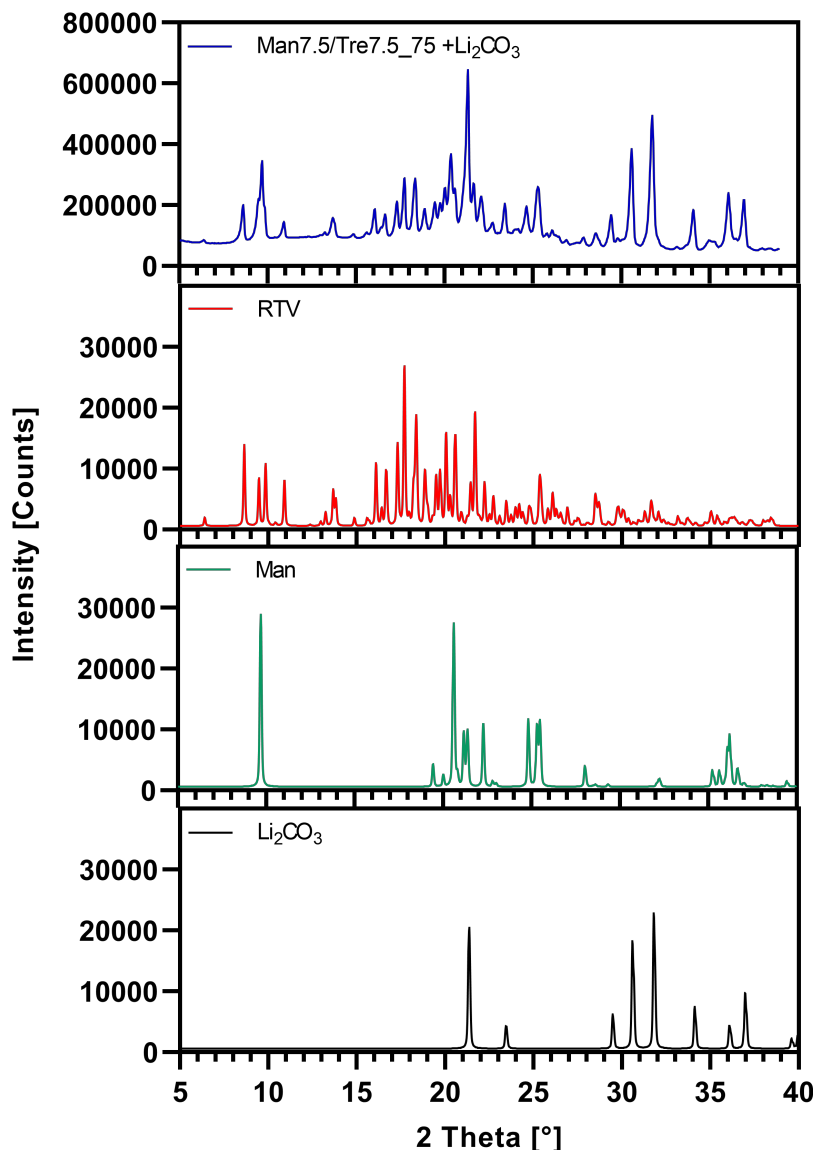


Figure 6.S2: PXRD pattern of pure ritonavir (RTV), mannitol (Man) and lithium carbonate (Li_2CO_3), and vacuum drum dried intermediate (Man7.5/Tre7.5_75_large) spiked with lithium carbonate as reference

TRANSFORMATION OF RITONAVIR NANOCRYSTAL SUSPENSIONS INTO A REDISPERSIBLE DRUG PRODUCT VIA VACUUM DRUM DRYING

6.13.3 Encapsulation process

Table 6.S1 summarizes the results of the in-process control and process control samples combined with machine protocol data reflecting an acceptable encapsulation process.

Table 6.S1: Encapsulation – Weight control results for capsule fill weight obtained from in-process samples, process sample, and in-process control module

	In-Process Control (n=20) according to Ph. Eur. 2.9.5			Process Sample (n=100)	IPC Module (n=all)
	Start	Middle	End		
Mean [mg]	158.7	160.2	160.5	154.7	157.8
SD [mg]	4.7	5.0	5.4	6.2	5.8
RSD [%]	3.0	3.1	3.3	4.0	3.7
Min [mg]	150.8	151.3	152.2	143.3	141.2
Max [mg]	164.5	164.7	165.6	173.7	171.7

6.14 References

1. Loftsson T, Brewster ME. Pharmaceutical applications of cyclodextrins: basic science and product development. *Journal of Pharmacy and Pharmacology*. 2010;62(11):1607-21. doi: <https://doi.org/10.1111/j.2042-7158.2010.01030.x>.
2. Lipinski CA, Lombardo F, Dominy BW, Feeney PJ. Experimental and computational approaches to estimate solubility and permeability in drug discovery and development settings. *Advanced Drug Delivery Reviews*. 2001;46(1):3-26. doi: [https://doi.org/10.1016/S0169-409X\(00\)00129-0](https://doi.org/10.1016/S0169-409X(00)00129-0).
3. Khan KU, Minhas MU, Badshah SF, Suhail M, Ahmad A, Ijaz S. Overview of nanoparticulate strategies for solubility enhancement of poorly soluble drugs. *Life Sciences*. 2022;291:120301. doi: <https://doi.org/10.1016/j.lfs.2022.120301>.
4. Dolenc A, Kristl J, Baumgartner S, Planinšek O. Advantages of celecoxib nanosuspension formulation and transformation into tablets. *International Journal of Pharmaceutics*. 2009;376(1):204-12. doi: <https://doi.org/10.1016/j.ijpharm.2009.04.038>.
5. Merisko-Liversidge E, Liversidge GG. Nanosizing for oral and parenteral drug delivery: A perspective on formulating poorly-water soluble compounds using wet media milling technology. *Advanced Drug Delivery Reviews*. 2011;63(6):427-40. doi: <https://doi.org/10.1016/j.addr.2010.12.007>.
6. Müller RH, Peters K. Nanosuspensions for the formulation of poorly soluble drugs: I. Preparation by a size-reduction technique. *International Journal of Pharmaceutics*. 1998;160(2):229-37. doi: [https://doi.org/10.1016/S0378-5173\(97\)00311-6](https://doi.org/10.1016/S0378-5173(97)00311-6).
7. Liu P, Rong X, Laru J, van Veen B, Kiesvaara J, Hirvonen J, et al. Nanosuspensions of poorly soluble drugs: Preparation and development by wet milling. *International Journal of Pharmaceutics*. 2011;411(1):215-22. doi: <https://doi.org/10.1016/j.ijpharm.2011.03.050>.
8. Choi J-Y, Yoo JY, Kwak H-S, Uk Nam B, Lee J. Role of polymeric stabilizers for drug nanocrystal dispersions. *Current Applied Physics*. 2005;5(5):472-4. doi: <https://doi.org/10.1016/j.cap.2005.01.012>.
9. Jermain SV, Brough C, Williams RO. Amorphous solid dispersions and nanocrystal technologies for poorly water-soluble drug delivery – An update. *International Journal of Pharmaceutics*. 2018;535(1):379-92. doi: <https://doi.org/10.1016/j.ijpharm.2017.10.051>.
10. Singhal M, Baumgartner A, Turunen E, van Veen B, Hirvonen J, Peltonen L. Nanosuspensions of a poorly soluble investigational molecule ODM-106: Impact of milling bead diameter and stabilizer concentration. *International Journal of Pharmaceutics*. 2020;587:119636. doi: <https://doi.org/10.1016/j.ijpharm.2020.119636>.
11. Lee J. Drug Nano- and Microparticles Processed into Solid Dosage Forms: Physical Properties. *Journal of Pharmaceutical Sciences*. 2003;92(10):2057-68. doi: <https://doi.org/10.1002/jps.10471>.
12. Chaubal MV, Popescu C. Conversion of nanosuspensions into dry powders by spray drying: a case study. *Pharmaceutical Research*. 2008;25(10):2302-8. doi: <https://doi.org/10.1007/s11095-008-9625-0>.
13. Möschwitzer JP. Drug nanocrystals in the commercial pharmaceutical development process. *International Journal of Pharmaceutics*. 2013;453(1):142-56. doi: <https://doi.org/10.1016/j.ijpharm.2012.09.034>.
14. Czyz S, Wewers M, Finke JH, Kwade A, van Eerdenbrugh B, Juhnke M, et al. Spray drying of API nanosuspensions: Importance of drying temperature, type and content of matrix

TRANSFORMATION OF RITONAVIR NANOCRYSTAL SUSPENSIONS INTO A REDISPERSIBLE DRUG PRODUCT VIA VACUUM DRUM DRYING

- former and particle size for successful formulation and process development. *European Journal of Pharmaceutics and Biopharmaceutics.* 2020;152:63-71. doi: <https://doi.org/10.1016/j.ejpb.2020.04.021>.
15. Hou Y, Shao J, Fu Q, Li J, Sun J, He Z. Spray-dried nanocrystals for a highly hydrophobic drug: Increased drug loading, enhanced redispersity, and improved oral bioavailability. *International Journal of Pharmaceutics.* 2017;516(1):372-9. doi: <https://doi.org/10.1016/j.ijpharm.2016.11.043>.
 16. Van Eerdenbrugh B, Van den Mooter G, Augustijns P. Top-down production of drug nanocrystals: Nanosuspension stabilization, miniaturization and transformation into solid products. *International Journal of Pharmaceutics.* 2008;364(1):64-75. doi: <https://doi.org/10.1016/j.ijpharm.2008.07.023>.
 17. Kesisoglou F, Panmai S, Wu Y. Nanosizing — Oral formulation development and biopharmaceutical evaluation. *Advanced Drug Delivery Reviews.* 2007;59(7):631-44. doi: <https://doi.org/10.1016/j.addr.2007.05.003>.
 18. Schönenfeld BV, Westedt U, Wagner KG. Vacuum drum drying – A novel solvent-evaporation based technology to manufacture amorphous solid dispersions in comparison to spray drying and hot melt extrusion. *International Journal of Pharmaceutics.* 2021;596:120233. doi: <https://doi.org/10.1016/j.ijpharm.2021.120233>.
 19. Schönenfeld BV, Westedt U, Wagner KG. Compression of amorphous solid dispersions prepared by hot-melt extrusion, spray drying and vacuum drum drying. *International Journal of Pharmaceutics: X.* 2021;100102. doi: <https://doi.org/10.1016/j.ijpx.2021.100102>.
 20. Bhandari B, Bansal N, Zhang M, Schuck P. 4.1 Introduction. *Handbook of Food Powders - Processes and Properties.* Woodhead Publishing; 2013.
 21. Vorländer K, Kampen I, Finke JH, Kwade A. Along the Process Chain to Probiotic Tablets: Evaluation of Mechanical Impacts on Microbial Viability. *Pharmaceutics.* 2020;12(1):66. doi: <https://doi.org/10.3390/pharmaceutics12010066>.
 22. Malamatari M, Somavarapu S, Kachrimanis K, Buckton G, Taylor KMG. Preparation of respirable nanoparticle agglomerates of the low melting and ductile drug ibuprofen: Impact of formulation parameters. *Powder Technology.* 2017;308:123-34. doi: <https://doi.org/10.1016/j.powtec.2016.12.007>.
 23. Zuo B, Sun Y, Li H, Liu X, Zhai Y, Sun J, et al. Preparation and in vitro/in vivo evaluation of fenofibrate nanocrystals. *International Journal of Pharmaceutics.* 2013;455(1):267-75. doi: <https://doi.org/10.1016/j.ijpharm.2013.07.021>.
 24. Wang W. Lyophilization and development of solid protein pharmaceuticals. *International Journal of Pharmaceutics.* 2000;203(1):1-60. doi: [https://doi.org/10.1016/S0378-5173\(00\)00423-3](https://doi.org/10.1016/S0378-5173(00)00423-3).
 25. Jackson CL, McKenna GB. The melting behavior of organic materials confined in porous solids. *The Journal of Chemical Physics.* 1990;93(12):9002-11. doi: <https://doi.org/10.1063/1.459240>.
 26. Medarević D, Djuriš J, Ibrić S, Mitrić M, Kachrimanis K. Optimization of formulation and process parameters for the production of carvedilol nanosuspension by wet media milling. *International Journal of Pharmaceutics.* 2018;540(1):150-61. doi: <https://doi.org/10.1016/j.ijpharm.2018.02.011>.
 27. Zhang X, Guan J, Ni R, Li LC, Mao S. Preparation and Solidification of Redispersible Nanosuspensions. *Journal of Pharmaceutical Sciences.* 2014;103(7):2166-76. doi: <https://doi.org/10.1002/jps.24015>.

TRANSFORMATION OF RITONAVIR NANOCRYSTAL SUSPENSIONS INTO A
REDISPERISIBLE DRUG PRODUCT VIA VACUUM DRUM DRYING

28. Nair A, Khunt D, Misra M. Application of quality by design for optimization of spray drying process used in drying of Risperidone nanosuspension. *Powder Technology*. 2019;342:156-65. doi: <https://doi.org/10.1016/j.powtec.2018.09.096>.
29. Kayaert P, Van den Mooter G. Is the amorphous fraction of a dried nanosuspension caused by milling or by drying? A case study with Naproxen and Cinnarizine. *European Journal of Pharmaceutics and Biopharmaceutics*. 2012;81(3):650-6. doi: <https://doi.org/10.1016/j.ejpb.2012.04.020>.
30. Kumar S, Gokhale R, Burgess DJ. Sugars as bulking agents to prevent nano-crystal aggregation during spray or freeze-drying. *International Journal of Pharmaceutics*. 2014;471(1):303-11. doi: <https://doi.org/10.1016/j.ijpharm.2014.05.060>.

7. SUMMARY AND OUTLOOK

Enabling formulation principles became more pronounced in the last years addressing the poor water-solubility and linked poor bioavailability of drug candidates in the pharmaceutical pipeline. Several technologies exist for the various enabling formulation principles all exhibiting advantages, disadvantages, and limitations. A well-known drying technology in the food and chemical industry is vacuum drum drying, which is rarely known in the pharmaceutical development of solid dosage forms. However, the current work demonstrated the applicability of vacuum drum drying as novel technology in the pharmaceutical field for two enabling formulation principles: a) manufacture of amorphous solid dispersions (ASD) and b) processing nanosuspensions into solidified nanocrystals. Moreover, the downstream processability to final dosage forms was investigated for both cases.

For the ASD approach, ritonavir (15% w/w) in a copovidone/sorbitan monolaurate matrix was used as model formulation. Vacuum drum drying as solvent-evaporation based technology was presented as valid alternative compared to the conventional techniques, namely hot-melt extrusion (HME) and spray drying (SD). The present work demonstrated that all investigated ASD intermediates showed similar results regarding critical quality attributes and solid-state characterization on the intermediate level, such as drug substance related absence of crystallinity, assay, and degradation products (see chapter 3). However, differences were observed in particle morphology and related powder properties such as flowability and bulk density. HME was identified as most beneficial technology considering powder properties, while VDD was slightly superior compared to SD, both solvent-evaporation based methods. Besides, the compression behavior of the ASD intermediates and respective tablet blends (TB; addition of filler, glidant, lubricant (12.9% w/w)) was studied including X-ray μ CT (microcomputed tomography) images for the inner structure of the tablets. The present work indicated that downstream processability as well as compression behavior was not entirely defined by the solid-state of the respective ASD. All ASDs prepared by different approaches showed similar solid-state characterization results such as drug substance related residual crystallinity or glass transition temperature. In fact, the compression behavior seemed to be mostly affected by the observed particle morphology differences – at least for the assessed model formulation (see chapter 4). Advantageously, the VDD intermediate was directly compressible, whereas the SD material was not, resulting in tablets with defects (capping) based on a high degree of elastic recovery. Compared to HME, the VDD material showed similar tabletability on the ASD intermediate level and substantially improved

tabletability when formulated as tablet blend, resulting in stronger compacts at even lower solid fraction values. In general, the addition of outer phase excipients diminished differences between the tested ASD intermediates. This results in tablets with less voids or cracks in the inner structure, which is most likely linked to improved flowability, reduced inner wall friction and the addition of a brittle filler increasing the bonding surface additionally. Interestingly, dissolution testing of the ASD intermediates (powder in capsules) by using an automated biphasic assay setup (BiPHa+) indicated no impact of the manufacturing technique (see chapter 3). This was in accordance with the disintegration and dissolution data (USP II apparatus) of tablets consisting of pure ASDs or ASD tablet blends (see chapter 4).

In conclusion, the manufacturability of an ASD is affected by the manufacturing technology, whereas the dissolution seemed not to be impacted assuming no influence on associated bioavailability - in this specific case. Thus, the decision on the appropriate technology for a respective compound should be made individually for each pipeline compound based on:

- a) the physico-chemical properties of the compound (e.g., chemical stability, melting point, solubility in solvents),
- b) the target drug product profile which defines the dosage, dosage form as well as route of application and
- c) the business-related aspects such as technology availability and inhouse scale-up options.

In chapter 5 the compression modulus of polymeric excipients commonly used in ASD manufacture or tableting was assessed compared to non-polymeric ones. It was found that the particle density (via helium pycnometer) was already exceeded at low compaction pressures (< 200 MPa) for polymeric excipients (Kollidon®VA64, Soluplus®, AQOAT®AS-MMP, Starch1500®, Avicel®PH101), whereas either never reached for brittle fillers such as DI-CAFOS®A60 and tricalcium citrate or exceeded at compaction pressures above 350 MPa in the case of FlowLac®100, Pearlitol®100SD. We found that the threshold for exceeding particle density was in accordance with the start of linear increase in elastic recovery in-die and thus, with predominantly elastic deformation. This could be confirmed by the calculation of the elastic modulus based on a presented equation including the slope of the linear increase in elastic recovery in-die. In conclusion, the knowledge of the threshold provides guidance for the selection of suitable excipients in the formulation development to mitigate the risk for tablet defects related to stored elastic energy, like capping and lamination. The introduced threshold of exceedance of the particle density might be another approach worthy to be included in the risk assessment for drug product development.

Moreover, the general applicability of the particle density for compression analysis was discussed exemplarily for the Heckel analysis. The present work demonstrated that the Heckel compression analysis was not valid at high compaction pressures considering the particle density for calculation in case of polymeric excipients. Instead, it was shown that using the so-called “density under pressure” resulted in reasonable Heckel plots. However, it should be discussed and investigated in future work, whether it is advisable to apply Heckel analysis for polymeric excipients in general, especially above the determined threshold, at which most of the compaction energy is translated into elastic deformation.

Finally, the present work demonstrated the applicability of vacuum drum drying for the solidification of crystalline ritonavir nanosuspensions prepared by wet-ball milling (chapter 6) – another enabling formulation principle. Several technologies already exist for solidification such as spray drying, spray coating or freeze drying. However, each technology has its own limitations, and there seems to be a lack for continuous manufacturing or for easy downstream processing to tablets or capsules. In principle, the solidification step of a nanosuspension is known to be critical because of destabilizing the nanocrystal system leading potentially to crystal growth as well as particle agglomeration/aggregation. Therefore, drying protectants are usually added to avoid particle growth. In the present study different drying protectants (mannitol, lactose, or trehalose) were tested by being added to the nanosuspension prior drying. The nanoparticulate redispersibility and remaining crystallinity was still given after the solidification process via vacuum drum drying, and further not negatively affected by neither tabletability nor encapsulation process for a selected formulation consisting of mannitol combined with trehalose as drying protectants. Beneficially, the resulting powder of the investigated different VDD intermediates was easy-flowing and exhibited appropriate bulk density. In general, the particle size and thus, the power properties are adjustable by milling of the VDD intermediate to powder offering potential to even optimize downstream processability. Moreover, a formulation specific drum temperature T_{crit} was identified as critical for remaining ritonavir nanoparticulate redispersibility and crystallinity. It was observed that the T_{crit} might be correlated with the glass transition temperature ($T_{g,wet}$) of the formulation, which seemed to be mostly dominated by the T_g of the pure drying protectant. However, further mechanistic clarification is needed in this field. In conclusion, stabilizers for the nanosuspension and drying protectants for the drying liquid formulation should be carefully selected during formulation development to ensure drying processability via vacuum drum drying.

In sum, the current work identified several benefits of vacuum drum drying and highlighted its potential as alternative technique for enabling formulation principles, especially compared

to spray drying. SD and VDD are both techniques applicable for thermally labile and shear-sensitive drug substances compared to HME, since reduced temperatures can be used by applying vacuum to ensure proper drying. However, the VDD demonstrated its suitability as one-step drying process by removing organic solvents and even water effectively requiring no subsequent drying step (see chapter, 3, 4 and 6). In contrast, SD requires a secondary drying step afterwards in most cases. The elimination of a subsequent drying step is economically beneficial by reducing the total number of process steps, but also from stability point of view, since residual solvents/ moisture knowingly impact physical stability of both, ASDs and solidified nanocrystals. Another advantage of VDD is its dosing principle via nip feeding resulting in less viscosity limitations, since even pastes can be dosed between the gap of the two drums. Thus, high solid loads can be aimed for processing if the solubility of the respective drug substance and excipients is given. This reduces the total amount of solvents positively, which indeed, is environment-friendly and economical by increasing the solid throughput and thus, reducing the overall processing time. The overall process time is shorter for the VDD process since the time-consuming secondary drying step is not required. Furthermore, vacuum drum drying is semi-continuous process, where the feeding solution must be prepared in batches, but the drying step itself can be conducted continuously. Limitations are the cleaning need for the border plates at the end of the drums over time and the condensate bin emptying leading to an interruption of the process by stopping the vacuum pump.

Moreover, vacuum drum drying offers advantages in scaling up the process from pilot to production scale since the retention time on the drums is key for the product quality affected by drum diameter and drum speed. Another important factor is the product layer thickness on the drums, which should be widely similar if keeping speed and geometry of the gap comparable. In addition, comparing vacuum drum drying with spray drying the production-scale equipment for VDD has a much lower footprint – especially considering no need for secondary drying step equipment such as a conical dryer.

However, also disadvantageous were observed as a potentially longer residence time of the product on the drum leading to an increase in thermal exposure, which needs further evaluation. In addition, sedimentation or phase separation might occur in the liquid reservoir above the drums gap considering higher concentration of the solution/suspension induced by the evaporation process. Especially if using solvent mixtures instead of pure solvents where one compound evaporates faster than the other. Moreover, even though the requirement of a certain viscosity (ensuring adhesion of the product to the drums) allows the processability of even honey-like liquids, it leads to challenges if only low solid loads can be processed due to

limited solubility of the API or excipients in solvents. The addition of viscosity enhancers would become necessary decreasing the overall drug load of the intermediate and thus, increasing potentially the pill burden.

In sum, the presented technical set-up of the vacuum drum dryer in a GMP pilot plant was demonstrated to be feasible for development purposes of amorphous solid dispersions and solidified nanocrystals. Thus, vacuum drum drying can be considered for first-in-human clinical trial supply manufactures in future. Moreover, vacuum drum drying might become a frequently used technology for toxicological study supply as well.

However, vacuum drum drying should be assessed in more detail in future regarding both enabling formulation principles including the following aspects:

- Increasing of process understanding especially of the interplay of process parameters
- Identification of critical process parameters and their impact on critical quality attributes statistically and for more than one model formulation (e.g., fast recrystallizing API for ASDs)
- Identification of the interplay of critical process parameters with critical material attributes of the feeding solution/suspensions
- Identification of limitations for the VDD process itself, e.g., viscosity limitations for the feeding solution
- Identification of mandatory requirements, e.g., certain viscosity of the feeding solution to avoid the solution to flow through the gap and to ensure proper adhesion to the drums
- Assessment of more excipients commonly used in the manufacture of ASDs and solidification of nanosuspensions (e.g., drying protectants) and their processability via VDD

8. PUBLICATIONS

Parts of this work are already published as articles:

Title	Authors	Journal	Year	DOI	Outcome/Highlights
Vacuum drum drying – a novel solvent-evaporation based technology to manufacture amorphous solid dispersions in comparison to spray drying and hot-melt extrusion	B. V. Schönenfeld, U. Westedt, K. G. Wagner	International Journal of Pharmaceutics	2021	https://doi.org/10.1016/j.ijpharm.2021.120233	<ul style="list-style-type: none"> • VDD = alternative technology to manufacture amorphous solid dispersions (ASDs) • No differences in solid-state characterization, nor in assay/ degradation products and biphasic dissolution testing • Differences in particle morphology and related powder properties • VDD beneficial compared to SD
Compression of amorphous solid dispersions prepared by hot-melt extrusion, spray drying and vacuum drum drying	B. V. Schönenfeld, U. Westedt, K. G. Wagner	International Journal of Pharmaceutics X	2021	https://doi.org/10.1016/j.ijpx.2021.100102	<ul style="list-style-type: none"> • ASD technology has influence on particle morphology • Compression behavior dominated by particle morphology • VDD material directly compressible into tablets; better tabletability compared to extrudate • ASD technology no impact on disintegration/ dissolution
Compression modulus and apparent density of polymeric excipients during compression – impact on tabletability	B. V. Schönenfeld, U. Westedt, K. G. Wagner	Pharmaceutics	2022	https://doi.org/10.3390/pharmaceutics14050913	<ul style="list-style-type: none"> • Exceeding particle density (via helium pycnometer) already at low compaction pressures (CPs) for polymeric excipients • Exceeding particle density either never reached for brittle fillers or reached at high CPs • Exceeding particle density directly linked with start of increasing elastic recovery in-die and thus, associated with predominantly elastic deformation during compression
Transformation of ritonavir nanocrystal suspensions into a redispersible drug product via vacuum drum drying	B. V. Schönenfeld, B.-L. Keller, U. Westedt, K. G. Wagner	AAPS PharmSciTech	2022	https://doi.org/10.1208/s12249-022-02283-z	<ul style="list-style-type: none"> • VDD is a suitable technology for solidification of crystalline drug substance nanosuspensions • Critical drum temperature identified for remaining nanoparticulate redispersibility and crystallinity • Glass transition temperature of drying protectant has impact on remaining redispersibility